DEPARTMENT OF CHEMISTRY, UNIVERSITY OF JYVÄSKYLÄ
RESEARCH REPORT No. 190

Solid state conformational behavior and interactions of a series of aromatic oligoamide foldamers

BY

AKU SUHONEN

Academic Dissertation for the Degree of
Doctor of Philosophy

To be presented, by permission of the Faculty of Mathematics and Science of the University of Jyväskylä, for public examination in YAA303, on February 19th, 2016 at 12 noon.

UNIVERSITY OF JYVÄSKYLÄ

Jyväskylä, Finland
ISBN 978-951-39-6529-7
ISSN 0357-346X

ABSTRACT

Suhonen, Aku
Solid state conformational behavior and interactions of a series of aromatic oligoamide foldamers
Jyväskylä: University of Jyväskylä, 2016, 68 p.
(Department of Chemistry, University of Jyväskylä Research Report
ISSN 0357-346X)
ISBN 978-951-39-6529-7

The topic of this thesis is aromatic oligoamide foldamers. The literary review of the thesis discusses the general features of foldamers and their design and then focuses on the specific examples of aromatic oligoamide foldamers.

The experimental part of the thesis discusses the design and preparation of a family of aromatic oligoamide foldamers that can adopt a helical conformation. The folding is directed by intramolecular hydrogen bonding and stabilized by intramolecular aromatic interactions. The focus of the thesis is the analysis of the solid state conformations of ten foldamer analogues. The analysis is based on forty different crystal structures which are determined using single crystal X-ray diffraction. In selected cases the solution behavior of the compounds is analyzed using NMR spectroscopy, and the conformations are compared to DFT calculations.

Three types of aromatic oligoamide foldamers were synthesized: a benzene foldamer and its sulfonamide analogue, where two of the amide bonds were replaced by a sulfonamide bond, and a series of pyridine foldamers. The benzene foldamer, while able to fold in a fairly open helical conformation, was found to have high flexibility that hinders the design of consistently folding molecules. DFT calculations showed that the sulfonamide foldamer could fold in a highly folded helical conformation, but the folding was not observed experimentally.

Pyridine foldamers have a central 2,6-pyridine core unit that is planar and directs the adjacent amide N-H groups towards the inner face of the folded conformation. The first pyridine foldamer, the analogue of the benzene foldamer, showed improved folding predictability and solubility. The other pyridine foldamers are asymmetric analogues designed to study the effect of the different electron density donating properties, as well as, the presence, size and bulkiness of the substituent to the folding properties of the compounds.

Keywords: foldamer, oligoamide, hydrogen bonding, intramolecular interactions, structural chemistry, X-ray diffraction, NMR spectroscopy, polymorph, solvate

Author's address

Aku Suhonen
Department of Chemistry
Nanoscience Center
University of Jyväskylä
P.O. Box 35
FI-40014 University of Jyväskylä
Finland
Aku.suhonen@jyu.fi

Supervisor

Professor Maija Nissinen
Department of Chemistry
Nanoscience Center
University of Jyväskylä
P.O. Box 35
FI-40014 University of Jyväskylä
Finland

Reviewers

Professor Janne Jänis
Department of Chemistry
University of Eastern Finland
Finland

Dr. Ivan Huc
Institut Européen de Chimie Biologie
Université Bordeaux
France

Opponent

Professor Mir Wais Hosseini
Laboratoire de Tectonique Moléculaire
Université de Strasbourg
France

PREFACE

The work presented in this thesis was carried out at the Department of Chemistry, Nanoscience center, University of Jyväskylä between 2012 and 2015 and was funded by the University of Jyväskylä Graduate School for Doctoral Studies. Several other sources of funding have also contributed to this thesis in the form of travel grants that have allowed me to participate in several international conferences and training courses. I would like to thank the doctoral school as well as the Gustaf Komppa fund of the Alfred Kordelin foundation, Oskar Öflund foundation, Magnus Ehrnrooth foundation, NGS-nano and OCCB for enabling me to conduct the research discussed in this thesis.

I would like to thank my supervisor Professor Maija Nissinen for giving me this interesting project and introducing the interesting fields of foldamers and X-ray diffraction to me. I would also like to thank her for all the advice and support during this project. Also big thanks to my master's thesis supervisors and later colleagues Dr. Elisa Nauha for teaching me most of what I know about practical X-ray diffraction and Dr. Kaisa Helttunen for her help and guidance in the synthesis and characterization of the foldamers I prepared during the project. A big thank you also goes to the other current and former members of the group, Dr. Tiia-Riikka Tero, Riia Annala and Dr. Kirsi Salorinne for their valuable help and advice.

My coworkers in the Department of Chemistry and especially Nanoscience Center are thanked for the motivating and inspiring environment. It has been a pleasure working here. I would especially like to thank Dr. Gerrit Groenhof, Professor Perttu Permi, Professor Petri Pihko and Professor Heikki Tuononen for collaborating with this project and for their valuable advice. I would also like to thank the reviewers of this thesis Dr. Ivan Huc and Professor Janne Jänis, who thoroughly inspected this thesis, for their effort and valuable comments.

Last I would like to thank my parents Marjatta and Pekka for their support throughout my studies, and my friends Kimmo, Marika, Esa, Anni, Mika, Elisa, Olli, Juuso and Katja for their friendship, and for helping me take my mind off work and have fun when things were stressful or tiring.

Jyväskylä, January 18th 2016

Aku Suhonen

LIST OF ORIGINAL PUBLICATIONS

This dissertation is based on the original publications listed below and they are herein referred to by their Roman numerals.

I A. Suhonen, E. Nauha, K. Salorinne, K. Helttunen and M. Nissinen, Structural analysis of two foldamer-type oligoamides – the effect of hydrogen bonding on solvate formation, crystal structures and molecular conformation, *CrystEngComm* 14 (2012), 7398-7407. DOI: 10.1039/c2ce25981h.

II M. Kortelainen, A. Suhonen, A. Hamza, I. Pápai, E. Nauha, S. Yliniemelä-Sipari, M. Nissinen and P. M. Pihko, Folding Patterns in a Family of Oligoamide Foldamers, *Chem. Eur. J.* 21 (2015), 9493-9504. DOI: 10.1002/chem.201406521.

III A. Suhonen, I. S. Morgan, E. Nauha, K. Helttunen, H. M. Tuononen and M. Nissinen, The Effect of a Rigid Sulfonamide Bond on Molecular Folding: A Case Study, *Cryst. Growth Des.* 15 (2015), 2602-2608. DOI: 10.1021/acs.cgd5b00424.

IV A. Suhonen, M. Kortelainen, E. Nauha, S. Yliniemelä-Sipari, P. Pihko and M. Nissinen, Conformational Properties and Folding analysis of a series of Seven Oligoamide Foldamers, **2015**, *manuscript*.

For papers I, III and IV the author is the primary author, and has carried out most of the crystallography work for papers I-IV, all of the synthetic work for papers I and III and some of the synthetic work for paper IV. He has carried out most of the characterization and NMR analysis work for papers I and III and some of the characterization and NMR analysis work for papers II and IV.

ABBREVIATIONS

Boc	*tert*-butyloxycarbonyl protecting group
Cbz	carboxybenzyl
CD	circular dichroism
DCC	*N*,*N*'-dicyclohexylcarbodiimide
DCE	dichloroethane
DCM	dichloromethane
DFT	density functional theory
Diox	dioxane
DMA	dimethylacetamide
DMB	dimethoxybenzyl
DMF	*N*,*N*-dimethylformamide
DMSO	dimethyl sulfoxide
DNA	deoxyribonucleic acid
EDC	1-Ethyl-3-(3-dimethylaminopropyl)carbodiimide
Et	ethyl
EtOAc	ethylacetate
Fmoc	fluorenylmethyloxycarbonyl
*i*Pr	isopropyl
IR	infrared
MD	molecular dynamics
Me	methyl
MeCN	acetonitrile
mp	melting point
NMR	nuclear magnetic resonance
NOE	nuclear Overhauser effect
NOESY	nuclear Overhauser effect spectroscopy
Ph	phenyl
PMB	*p*-methoxybenzyl ether
PXRD	powder X-ray diffraction
RNA	ribonucleic acid
rt	room temperature
SPPS	solid-phase peptide synthesis
TBA-F	tetrabutylammonium fluoride
*t*Bu	*tert*-butyl
TGA	thermogravimetric analysis
THF	tetrahydrofuran
VT	variable temperature
XRD	X-ray diffraction

CONTENTS

1 REVIEW OF THE LITERATURE

1.1 Introduction

Within nature proteins serve a variety of functions despite the limited number of building blocks they are composed of and interactions they can employ. They carry out sophisticated functions, like catalysis or selective binding, with high efficiency and often with stereospecificity in complex intra- and intercellular circumstances. The vast abilities of the biological molecules represent a huge potential for chemists to learn and adapt them for chemical applications.

Foldamers are synthetic oligomers and polymers are designed to mimic the structure and interactions of biopolymers, and fold into well-defined conformations.[1] Foldamer-type molecules have vast potential in the pharmaceutical industry, for example as potential transporters for drugs and other bioactive molecules[2] and as complex drug molecules with the ability to participate in protein-protein interactions[3]. They also have potential as organic catalysts[4] with high efficiency and specificity, and as allosteric controls and biomimetic receptors[5] and sensors[6], antimicrobial polymers[7] or other materials[8]. While proteins have many advantages over synthetic molecules the intrinsic nature of synthetic foldamers can also give them beneficial properties, such as better endurance for temperature, pH and salt concentrations, the possibility to function in organic solvents, modifiability of the size of the molecule and extracellular stability.

Foldamers are typically divided in two broad categories. Aliphatic foldamers are composed of aliphatic monomers, often peptidomimetics, such as β-peptides, whereas aromatic foldamers are composed of aromatic monomer units. An interesting class of foldamers are aromatic oligoamides,[9] which contain both primary and secondary rigid and predictable structures, provided by both the aromatic rings and the amide bond. Planar aromatic rings provide a fixed position and directionality for possible substituents. They also have the potential to affect the conformation and secondary structure of the foldamer through steric effects and π stacking interactions both in solution and in the

solid state. Equally important for the predictability and folding of aromatic oligoamides are the amide bonds. Due to the partial double bond nature of the carbonyl C-N bond the amide bond is also planar and rigid and the energy barrier for flipping the bond is higher than for a single bond, which increases the stability of a folded conformation. The most important feature of the amide bond, however, is the presence of both the hydrogen bond donor and acceptor moieties. The hydrogen bonding motifs are fairly predictable and strong enough to significantly stabilize the secondary structure of the foldamer.

1.2 Foldamer concepts

1.2.1 Synthesis

In foldamer synthesis there are seemingly as many methods as there are chemists, but only a few principles have emerged that are found throughout the field. The synthesis routes are often designed to be repetitive and as simple as possible with unified purification methods (Figure 1). Usually one unit is attached at a time, which allows for the variation of the attached units and easy access to the reaction intermediates, as the attached units are usually either commercially available or their immediate derivatives. The yields of the reactions are also improved and the handling of the reactants is simplified due to better solubility of the smaller units.

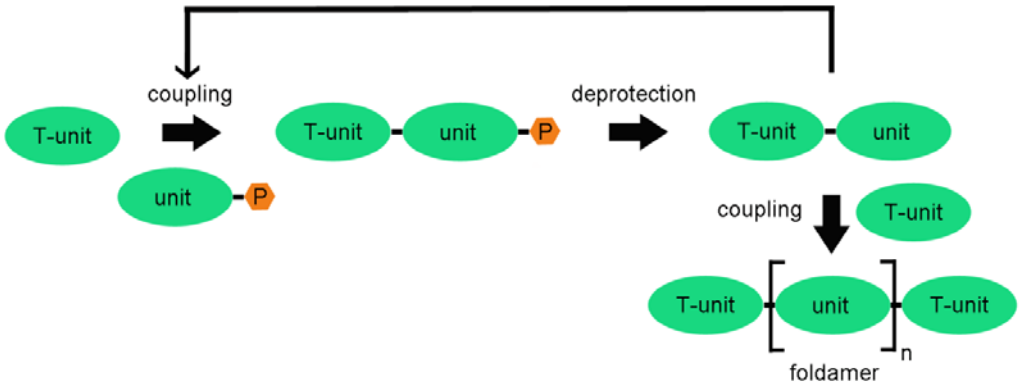

Figure 1. A Schematic example of a repeatable foldamer synthesis that utilizes protection groups. The protection group is presented in orange and the foldamer units are green. T-units are terminal units meant to cap the foldamer.

The synthesis of the amide, or peptide, bond has a long history. The first synthetic methods were published over 100 years ago.[10] Since then new methods have been developed to serve different synthetic needs. The most important directions for the foldamer field have been the solid-phase peptide synthesis (SPPS)[11] and chemical ligation,[12,13] which were developed from the earlier synthetic inventions, such as utilization of different coupling methods,

for example acid chlorides[10,14] and carbodiimides,[15] and protective groups[16–19] in peptide synthesis. Small β-peptides and α/β-peptide hybrids are usually prepared either using Fmoc SPPS or Boc solution phase methods.[10]

The methods for the synthesis of the aromatic oligoamides vary greatly. Especially smaller aromatic oligoamides have been prepared using many different protecting groups, activating reagents and/or acid chlorides. The units have been attached one at a time or as dimers or even trimers. The methods often depend on the properties of the individual target compound and on the preferences of the chemist. However, some systematic methodology has been used. Huc *et al.*[20] have used acid chlorides for the sake of efficiency and the lack of hybridization, and Boc-protection instead of the Cbz-protection due to the ease of the deprotection. The synthesis route was intended to be repetitive and to suit the properties of the product foldamers that fold better which leads to steric hindrance that lowers the reaction yields when larger units are used. Kilbinger *et al.*[21] employed a solid state method and PMB and Fmoc-protection in the preparation of oligobenzamide foldamers.

The methods for the synthesis of foldamer backbones without the amide bond follow the same general principles. Tanatani *et al.*[22], for example, prepared aromatic oligourea foldamers from nitroanilines and aromatic isocyanates in repetitive coupling cycles. In another non-amide type example Lehn *et al.*[23] prepared naphthyridine foldamers through a modulated process using repeated condensation and acid hydrolysis steps.

1.2.2 Folding interactions

Important general features for the foldamer folding are the predictability of the folding motif, the ability to unfold and change conformation and the continuity of the folding effect or effects to allow the production of stable oligomeric structures. In foldamers this is achieved through a variety of interactions, the most common of which is hydrogen bonding.[24,25] However, aromatic interactions,[22,26–29] solvophobic forces,[30] metal coordination[31,32] and so called conformational preferences[26,27] have also been used.

Hydrogen bonds are prevalent in biological systems and their formation and breaking based on the changes of environment or biological signals is the basis of many crucial biological processes. Their stability and directionality allow the design and use of reliable hydrogen bond synthons that strongly direct the folding of oligomers. The use of hydrogen bond synthons can be complicated, however, due to the interference of additional hydrogen bond acceptors or donors that may disrupt the formation of the desired hydrogen bond synthon. Also, the hydrogen bonding properties of solvents have to be taken into account as many solvents can hinder or alter the folding of a compound.

The most common hydrogen bonding group used in the foldamer design is the amide bond. The amide bond, or peptide bond in proteins, has both hydrogen bond donor and acceptor groups which makes it a versatile tool for the design of a hydrogen bond network. The bond between the nitrogen and

the carbonyl carbon of the amide bond has a double bond character which brings planarity and rigidity to the bond and causes a significant energy barrier for bond flipping, which stabilizes the folded structure. Other hydrogen bonding groups used in foldamers are the urea bond, which has two hydrogen bond donors for every hydrogen bond acceptor[33] and the sulfonamide bond, which somewhat resembles the amide bond, but the geometry of the bond is very different.[34] The sulfonamide bond has two hydrogen bond acceptors, which are weaker than the amide carbonyl oxygen, and the N-H proton, which is more acidic than the amide N-H making it a more powerful hydrogen bond donor. Other hydrogen bond contributing groups used in conjunction with the previously discussed groups in foldamers include, for example, pyridine, pyrimidine and isobutoxy groups.

Aromatic interactions are also important for folding, as they have some directionality and rigidity, which, with proper positioning, can be used to induce folding. The utilization of solvophobic effects requires careful positioning of hydrophobic and hydrophilic groups to support the desired folding. Metal coordination induced folding is typically caused by the wrapping of the foldamer backbone around a metal atom. Conformational preferences are an example of a variety of methods available for a researcher to design a foldamer. For example, Lehn *et al.*[26] used the preference of nitrogen containing aromatic rings, like pyridine and pyrimidine, to form the conformations where the nitrogen atoms are not close to each other in order to produce helical folding which is additionally stabilized by aromatic interactions.

1.2.3 Foldamer secondary structure

The secondary structure of foldamers is based on the same principles as the secondary structure of proteins. The most common secondary folding motif in both foldamers and proteins is a helix.[35] A helix is either right or left-handed and a preference for either form is often decided based on the chirality of the folding molecule. Other biological folding motifs mimicked in foldamer research are a sheet[28,29] and some beta turns[36] which are important, for example, in the stacking of the sheets and as receptor counterparts. The secondary structure of foldamers is not limited to the biological motifs and several other motifs have emerged that are based on the properties of the foldamer units or a specific non-biological shape. These motifs are rigid linear strands[37] that can sometimes be curved, zigzag shapes[38] and different helical capsule motifs[39,40] that are held together by weak interactions.

1.3 Aromatic oligoamide foldamers

1.3.1 2,6-Pyridine foldamers

Oligoamide foldamers composed solely of 2,6-pyridines have been prepared by Lehn *et al.*[41–45] and Huc *et al.*[20,46–49] (Scheme 1). The length of the foldamers varies from three to fifteen aromatic units and they are separated by amide bonds with alternating directionality. The ends of the molecules often contain various aliphatic, aromatic or amine groups. In many cases all or half of the pyridine rings are substituted at 4-position with various substituents.

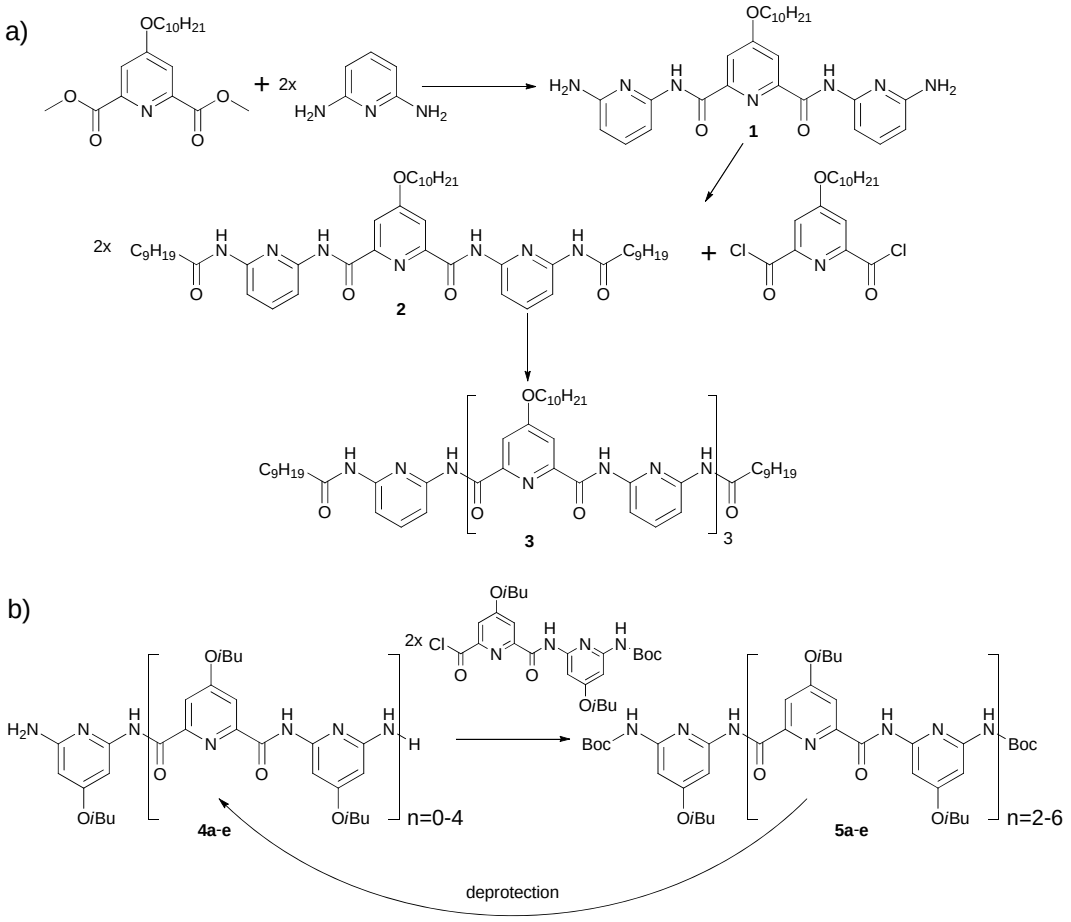

Scheme 1. Examples of the structure and synthesis of 2,6-pyridine foldamers through a) a modular[42] and b) stepwise approach.[20]

The most common synthesis method for 2,6-pyridine foldamers is a modular approach,[41,42,47] but a stepwise approach[20] or a combination using elements from both approaches[49] can also be employed. For example, Lehn *et al.*[42] used a modular approach where smaller components were combined with larger components which were further combined with foldamers (Scheme 1a). When designing larger foldamers (up to 2.7 kDa) Huc *et al.*[20] used a stepwise addition of small units (Scheme 1b). In this method steric hindrance produced

by the folding of the larger foldamers was mitigated and the method proved to be an easy way to create larger foldamers by adding small units to the previously prepared foldamers. The amide linkage was made through the attachment of lithium amine salts to esters or by using acid chlorides and protected amines. Several protection groups for amine were tested (Fmoc, Cbz and Boc). In the longest foldamers the Boc group was found to be the most promising. In a combination method Huc *et al.*[49] first prepared pyridine oligomers of different lengths by adding a single unit in a repetitive reaction cycle and then combining these oligomers to produce the final foldamers.

The crystal structures indicate that in the solid state the 2,6-pyridine foldamers prefer helical single or multi-stranded structures (Figures 2 and 3, Scheme 2). The aromatic rings and amide bonds and conjugation of π-orbitals throughout the molecules limit the conformational freedom of the foldamers. The folding is mainly directed by intramolecular hydrogen bonding between consecutive units, but there are also favorable π-stacking interactions. The intramolecular hydrogen bonds are located inside the molecule shielding them from the surrounding environment. The adoption of the helical conformation through conformational restraints, hydrogen bonding between the consecutive units and stacking interactions allows the foldamers to breathe and extend with minimal distortion of the hydrogen bond network. All foldamers of this type have hollow cavities within the molecule, which often are filled with water molecules that are strongly hydrogen-bonded to the surrounding helices (Figures 2 and 3).

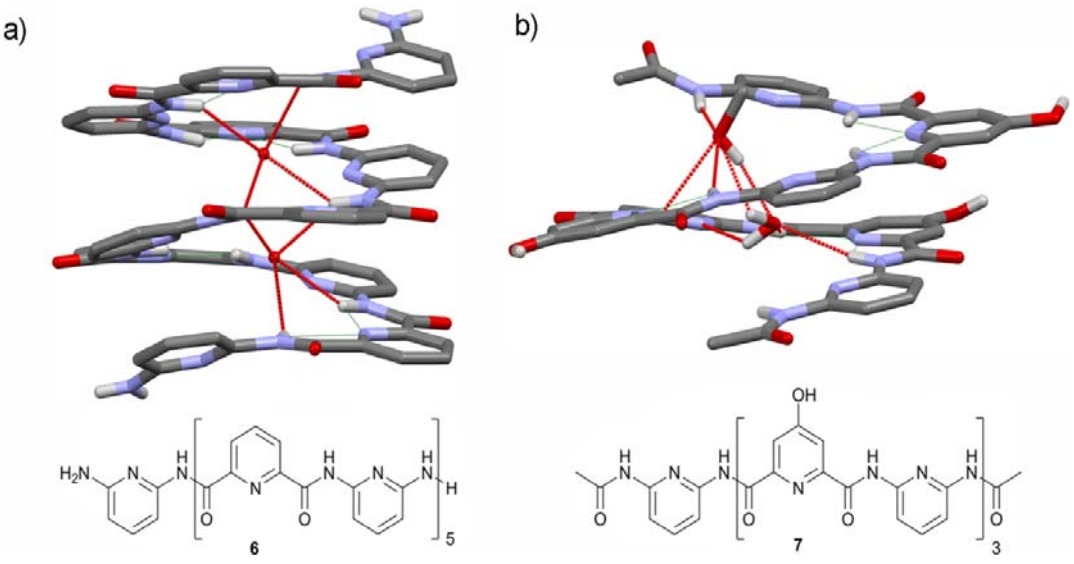

Figure 2. Examples of single stranded crystal structures of the 2,6-pyridine foldamers. a) An eleven ring foldamer **6** with two water molecules in the foldamer cavity[42] and b) seven ring foldamer **7** with methanol and water in the foldamer cavity.[46] Non-contact hydrogen atoms have been removed for clarity.

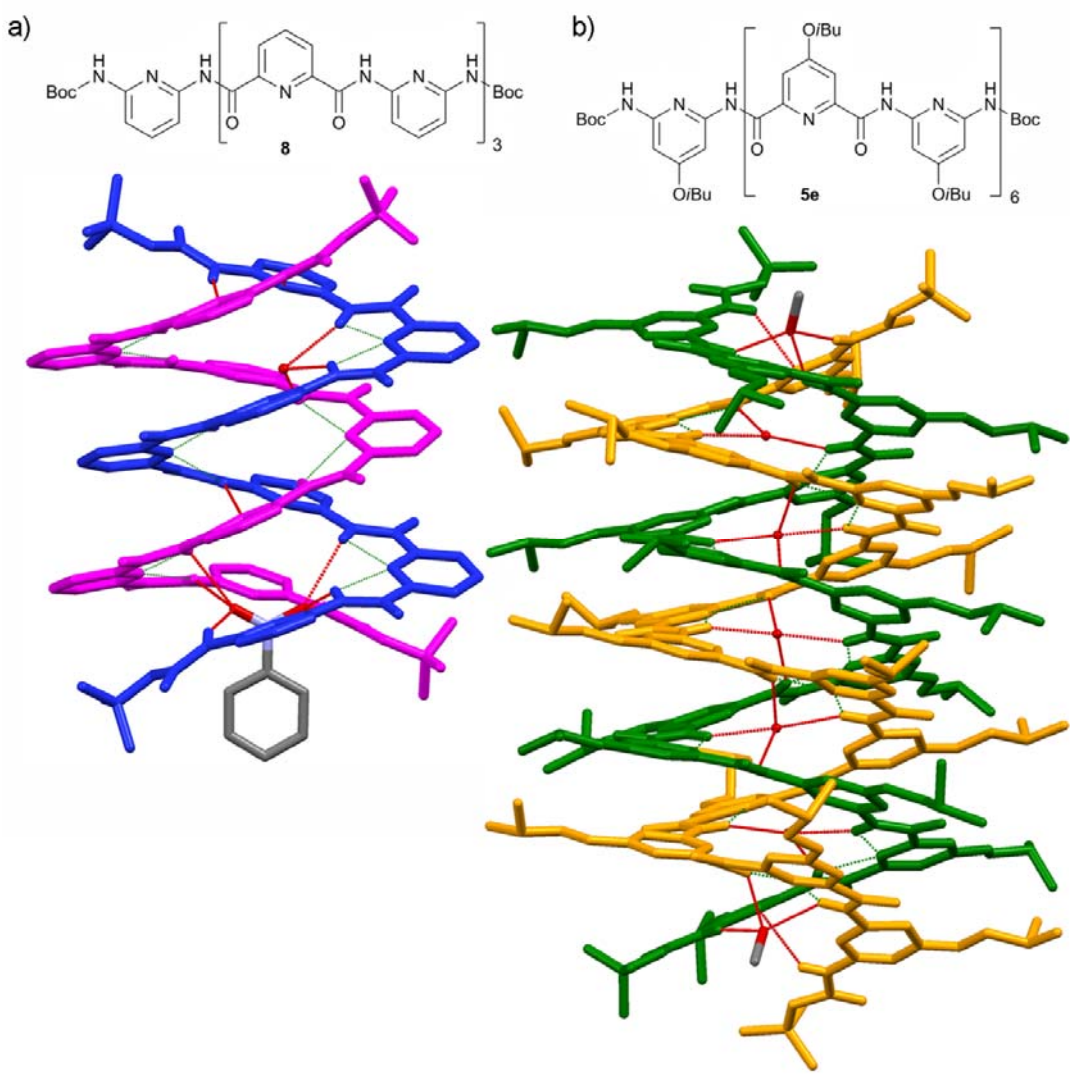

Figure 3. Examples of double-stranded crystal structures of the 2,6-pyridine foldamers. a) A seven ring foldamer **8** in a double helix with water and nitrobenzene in the foldamer cavity;[41,43] and b) a thirteen ring foldamer **5e** forming a double helix with water and methanol molecules in the foldamer cavity.[20] Non-contact hydrogen atoms were removed for clarity.

The solution state properties of the foldamers were studied using NMR[20,41–43,46]. The results show that the helical shape of the foldamers is maintained in the solution and double helix assemblies are also present. The monomer and dimeric states are continuously in a slow exchange. The supporting MD simulations suggest that both monomer and double helix species are stable in solution.[42,43]

In several cases the pyridine-2,6-diamine rings of the foldamers were additionally protonated using triflic acid,[44,45,47,48] which led to the foldamer adopting an undulating structure instead of the helix (Figure 4). NMR data indicates that this form is also found in solution.

The induction of chirality in the foldamer design was introduced either externally by using a chiral solvent, or internally through the addition of a chiral fragment to a foldamer.[45,47] CD spectroscopy measurements in chiral solvents and for the foldamers with a chiral substituent or a group at the center of the molecule showed that the handedness of the helix can be directed.

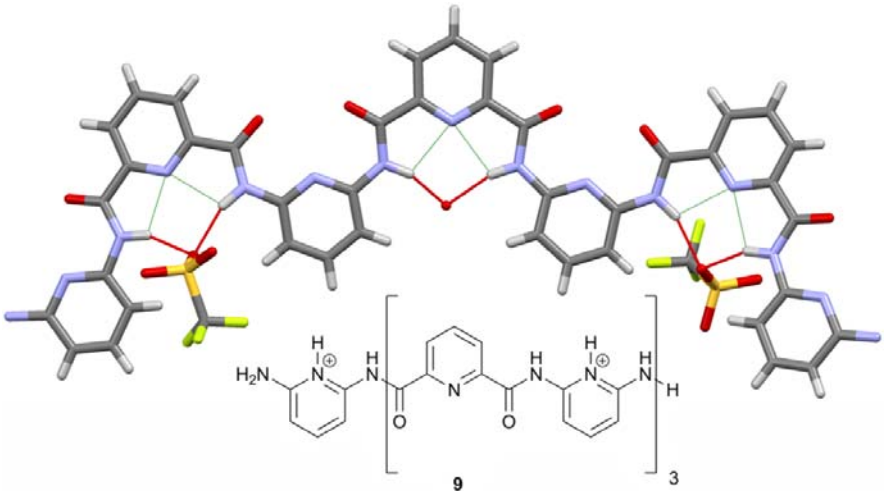

9

Figure 4. An example of the undulating structure of the protonated 2,6-pyridine foldamer **9**.[44,45]

1.3.2 Anthranilamide foldamers

Hamilton *et al.*[50–52] have prepared anthranilamide foldamers with two basic structural types, linear and helical (Scheme 2). The synthesis of the linear strand foldamers follows a stepwise approach where the anthranilamide strands are synthesized from 2-nitrobenzoyl chloride and methyl anthranilates (Scheme 2a). After the initial reaction the nitro group of the product is reduced to an amine and the reaction is repeated. The helicity is introduced to the structure by a pyridine-based turn unit. These foldamers are synthesized in a modular approach from the shorter linear strands in one or two major steps (Scheme 2b-c). The anthranilamide foldamers are easily functionalizable to their aromatic rings with only a small effect on their conformational behavior.

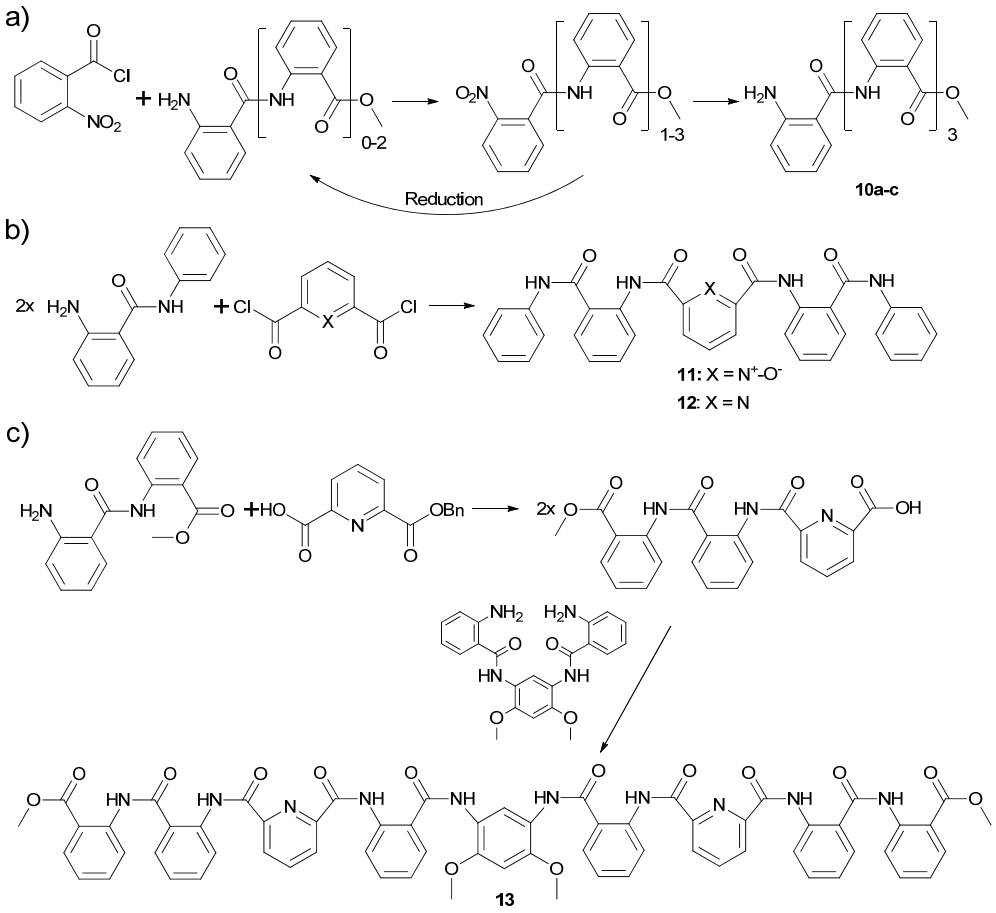

Scheme 2. Examples of the molecular structure and the synthesis of anthranilamide foldamers. a) A stepwise synthesis of linear strand foldamers,[51] and a modular synthesis of helical foldamers b) with one turn,[50,51] and c) two turns[52].

The linear strand foldamers **10a-c** vary in size from two to four aromatic rings. NMR data indicates that the linear conformation, seen in a crystal structure of a shorter molecule (Figure 5a), remains constant in all foldamers of this type and even the substituents attached to either one or both ends of the molecule or to the phenyl rings did not alter the linear conformation.

The longer, helical foldamers **11-13** adopt different helical conformation types depending on the length and composition of the molecule (Figures 5b-c and 6a-b). The pyridine-2,6-dicarboxamide *N*-oxide anthranilamide foldamer **11** crystallizes in a relatively open helical conformation with intramolecular hydrogen bonding and a stable planar structure with a 120° angle between the phenyl amide bonds (Figure 5b). The 2,6-pyridine anthranilamide foldamer **12** has similar properties, but the hydrogen bonds are in a wider, roughly 110° angle and the foldamer adopts a compact helical conformation (Figure 5c).

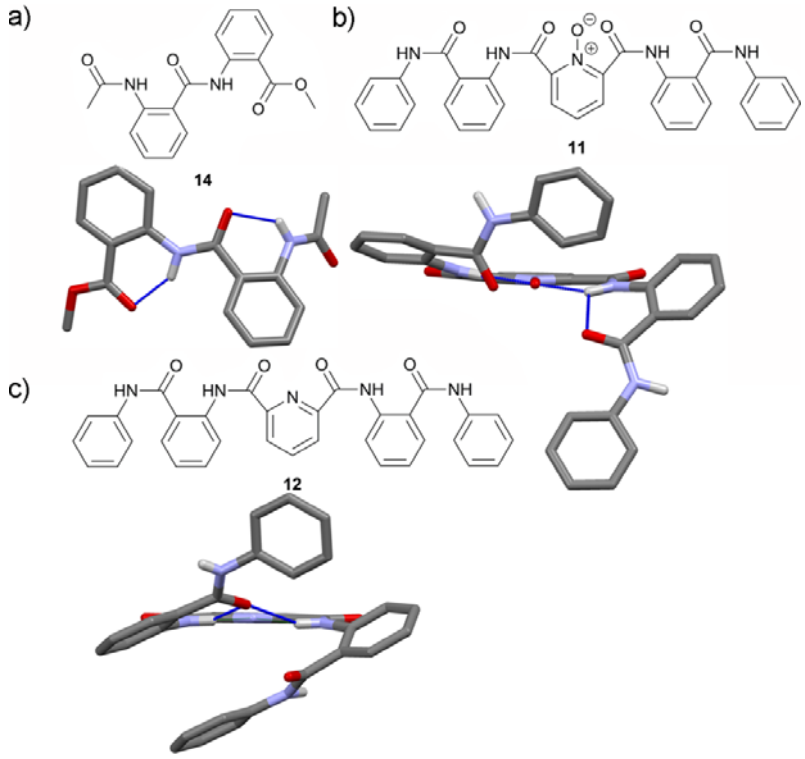

Figure 5. Examples of the crystal structures of anthranilamide foldamers. a) A prototype of a linear strand sheet structure (**14**);[51] b) a pyridine-2,6-*N*-oxide anthranilamide foldamer **11** in an open helical conformation;[50,51] c) a 2,6-pyridine anthranilamide foldamer **12** in a helical conformation.[50,51] Non-amide hydrogen atoms have been removed for clarity.

Longer nine aromatic rings containing foldamer **13** having 4,6-dimethoxy-1,3-diaminobenzene anthranilamide forms intramolecular hydrogen bonds between the amino and methoxy groups pointing outside of the molecule, which causes similar planar effect as with the pyridine turn units. Foldamer **13** crystallizes in two different helical conformations (Figure 6a-b); a more compact conformer with two helical parts, one of which is right-handed and the other left-handed (Figure 6a), and the other conformer with same-handed parts and a more open end of the molecule (Figure 6b). Solution state data indicates that the helical conformations of foldamers **11-13** are retained in solution and that the longer foldamer **13** is present in various populations of both helical conformations (Scheme 2c, Figure 6a-b).

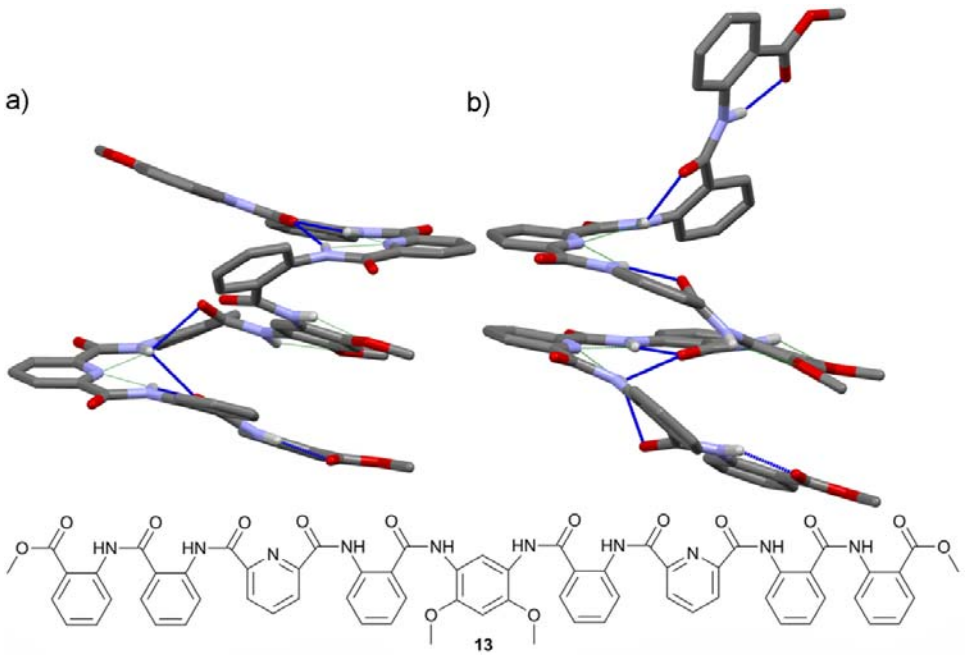

Figure 6. Crystal structures of a 2,6-pyridine-4,6-dimethoxy anthranilamide foldamer **13**[52] a) in a compact helical conformation and b) in an open-ended helical conformation. Non-amide hydrogen atoms have been removed for clarity.

1.3.3 Quinoline foldamers

Quinoline based foldamers and quinoline-pyridine hybrid foldamers have been widely studied by Huc *et al.*[39,40,53–77] (Scheme 3). The principle behind the quinoline foldamers is the predictability of the rigid structure. The folding is a result of intramolecular hydrogen bonding between the consecutive units, which can be predicted based on the behavior of the shorter strands. The quinoline unit was designed to produce relative sharp turns in the helical structure by placing the substitutes of the amide bond at a roughly 60° angle to each other. This allows for efficient folding without the need for specific turn units. The amide bonds face towards the inside of the molecule shielding them from solvent molecules and filling the inner part of the molecular fold. Synthetic modifications have also been made to the quinoline sequence by introducing 2,6-pyridine based units, or by modifying the quinoline unit itself. For example, a container[39,40,59] or a multi stranded helix[71–74] have been made and the flexibility and the reactivity of the foldamer increased to allow the synthesis of larger molecules[64].

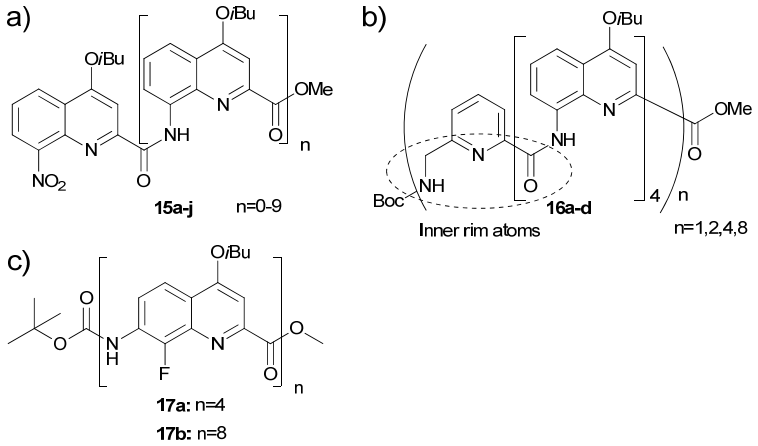

Scheme 3. Examples of quinoline and quinoline-pyridine hybrid foldamers: a) a quinoline foldamer **15**[53,54], b) a quinoline-pyridine hybrid **16**[64] and c) fluoroquinoline foldamer **17**[71].

1.3.3.1 Synthesis of quinoline foldamers

The principal synthesis of the quinoline foldamers is modular[53,54], and the focus has been on increasing the foldamer size in as few steps as possible (Scheme 4). The basic quinoline unit **15a** is repetitively coupled with amide bonds after the reduction of the nitro group and turning the ester group to an acid chloride. The process works well for the foldamers containing up to eight quinoline units (**15c-h**), though the reaction time and/or temperature has to be increased in the reduction and saponification steps of the reaction. Even then the yield of the small scale reaction of the eight unit foldamer **15h** remained very low (<10%). Adding a small two unit precursor to the eight unit foldamer produced good yields suggesting that adding a smaller unit in a stepwise fashion is favorable with the larger foldamers. This method also provides the added benefit of the selective addition of different units to the foldamer sequence.

The quinoline based and quinoline-pyridine hybrids are synthesized by combining oligomeric sequences composed of a single unit, or in few cases a sequence composed of several different units, into a foldamer using the modular method. Several different types of foldamers have been synthesized from modified quinoline units, such as 8-fluoroquinoline[71], naphthyridine[72] and pyridoquinoline[73] or their combinations[74]. Examples of quinoline-pyridine hybrids[39,40,59,64] include foldamer capsules[39,40,59,77] and quinoline-aminomethylpyridine hybrid foldamers[64]. The synthesis of the quinoline-aminomethylpyridine hybrid foldamers was similar to the modular method discussed above, but because the aliphatic parts of the pyridine units were more reactive than the quinolines larger foldamers, even up to 40 units in length, could be prepared.[64]

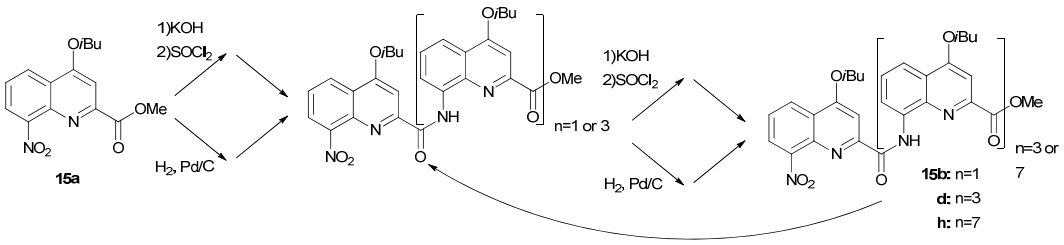

Scheme 4. Example of the modular synthesis method of quinoline foldamers.[54]

Another method for the preparation of the quinoline foldamers **18a-c** is a modification of the solid phase synthesis[66] used for preparing peptides and aliphatic foldamers (Scheme 5).[10] Wang resin is used as a solid support, and Fmoc protected amines and small acid chloride units are used for coupling.[66] The yields for the reactions vary, and the increase in length proved to be a problem as the molecules folded around each other slowing down the reaction rate and lowering the yield. A lower foldamer density on the resin, and the use of microwave radiation sped up the process and improved the yield.

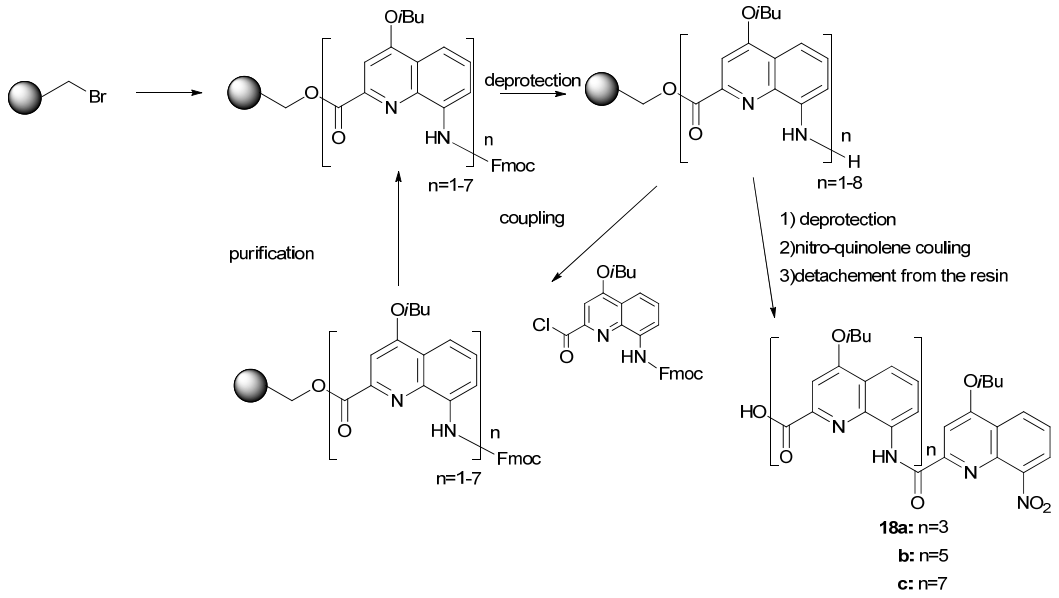

Scheme 5. Example of the synthesis of quinoline foldamers **18a-c** using the solid phase synthesis method.[66]

1.3.3.2 Structure of quinoline foldamers

The basic quinoline foldamers (**15a-j**) produce a tight single-handed helix without solvents at the center of the foldamer (Figure 7a). The quinoline units form hydrogen bonds to neighboring quinoline units forming a helix, which is also stabilized by numerous aromatic interactions between the different quinoline units. The largest foldamers of this type, up to 40 units, are quinoline-pyridine hybrid foldamers **16a-d**. The folding was designed to utilize the higher flexibility and rotational freedom of the pyridine units while maintaining a

stable and tight helical folding motif conveyed by the quinoline units (Figure 7b). The pyridine units have the same curvature as the quinolines and the atoms forming the inner rim of the helix are the same (Scheme 3b).

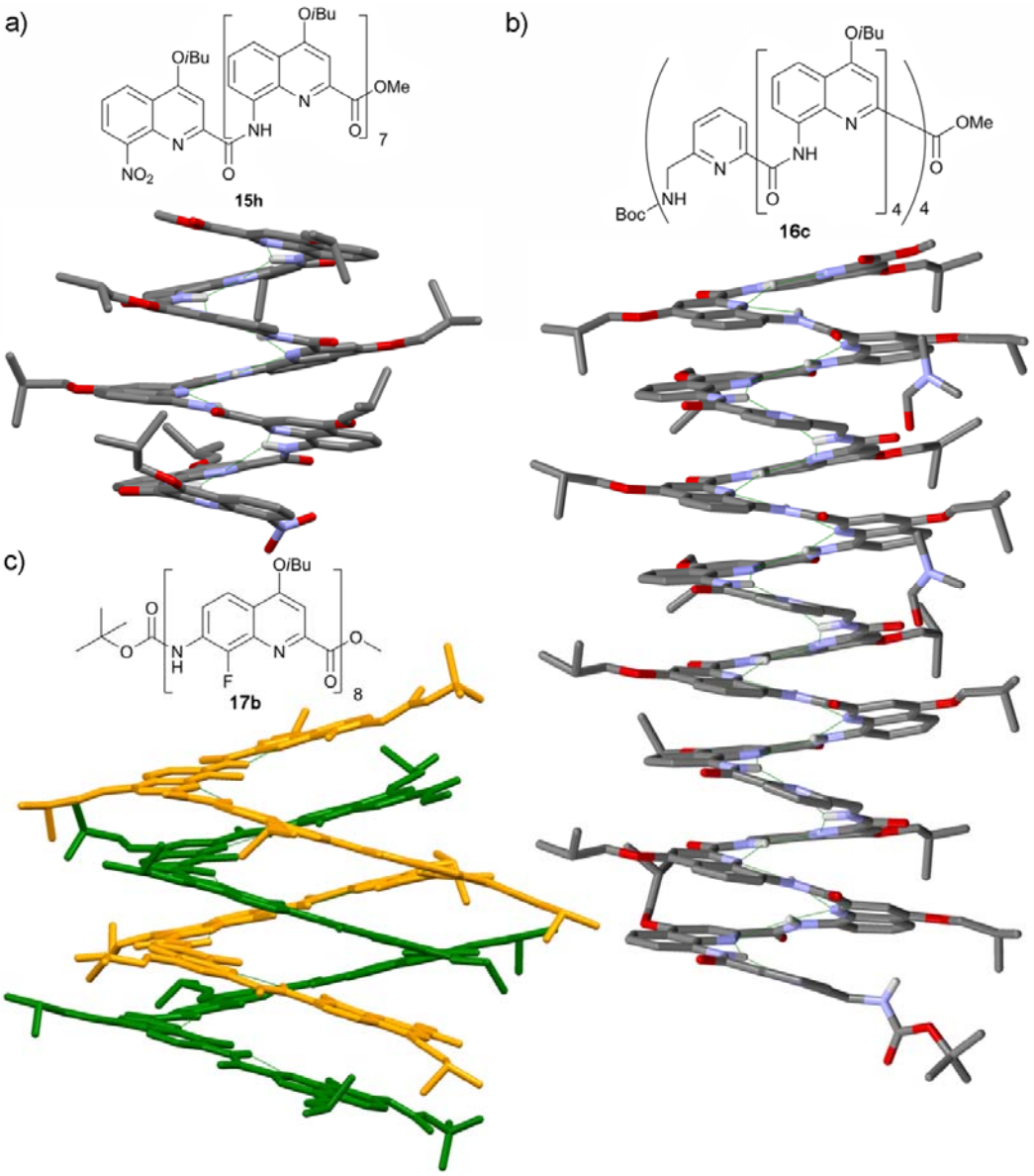

Figure 7. Examples of quinoline and quinoline hybrid foldamers: a) an eight unit quinoline foldamer **15h**[53], b) a 20 unit pyridine-quinoline hybrid **16c**[64] and c) an eight unit fluoride modified quinoline double strand **17b**[71]. Non-contact hydrogen atoms have been removed for clarity.

Foldamers composed of fluoroquinoline monomers[71] (**17**) are a modification of the quinoline foldamers that were designed to produce a wider helix with an intramolecular cavity. The fluoroquinoline foldamers produced double and even quadruple stranded helices (Figure 7c). Hollow parallel and antiparallel double helices were also prepared using naphthyridine units.[72]

Quinoline-pyridoquinoline hybrids were prepared in order to create a foldamer with a pyridoquinoline double helical segment in the middle of the molecule, and single stranded quinoline helices at the end to increase the size of the helical cavity.[73]

The handedness of the longer quinoline foldamers was monitored with NMR measurements, and it was found to change very slowly.[55–57,69,70] The change took from hours to days, or even longer. Chirality and also specificity for a certain handedness of the foldamer helix could be induced by adding a chiral group to the end of the foldamer.[57] The handedness of a foldamer could also be switched by attaching a group that induces mutual steric exclusion on the two halves of the foldamer in the middle of the foldamer.[56]

1.3.3.3 Applications of quinoline foldamers

Quinoline-pyridine hybrids have been used as molecular capsules consisting of one (**19**)[39,59,77] or two strands (**20** and **21**)[40] depending on the foldamer. So-called molecular apple peel **19** (Figure 8a, Scheme 6a) is a loosely cohesive unimolecular container with a polar interior cavity.[39,59] The size of the cavity varies roughly from 20 to 70 Å^3 depending on the length of the foldamer. The smallest cavity was able to bind water molecule while the larger could accommodate larger guests like methanol.

The smaller two-stranded capsule **20** consists of a single strand cap with only a small non-solvent accessible cavity and a larger double-stranded cavity at the other end (Figure 8b, Scheme 6b).[40] The larger two-stranded capsule **21** has an additional four unit quinoline cap at the end of the molecule that has no cavity (Figure 8c, Scheme 6c). The smaller double-stranded capsule could contain up to two DMSO molecules inside the cavity while the larger capsule could bind even a 1,10-decanediol molecule. Yet another example of capsular applications are quinoline-pyridine-naphthyridine foldamers with a pyridine-pyridazine-pyridine center, which were designed to capture a chiral target non-permanently inside a single-stranded helical capsule.[77] The encapsulation of guest molecules from the surrounding solvent has potential applications in catalysis and molecular recognition, as well as in protection from degradation of the guest by its surroundings.

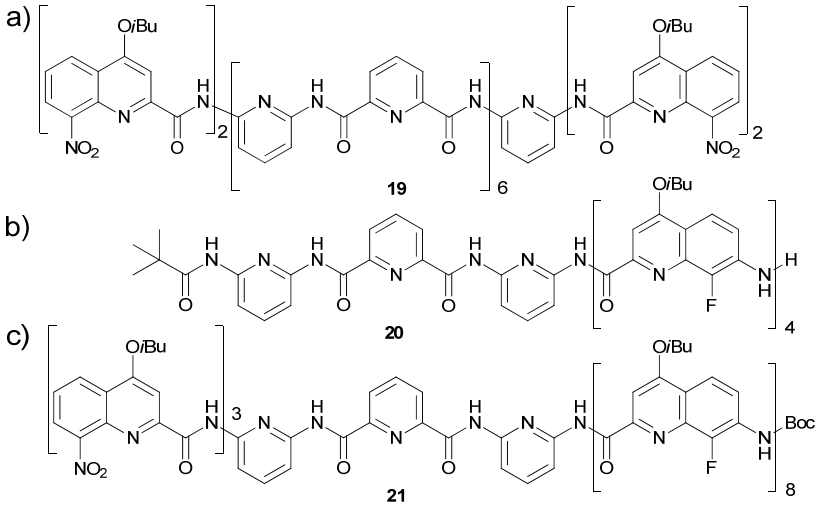

Scheme 6. Examples of quinoline-pyridine foldamer capsules: a) an apple peel capsule forming foldamer **19**[39,59], b) a pyridine-fluoroquinoline capsule forming foldamer **20**[40], and c) a quinoline-pyridine-fluoroquinoline capsule forming foldamer **21**[40].

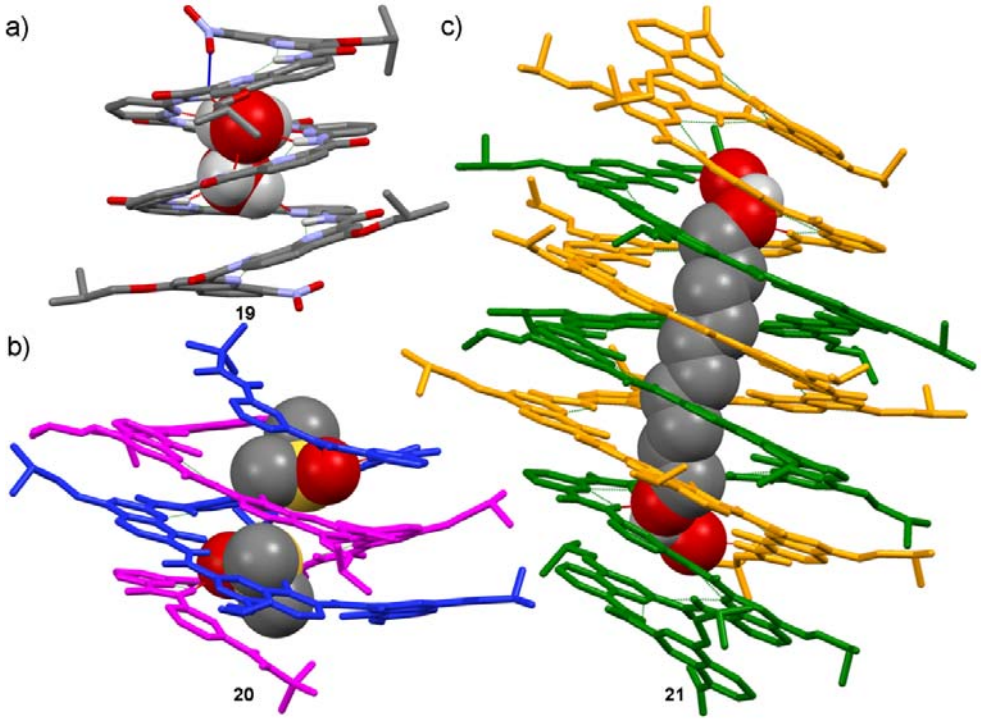

Figure 8. Examples of quinoline-pyridine foldamer capsules: a) a single-stranded apple peel capsule (**19**) with two water molecules inside the cavity[39,59], b) a double-stranded pyridine-fluoroquinoline capsule (**20**) with two DMSO molecules inside the cavity[40], and c) a double-stranded quinoline-pyridine-fluoroquinoline capsule (**21**) with two water molecules and a 1,10-decanediol molecules inside the cavity[40]. Non-contact hydrogen atoms have been removed for clarity.

Many potential applications also lie in the biological functions, and with this in mind the water solubility of the quinoline and quinoline hybrid foldamers have been enhanced in two different ways.[60,62] Amphipathic quinoline helices have isobutoxy chains as a hydrophobic side and aminopropoxy groups as a hydrophilic side.[60] The solubility was improved, but complete water solubility was not achieved. Amino and diamino containing functional groups, however, increased the water solubility.[62,74] Water soluble foldamers with charged side chains, usually an amino based, bind to DNA G-quadruplexes that are suspected to have a function in gene expression.[63,67,68] Another biological application is quinoline based foldamers of varying types and strength with proteinogenic side chains, which have shown potential for protein-foldamer interactions.[75,76] A study has also been carried out on larger molecules combining several helical segments linked by a spacer unit to create protein-like foldamers.[61]

The quinoline foldamers have also been used as a helical bridge between an electron donor and an acceptor in a photoinduced charge transfer reaction.[65] The well-established conformation of the quinoline foldamers allows the precise positioning of the chromophores. The results show low attenuation factors, but the exact mechanism for the electron transfer is still unclear.

1.3.4 Phenanthroline foldamers

Foldamers composed of alternating phenanthroline and *o*-phenylenediamine units, with alternating amide bond directionality were prepared by modular approach from monomer, dimer, trimer or tetramer units attached to a phenylene mono or diamine unit (Figure 9).[78] Both phenanthroline and *o*-phenylenediamine monomers were chosen in the design process due to the 60° angle they define, which induces the adoption of a helical conformation stabilized by intramolecular hydrogen bonds and aromatic interactions. In addition, two *iso*-butoxy groups were added to the phenanthroline to increase the solubility of the foldamers. Later, the group of phenanthroline based foldamers was expanded to chiral oligoamides and foldamer based super secondary structures where two foldamers were attached to an aromatic linker.[79,80]

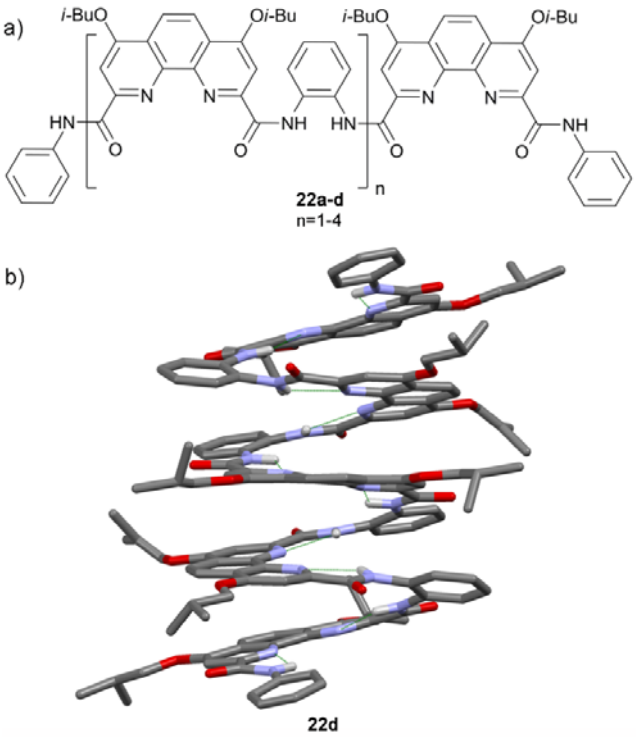

Figure 9. a) Phenanthroline foldamers **22a-d** and b) the crystal structure of a four unit phenanthroline foldamer **22d**.[78] Non-contact hydrogen atoms have been removed for clarity.sc

1.3.5 Benzene foldamers

Benzene oligoamide foldamers composed of various substituted benzene units can be roughly divided into three categories based on the shape of the folding; helical, linear and zig-zag. The folding is based on the position and rigidity of the aromatic bonds, and the intramolecular hydrogen bonding between the benzene substituents and the amide N-H hydrogens. The helical foldamers adopt mostly planar conformations with continuous unidirectional turn in the fold that results in the overlap of the oligomer units. The linear foldamers adopt a planar, linear and relatively rigid conformation, whereas the zig-zag foldamers are planar and rigid, but adopt a conformation with sharp turns.

1.3.5.1 Helical foldamers

Helical foldamers by Gong *et al.*[81–86] (Scheme 7) and Li *et al.*[87–93] (Scheme 8) can adopt crescent and helical shapes and they all have a cavity at the center of the helix. The size and shape of the cavity, as well as the solubility of the foldamer can be altered with different building units, such as *para*-substituted benzene derivatives, and by varying the length of the foldamer. The folding is based on the position and rigidity of the aromatic bonds, and on the three-center intramolecular hydrogen bonding between hydrogen bond acceptors attached to the benzene unit and the amide N-H hydrogens. The hydrogen bond

acceptors are usually alkoxy groups, but foldamers with fluoride acceptors were also prepared to test if covalently-bound fluoride atoms were strong enough hydrogen bond acceptors to form a helical conformation in a suitably designed aryl oligoamide backbone.[87] Three centered hydrogen bonds can point either outside or inside the helix interior, but in all cases they enforce both planarity and a continuous turn in the foldamer. The hydrogen bonds are always only to the neighboring units which makes the conformation of foldamers easier to predict. Intramolecular aromatic interactions are also found in overlapping parts of the helical foldamer structures and they contribute to the overall stability of the conformation. Seven units or more are required to form a helical turn, more if both para and *meta*-units are used.

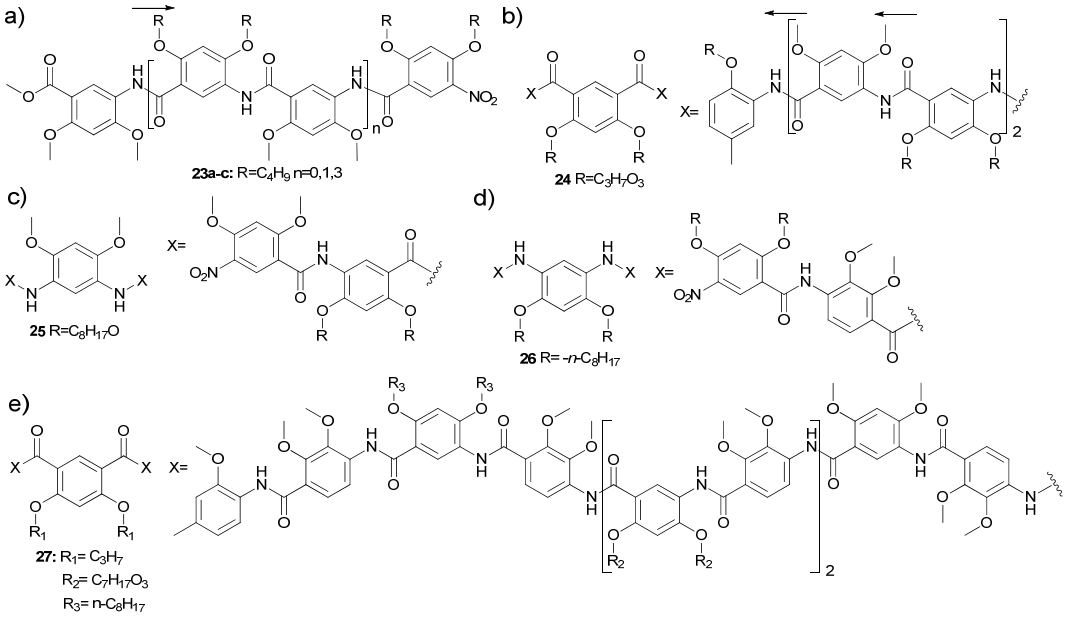

Scheme 7. Example structures of helical foldamers by Gong *et al.*: a) unidirectional foldamer **23**,[86] b) bidirectional foldamer with a dicarboxamide center unit and meta substituted aromatic units **24**,[85] c) bidirectional foldamers with diamine center unit and meta substituted aromatic units **25**,[85] d) bidirectional foldamers with diamine center unit and both meta and para substituted aromatic units **26**[85] and e) bidirectional foldamers with a dicarboxamide center unit and both meta and para substituted aromatic units **27**[83]. The arrows indicate the direction of the amide bonds.

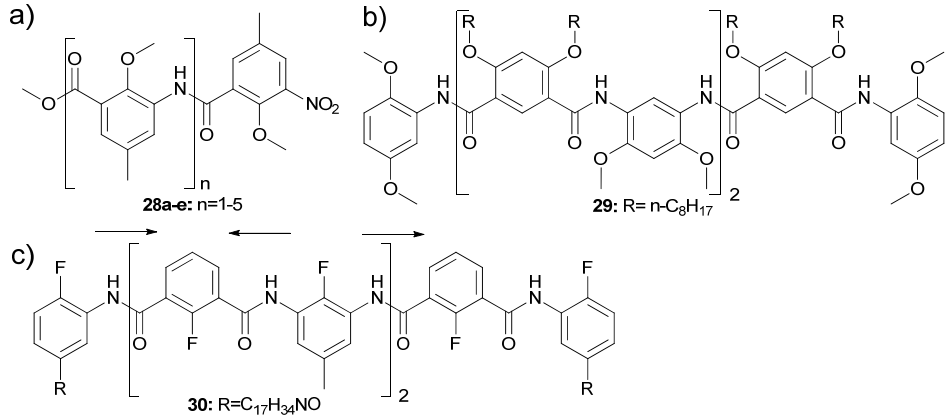

Scheme 8. Example structures of helical foldamers by Li *et al.*: a) unidirectional helical foldamer **28**[89], b) helical dialkoxy foldamer **29**[88] and c) helical fluoride foldamer **30**[87]. The arrows indicate the direction of the amide bonds (c).

The unidirectional foldamers with all amide bonds in the same direction were synthesized by a step-wise method from aromatic acid chlorides that have nitro groups at the *meta*-position in respect to acid chloride functionality (Scheme 9a).[82,89] The same method was also used for the precursor oligoamides of the bidirectional foldamers with a dicarboxamide center unit. Bidirectionality was achieved by attaching the oligoamides to an aromatic diamine or diacid chloride center in a modular reaction step (Scheme 9b).[83–85] The synthesis of the helical foldamers with alternating amide bond directionality is also modular.[87-93] The foldamers are prepared by the coupling of trimer or dimer units and diacid chloride or diacid unit. Due to the increasing difficulty of synthesis as the length and steric hindrance of the foldamers increased Gong *et al.*[86] devised a synthesis method where the folding is disrupted temporarily by replacing the N-H hydrogens of the amide bonds by a protecting group, 2,4 DMB (Scheme 9c). The studies showed that if too many DMB replacements are used the synthesis is again hindered, this time by crowded conformations caused by the large DMB group. The reaction rates are the highest when one DMB group is used per 3-5 amide bonds. The solubility of the foldamer precursors with the DMB was also improved.

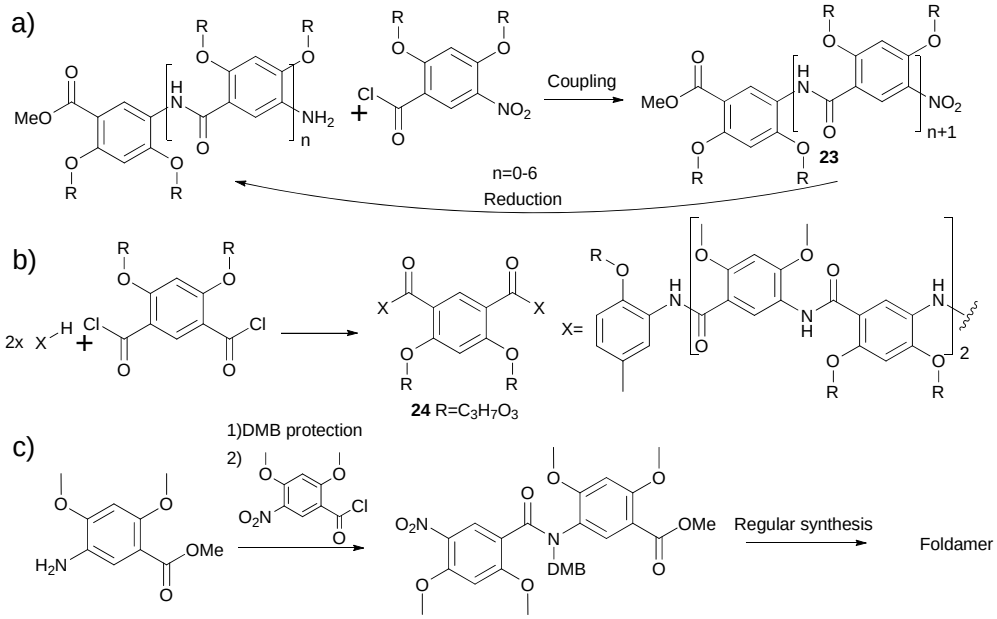

Scheme 9. Example synthesis methods for helical foldamers: a) a unidirectional foldamer **23**,[82] b) a bidirectional foldamer with dicarboxamide center unit **24**,[83–85] and c) DMB-protected dimer[86].

The *meta*-linked foldamers, such as foldamers **23**-**25** and **28**-**30** (Scheme 7a-c and 8) have smaller cavities, up to 9 Å diameter, whereas the foldamers with both *meta*- and *para*-units **26**-**27** (Scheme 7d-e) can have a cavity with a diameter of over 30 Å. The inner surfaces of the cavities have different properties depending on the hydrogen bond motif of the folding. The foldamers where the hydrogen bonds are on the outer groove of the helix have many carbonyl groups at the inner edge of the foldamer, while those with the hydrogen bonding inside the foldamer have many hydrogen bond donor groups (N-H) and alkoxy or fluoride acceptors at the inner face of the foldamers. Crystal structures of the foldamers were not obtained, but the hydrogen bonding motif is similar to compounds **31** and **32** (Figure 10).

Potential applications for these foldamers are ammonium ion[89], and alkali metal cation[91] binding and the effect of the binding on the reactivity of alkaline hydroxides. In addition foldamers with length of up to seven units were used to bind saccharides.[88] The fluoride containing foldamers were observed to bind dialkylammonium ions and form supramolecular networks by binding to fullerenes[90]. Fluoride-containing foldamers were also used as a starting material for dipodal molecules which stack into vesicular structures.[92] Unidirectional foldamers have been used as polymer cross-linkers to modulate the thermal and mechanical properties of polymers.[93]

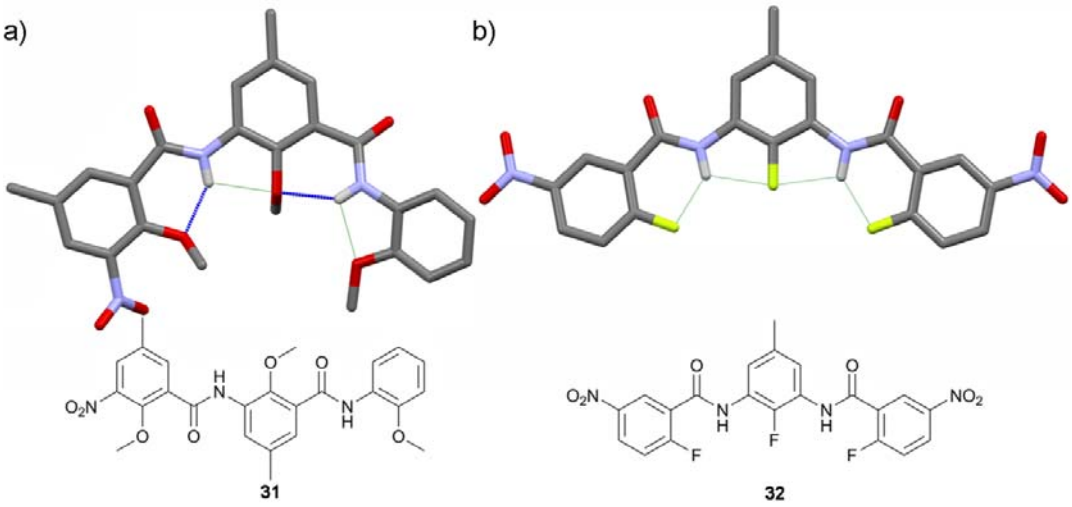

Figure 10. Examples of three-unit helical foldamers and their hydrogen bonding motifs. a) a unidirectional helical foldamer **31**[91] and b) a fluoride foldamer **32**[87] with alternating amide bond directionality. Non-contact hydrogen atoms have been removed for clarity.

1.3.5.2 Linear foldamers

The linear foldamers have been studied by groups of DeGrado (**33**)[94], Hamilton (**34** and **36**)[95–98], Li (**37**)[99,100] and Wilson (**35**)[101,102] (Scheme 10). Linear foldamers have usually unidirectional amide bonds, but examples of alternating amide bond directionality are also acknowledged.[99,100] Linear foldamers are prepared from *para*- or *meta*-substituted aromatic units by a stepwise process, except for the alternating directionality foldamers which are prepared by a modular process. Both processes are very similar to the one described in the previous chapter. Solution based syntheses are commonly used, but solid state methods have also been applied.[94,101,102] In the solid state method the foldamer precursor is attached to a solid resin and coupling and deprotection steps are repeated until the foldamer reaches the desired size after which the foldamer is cleaved from the resin.

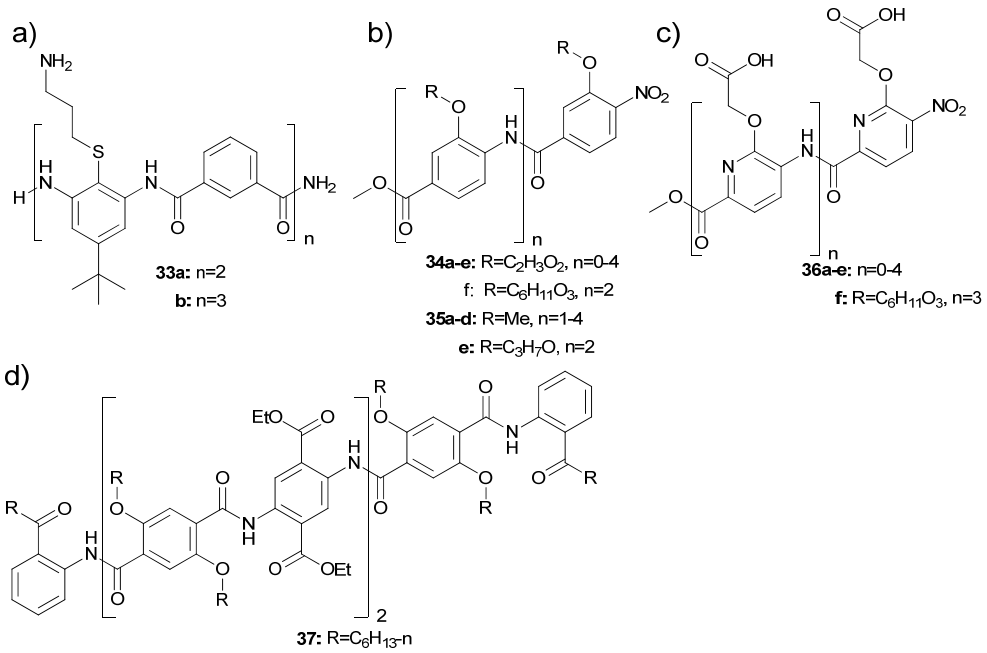

Scheme 10. Examples of structures of linear foldamers. a) *meta*-Substituted thiafoldamer **33** with alternating directionality,[94] b) alkoxy substituted unidirectional foldamers **34-35**,[97,101,102] c) 2,5-pyridine analogue of the alkoxy substituted unidirectional foldamer **36**[97] and d) dialkoxy foldamer **37** with alternating directionality.[99]

The *para*- or *meta*-substitution and hydrogen bonding force the foldamers to adopt a planar, linear and relatively rigid conformation. Three-center hydrogen bonding is the most common motif, but the specifics of the bonding differ. Alkoxy group oxygens are the most common hydrogen bond acceptors, but a thia sulfur was also used as an acceptor.[94] The foldamers always form at least one S(5) motif hydrogen bond between the amide N-H and the alkoxy or thia group (Figure 11). In addition to linear benzene based foldamers Hamilton *et al.*[95–98] have also prepared 2,5-pyridine analogues **36**, which have an extra intramolecular hydrogen bond from the amide bond N-H to the pyridine nitrogen.

Foldamer **33** has *meta*-substituted units similarly to compound **36** instead of the more common *para*-units (Figure 11a) which cause the foldamers to have small zig-zag turns between the units. Foldamers **34-36** have a slight curve induced by the hydrogen bonding on the same side of the foldamer, which is especially seen in the pyridine foldamer **34** (Figure 11c-e). Foldamer **37** is nearly linear due to three-center hydrogen bonding on alternate sides of the foldamer and the *para*-substitution of the units similar to compound **39** (Figure 11d).

Potential applications of linear foldamers include low molecular weight α-helix and double α-helix analogues that could interact with protein surfaces.[94-98,101,102] A five unit linear foldamer backbone functionalized by cholesterol at the ends of the foldamer was found to produce liquid crystals.[100]

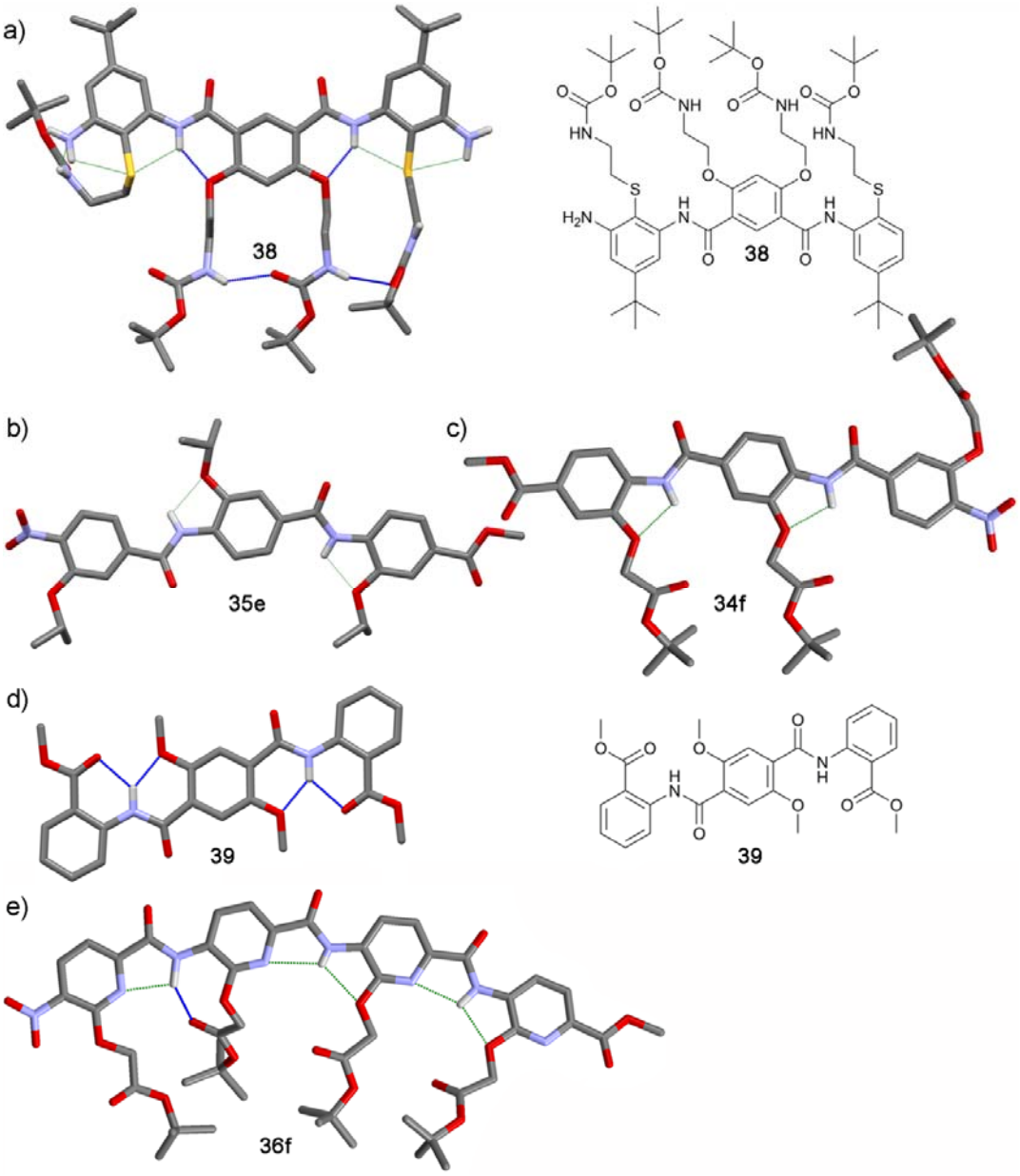

Figure 11. Examples of linear foldamers. a) A three-unit thia-compound **38**,[37] b) a three-unit mono alkoxy foldamer **35e**,[102] c) a three-unit mono alkoxy foldamer **34f**,[103] d) a three-unit dialkoxy foldamer **39**[99] and e) a four-unit 2,5-pyridine foldamer **36f**[97]. Non-contact hydrogen atoms have been removed for clarity.

1.3.5.3 Zig-zag foldamers

The zig-zag foldamers **40** are planar and rigid like the linear foldamers, but adopt a conformation which has sharp turns. Their hydrogen bonding is an adaptation of the linear foldamer three-center hydrogen bonding motif as the hydrogen bonding pattern combines two three-center motifs (Figure 12). The conformation of zig-zag foldamers is planar and relatively rigid and the turns correspond to the *meta*-substitution of the amide bond comprising groups.[104]

The stable conformation of the zig-zag foldamers was used to preorganize complementary amido and ureido recognition units to create foldamer duplexes.[105,106]

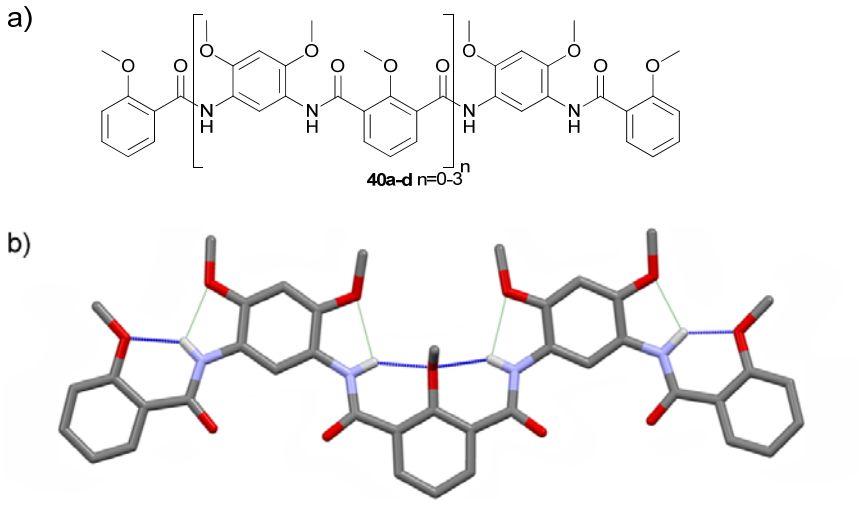

Figure 12. a) An example of a zig-zag foldamer **40** and b) a five unit zig-zag foldamer **39b**.[104] Non-contact hydrogen atoms have been removed for clarity.

The synthesis of the zig-zag foldamers is modular.[104] The synthesis route is very similar to the modular methods discussed earlier. The foldamers are prepared from dimer, trimer or even tetramer units attached to a mono or diacid chloride or diacid units or oligomers to form the foldamers (Scheme 11). The coupling is done either with an amide bond coupling agent or with acid chlorides.

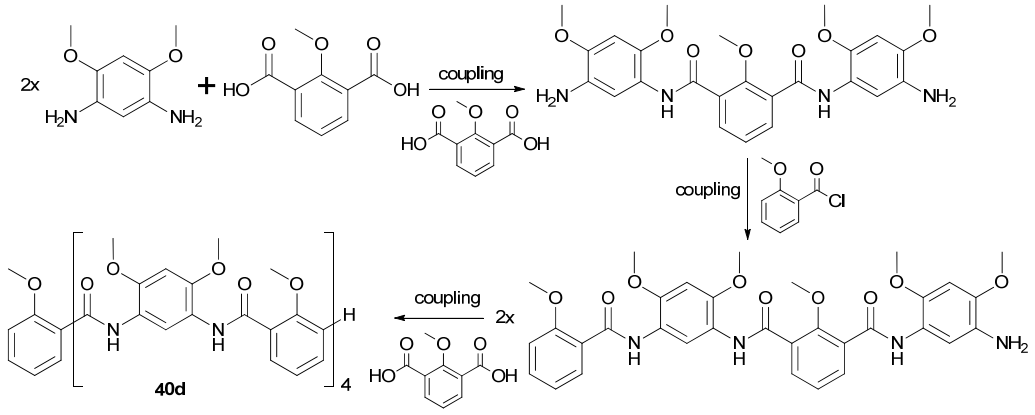

Scheme 11. Example of the modular synthesis method used to prepare a nine-unit zig-zag foldamer **40d**.[104]

2 EXPERIMENTAL

2.1 Aims and background of the work

The purpose of the work was the synthesis and structural study of a new aromatic oligoamide foldamer backbone. The starting points of the study were the benzene (**41**) and pyridine (**43**) foldamers, of which the pyridine foldamer **43** was found to adopt a protohelical conformation, which was later designated as the @-conformation. In order to deepen the understanding of the folding process and the stability of the fold a sulfonamide analogue **42** of the benzene foldamer and a series of asymmetrical analogues of the pyridine foldamer (**44**-**50**) were synthesized and characterized (Scheme 12).

The main tool in the structural studies was single crystal X-ray diffraction which provides detailed structural information in the solid state. The solid state studies were complemented in selected cases by powder X-ray diffraction studies, as well as by IR- spectroscopy and thermogravimetric methods. The crystal structures were used as the starting conformations in the DFT calculations and in the analysis of the solution state conformational data. The solution state information was obtained by NMR spectroscopic methods, including the characterization of the secondary structure of foldamer **46** by NOESY NMR, where the spatial correlations of protons could be measured.

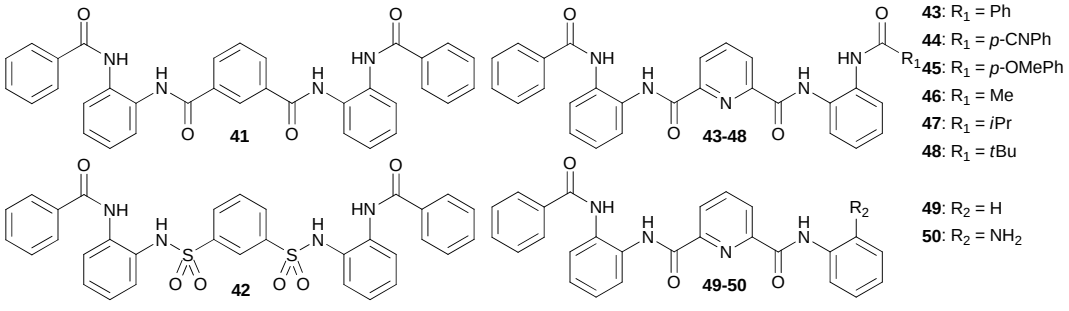

Scheme 12. Molecular structures of the foldamers presented in the thesis.

2.2 Synthesis of aromatic oligoamide foldamers

2.2.1 Symmetric benzene, pyridine and sulfonamide foldamers[I,III]

The symmetric benzene, pyridine and sulfonamide foldamers were synthesized by an acylation reaction between acid chlorides or acid sulfonyl chlorides and primary amines (Scheme 13).

Benzene foldamer **41** was originally synthesized in the master's thesis project of M.Sc. Jussi Ollikka.[107] The yield of the reaction was not satisfactory and a new method was devised and later published in paper I.[I] The pyridine **43** and sulfonamide **42** foldamers were synthesized as analogues of the benzene foldamer **41** using variations of the new method.[I,III]

The original method differed from the published method mainly in the route taken to get to the final product. In the original route *o*-phenylenediamine was coupled to isophthaloyl chloride and the intermediate product **51** was then coupled to benzoyl chloride to afford the benzene foldamer **41**. In the new method the benzoyl chloride was first coupled with *o*-phenylenediamine and only after that with isophthaloyl chloride (Scheme 13). This route proved not only to have far better yields, but the intermediate product **52a** could also be used in the preparation of foldamers **42** and **43** and as an intermediate product of the asymmetric foldamers **44-50**.

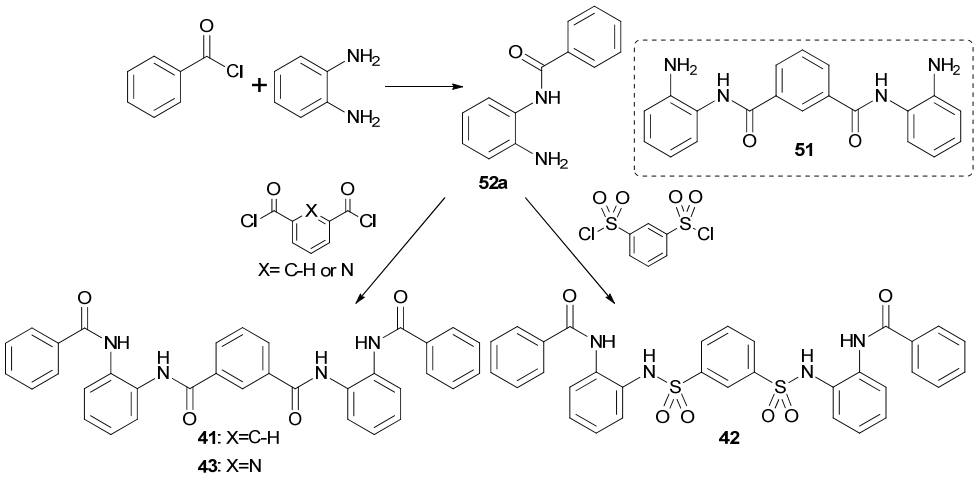

Scheme 13. Synthesis of symmetric foldamers **41-43** and the intermediate **52a**.[I,III]

2.2.2 Asymmetric pyridine foldamers[II,IV]

Similar approaches were used in the synthesis of the asymmetric foldamers **44-50** (Scheme 14a). Acylation reaction with acid chlorides was used in the synthesis of intermediates **52c-f** for foldamers **45-48**.[II] Nitrated intermediates **53c-f** were synthesized first and then reduced to amines **52c-f** using Pd/C and H_2 because in the reaction with the diamine a disubstituted by-product would

form and lower the yield. In the case of the intermediate **52b** for cyanofoldamer **44** the amide bond was formed with an amide bond crosslinker (EDC). The intermediate products were then coupled to an intermediate **53** in the case of foldamers **44-48**[II] and **50**[IV] or intermediate **55** in the case of foldamer **49**[II] using EDC coupling (Scheme 14b).

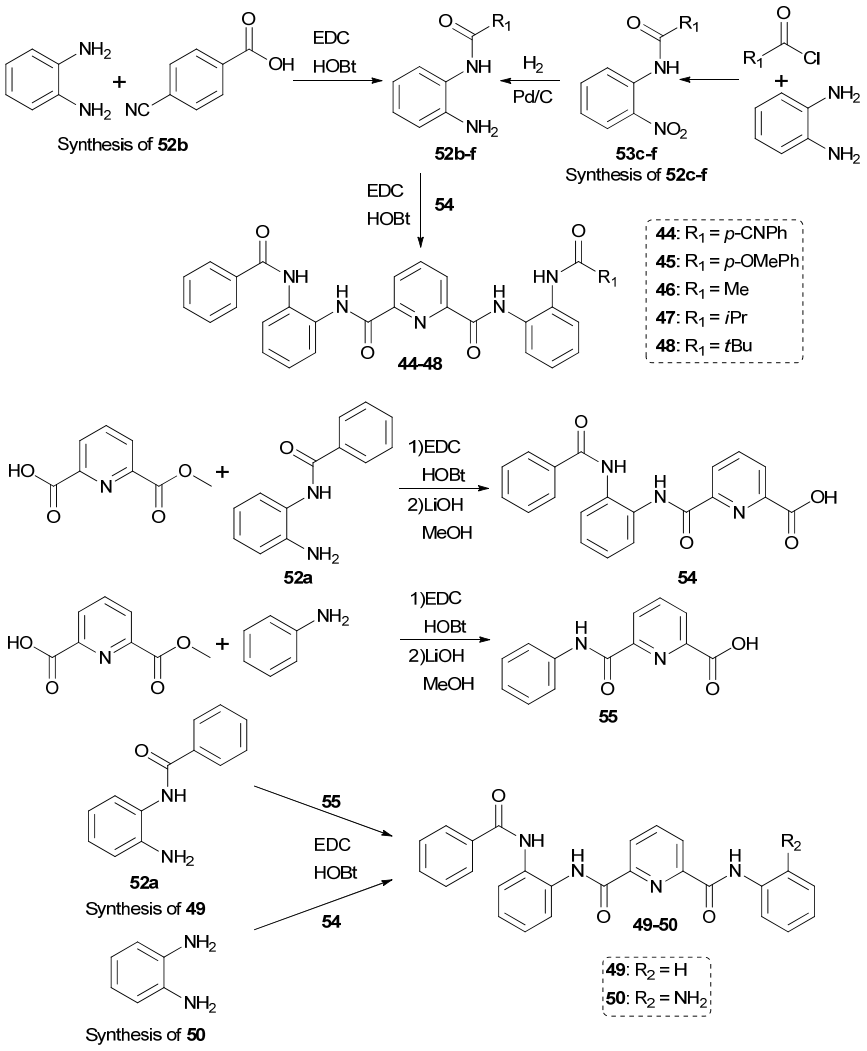

Scheme 14. An example of the synthesis of asymmetric foldamers **44-50** and their intermediates (**52b-f**, **53c-f**, and **54-55)**.[II,IV]

2.3 Structural studies of benzene foldamer 41[I]

Three crystal structures were obtained of the benzene foldamer **41** (Figure 13).[I] Two were DMSO solvates and one was an unsolvated structure which was crystallized from DMF. In all structures the foldamer forms two intramolecular hydrogen bonds (S(7) motif) and the crystal packing motif is a double chain

($C_2^2(24)$) where each foldamer molecule forms four intermolecular hydrogen bonds to two neighboring foldamer molecules. In one of the DMSO solvates (Figure 13c) an additional hydrogen bond forms to a DMSO solvent molecule.

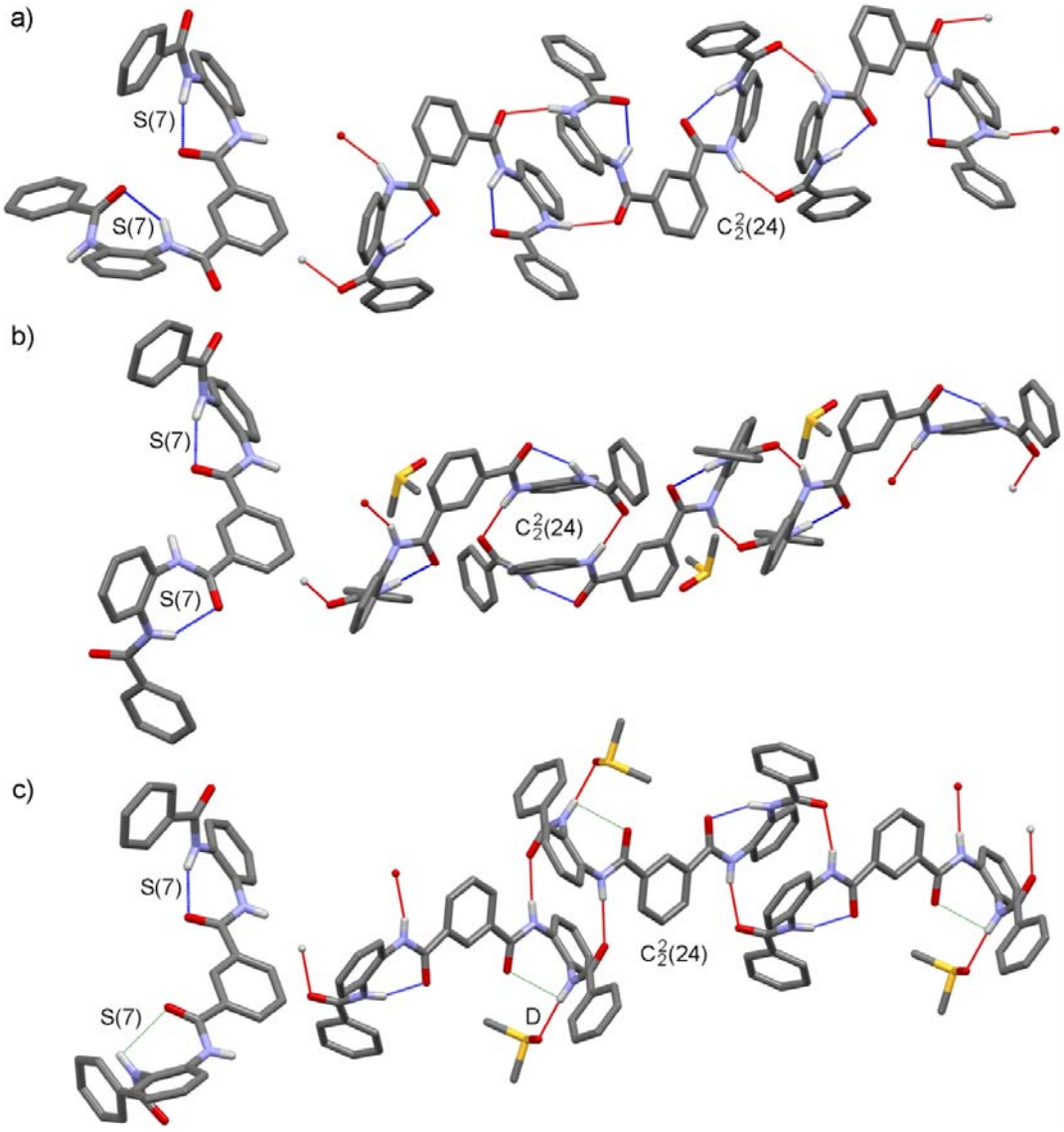

Figure 13. Molecular conformations and crystal packing motifs of the benzene foldamer **41**.[I] a) Unsolvated form I with a slightly folded conformation, b) DMSO solvate I with an open, almost linear conformation and with no hydrogen bonds with the DMSO molecules and c) DMSO solvate II with more compact, but still relatively open conformation. One of the intramolecular hydrogen bonds (green) is weak due to the intermolecular hydrogen bond with DMSO. Non-contact hydrogen atoms were removed for clarity.

Despite the similarity of hydrogen bonding, the conformations of the foldamer are different in all structures.[I] The unsolvated form I (Figure 13a) adopts a conformation that is closest to the @-conformation seen in the pyridine foldamers (Figure 14), but in this case only one of the inner amide bond N-H

hydrogens points inside the fold and only one hydrogen bond is formed per hydrogen bond acceptor. In the DMSO solvates (Figure 13b-c), the benzene foldamer **41** is in a more open conformation. In the DMSO solvate I (Figure 13b) the intramolecular hydrogen bonds are both formed to the inner amide bond C=O groups. Due to this the foldamer molecules adopt a more linear conformation. In the DMSO solvate II an intermolecular hydrogen bond to the DMSO solvent stabilizes an intermediate conformation between the "almost folded" form I and nearly linear conformation of solvate I where one of the intramolecular hydrogen bonds (S(7) motif, green in Figure 13c) becomes much weaker (Figure 13c).

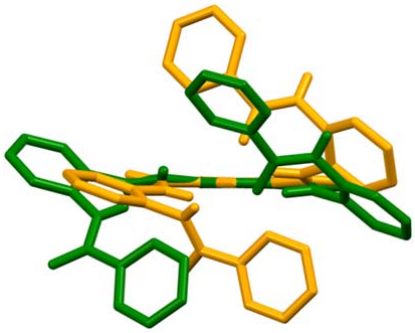

Figure 14. Overlay structure of the almost folded conformation of the benzene foldamer **41** form I (green) and pyridine foldamer **43** form I in the @-conformation (orange).[I] Non-contact hydrogen atoms were removed for clarity.

PXRD patterns indicate that the benzene foldamer **41** has several other solvate crystal forms where the molecular conformation and/or the crystal packing form differ from the obtained XRD structures.[I] Compared to the pyridine foldamer **43**, the lack of a stabilizing pyridine core unit hydrogen bond (S(5) motif), makes the benzene foldamer **41** more flexible and its secondary structure more difficult to predict. Therefore the benzene foldamer **41** is not as suitable as a starting point towards more complex foldamers. Another drawback is the relatively low solubility of the benzene foldamer **41** even to solvents like DMSO, which would only become more difficult if the size of the molecule was increased without the addition of functional groups that would improve the solubility of the foldamer.

2.4 Structural studies of sulfonamide foldamer 42[III]

Sulfonamide foldamer **42** was prepared as an analogue to the benzene foldamer **41**.[III] The sulfonamide bond is an interesting bond often used in the pharmaceutical industry.[108] The properties of the sulfonamide group resemble an amide bond in some respects, but geometry and hydrogen bonding are different due to sp^3 sulfur which replaces the sp^2 carbon in the bond. The difference in the OSN and OCN angles, 106° and 120°, respectively, leads to a

significant difference in the orientation of the bond and also, therefore, in the conformation of the molecule. Although the sulfonamide group has an extra hydrogen bond acceptor compared to the amide group, the tendency to act as a hydrogen bond acceptor is lower. This is due to the presence of the second oxygen in the sulfonamide group, which leads to smaller negative dipole moments in the oxygen atoms.

The folding preferences of the sulfonamide foldamer **42** were studied using XRD and DFT calculations.[III] As a result two conformations were identified experimentally and a third additional conformation was identified from the DFT calculations. One of the solid state conformations obtained either from DCE or THF is unfolded and forms only two weak intramolecular hydrogen bonds (Figure 15a, S(5) motif). The other folded conformation is obtained either from ethyl acetate or acetonitrile and, in addition to the two weak hydrogen bonds (S(5) motif), it forms an intramolecular hydrogen bond (Figure 15b, S(13) motif). The foldamer in the unfolded conformation packs into double chains ($C_2^2(20)$ motif) with the molecules in a head-to-tail arrangement. The foldamers in a folded conformation pack are in sheet-like assemblies where chains (C(7) motif) are connected to one another by two intermolecular hydrogen bonds that form a ring structure ($R_2^2(16)$ motif, Figure 15b).

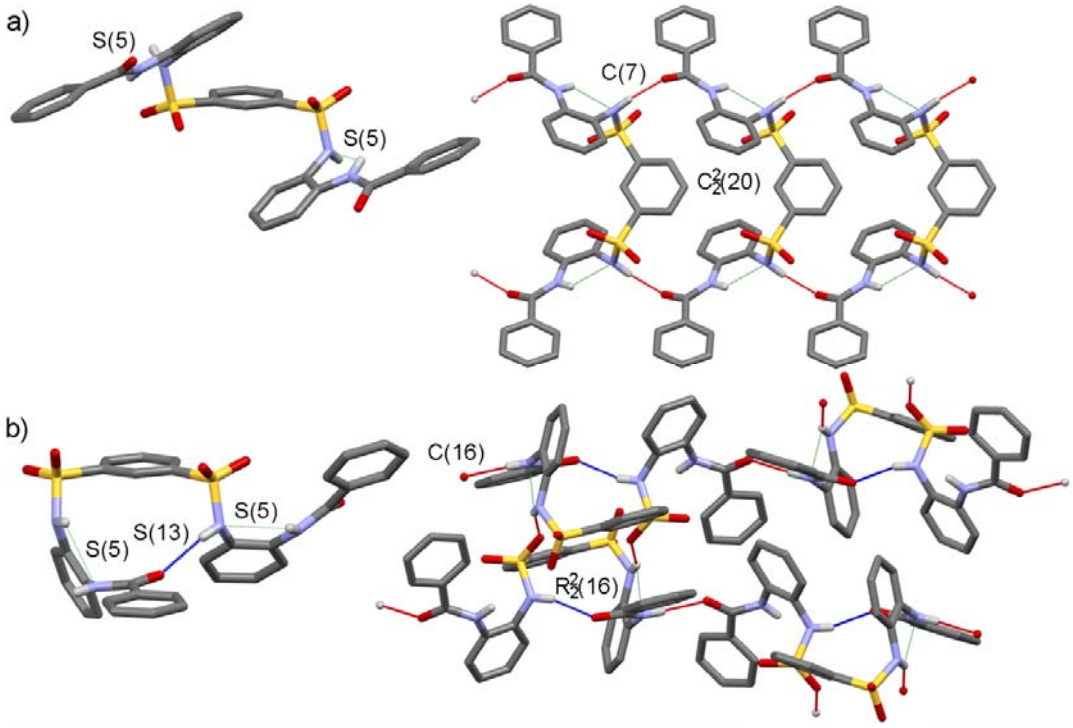

Figure 15. Conformations and crystal packing motifs of the sulfonamide foldamer **42**. a) An unfolded conformation and b) a folded conformation.[III] Non-contact hydrogen atoms were removed for clarity.

A clear reason for two different solid state conformations could not be identified. The environmental conditions (temperature, moisture, crystallization

vessel) were as identical as possible and the physical and chemical properties of the solvents do not show a clear trend. This, together with DFT calculations, suggests that the conformations are close in energy. The folded conformation retains its fold in the DFT calculations; it is therefore likely that this form is also found in solution (Figure 16c).[III] Based on the DFT calculations the unfolded conformation, on the other hand, does not seem to be as stable. In the calculations the unfolded conformation tends to adopt a more folded conformation with two intramolecular hydrogen bonds (Figure 16a). This more folded conformation seems to be more stable in the gas state and unfolds into an efficient and stable crystal packing structure stabilized by intermolecular hydrogen bonds in the solid state. Evidence for this conformational change could be seen when a system of two molecules were calculated. It was found that one of the molecules changed to a more folded conformation, but the other one remained in an unfolded conformation (Figure 16b). This indicates that, once formed, the dimer is able to direct the formation of an intermolecular hydrogen bond network.

The third conformer found in the DFT calculations has four intramolecular hydrogen bonds, which makes it lower in energy than the experimentally found conformers (Figure 16d).[III] However, large energy barriers of rotation of the bulky aromatic side chains likely prevent the formation of the conformation experimentally. Also the role of solvents as competing hydrogen bond formers can hinder the adoption of the conformer.

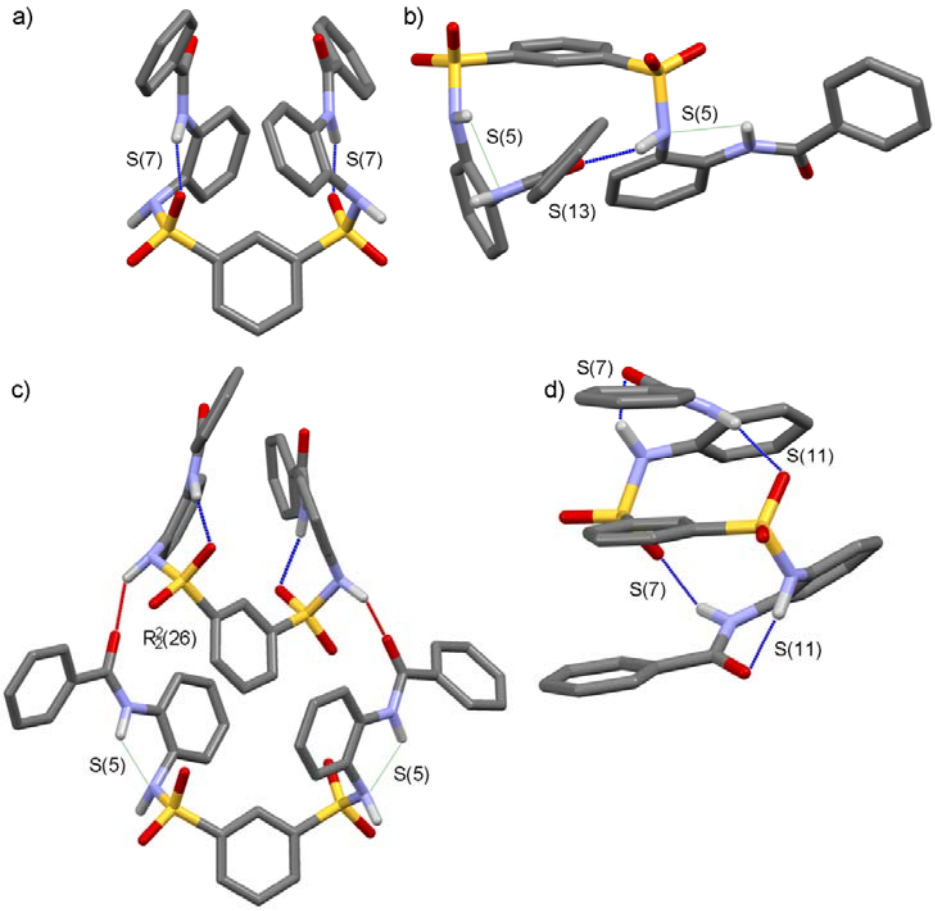

Figure 16. Calculated conformers of the sulfonamide foldamer **42**.[III] a) A folded conformation adopted from the experimentally found unfolded conformation, b) a folded conformation that is nearly identical with the experimentally found folded conformer, c) an optimized dimeric pair, where one of the molecules stays roughly at the starting conformation and the other adopts a more folded conformation and d) a strongly folded conformation found only in the DFT calculations. Non-contact hydrogen atoms were removed for clarity.

A NOESY spectra of compound **42** was measured in acetone-d_6, but no evidence supporting any particular conformation was found.[III] VT-NMR measurements did not show any clear evidence of interconversion from one conformation to another either, although broadening of some peaks was detected. These results suggest that the conformation in solution may yet be different from those found in the solid state or DFT calculations and that the environmental factors contribute to the choice of conformation in an unpredictable way. Nevertheless, neither of the solid state conformers of the sulfonamide foldamer **42** is in a desired folded, protohelical conformation, which together with the unpredictability of the conformers make the sulfonamide bond a challenging component when planning and preparing foldamers.

2.5 The conformational properties of pyridine foldamers 43-50[I,II,IV]

The symmetric pyridine foldamer **43** was originally prepared as an analogue of the benzene foldamer **41**.[I] In the molecule the central *m*-substituted phenyl ring was replaced by a pyridine. This change had been used in many previous studies with good results.[50–52] Indeed, the foldamer was found to fold in a stable, tightly folded, protohelical conformation with predictable behavior. In addition to the pyridine foldamer **43** seven asymmetric analogues (**44-50**) were prepared in order to study the folding ability of the pyridine foldamers (**43-50**) in greater detail.[II,IV]

In general the predictability and stability of the pyridine foldamer conformations originate from two structural properties (Scheme 15). One is the *o*-disubstituted side unit which forces a sharp and rigid turn in the foldamer backbone and increases its ability to form π-stacking interactions. The other important structural feature is the pyridine core where two weak intramolecular hydrogen bonds are formed to the N-H groups of the amide bonds closest to the pyridine nitrogen atom (S(5) motif). This enforces a roughly planar geometry to the core in almost all cases and creates a position where two hydrogen bond donors are very close to each other.

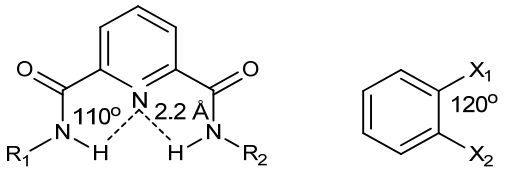

Scheme 15. Pyridine foldamer units, pyridine core (left) and *o*-disubstituted side unit (right)

The most interesting aspect of the pyridine foldamer **43**, however, is the three simultaneous intramolecular hydrogen bonds to the same hydrogen bond acceptor instead of a fold with two S(7) motif intramolecular hydrogen bonds as seen with the benzene foldamer **41**. These hydrogen bonds not only gave the pyridine foldamer **43** a tightly folded protohelical conformation—an interesting property for the preparation of new foldamers—but the conformation resembles an active site found in some enzymes, called the oxyanion hole (Scheme 16).[109,110] The oxyanion hole is a fold in an enzyme where several hydrogen bond donor groups are forced into close proximity by the secondary structure of an enzyme. In this position several intermolecular hydrogen bonds or ion-dipole bonds can form to a single ion or a hydrogen bond acceptor, which enables the catalysis of reactions that involve tetrahedral intermediates, such as hydrolytic cleavage of esters, thioesters and amides, and reactions that involve enolate intermediates. The oxyanion hole structure lowers the reaction energy and stabilizes high-energy reaction intermediates because of hydrogen and ion-dipole bonds.

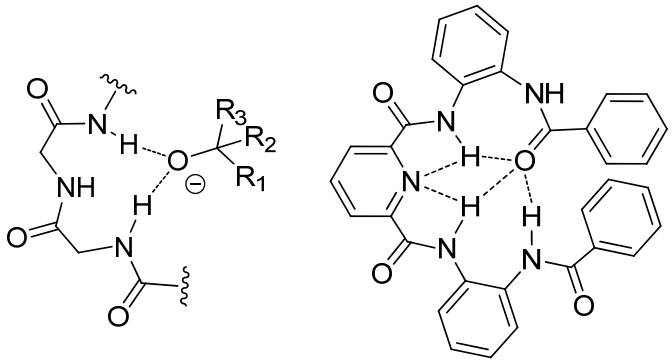

Scheme 16. A schematic structure of an oxyanion hole (left) and foldamer **43** in the @-conformation resembling an oxyanion hole motif (right).

2.5.1 Pyridine foldamer analogues[I,II,IV]

Due to the resemblance between the pyridine foldamer **43** and the oxyanion hole the stability of the @-conformation was tested by preparing a series of asymmetric foldamers. In foldamers **44** and **45** (Scheme 12) a terminal phenyl group of the foldamer is para-substituted with either a cyano or a methoxy group, respectively. The cyano group was attached to withdraw electron density from the carbonyl oxygen closest to it and thus make it a weaker hydrogen bond acceptor. The methoxy group, on the other hand, was attached to increase the electron density. With foldamers **46**-**48** one of the terminal phenyl rings was replaced by an aliphatic group (Scheme 12). This change served two purposes: The aliphatic group increases the electron density of the nearest C=O group and the variance of the size of the group affects the steric hindrance on the secondary structure of the foldamer. The shorter foldamers **49** and **50** were synthesized to see if only three amide bonds are sufficient to cause an @-conformation and what the effect of a terminal amine group on folding is.

The eight different variants of pyridine foldamer (Scheme 12) produced 33 different crystal structures (Table 1), as both solvates and polymorphic forms. Despite the eight slightly different compounds and a great variety of different crystal structures only two major conformation types were discovered; one in a tight protohelical @-conformation with several intramolecular hydrogen bonds to a single hydrogen bond acceptor and a more open, S-shaped conformation. Foldamers **44**, **47** and **49** were found to adopt both @- and S-conformations whereas foldamers **43** and **50** crystallized exclusively in the @-conformation and foldamers **46** and **48** only in the S-conformation. No crystal structures were obtained for foldamer **45**.

Table 1. Pyridine foldamer **43**-**44** and **46**-**50** crystal structures, their conformations, crystal packing and crystallization solvents.[I,II,IV]

Structure	Packing motif	Crystallization solvent	Structure	Packing motif	Crystallization solvent
43@-Form I	$R_2^2(14)$	EtOAc	**46S$_1$**-Form I	$R_2^2(32)$	Acetone
43@-Form II	$R_4^4(46), 2R_3^3(39)$	DMSO-d_6 (**43**:TBA-F•3H_2O, 5:1)	**46S$_1$**-Form II	$R_2^2(32)$	EtOAc
43@-acetone	C(7)	Acetone-d_6 (**43**:TBA-Cl 3:1)	**46S$_1$**-Diox	$R_2^2(32)$	1,4-diox
43@-DMA	C(7)	DMA	**46S$_1$**-DMSO	D	DMSO
43@-DMF	C(7)	DMF	**47@'$_2$**-Form I	$C_2^2(23)$	EtOAc
43@'-DMSO	C(11)	DMSO	**47S$_1$**-Form II	$R_2^2(14)$	Toluene
43@-DMSO-H_2O	C(7), $D_2^2(5)$	DMSO-d_6 (**43**:TBA-F•3H_2O, 1:4)	**48S$_2$**-Form I	C(11)	Acetone
43@-EtOAc	C(11)	EtOAc	**48S$_2$**-Diox	C(11)	1,4-diox
43@-EtOH	C(16)	EtOH	**49@**-Form I	C(11)	Acetone
43@-MeCN	C(7)	MeCN	**49@**-Form II	C(7)	DMA
43@-MeOH	C(16)	MeOH	**49S**-DCM-1	$2R_2^1(10)$	DCM
43@-toluene	C(11)	Toluene	**49S**-DCM-2	$2R_2^1(10)$	DCM
44@$_2$-Form I	C(7)	MeCN	**49@**-DMA	D	DMA/1,4-diox
44S$_1$-$CHCl_3$	$R_2^2(14)$	$CHCl_3$	**49@**-S-DMF	$R_2^2(14), 2R_2^1(10)$	DMF
44S$_1$-DMA	$R_2^2(14)$	DMA	**49S**-MeCN	$2R_2^1(10)$	MeCN
44S$_1$-EtOAc	$R_2^2(14)$	EtOAc	**50@**-Form I	$C_2^1(16)$	MeCN
44S$_1$-THF	$R_2^2(14)$	THF			

Both conformers have variants depending on the amount of hydrogen bonds and which amide moieties form intramolecular bonds (Scheme 17). In the @-conformation the molecule is tightly folded around the pyridine core and three intramolecular hydrogen bonds (S(7), S(13) and S(16) motif) are formed to a single hydrogen bond acceptor (Scheme 17). If only two intramolecular hydrogen bonds (S(7) and S(13) motif) form the conformation is denoted as @'. In the case of asymmetric foldamers **44**-**48** the conformations are further divided into two categories depending on which end of the molecule acts as a hydrogen bond acceptor for the pyridine core amide bonds. Category 2 is used when C=O of the unsubstituted phenyl end of the molecule acts as a hydrogen bond acceptor. The sigmoidal S-conformation is stabilized by two intramolecular hydrogen bonds from the pyridine core N-H groups to a hydrogen bond acceptor (S(7) and S(13) motif) and a hydrogen bond from an outer amide N-H to a pyridine core C=O group (S(7) motif). Two weak hydrogen bonds to the pyridine ring nitrogen atom further stabilize the conformation. With foldamer **49** an S-conformation, however, forms through intermolecular hydrogen bonding and the intramolecular hydrogen bonds to the amide bonds around the pyridine and (S(7) and S(13) motif) are replaced by intermolecular bonds to another foldamer **49** molecule ($R_2^1(10)$ motif). DFT-calculations on foldamers **43**-**46** and **48**-**49** also suggest a helical conformation with a different intramolecular hydrogen bonding network (S(7) and S(16) motif) where the pyridine-amide core unit is non-planar and only one intramolecular hydrogen bond is formed per hydrogen bond acceptor (Scheme 17).

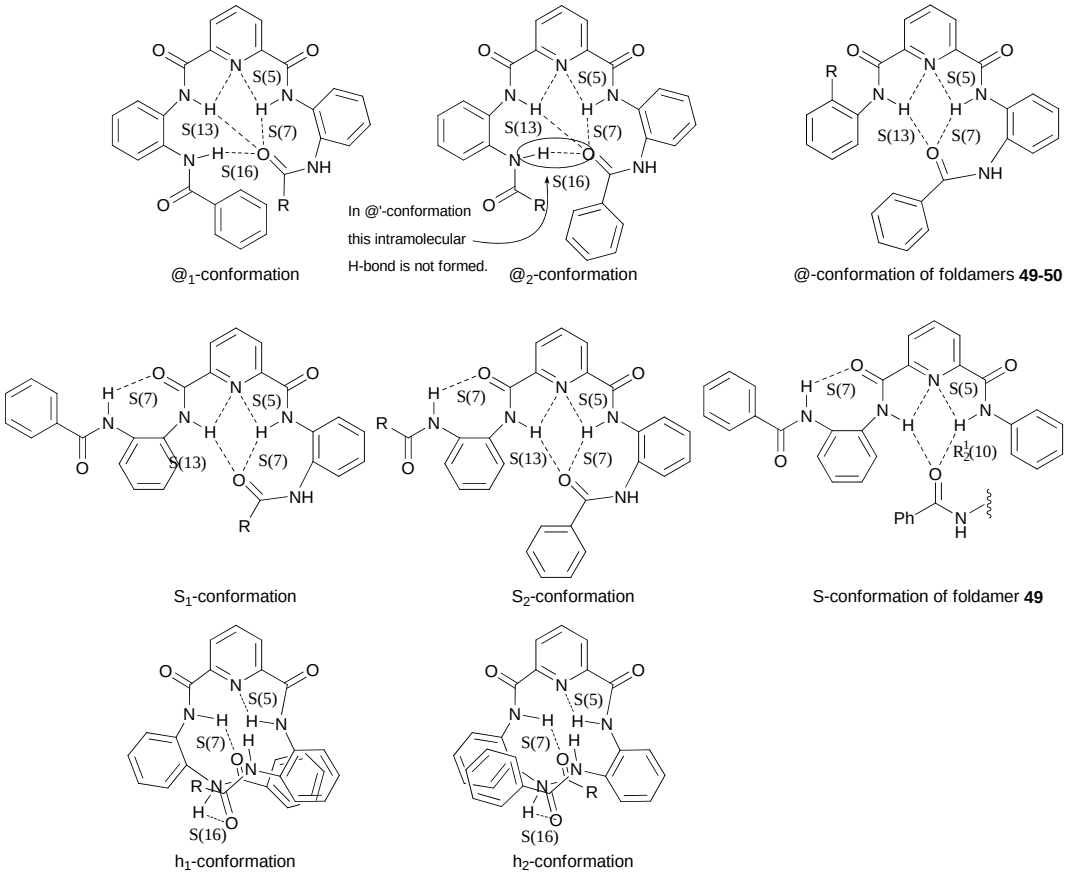

Scheme 17. Schematic presentation and denotations of the @-, S- and h-conformations.[II] The subscript describes which of the outer carbonyl groups acts as a hydrogen bond acceptor. In the @-conformation the apostrophe is used if only two intramolecular hydrogen bonds to the same hydrogen bond acceptor are formed.

2.5.2 Conformers and crystal packing of individual compounds

2.5.2.1 Pyridine foldamer 43[I,II,IV]

The pyridine foldamer **43** was found to have an impressive ability to produce good quality crystals. Altogether 12 crystal structures were obtained, two of which are polymorphs, and ten are solvates (Table 1).[I,IV] In all crystal structures foldamer **43** was found to adopt the @-conformation or a conformation very close to the @-conformation (Figure 17). In addition to the intramolecular hydrogen bonds the conformation is in all cases stabilized by t-shaped π-stacking interactions between the outer and inner phenyl rings. The slightly different conformations were observed in the structures of DMSO solvate and the polymorphic form II. A DMSO solvate of foldamer **43** is found in the @'-conformation where the S(16) motif intramolecular hydrogen bond is not formed. Instead an intermolecular hydrogen bond is formed to the DMSO solvent molecule (Figure 17b). This suggests that the S(16) motif bond is the weakest of the intramolecular hydrogen bonds. In the polymorphic form II one

molecule out of three in the asymmetric unit adopts a more open conformation which, nevertheless, closely resembles the @-conformation (Figure 17c). The more open conformer has only one moderately strong intramolecular hydrogen bond, S(7), and three weaker bonds, an S(7) bond and two S(5) bonds to the pyridine nitrogen.

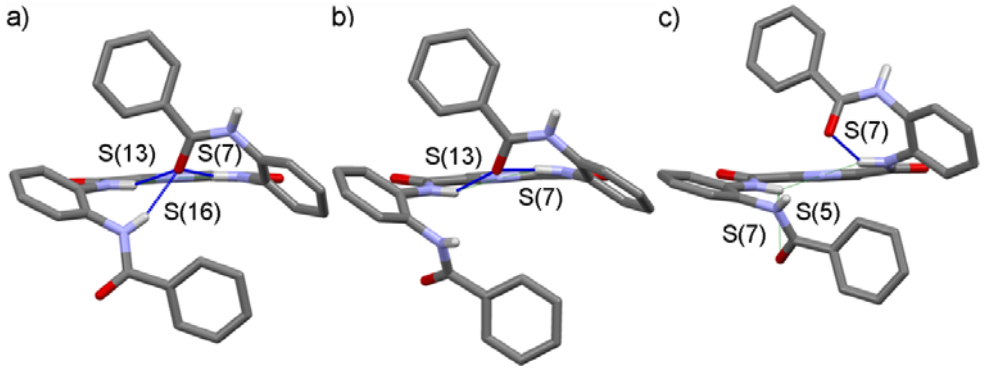

Figure 17. Pyridine foldamer **43** a) in the @-conformation, b) in the @′-conformation and c) in a more open conformation resembling the @-conformation.[I,IV]

NMR and DFT studies were done to shed light on the solution state conformations of the pyridine foldamer **43**.[I,II] The NOESY spectra measured for the pyridine foldamer **43** in THF-d_8 and acetone-d_6 suggests

that the compound is folded in solution, though the conformation can be either @-, S- or helical (Figure 18). The DFT results suggest that the S-conformation would be the most energetically favorable followed by a helical conformation, which was unseen experimentally, and the least favorable would be the @- and @′-conformations with equal energies (Figure 18). Gibbs free energies of the conformations relative to the most stable conformation, however, were 0.0 (S), 0.4 (helix) and 1.3 kcal·mol^{-1} (@ and @′), i.e. the conformers are very close in energy, which suggests that in solution many conformers are likely present and their ratio varies based on the solution conditions. DFT calculations indicate stabilization by intramolecular parallel displaced π-stacking interactions, whereas they are t-shaped in the crystal structures indicating the difference caused by crystal packing effects.

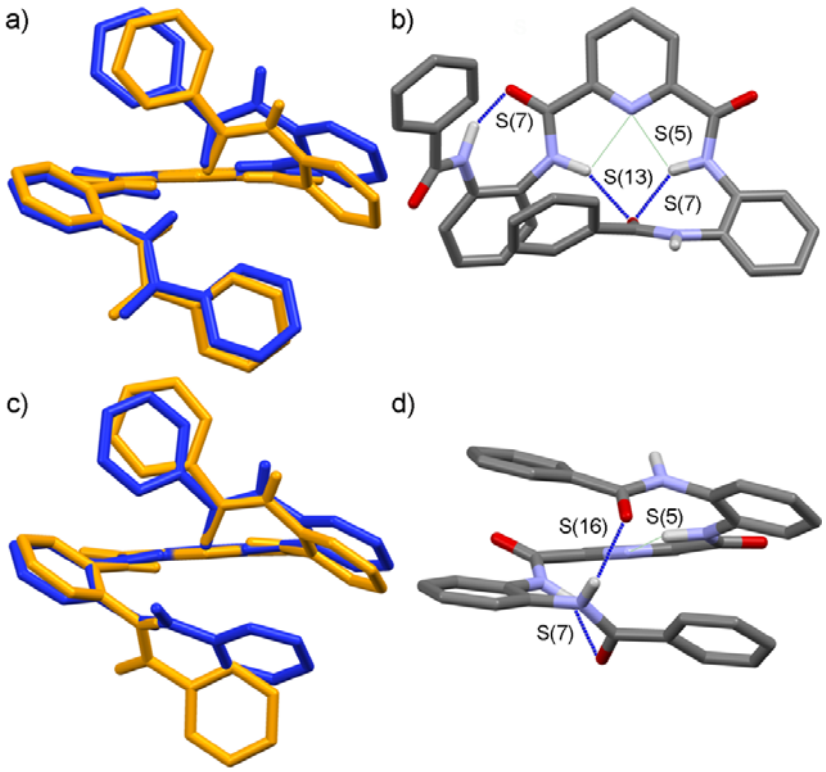

Figure 18. a) An overlay of the calculated @-conformation (blue) and the @-conformation of foldamer **43** from an acetone solvate (orange), b) the calculated S-conformation of foldamer **43**, c) an overlay of the calculated @′-conformation (blue) and the @′-conformation of foldamer **43** from a DMSO solvate (orange) and d) the calculated h-conformation of foldamer **43**.[I,II,IV] Non-contact hydrogen atoms were removed for clarity.

The pyridine foldamer **43** crystallizes in five different crystal packing motifs with some variation due to solvent molecules (Figure 19).[I,IV] Chain-like packing is the most common as ten out of the twelve crystal structures exhibit it. The two polymorphic forms pack in ring assemblies. The pyridine foldamer **43** in the @-conformation has three unused hydrogen bond acceptors and one free hydrogen bond donor. This allows for three chain motifs (C(7), C(11) and C(16), Figure 19b-d), with C(7) motif chains being the most popular. All chains are also solvates suggesting that the chain motifs are not very efficient and solvent accessible spaces are left in the crystal lattice. The ring packing of form I is defined by a relatively simple $R_2^2(14)$ motif (Figure 19a), while form II adopts a more complex structure composed of six molecules that form three rings ($R_4^4(46)$ and two $R_3^3(39)$ motifs). In this structure one of the pyridine foldamers **43** deviates from the @-conformation to allow the packing structure (Figure 19e).

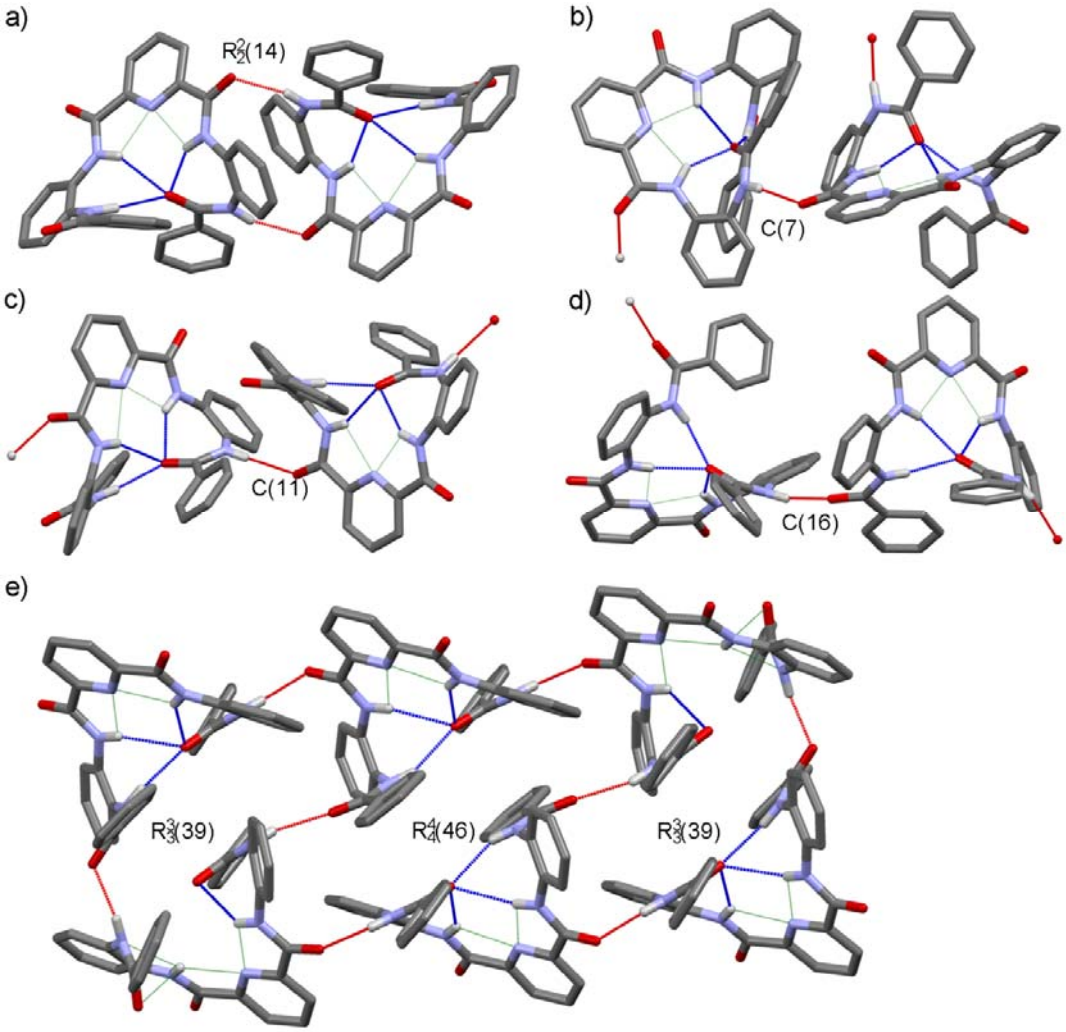

Figure 19. Pyridine foldamer **43** a) form I ring structure, b) a C(7) motif chain from a DMA solvate, c) a C(11) motif chain from an EtOAc solvate, d) a C(16) motif chain from an EtOH solvate and e) form II ring structure.[I,IV] Non-contact hydrogen atoms were removed for clarity.

2.5.2.2 Cyano foldamer 44 and methoxy foldamer 45[II,IV]

The cyano foldamer **44** and methoxy foldamer **45** are near analogues of the pyridine foldamer **43** with the only difference being a cyano group (**44**) or a methoxy group (**45**) at para position at the other end of the molecule. The cyano group withdraws electron density from the closest carbonyl oxygen thus making it a weaker hydrogen bond acceptor, which should lead to the preference of the @$_2$- and S$_2$-conformations. In the case of the methoxy group the effect is the opposite, and the @$_1$- and S$_1$-conformations would be more favorable. In the solid state, however, @$_2$- and S$_1$-conformers were obtained for the cyano foldamer **44**, whereas no crystal structures were obtained for the methoxy foldamer **45**.

Five cyano foldamer **44** crystal structures were determined, one of which is unsolvated (Figure 20a) with an @$_2$-conformation, and four nearly isomorphous solvates in an S$_1$-conformation (Figure 20, Table 1).[II,IV] The @$_2$-conformation (Form I) packs in a C(7) motif chain common to the @-conformation structures. The solvates in the S$_1$-conformation pack in parallel displaced pairs ($R_2^2(14)$ motif, Figure 20). The solvent molecules are always located near the cup shaped areas of the stacked pairs and, depending on the size and shape of the solvent, a small void can remain in the cup.

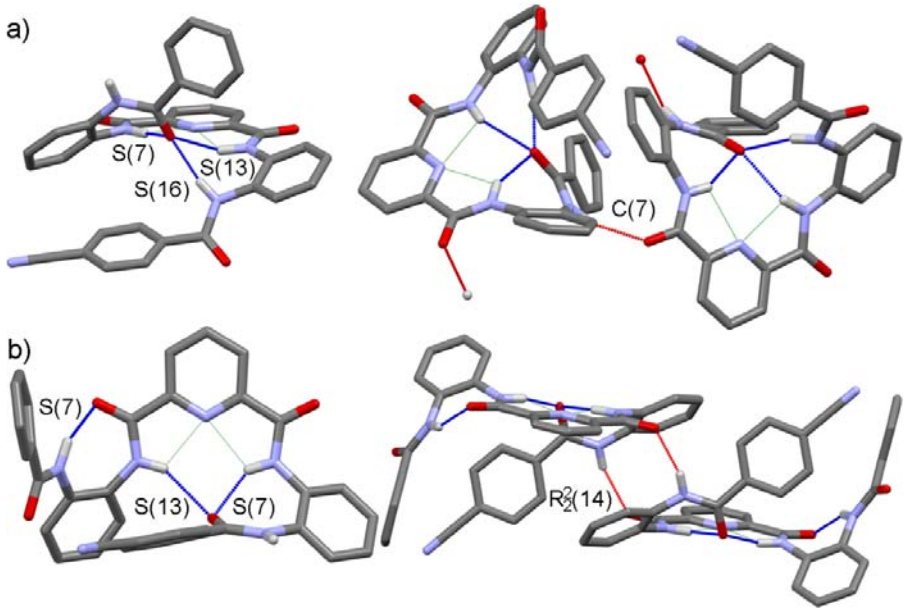

Figure 20. Cyano foldamer **44** conformations and packing. a) @$_2$-conformation and C(7) motif packing of unsolvated form I and b) S$_1$-conformation and $R_2^2(14)$ motif packing of an EtOAc solvate. Non-contact hydrogen atoms were removed for clarity.

In DTF calculations cyano foldamer **44** prefers the S$_2$-conformation though @'$_2$- and h$_1$-conformations were very close in energy (0.7 and 0.2 kcal·mol^{-1} were higher in energy, respectively, Figure 21a and 21d-e).[II] The @$_2$- and S$_1$-conformations (Figure 21b) found experimentally were also relatively close in energy (3.4 and 2.5 kcal·mol^{-1} were higher in energy, respectively). The calculated S$_2$-conformer fulfills the original assumption of the effect of the electron-withdrawing cyano group. In its solid state, however, the efficiency of the crystal packing as well as other steric reasons may be the reason for the opposing S$_1$-conformer.

In DFT calculations the @$_1$-, S$_1$ and h$_2$-conformers of the methoxy foldamer **38** were lower in energy than the opposite conformations.[II] The S$_1$-conformer was the most favorable in energy, but the h$_2$-conformer was only 0.9 and the @$_2$-conformer 2.5 kcal·mol^{-1} higher in energy (Figure 21c and 21f).

Based on the DFT calculations the design strategy for the foldamers seems sound. In both cases the foldamers favor the S-conformation over the @-conformation in the DFT calculations. This is likely due to the para-position

groups. In the solid state other factors, such as crystal packing, have an effect on the conformational preferences of the foldamers, at least in the case of the cyano foldamer **44**.

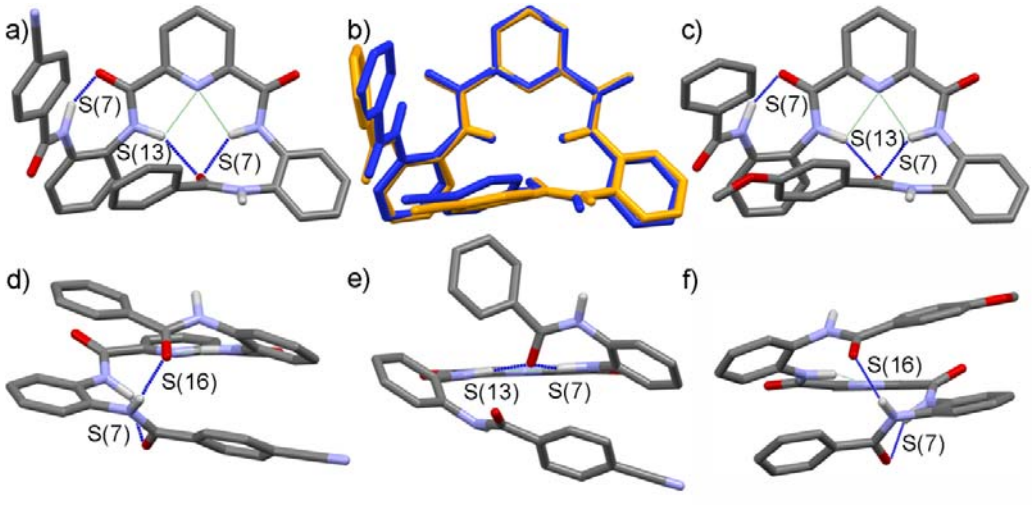

Figure 21. DTF optimized conformations of foldamers **44** and **45**.[II] a) S_2-conformation of foldamer **44** b) an overlay of the DFT optimized S_1-conformation (blue) and the S_1-conformation of foldamer **44** from an EtOAc solvate (orange), c) S_1-conformation of foldamer **45**, d) the h_1-conformation of foldamer **44**, e) the @'-conformation of foldamer **44** and f) the h_2-conformation of foldamer **45**. Non-contact hydrogen atoms were removed for clarity.

2.5.2.3 Aliphatic foldamers 46-48[II,IV]

Three foldamers with increasing sizes of aliphatic groups at one end of the molecule were prepared (**46-48**). The aliphatic group makes the C=O group closest to it a more potent hydrogen bond acceptor, and presumably directs the foldamers towards type 1 conformations. The different sizes of the groups offer information on the effect of the substituent bulkiness on the conformation adopted. The groups are also non-planar and unable to form π-stacking interactions, which is a marked difference compared to foldamers with mainly aromatic groups.

The crystallizations of the acetyl foldamer **46** produced two polymorphic forms and two solvates (Table 1). In all structures the conformation was S_1 (Figure 22a). Although type 1 folding was expected, the prevalence of the S-conformation was rather surprising. Acetyl foldamer **46** packs in three crystal structures as stacked pairs ($R_2^2(32)$ motif), which seems to be a fairly efficient packing motif (Figure 22b). The only exception to the packing is the DMSO solvate where the acetyl foldamer **46** forms an intermolecular hydrogen bond with the DMSO molecule instead of stacked pairs (Figure 22c).

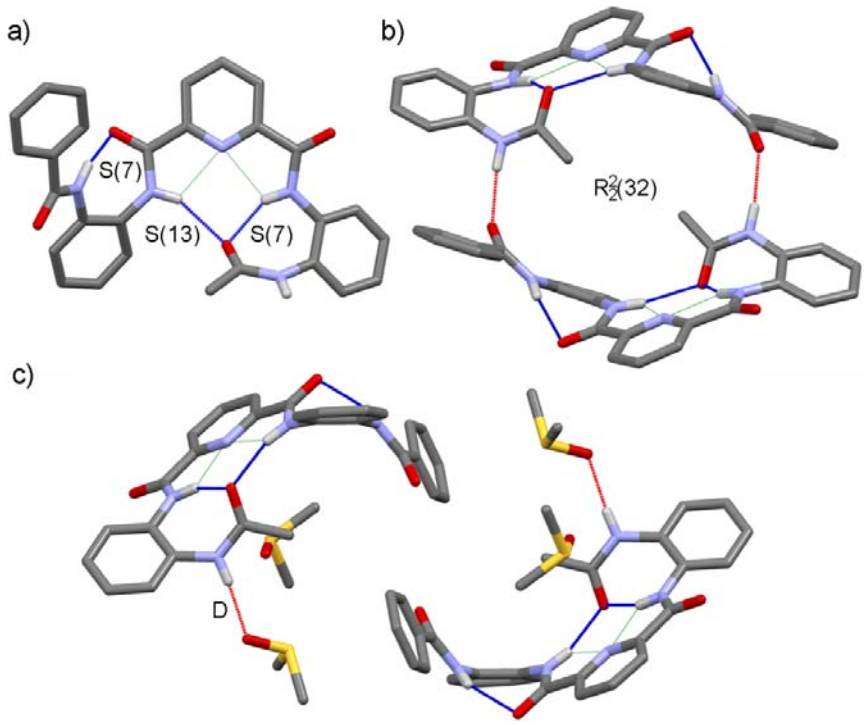

Figure 22. Acetyl foldamer **46**. a) S_1-conformation, b) $R_2^2(32)$ motif packing of unsolvated form I and c) D motif packing of the DMSO solvate. Non-contact hydrogen atoms were removed for clarity.

The isopropyl foldamer **47** crystallized only as two polymorphic forms with different conformations. In form I the isopropyl foldamer **47** adopts a $@'_2$-conformation and in form II an S_1-conformation (Figure 23, Table 1). The reason behind the $@'_2$-conformation over the presumably more favorable $@_1'$-conformation or a $@_1$-conformation are not clear. Form I packs in double chains where the amide bond near the isopropyl group is involved in two intermolecular hydrogen bonds ($C_2^2(23)$ motif). This is likely an efficient packing motif and could, at least in part, explain the $@'_2$-conformation. The bulky isopropyl group may prevent the formation of the S(16) motif intramolecular hydrogen bond, whereas the electron-donating properties of the aliphatic group still increase hydrogen bond acceptor properties and facilitate the formation of stabilizing intermolecular hydrogen bonds. T-shaped π-stacking interactions (Figure 23a) could not form in the type 1 conformation either. In form II the isopropyl foldamer **47** is in the expected S_1-conformation and packs in parallel displaced pairs very similar to the cyano foldamer **44** solvates ($R_2^2(14)$ motif). The structure even has a void (26 Å^3) in the area where the cyano foldamer **44** would have had the solvent molecule.

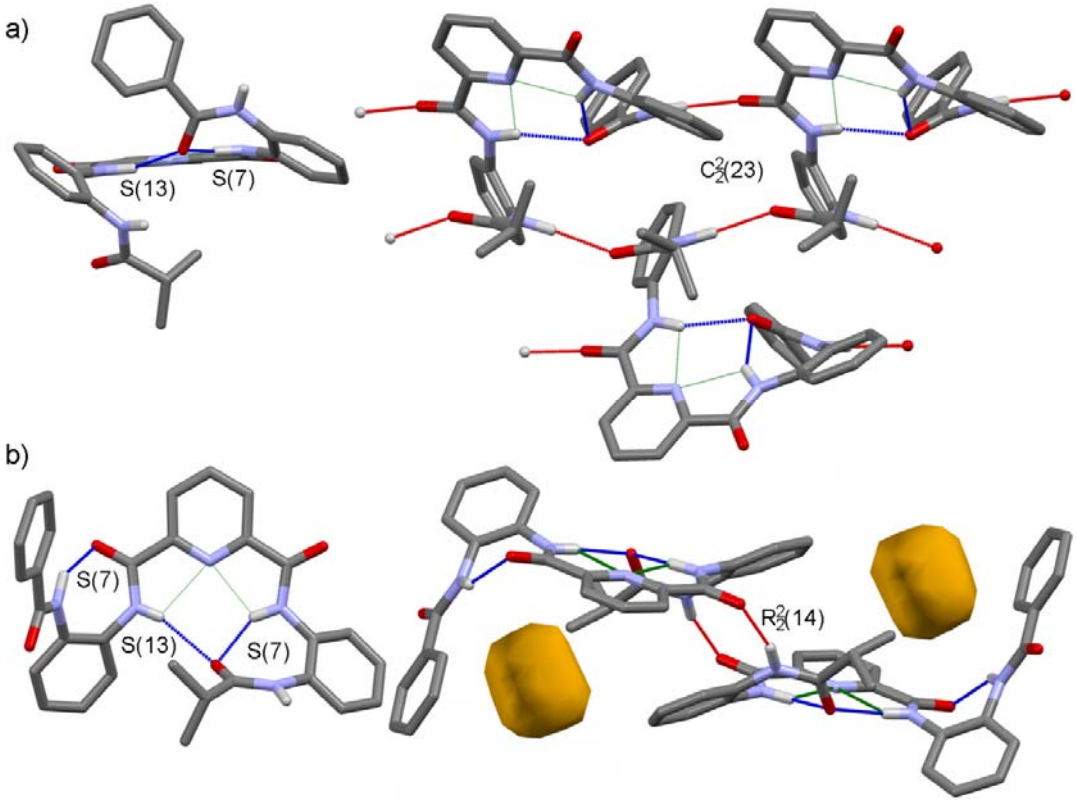

Figure 23. The conformations and crystal packing of isopropyl foldamer **47**. a) @'$_2$-conformation and $C_2^2(23)$ motif packing of form I and b) S_1-conformation and $R_2^2(14)$ motif packing form II and 26 Å^3 structural voids (orange). Non-contact hydrogen atoms were removed for clarity.

The crystallizations of the *tert*-butyl foldamer **48** produced two crystal structures, an unsolvated form and a 1,4-dioxane solvate (Table 1). In both structures foldamer **48** adopts an S_2-conformation, which is not observed in any other foldamer (Figure 24a). The conformation is likely a result of considerable steric hindrance caused by the *tert*-butyl group, with additional stabilization from a t-shaped π-stacking interaction between the outer phenyl ring and the phenyl ring closest to the *tert*-butyl group. The packing of the *tert*-butyl foldamer **48** is equally unique, for S-conformers, as in both structures the foldamer packs in chains (C(11) motif, Figure 24b) because of the bulky *tert*-butyl group.

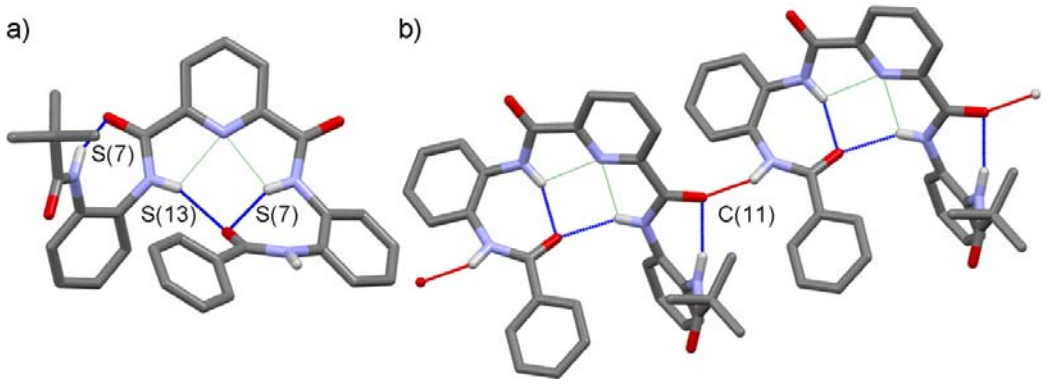

Figure 24. *tert*-Butyl foldamer **48** a) S_2-conformation and b) C(11) motif packing of unsolvated form I. Non-contact hydrogen atoms were removed for clarity.

In the DFT calculations of foldamer **46** the S_2-conformation had the lowest energy (Figure 25a).[II] The S_1-conformation, also seen in the crystal structures, had an energy difference of 2.0 kcal·mol^{-1} (Figure 25b). DFT calculations were not done on foldamer **47**, but as with the acetyl foldamer **46** the DFT calculations for *tert*-butyl foldamer **48** suggest that the S_2-conformation is the most favorable conformation in the gas phase (Figure 25c). As with the other foldamers most of the other @-, S- and h-conformations are only 1-2 kcal·mol^{-1} higher in energy for both foldamers **46** and **48**. The reason why S_2-conformers are more favorable in DFT optimized structures can be explained by the intramolecular parallel displaced π-stacking interaction seen in the DFT optimized conformations between the outer phenyl ring of the foldamer and the phenyl ring closest to the aliphatic group in the S_2-conformations.

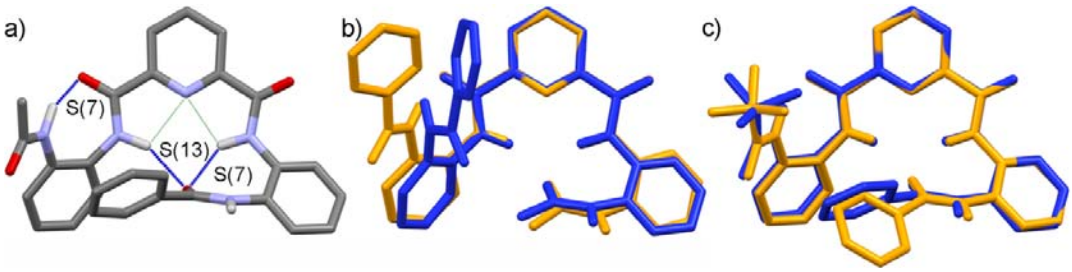

Figure 25. a) The calculated S_2-conformation of foldamer **46**, b) an overlay of the calculated S_1-conformation (blue) and the S_1-conformation of foldamer **46** from unsolvated form I (orange) and c) an overlay of the calculated S_2-conformation (blue) and the S_2-conformation of foldamer **48** from unsolvated form I (orange). Non-contact hydrogen atoms were removed for clarity.

The secondary structure of the acetyl foldamer **46** was also studied in the solution state using NOESY and NOE NMR techniques.[II] The acetyl foldamer **46** was chosen for the solution state studies because of its good solubility, improved by the small aliphatic group, and the methyl group which is easily distinguishable in the NMR spectra. The NOESY spectra suggested that the

acetyl foldamer **46** is folded, but specific conformation could not be inferred. Three diagnostic NOE-spectra measured by irradiating the outer amide bond N-H protons and methyl protons gave more information and suggested that in $CDCl_3$ solution and in the NMR timescale the molecule alternates between @-, h-, and S-conformations. Neither @- nor S-conformation could account for all the peaks, and the best correspondence to the data was found when the h_1-conformation DFT structure was compared to the data (Figure 26).

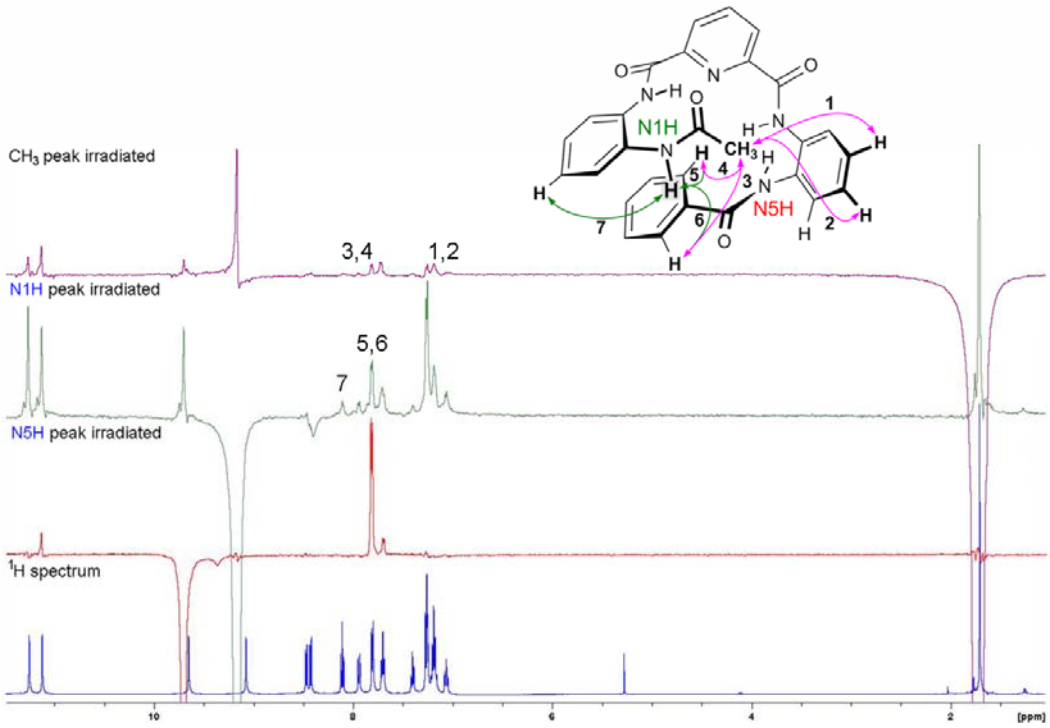

Figure 26. NOE NMR-spectra measured of the acetyl foldamer **46**. The schematic representation is the acetyl foldamer **46** in the h_1-conformation that matches best with the NOE-data. The arrows mark some selected NOE-interactions.

Some trends can be seen in the conformations of the solid state structures and the DFT optimized conformations. The presence of the aliphatic group leads foldamers **46** and **47** to favor the S_1-conformation, whereas the @′$_2$- and S_2-conformations of foldamers **47** and **48**, respectively, suggest that other factors are also important. The increasing size of the aliphatic group shows a much clearer trend. Foldamers **46** and **47** can adopt the more sterically hindered S_1-conformation, while foldamer **47** is unable to fold even to the more open @$_2$-conformation and foldamer **48** can only fold to the least hindered S_2-conformation. The DFT calculations show the importance of the π-stacking interactions that cause the S_2-conformers to be lower in energy despite the hydrogen bond acceptor improving effect of the aliphatic group.

2.5.2.4 Truncated foldamers 49 and 50[II,IV]

Truncated foldamers **49** and **50** are shorter analogues of the pyridine foldamer **49** with only three amide bonds and thus also fewer hydrogen bond donors and correspondingly only four aromatic rings. Foldamer **50** has an amino substituent at the ortho position of the phenyl ring at the truncated end of the molecule.

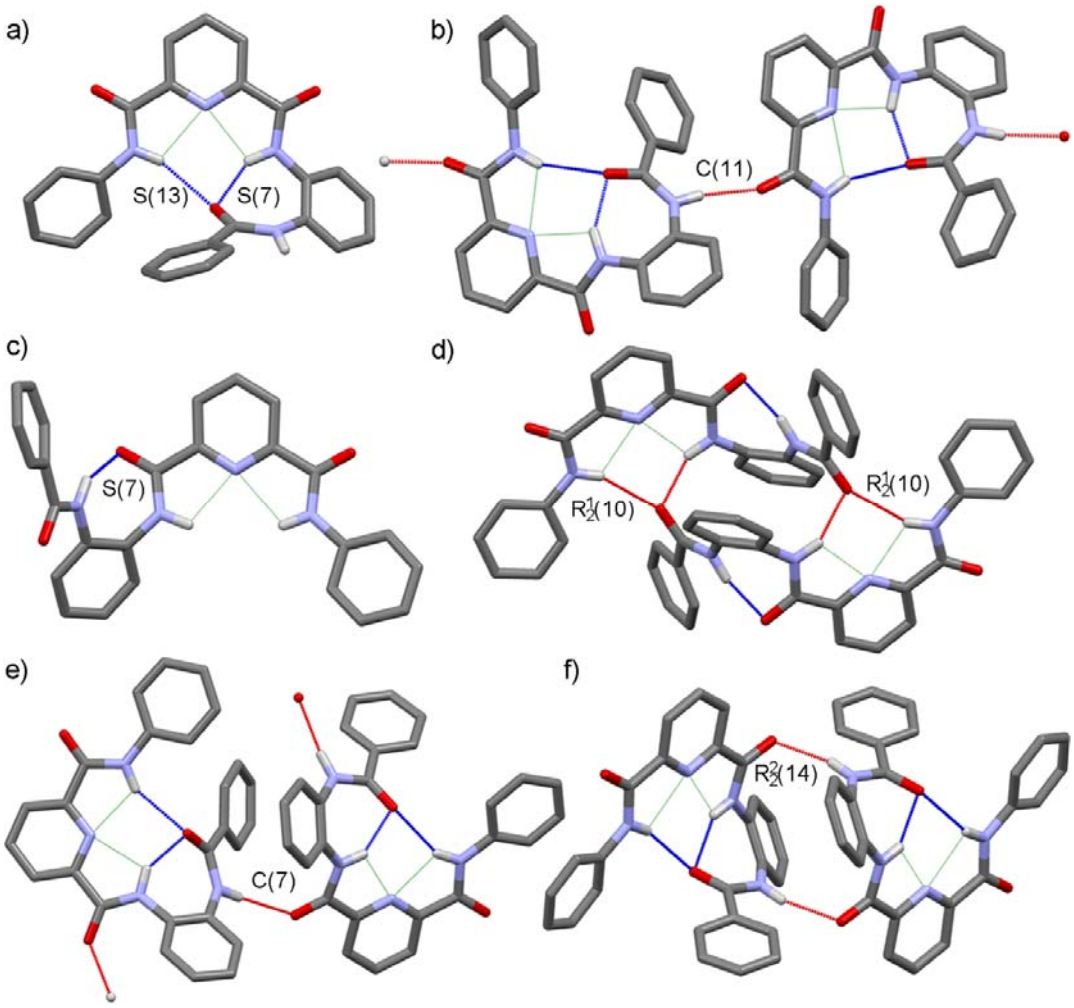

Figure 27. Solid state conformations and crystal packing structures of foldamer **49** a) @-conformation (form I), b) C(11) motif chain (form I), c) S-conformation (MeCN solvate), d) $2R_2^1(10)$ motif pair (seed crystallization DCM solvate), e) C(7) motif chain (form II) and f) $R_2^2(14)$ motif pair (DMF solvate). Non-contact hydrogen atoms were removed for clarity.

Seven crystal structures were obtained for foldamer **49**; two unsolvated polymorphs, and five solvates (Table 1). The foldamer was found in both @- and S-conformations (Figure 27a and 27c); both conformations are even simultaneously present in the structure of the DMF solvate (Figure 28). The unsolvated structures crystallize in @-conformation, but with different crystal packing. In form I the molecules pack in C(11) motif chains while in form II the

foldamers pack with the other possible, C(7), chain motif (Figure 27b and 27e). Interestingly, the crystal structure of form I is non-centrosymmetric and the molecules pack in a one-handed helical superstructure throughout the crystal. In the DMF solvate where both @- and S-conformations are present the @-conformers pack in $R_2^2(14)$ motif pairs (Figure 25f), while the S-conformer packs in $2R_2^1(10)$ motif pairs. The pair motif is likely crucial to the stability of the S-conformation as the molecule lacks the fourth amide bond and cannot form the intramolecular hydrogen bonds with the C=O groups around the pyridine core. Instead, the hydrogen bonds are intermolecular to another foldamer molecule (Figure 27c). This pair motif is present in all S-conformation structures of foldamer **49**.

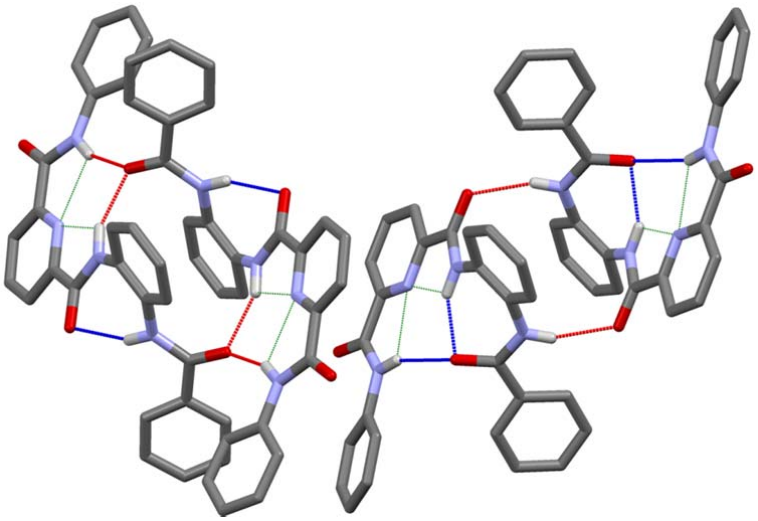

Figure 28. Foldamer **49** DMF solvate crystal structure with both @- and S-conformations in a single crystal structure. Non-contact hydrogen atoms were removed for clarity.

The crystallization behavior of foldamer **50** is very different from foldamer **49**. Foldamer **50** produced crystals from many solvents (MeCN, DMF, MeOH, EtOAc and acetone), but the result was always the same unsolvated form where foldamer **50** is in an @-conformation and packed in double chains ($C_2^1(16)$ motif, Figure 29). Surprisingly, the amino group does not participate in the intramolecular hydrogen bonding. Instead an intermolecular hydrogen bond is formed to carbonyl oxygen of the adjacent foldamer ($C_2^1(16)$ motif) which directs the crystal packing to a double chain.

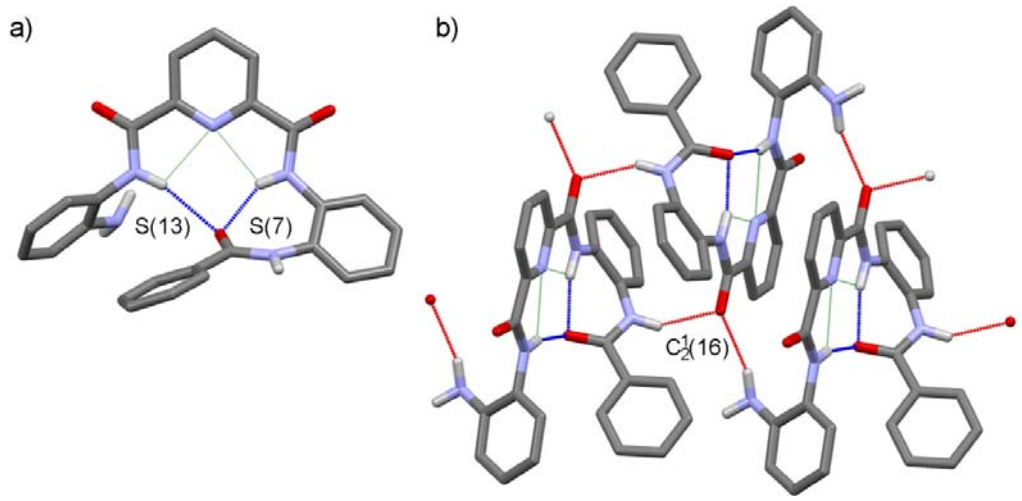

Figure 29. Foldamer **44** a) @-conformation and b) $C_2^1(16)$ motif double chain. Non-contact hydrogen atoms were removed for clarity.

In DFT calculations the @-conformation of foldamer **49** was found to clearly have the lowest energy in the gas phase as the energies of h- and S-conformations were 4.2 and 5.4 kcal·mol^{-1} higher, respectively, (Figure 30).[II] The energy barrier between the forms is higher than in the other foldamers. The clear difference can be explained by the intramolecular hydrogen bonding differences of the conformations: The @-conformation has two hydrogen bonds and additionally two weak hydrogen bonds to the pyridine core, while the S-conformation has only one hydrogen bond and the h-conformation has none. Additionally parallel displaced π-stacking interactions were observed only with @-conformation.

Figure 30. a) An overlay of the calculated @-conformation (blue) and the @-conformation of foldamer **49** taken from form I (orange), b) an overlay of the calculated S-conformation (blue) and the S-conformation of foldamer **49** taken from a MeCN solvate (orange) and c) the calculated h-conformation of foldamer **49**. Non-contact hydrogen atoms were removed for clarity.

The presence of the @-conformation for both foldamers **49** and **50** suggests that the third hydrogen bond (S(16) motif) is not crucial for the @-conformation. The @'-conformation structures seen with foldamers **43** and **47** also support this notion. In fact, DTF calculations of foldamer **49** suggest that the S-conformation is more affected by the lack of the fourth bond as the foldamer lacks the

necessary fourth hydrogen bond acceptor for the pyridine core hydrogen bonds. The same may not be true for foldamer **50** as the amine group is in the position to be able to provide the hydrogen bond donor for the signature S(7) motif bond of the S-conformation. The difference in the amount of different types of crystal structures between the foldamers is also interesting. The stability of the double chain of foldamer **50** could be a reason why only one particular conformation and crystal structure are seen.

3 SUMMARY AND CONCLUSIONS

Ten aromatic oligoamide foldamers were prepared and their structural properties were studied experimentally in solid and solution state, and by DFT calculations. Forty crystal structures were determined and the structures provided a good understanding of the conformational behavior of the compounds with complementary information from the interpretation of the DFT and solution state data.

Eight of the foldamers are classified as pyridine foldamers based on their central pyridine core unit. The pyridine core was found to be useful as its properties and behavior remained almost constant in the majority of crystal structures. The pyridine core brings two hydrogen bond donors close to each other and enables folding through relatively powerful intramolecular hydrogen bonding. The most prominent example of the strength of the resulting fold is the proto-helical @-conformation. In the @-conformation three intramolecular hydrogen bonds are formed to one hydrogen bond acceptor. This motif also has potential as a starting point for longer helical foldamers with a width far smaller than most of the previous aromatic foldamers and without the solvent filled central cavity seen in most similar examples. The small width of the foldamers is fairly close to the width of the average amino acid α-helix indicating, for example, a potential as protein mimics in protein-protein recognition processes. The @-conformation also shows, through its resemblance with the oxyanion hole, the potential of these type of foldamers as organocatalysts or at least as good analogues in the study of the active sites of enzymes.

The two other types of foldamers, benzene foldamer **41** and sulfonamide foldamer **42**, proved to be interesting molecules with more flexibility than pyridine foldamers. The flexibility makes them difficult to use as foldamer prototypes, though they did provide interesting information on the hydrogen bonding behavior of aromatic oligoamide foldamers without a pyridine core and with sulfonamide bonds. The benzene foldamer **41** favors more open, even linear, conformation where only one intramolecular hydrogen bond is formed to a hydrogen bond acceptor. With sulfonamide foldamer **42** the sharp turns

caused by the sulfonamide group seem to discourage helical folding of the molecule, though an interesting, well folded, conformation was found in the DFT calculations.

In addition to the valuable structural information obtained from this type of aromatic oligoamide foldamers, useful preparation and characterization methods of aromatic foldamers were obtained. This information creates a solid foundation for future projects aiming at more advanced foldamers with properties, for example, as supramolecular hosts, and eventually in useful applications such as organocatalysts, receptors or bioactive compounds.

REFERENCES

1 Gellman, S. H. *Acc. Chem. Res.* **1998**, *31*, 173–180.

2 Douat, C.; Aisenbrey, C.; Antunes, S.; Decossas, M.; Lambert, O.; Bechinger, B.; Kichler, A.; Guichard, G. *Angew. Chem Int. Ed.* **2015**, *54*, 11133–11137.

3 Horne, W. S.; Johnson, L. M.; Ketas, T. J.; Klasse, P. J.; Lu, M.; Moore, J. P.; Gellman, S. H. *Proc. Natl. Acad. Sci. U. S. A.* **2009**, *106*, 14751–14756.

4 Müller, M. M.; Windsor, M. A.; Pomerantz, W. C.; Gellman, S. H.; Hilvert, D. *Angew. Chem Int. Ed.* **2009**, *48*, 922–925.

5 Hou, J. L.; Shao, X. Bin; Chen, G. J.; Zhou, Y. X.; Jiang, X. K.; Li, Z. T. *J. Am. Chem. Soc.* **2004**, *126*, 12386–12394.

6 Zhao, Y.; Zhong, Z. *J. Am. Chem. Soc.* **2006**, *128*, 9988–9989.

7 Tew, G. N.; Scott, R. W.; Klein, M. L.; Degrado, W. F. *Acc. Chem. Res.* **2010**, *43*, 30–39.

8 Guichard, G.; Huc, I. *Chem. Commun.* **2011**, *47*, 5933–5941.

9 Huc, I. *Eur. J. Org. Chem.* **2004**, 17–29.

10 Kimmerlin, T.; Seebach, D. *J. Pept. Res.* **2005**, *65*, 229–260.

11 Merrifield, R. B. *J. Am. Chem. Soc.* **1963**, *85*, 2149.

12 Kemp, D. S.; Leung, S.-L.; Kerkman, D. J. *Tetrahedron Lett.* **1981**, *22*, 181–184.

13 Kemp, D. S.; Kerkman, D. J. *Tetrahedron Lett.* **1981**, *22*, 185–186.

14 Curtius, T. *J. für Prakt. Chemie* **1882**, *26*, 145–208.

15 Lerner, A. B.; Lee, T. E. H. H.; Sheehan, J. C.; Hess, G. P. *J. Am. Chem. Soc.* **1955**, *77*, 1067–1068.

16 Bergmann, M. *Science* **1934**, *79*, 439–445.

17 Carpino, L. A. *J. Am. Chem. Soc.* **1957**, *79*, 4427–4431.

18 McKay, F. C.; Albertson, N. F. *J. Am. Chem. Soc.* **1957**, *79*, 4686–4690.

19 Carpino, L. A.; Han, G. Y. *J. Am. Chem. Soc.* **1970**, *92*, 5748–5749.

20 Baptiste, B.; Zhu, J.; Haldar, D.; Kauffmann, B.; Leger, J. M.; Huc, I. *Chem. Asian J.* **2010**, *5*, 1364–1375.

21 König, H. M.; Abbel, R.; Schollmeyer, D.; Kilbinger, A. F. M. *Org. Lett.* **2006**, *8*, 1819–1822.

22 Kudo, M.; Katagiri, K.; Azumaya, I.; Kagechika, H.; Tanatani, A. *Tetrahedron* **2012**, *68*, 4455–4463.

23 Petitjean, A.; Cuccia, L. a.; Schmutz, M.; Lehn, J. M. *J. Org. Chem.* **2008**, *73*, 2481–2495.

24 Hill, D. J.; Mio, M. J.; Prince, R. B.; Hughes, T. S.; Moore, J. S. *Chem. Rev.* **2001**, *101*, 3893–4011.

25 Arunan, E.; Desiraju, G. R.; Klein, R. A.; Sadlej, J.; Scheiner, S.; Alkorta, I.; Clary, D. C.; Crabtree, R. H.; Dannenberg, J. J.; Hobza, P.; Kjaergaard, H. G.; Legon, A. C.; Mennucci, B.; Nesbitt, D. J. *Pure Appl. Chem.* **2011**, *83*, 1637–1641.

26 Ohkita, M.; Lehn, J.-M.; Baum, G.; Fenske, D. *Chem. Eur. J.* **1999**, *5*, 3471–3481.

27 Gardinier, K. M.; Khoury, R. G.; Lehn, J. M. *Chem. Eur. J.* **2000**, *6*, 4124–4131.

28 Sebaoun, L.; Maurizot, V.; Granier, T.; Kauffmann, B.; Huc, I. *J. Am. Chem. Soc.* **2014**, *136*, 2168–2174.

29 Sebaoun, L.; Kauffmann, B.; Delclos, T.; Maurizot, V.; Huc, I.; Granier, T.; Kauffmann, B.; Huc, I. *Org. Lett.* **2014**, *136*, 2326–2329.

30 Zhao, Y.; Moore, J. S. In *Foldamers: Structures, Properties and Applications*; Hecht, S., Huc, I., Eds.; Wiley-VCH, 2007; pp 75–108.

31 Miyake, H.; Tsukube, H. *Chem. Soc. Rev.* **2012**, *41*, 6977–6991.

32 Tashiro, S.; Matsuoka, K.; Minoda, A.; Shionoya, M. *Angew. Chem Int. Ed.* **2012**, *51*, 13123–13127.

33 Fischer, L.; Claudon, P.; Pendem, N.; Miclet, E.; Didierjean, C.; Ennifar, E.; Guichard, G. *Angew. Chem Int. Ed.* **2010**, *49*, 1067–1070.

34 Baruah, P. K.; Sreedevi, N. K.; Majumdar, B.; Pasricha, R.; Poddar, P.; Gonnade, R.; Ravindranathan, S.; Sanjayan, G. J.; Guichard, G.; Huc, I.; Nakashima, K.; Murahashi, M.; Yuasa, H.; Ina, M.; Norihiro, T.; Itoh, A.; Hirashima, S. I.; Koseki, Y.; Miura, T.; Ramesh, V. V. E.; Kale, S. S.; Kotmale, A. S.; Gawade, R. L.; Puranik, V. G.; Rajamohanan, P. R.; Sanjayan, G. J.; Sanphui, P.; Sarma, B.; Nangia, A.; Terada, S.; Katagiri, K.; Masu, H.; Danjo, H.; Sei, Y.; Kawahata, M.; Tominaga, M.; Yamaguchi, K.; Azumaya, I.; Zhang, D. W.; Zhao, X.; Hou, J. L.; Li, Z. T. *Cryst. Growth Des.* **2013**, *12*, 5933–5941.

35 Sanford, A. R.; Gong, B. *Curr. Org. Chem.* **2003**, *7*, 1649–1659.

36 Srinivas, D.; Gonnade, R.; Ravindranathan, S.; Sanjayan, G. J. *J. Org. Chem.* **2007**, *72*, 7022–7025.

37 Choi, S.; Isaacs, A.; Clements, D.; Liu, D.; Kim, H.; Scott, R. W.; Winkler, J. D.; DeGrado, W. F. *Proc. Natl. Acad. Sci. U. S. A.* **2009**, *106*, 6968–6973.

38 Angelo, N. G.; Arora, P. S. *J. Am. Chem. Soc.* **2005**, *127*, 17134–17135.

39 Garric, J.; Léger, J. M.; Huc, I. *Chem. Eur. J.* **2007**, *13*, 8454–8462.

40 Bao, C.; Gan, Q.; Kauffmann, B.; Jiang, H.; Huc, I. *Chem. Eur. J.* **2009**, *15*, 11530–11536.

41 Berl, V.; Huc, I.; Khoury, R. G.; Krische, M. J.; Lehn, J. M. *Nature* **2000**, *407*, 720–723.

42 Berl, V.; Huc, I.; Khoury, R. G.; Lehn, J. M. *Chem. Eur. J.* **2001**, *7*, 2798–2809.

43 Berl, V.; Huc, I.; Khoury, R. G.; Lehn, J. M. *Chem. Eur. J.* **2001**, *7*, 2810–2820.

44 Kolomiets, E.; Berl, V.; Odriozola, I.; Stadler, A.; Kyritsakas, N.; Lehn, J.-M. *Chem. Commun.* **2003**, 2868–2869.

45 Kolomiets, E.; Berl, V.; Lehn, J. M. *Chem. Eur. J.* **2007**, *13*, 5466–5479.

46 Huc, I.; Maurizot, V.; Gornitzka, H.; Léger, J.-M. *Chem. Commun.* **2002**, 578–579.

47 Maurizot, V.; Dolain, C.; Huc, I. *Eur. J. Org. Chem.* **2005**, No. 7, 1293–1301.

48 Dolain, C.; Maurizot, V.; Huc, I. *Angew. Chem Int. Ed.* **2003**, *42*, 2738–2740.

49 Jiang, H.; Maurizot, V.; Huc, I. *Tetrahedron* **2004**, *60*, 10029–10038.

50 Hamuro, Y.; Geib, S. J.; Hamilton, A. D. *Angew. Chem Int. Ed.* **1994**, *33*, 446–448.

51 Hamuro, Y.; Geib, S. J.; Hamilton, A. D. *J. Am. Chem. Soc.* **1996**, *118*, 7529–7541.

52 Hamuro, Y.; Geib, S. J.; Hamilton, A. D. *J. Am. Chem. Soc.* **1997**, *119*, 10587–10593.

53 Jiang, H.; Léger, J. M.; Huc, I. *J. Am. Chem. Soc.* **2003**, *125*, 3448–3449.

54 Jiang, H.; Léger, J. M.; Dolain, C.; Guionneau, P.; Huc, I. *Tetrahedron* **2003**, *59*, 8365–8374.

55 Jiang, H.; Dolain, C.; Léger, J. M.; Gornitzka, H.; Huc, I. *J. Am. Chem. Soc.* **2004**, *126*, 1034–1035.

56 Maurizot, V.; Dolain, C.; Leydet, Y.; Léger, J. M.; Guionneau, P.; Huc, I. *J. Am. Chem. Soc.* **2004**, *126*, 10049–10052.

57 Dolain, C.; Jiang, H.; Léger, J. M.; Guionneau, P.; Huc, I. *J. Am. Chem. Soc.* **2005**, *127*, 12943–12951.

58 Dolain, C.; Grélard, A.; Laguerre, M.; Jiang, H.; Maurizot, V.; Huc, I. *Chem. Eur. J.* **2005**, *11*, 6135–6144.

59 Garric, J.; Léger, J. M.; Huc, I. *Angew. Chem Int. Ed.* **2005**, *44*, 1954–1958.

60 Gillies, E. R.; Dolain, C.; Léger, J. M.; Huc, I. *J. Org. Chem.* **2006**, *71*, 7931–7939.

61 Delsuc, N.; Léger, J. M.; Massip, S.; Huc, I. *Angew. Chem Int. Ed.* **2007**, *46*, 214–217.

62 Gillies, E. R.; Deiss, F.; Staedel, C.; Schmitter, J. M.; Huc, I. *Angew. Chem Int. Ed.* **2007**, *46*, 4081–4084.

63 Shirude, P. S.; Gillies, E. R.; Ladame, S.; Godde, F.; Shin-ya, K.; Huc, I.; Balasubramanian, S. *J. Am. Chem. Soc.* **2007**, *129*, 11890–11891.

64 Sánchez-García, D.; Kauffmann, B.; Kawanami, T.; Ihara, H.; Takafuji, M.; Delville, M. H.; Huc, I. *J. Am. Chem. Soc.* **2009**, *131*, 8642–8648.

65 Wolffs, M.; Delsuc, N.; Veldman, D.; Anh, N. V.; Williams, R. M.; Meskers, S. C. J.; Janssen, R. A. J.; Huc, I.; Schenning, A. P. H. J. *J. Am. Chem. Soc.* **2009**, *131*, 4819–4829.

66 Baptiste, B.; Douat-Casassus, C.; Laxmi-Reddy, K.; Godde, F.; Huc, I. *J. Org. Chem.* **2010**, *75*, 7175–7185.

67 Delaurière, L.; Dong, Z.; Laxmi-Reddy, K.; Godde, F.; Toulmé, J. J.; Huc, I. *Angew. Chem Int. Ed.* **2012**, *51*, 473–477.

68 Müller, S.; Laxmi-Reddy, K.; Jena, P. V.; Baptiste, B.; Dong, Z.; Godde, F.; Ha, T.; Rodriguez, R.; Balasubramanian, S.; Huc, I. *ChemBioChem* **2014**, *15*, 2563–2570.

69 Dawson, S. J.; Mészáros, Á.; Peth, L.; Colombo, C.; Csékei, M.; Kotschy, A.; Huc, I. *Eur. J. Org. Chem.* **2014**, *2014*, 4265–4275.

70 Qi, T.; Maurizot, V.; Noguchi, H.; Charoenraks, T.; Kauffmann, B.; Takafuji, M.; Ihara, H.; Huc, I. *Chem. Commun.* **2012**, *48*, 6337.

71 Gan, Q.; Bao, C.; Kauffmann, B.; Grélard, A.; Xiang, J.; Liu, S.; Huc, I.; Jiang, H. *Angew. Chem Int. Ed.* **2008**, *47*, 1715–1718.

72 Ferrand, Y.; Kendhale, A. M.; Garric, J.; Kauffmann, B.; Huc, I. *Angew. Chem Int. Ed.* **2010**, *49*, 1778–1781.

73 Singleton, M. L.; Pirotte, G.; Kauffmann, B.; Ferrand, Y.; Huc, I. *Angew. Chem. Int. Ed. Engl.* **2014**, *53*, 13140–13144.

74 Shang, J.; Gan, Q.; Dawson, S. J.; Rosu, F.; Jiang, H.; Ferrand, Y.; Huc, I. *Org. Lett.* **2014**, *16*, 4992–4995.

75 Buratto, J.; Colombo, C.; Stupfel, M.; Dawson, S. J.; Dolain, C.; Langlois d'Estaintot, B.; Fischer, L.; Granier, T.; Laguerre, M.; Gallois, B.; Huc, I. *Angew. Chem. Int. Ed. Engl.* **2014**, *53*, 883–887.

76 Kudo, M.; Maurizot, V.; Kauffmann, B.; Tanatani, A.; Huc, I. *J. Am. Chem. Soc.* **2013**, *135*, 9628–9631.

77 Ferrand, Y.; Chandramouli, N.; Kendhale, A. M.; Aube, C.; Kauffmann, B.; Grélard, A.; Laguerre, M.; Dubreuil, D.; Huc, I. *J. Am. Chem. Soc.* **2012**, *134*, 11282–11288.

78 Hu, Z.-Q.; Hu, H.-Y.; Chen, C.-F. *J. Org. Chem.* **2006**, *71*, 1131–1138.

79 Hu, H.-Y.; Xiang, J.-F.; Yang, Y.; Chen, C.-F. *Org. Lett.* **2008**, *10*, 1275–1278.

80 Hu, H.-Y. H.-Y.; Xiang, J.-F. J.-F.; Chen, C.-F. C.-F. *Org. Biomol. Chem.* **2009**, *7*, 2534–2539.

81 Gong, B. *Acc. Chem. Res.* **2008**, *41*, 1376–1386.

82 Zhu, J.; Parra, R. D.; Zeng, H.; Skrzypczak-Jankun, E.; Zeng, X. C.; Gong, B. *J. Am. Chem. Soc.* **2000**, *122*, 4219–4220.

83 Gong, B.; Zeng, H.; Zhu, J.; Yuan, L.; Han, Y.; Cheng, S.; Furukawa, M.; Parra, R. D.; Kovalevsky, A. Y.; Mills, J. L.; Skrzypczak-Jankun, E.; Martinovic, S.; Smith, R. D.; Zheng, C.; Szyperski, T.; Zeng, X. C. *Proc. Natl. Acad. Sci. U. S. A.* **2002**, *99*, 11583–11588.

84 Yuan, L.; Zeng, H.; Yamato, K.; Sanford, A. R.; Feng, W.; Atreya, H. S.; Sukumaran, D. K.; Szyperski, T.; Gong, B. *J. Am. Chem. Soc.* **2004**, *126*, 16528–16537.

85 Yuan, L.; Sanford, A. R.; Feng, W.; Zhang, A.; Zhu, J.; Zeng, H.; Yamato, K.; Li, M.; Ferguson, J. S.; Gong, B. *J. Org. Chem.* **2005**, *70*, 10660–10669.

86 Zhang, A.; Ferguson, J. S.; Yamato, K.; Zheng, C.; Gong, B. *Org. Lett.* **2006**, *8*, 5117–5120.

87 Li, C.; Ren, S. F.; Hou, J. L.; Yi, H. P.; Zhu, S. Z.; Jiang, X. K.; Li, Z. T. *Angew. Chem Int. Ed.* **2005**, *44*, 5725–5729.

88 Yi, H.-P.; Shao, X.-B.; Hou, J.-L.; Li, C.; Jiang, X.-K.; Li, Z.-T. *New J. Chem.* **2005**, *29*, 1213.

89 Yi, H. P.; Li, C.; Hou, J. L.; Jiang, X. K.; Li, Z. T. *Tetrahedron* **2005**, *61*, 7974–7980.

90 Li, C.; Zhu, Y.-Y.; Yi, H.-P.; Li, C.-Z.; Jiang, X.-K.; Li, Z.-T.; Yu, Y.-H. *Chem. Eur. J.* **2007**, *13*, 9990–9998.

91 Yi, H.-P.; Wu, J.; Ding, K.-L.; Jiang, X.-K.; Li, Z.-T. *J. Org. Chem.* **2007**, *72*, 870–877.

92 Wang, L.; Xiao, Z.-Y.; Hou, J.-L.; Wang, G.-T.; Jiang, X.-K.; Li, Z.-T. *Tetrahedron* **2009**, *65*, 10544–10551.

93 Shi, Z.-M.; Huang, J.; Ma, Z.; Zhao, X.; Guan, Z.; Li, Z.-T. *Macromolecules* **2010**, *43*, 6185–6192.

94 Tew, G. N.; Liu, D.; Chen, B.; Doerksen, R. J.; Kaplan, J.; Carroll, P. J.; Klein, M. L.; DeGrado, W. F. *Proc. Natl. Acad. Sci. U. S. A.* **2002**, *99*, 5110–5114.

95 Ernst, J. T.; Becerril, J.; Park, H. S.; Yin, H.; Hamilton, A. D. *Angew. Chem Int. Ed.* **2003**, *42*, 535–539.

96 Hebda, J. A.; Saraogi, I.; Magzoub, M.; Hamilton, A. D.; Miranker, A. D. *Chem. Biol.* **2009**, *16*, 943–950.

97 Saraogi, I.; Hebda, J. A.; Becerril, J.; Estroff, L. A.; Miranker, A. D.; Hamilton, A. D. *Angew. Chem Int. Ed.* **2010**, *49*, 736–739.

98 Kulikov, O. V.; Thompson, S.; Xu, H.; Incarvito, C. D.; Scott, R. T. W.; Saraogi, I.; Nevola, L.; Hamilton, A. D. *Eur. J. Org. Chem.* **2013**, 3433–3445.

99 Wu, Z.-Q.; Jiang, X.-K.; Zhu, S.-Z.; Li, Z.-T. *Org. Lett.* **2004**, *6*, 229–232.

100 Wang, G.-T.; Zhao, X.; Li, Z.-T. *Tetrahedron* **2011**, *67*, 48–57.

101 Plante, J.; Campbell, F.; Malkova, B.; Kilner, C.; Warriner, S. L.; Wilson, A. J. *Org. Biomol. Chem.* **2008**, *6*, 138–146.

102 Murphy, N. S.; Prabhakaran, P.; Azzarito, V.; Plante, J. P.; Hardie, M. J.; Kilner, C. A.; Warriner, S. L.; Wilson, A. J. *Chem. Eur. J.* **2013**, *19*, 5546–5550.

103 Saraogi, I.; Incarvito, C. D.; Hamilton, A. D. *Angew. Chem Int. Ed.* **2008**, *47*, 9691–9694.

104 Zhu, J.; Wang, X. Z.; Chen, Y. Q.; Jiang, X. K.; Chen, X. Z.; Li, Z. T. *J. Org. Chem.* **2004**, *69*, 6221–6227.

105 Zhu, J.; Lin, J. Bin; Xu, Y. X.; Shao, X. Bin; Jiang, X. K.; Li, Z. T. *J. Am. Chem. Soc.* **2006**, *128*, 12307–12313.

106 Zhu, J.; Lin, J.-B.; Xu, Y.-X.; Jiang, X.-K.; Li, Z.-T. *Tetrahedron* **2006**, *62*, 11933–11941.

107 Ollikka, J. Abioottiset yksijuosteiset foldameerit, M.Sc. Thesis, University of Jyväskylä: Jyväskylä, 2009.

108 Supuran, C. T.; Casini, A.; Scozzafava, A. *Med. Res. Rev.* **2003**, *23*, 535–558.

109 Blow, D. *Structure* **2000**, *8*, 77–81.

110 Pihko, P. M.; Rapakko, S.; Wierenga, R. K. In *Hydrogen Bonding in Organic Synthesis*; 2009; pp 43–72.

ORIGINAL PAPERS

I

STRUCTURAL ANALYSIS OF TWO FOLDAMER-TYPE OLIGOAMIDES – THE EFFECT OF HYDROGEN BONDING ON SOLVATE FORMATION, CRYSTAL STRUCTURES AND MOLECULAR CONFORMATION

by

Aku Suhonen, Elisa Nauha, Kirsi Salorinne, Kaisa Helttunen & Maija Nissinen, 2012

CrystEngComm, **2012**, *14*, 7398-7407

CrystEngComm

Dynamic Article Links

Cite this: *CrystEngComm*, 2012, **14**, 7398–7407

www.rsc.org/crystengcomm

PAPER

Structural analysis of two foldamer-type oligoamides – the effect of hydrogen bonding on solvate formation, crystal structures and molecular conformation†

Aku Suhonen, Elisa Nauha, Kirsi Salorinne, Kaisa Helttunen and Maija Nissinen*

Received 19th June 2012, Accepted 17th August 2012
DOI: 10.1039/c2ce25981h

The crystal structures and molecular conformations of two foldamer-type oligoamides were analyzed. One polymorphic form and seven solvates were found for N^1,N^3-bis(2-benzamidophenyl)benzene-1,3-dicarboxamide (the benzene variant), and two polymorphic forms and six solvates for N^2,N^6-bis(2-benzamidophenyl)pyridine-2,6-dicarboxamide (the pyridine variant). Three crystal structures of the benzene variant and seven structures of the pyridine variant were solved using single crystal X-ray diffraction. The crystal structures showed that the different modes of intramolecular hydrogen bonding strongly affect the conformation and folding of the molecules, which is most evidently seen with the strongly folded helical structure of the pyridine variant. NOESY experiments suggest that the intramolecular hydrogen bonding is stable enough to retain a folded or partially folded conformation even in solution.

Introduction

Hydrogen bonding has been actively studied and discussed for almost a century and its relevance to the organization of molecules cannot be overestimated.[1] While hydrogen bonds are not as stable and rigid as covalent bonds, they still are a significant stabilizing force that results in a preferred molecular conformation in the solid state and even in solution. Hydrogen bonds are often used as key elements in crystal engineering because they are well understood and often predictable.[2] Their stabilizing effect usually causes the compounds to possess as many hydrogen bonds as possible and their directionality shapes the overall structure further by affecting the crystal packing. Multiple hydrogen bonding has even been observed to cause catalytic properties in some enzymes.[3] For example, hydrogen bonds can stabilize a negatively charged oxygen atom of the tetrahedral or enolate intermediate formed in many biological reactions, thus decreasing the enthalpic energy cost of the reaction. In these enzymes the hydrogen bond donor groups are also preorganized to stabilize the negatively charged intermediate, which in addition decreases the entropic energy cost of the reaction.[4] Examples of this catalytic effect include serine proteases[5] and triglyceride hydrolysis by cutinase.[6]

The crystal form of a compound, on the other hand, is decided by a multitude of different factors including the properties of the compound, the crystallization conditions, such as temperature and solvent, and by the interactions the compounds are able to form. Therefore, the same compound can crystallize in many different molecular conformations and crystal packing arrangements. This phenomenon is called polymorphism, which has many implications in, for example, industrial applications but which also has academic importance.[7] An equally important phenomenon in solid-state chemistry is the formation of multi-component crystals that are composed of two or more components, *i.e.* the formation of solvates and co-crystals, which change the physical and chemical properties of the compounds and affect, for example, their usability in commercial formulations and applications.[8]

Foldamers are an interesting group of synthetic oligomers which imitate some of the properties of biological macromolecules, such as peptides, proteins or DNA.[9,10] Because of these properties they can be used, for example, as biomimetic catalysts[11] or receptors,[12] or as models of protein folding.[13] The folding properties can be adjusted by designing the oligomers in such a way that weak intramolecular interactions, *e.g.* hydrogen bonds and π-stacking, between the key functional groups spontaneously direct the oligomer into a folded conformation.

In order to study the differences in the folding caused by subtle changes in the molecular structure, we designed two potential foldamers composed of five aromatic rings, which differ in their structure by containing either a phenyl (**2**) or a pyridine moiety (**3**) as the central aromatic ring (Scheme 1). Amide bonds, which

Nanoscience Center, Department of Chemistry, University of Jyväskylä, P.O. BOX 35 40014 JYU, Finland. E-mail: maija.nissinen@jyu.fi; Tel: +358 14 428 0804

† Electronic supplementary information (ESI) available: Crystal data and data collection parameters for isomorphous MeOH and toluene solvates, CIF files of the crystal structures and notes on the crystallographic data. Hydrogen bonding parameters of the structures. Solvent table for crystallizations of **2**. Lettering used in the NMR assignment. Assigned ^{1}H and ^{13}C spectra and 2D COSY, HMBC and HMQC spectra of compounds **2** and **3**. ^{1}H and ^{13}C spectra of compound **1**. NOESY spectra of compound **3** in THF-d_8 and acetone-d_6. TGA-DTA graphs of compound **2** and **3**-form II (MeCN) slurry of the pyridine variant **3**. CCDC reference numbers 885902–885911. See DOI: 10.1039/c2ce25981h

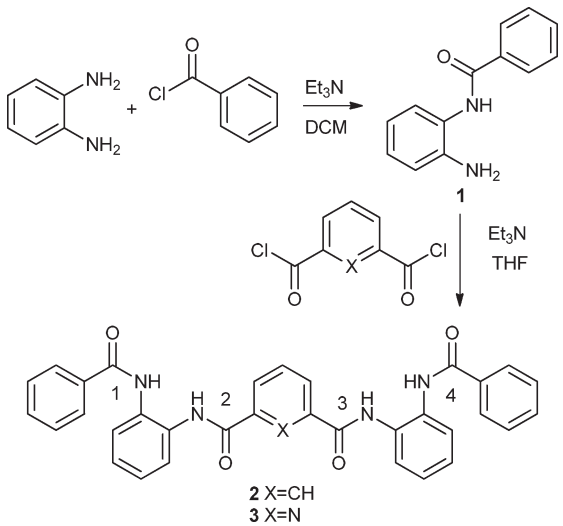

Scheme 1 The reaction scheme for the preparation of oligoamides **2** and **3** showing the amide bond numbering.

connect the aromatic rings of these two molecules and can act both as hydrogen bond acceptors and donors, are a common feature of foldamers because of their structural similarity to the peptide bond in biological molecules composed of amino acids.[10,12–25] It was anticipated that intramolecular hydrogen bonds could be formed between the two amide groups on both sides of the central aromatic ring, which would ultimately lead to folding like in similar oligoanthranilamides that have previously been shown to fold into intramolecular hydrogen bond stabilized helices both in solution and in the solid state.[15,16] Aromatic oligoamides composed of pyridine-2,6-dicarboxamide and *N*,*N*-pyridine-2,6-formamide monomers have been prepared and analyzed by Lehn *et al.*[17,18] and Huc *et al.*[19,20] Huc *et al.*[21–24] have also extensively studied aromatic oligoamide foldamers composed mainly of substituted quinoline monomers and naphthyridine monomers.[25]

In this paper we discuss the effects of weak intra- and intermolecular interactions on the molecular conformation, the folding properties, the crystal packing and the solvate formation, through a comprehensive solid-state structural analysis of two foldamer-type oligoamides. The analysis of these molecules offers insight which can help to design larger peptidomimetic foldamers with predictable secondary structures and properties. Both investigated compounds are capable of adopting a multitude of different conformational polymorphic forms and crystal packing patterns, including a strongly folded proto-helical conformation.

Experimental

Materials and methods

All starting materials were commercially available and used as such unless otherwise noted. Analytical grade solvents and Millipore water were used for crystallizations and slurries. NMR spectra were measured with a Bruker Avance DRX 500 spectrometer and the chemical shifts were calibrated to the residual proton and carbon resonance of the deuterated solvent. Melting points were measured in open capillaries using a Stuart Scientific SMP3 melting point apparatus and are uncorrected. ESI-TOF mass spectra were measured with a LCT Micromass spectrometer. Elemental analyses were done with a Vario EL III instrument. ATR-IR spectra were measured with a Bruker Tensor 27 spectrometer. TG-DTA measurements were performed with a Perkin Elmer STA600 simultaneous thermal analyzer.

Powder X-ray diffraction data was collected on a PANalytical X'Pert PRO MPD diffractometer in reflection mode with Cu-Kα_1 radiation (1.5406 Å). A 2θ angle range of 3–35° and step time of 75 s were used with a step resolution of 0.016°. Powder X-ray diffraction samples were pressed to a zero background silicon plate. The figures were drawn with X'Pert Highscore Plus.[26] Single crystal X-ray diffraction data was collected with a Bruker Nonius KappaCCD diffractometer at a temperature of 173 K using a Bruker AXS APEX II CCD detector and graphite-monochromated Cu-Kα-radiation (λ = 1.54178 Å). The structures were solved with direct methods and refined using Fourier techniques with the SHELX-97 software package.[27] Absorption correction was performed with Denzo-SMN 1997.[28] All non-hydrogen atoms were refined anisotropically, except for the disordered toluene solvent in structure **3**-toluene, and the hydrogen atoms were placed in the idealized positions except for the N–H hydrogen atoms that were found from the electron density map, and included in the structure factor calculations. Details of the crystal data and the refinement are presented in Tables 1 and 2 and in the ESI.† The crystal structures were analyzed by calculating packing coefficients[29] and fingerprint plots.[30] The graph set symbols[31] for hydrogen bonding were assigned and used to compare the bonding between the two molecules and the different crystal structures.

Synthesis

All syntheses were carried out under N_2 atmosphere. The glassware was dried at 120 °C prior to use. Dichloromethane was dried by distilling it over $CaCl_2$ and stored over Linde type 3 Å molecular sieves under nitrogen gas. Tetrahydrofuran was dried using sodium wire. Compound **1** was prepared by a slightly modified literature procedure with an improved yield.[32]

N-Benzoyl-2-aminoaniline 1[32]

O-Phenylenediamine (8.97 g; 83.1 mmol) was dissolved in dry dichloromethane (350 ml). Triethylamine (3.0 ml; 21.6 mmol) was added to the solution and the solution was heated to reflux with stirring. Benzoyl chloride (2.16 g; 20.7 mmol) dissolved in dry dichloromethane (200 ml) was added dropwise to the solution. The solution was allowed to reflux for two hours. The product was separated by column chromatography with a silica column, using an ethyl acetate–hexane (1 : 1) mixture as an eluent. Recrystallization from ethyl acetate–hexane afforded the product as a white solid, yield. 3.57 g (81%). mp. 149–151 °C; ^{1}H NMR (ESI†) (500 MHz, DMSO-d_6, 30 °C): δ = 4.87 (s, 2H; i), 6.60 (td, $^3J_{HH}$ = 1.2 Hz, $^3J_{HH}$ = 7.6 Hz, 1H; g), 6.79 (dd, $^3J_{HH}$ = 1.3 Hz, $^3J_{HH}$ = 8.1 Hz, 1H; e), 6.97 (td, $^3J_{HH}$ = 1.2 Hz, $^3J_{HH}$ = 7.6 Hz, 1H; f), 7.18 (d, $^3J_{HH}$ = 7.7 Hz, 1H; d), 7.51 (t, $^3J_{HH}$ = 7.4 Hz, 2H; b), 7.55–7.60 (m, 1H; a), 7.98 (d, $^3J_{HH}$ = 7.4 Hz, 2H; c), 9.63 (s, 1H; h) ppm; ^{13}C NMR (ESI†) (126 MHz, DMSO-d_6, 30 °C): δ = 116.1, 116.2, 123.3, 126.4, 127.6, 128.2, 131.2, 134.6,

Table 1 Crystal data and collection parameters for the benzene variant (**2**)

	2-form I	**2**-DMSO I	**2**-DMSO II
Formula	$C_{34}H_{26}N_4O_4$	$C_{34}H_{26}N_4O_4{\cdot}C_2H_6OS$	$C_{34}H_{26}N_4O_4{\cdot}C_2H_6OS$
M/g mol^{-1}	554.59	632.72	632.72
Crystal system	Monoclinic	Triclinic	Triclinic
Space group	$C2/c$	$P\bar{1}$	$P\bar{1}$
a/Å	39.6877(1)	8.8462(1	8.8810(4)
b/Å	8.3626(1)	9.6181(1)	14.2224(7)
c/Å	16.6713(1)	18.7208(1)	14.3149(6)
α (°)	90	84.621(1)	114.149(2)
β (°)	97.187(1)	85.074(1)	97.447(2)
γ (°)	90	81.720(1)	100.481(4)
V/Å^3	5489.6(1)	1565.1(1)	1579.8(1)
Z	8	2	2
ρ_c/g cm^{-3}	1.342	1.343	1.330
Meas. reflns	7913	6466	8159
Indep. reflns	4653	4997	5350
R_{int}	0.0813	0.0913	0.0582
R_1 [$I > 2\sigma(I)$]	0.0559	0.0677	0.0506
wR_2 [$I > 2\sigma(I)$]	0.1242	0.1413	0.1180
GooF	1.018	1.030	1.046

143.0, 165.2 ppm; MS (ESI-TOF) m/z: 235.08 [M + Na$^+$]; Elemental analysis calcd (%) for $C_{13}H_{12}N_2O$: C 73.6, H 5.7, N 13.2; found C 73.8, H 5.6, N 13.3.

General procedure for the preparation of the benzene and pyridine variants 2 and 3

N-Benzoyl-2-aminoaniline **1** (0.30 g; 1.42 mmol) was dissolved in dry tetrahydrofuran (25 ml). Triethylamine (0.2 ml; 1.44 mmol) was added and the mixture was stirred at room temperature for one hour. The solution was heated to reflux and isophthaloyl dichloride or 2,6-pyridinedicarbonyl dichloride (0.71 mmol) dissolved in dry tetrahydrofuran (15 ml) was added dropwise to the mixture. The solution was refluxed for two hours.

Benzene variant 2

Synthesis was done according to the general procedure using isophthaloyl dichloride as a reagent. After reaction the product precipitated from the mixture as a white solid. The precipitate was filtered out and washed with water. A second precipitate was collected from the filtrate after addition of water, and was washed with water. Combined precipitates were dried under vacuum. The product was a white solid, which contains approx. 1 molecule of THF for every molecule of **2** (according to NMR and TG analysis), yield 80%. mp. 253–254 °C; ^{1}H NMR (ESI†) (500 MHz, DMSO-d$_6$, 30 °C): δ = 7.29–7.42 (m, 4H, f and g), 7.47 (t, $^3J_{HH}$ = 7.5 Hz, 4H; b), 7.55 (tt, $^3J_{HH}$ = 1.4 Hz, $^3J_{HH}$ = 7.4 Hz, 2H; a), 7.64–7.73 (m, 5H; d, e and i), 7.93–7.96 (m, 4H; c), 8.13 (dd, $^3J_{HH}$ = 1.7 Hz, $^3J_{HH}$ = 7.7 Hz, 2H; h), 8.55 (s, 1H; j), 10.00 (s, 2H; k/l), 10.22 (s, 2H; k/l) ppm; ^{13}C NMR (ESI†) (126 MHz, DMSO-d$_6$, 30 °C): δ = 125.5 (f/g), 125.6 (f/g), 125.8 (d, e), 127.0 (j), 127.4 (c), 128.4 (b), 128.8 (i), 130.5 (h), 131.0 (d′), 131.4 (e′), 131.7 (a), 134.2 (c′), 134.6 (h′), 164.9 (l′), 165.4 (k′) ppm; MS (ESI-TOF) m/z: 577.14 [M + Na$^+$]; Elemental analysis calcd (%) for $C_{34}H_{26}N_4O_4$ 0.5(C_4H_8O): C 73.2, H 5.1, N 9.5; found C 73.3, H 5.1, N 9.3.

Table 2 Crystal data and collection parameters for the pyridine variant (**3**)

	3-form I	**3**-DMF	**3**-EtOAc[a]	3-EtOH[a]	3-DMSO
Formula	$C_{33}H_{25}N_5O_4$	$C_{33}H_{25}N_5O_4{\cdot}C_3H_7NO$	$C_{33}H_{25}N_5O_4{\cdot}0.5C_4H_8O_2$	$C_{33}H_{25}N_5O_4{\cdot}C_2H_6O$	$C_{33}H_{25}N_5O_4{\cdot}C_2H_6OS$
M/g mol^{-1}	555.58	628,68	599.63	601.65	633.71
Crystal system	Triclinic	Monoclinic	Monoclinic	Monoclinic	Monoclinic
Space group	$P\bar{1}$	$P2_1/c$	$P2_1/c$	$P2_1/c$	$P2_1/c$
a/Å	10.5379(7)	14.0456(7)	12.4871(5)	13.2559(4)	9.7193(5)
b/Å	11.5380(7)	19.2718(8)	16.7357(7)	16.6185(6)	18.6564(8)
c/Å	12.1818(7)	11.4694(5)	14.7175(7)	16.8199(6)	17.5185(8)
α (°)	78.559(3)	90	90	90	90
β (°)	74.708(3)	94.781(2)	90.296(2)	126.354(2)	92.741(2)
γ (°)	77.753(4)	90	90	90	90
V/Å^3	1380.2(2)	3093.8(2)	3070.1(2)	2984.1(2)	3172.9(3)
Z	2	4	4	4	4
ρ_c/g cm^{-3}	1.337	1.350	1.202	1.339	1.327
Meas. reflns	6344	8937	8295	8338	9190
Indep. reflns	4582	5250	4991	5123	5306
R_{int}	0.0826	0.0725	0.0529	0.0533	0.0700
R_1 [$I > 2\sigma(I)$]	0.0603	0.0575	0.0535	0.0551	0.0527
wR_2 [$I > 2\sigma(I)$]	0.1393	0.1253	0.1242	0.1231	0.1109
GooF	1.041	1.047	0.981	1.028	1.022

[a] Information on the isomorphous solvate structures is presented in the ESI.†

Pyridine variant 3

Synthesis was done according to the general procedure using 2,6-pyridinedicarbonyl dichloride as a reagent. After reflux, tetrahydrofuran was evaporated leaving a yellow-green precipitate. The precipitate was recrystallized from ethyl acetate as a white solid with a yield of 68%. mp. 251–253 °C; ^{1}H NMR (ESI†) (500 MHz, DMSO-d_6, 30 °C): δ = 7.21 (t, $^{3}J_{HH}$ = 7.9 Hz, 4H; b), 7.31–7.37 (m, 4H; f), 7.43 (tt, $^{3}J_{HH}$ = 1.2 Hz, $^{3}J_{HH}$ = 7.4 Hz, 2H; a), 7.63–7.71 (m, 4H; d, e), 7.75 (dd, $^{3}J_{HH}$ = 1.2 Hz, $^{3}J_{HH}$ = 7.1 Hz, 4H; c), 8.27–8.31 (m, 1H; h), 8.36–8.38 (m, 2H; g), 10.19 (s, 2H; i), 10.99 (s, 2H; j) ppm; ^{13}C NMR (ESI†) (126 MHz, DMSO-d_6, 30 °C): δ = 125.0 (g), 125.5 (e), 125.6 (f), 125.7 (d), 127.5 (c), 128.0 (b), 130.7 (d′), 131.1 (e′), 131.5 (a), 134.0 (c′), 140.3 (h), 148.2 (g′), 161.2 (j′), 165.9 (i′) ppm; MS (ESI-TOF) *m*/*z*: 578.16 [M + Na^+]; Elemental analysis calcd (%) for $C_{33}H_{25}N_5O_4$: C 71.3, H 4.5,N 12.6; found C 71.2, H 4.4, N 12.7.

Crystallizations

The benzene and pyridine variants, **2** and **3**, were crystallized in acetone, acetonitrile (MeCN), chloroform, 1,2-dichloroethane (DCE), dichloromethane (DCM), dimethylacetamide (DMA), dimethylformamide (DMF), dimethyl sulfoxide (DMSO), 1,4-dioxane, ethyl acetate (EtOAc), methanol (MeOH), tetrahydrofuran (THF) and toluene. In addition, compound **3** was crystallized from ethanol. Amounts of 3–50 mg of compounds **2** and **3** and 0.4–6 ml of solvent were used in the crystallization experiments. Due to the low solubility of compound **2** in most organic solvents, a small drop of DMA, DMF or DMSO (20–40 μl) were added to many solutions of **2**; in these cases the results of the crystallizations are referred to as solution mixtures in the text. Heating and stirring were used to help the dissolving process. After the compounds had dissolved, the solutions were allowed to evaporate at room temperature until crystals formed.

Slurries

Slurries of the oligoamides **2** and **3** were made by stirring 10–50 mg of the compound in 2–4 ml of solvent (MeCN, DCM, EtOAc or THF; in addition, EtOH was used for compound **2** and toluene for compound **3**) for two weeks at room temperature. After two weeks the mixtures were allowed to dry in open vessels.

Results and discussion

Synthesis and NMR

Compounds **2** and **3** were synthesized in two steps from acyl halides and substituted anilines using a nucleophilic substitution reaction with good to excellent yields (Scheme 1). In addition to ^{1}H and ^{13}C NMR spectroscopy, compounds **2** and **3** were characterized using 2D NMR spectroscopic techniques (COSY, HMQC and HMBC; see ESI for details†). The conformational properties of **3** in solution were studied with NOESY.† The NOESY spectra measured both in acetone-d_6 and in THF-d_8, showed correlations between the inner amide group peak (amide groups 2 and 3, Scheme 1) and an aromatic hydrogen peak of the outer phenyl rings. This indicates that oligoamide **3** is at least partially folded when dissolved in these solvents. NOESY spectra were not measured for **2** because of its poor solubility.

Crystal forms of the benzene variant 2

Three single crystal structures were obtained for the oligoamide **2**, namely, an unsolvated **2**-form I (crystallized from DMF), and two DMSO solvates (**2**-DMSO I and **2**-DMSO II), which were crystallized from DMSO–EtOAc and neat DMSO, respectively (Fig. 1, Table 1). Hydrogen bonding parameters for the structures can be found in the ESI.†

Structure **2**-form I has two intramolecular hydrogen bonds with an S(7) motif. One of the hydrogen bonds is formed between an inward bent inner C=O (Scheme 1, amides 2 and 3) and an outer N–H (amides 1 and 4), and the other bond between an outer C=O (1 or 4) and an inner N–H (2 or 3). These hydrogen bonds cause the molecule to adopt a loosely folded structure (Fig. 1a). Adjacent molecules connect to each other with hydrogen bonds between a carbonyl oxygen and an amide hydrogen (an $R_2^2(14)$ motif), which are available for the intermolecular hydrogen bonds, forming a chain structure (Fig. 1a). The molecular chains are connected by weak hydrogen bonds, van der Waals forces and parallel displaced π-stacking interactions between two of the 1,2-substituted phenyl rings.

The **2**-DMSO I solvate has two intramolecular hydrogen bonds with an S(7) motif similarly to **2**-form I, but both of these bonds are formed between the inner C=O groups (2 and 3) and the outer N–H groups (1 and 4). Therefore, the molecule has a more open conformation than **2**-form I (Fig. 1b and Fig. 2). Also, the crystal packing into chains of molecules is similar in comparison to **2**-form I, with two hydrogen bonds in an $R_2^2(14)$ motif (Fig. 1b). Interestingly, although DMSO is a powerful hydrogen bond acceptor it does not form any significant hydrogen bonds in this structure. It is only connected to other molecules with van der Waals interactions and weak hydrogen bonds and located in the structural cavities between the chains of molecules.

The **2**-DMSO II solvate has similar intramolecular hydrogen bonds S(7) between the inner C=O groups (2 and 3) and the outer N–H groups (1 and 4), as does the **2**-DMSO I solvate (Fig. 1c). However, unlike in the **2**-DMSO I solvate and **2**-form I, both of the inner C=O groups (2 and 3) are facing inwards to the molecule and form a curved conformation instead of an open or a folded one. Again, molecules connect to each other with two hydrogen bonds forming an $R_2^2(14)$ motif. The unexpected curved molecular conformation, where both of the inner C=O groups (2 and 3) are facing inwards, may in fact be caused by the DMSO that stabilizes the curved structure by forming a hydrogen bond into an amide hydrogen with a D motif. In both of the **2**-DMSO I and **2**-DMSO II solvates, the closest DMSO molecule to the benzene variant **2** is located near the central benzene ring. This may prevent tighter folding and cause more open molecular conformations.

The reason for the two different DMSO solvates is likely due to the presence of EtOAc in the crystallization of **2**-DMSO I. Since the DMSO does not form strong hydrogen bonds to the oligoamide in **2**-DMSO I, as it does in **2**-DMSO II, it is probable that the crystallization starts as an EtOAc solvate and later on the EtOAc molecules are forced out of the crystal and replaced by DMSO.

The packing efficiency of the three forms was compared using fingerprint plots of the structures (Fig. 1). The fingerprint plots

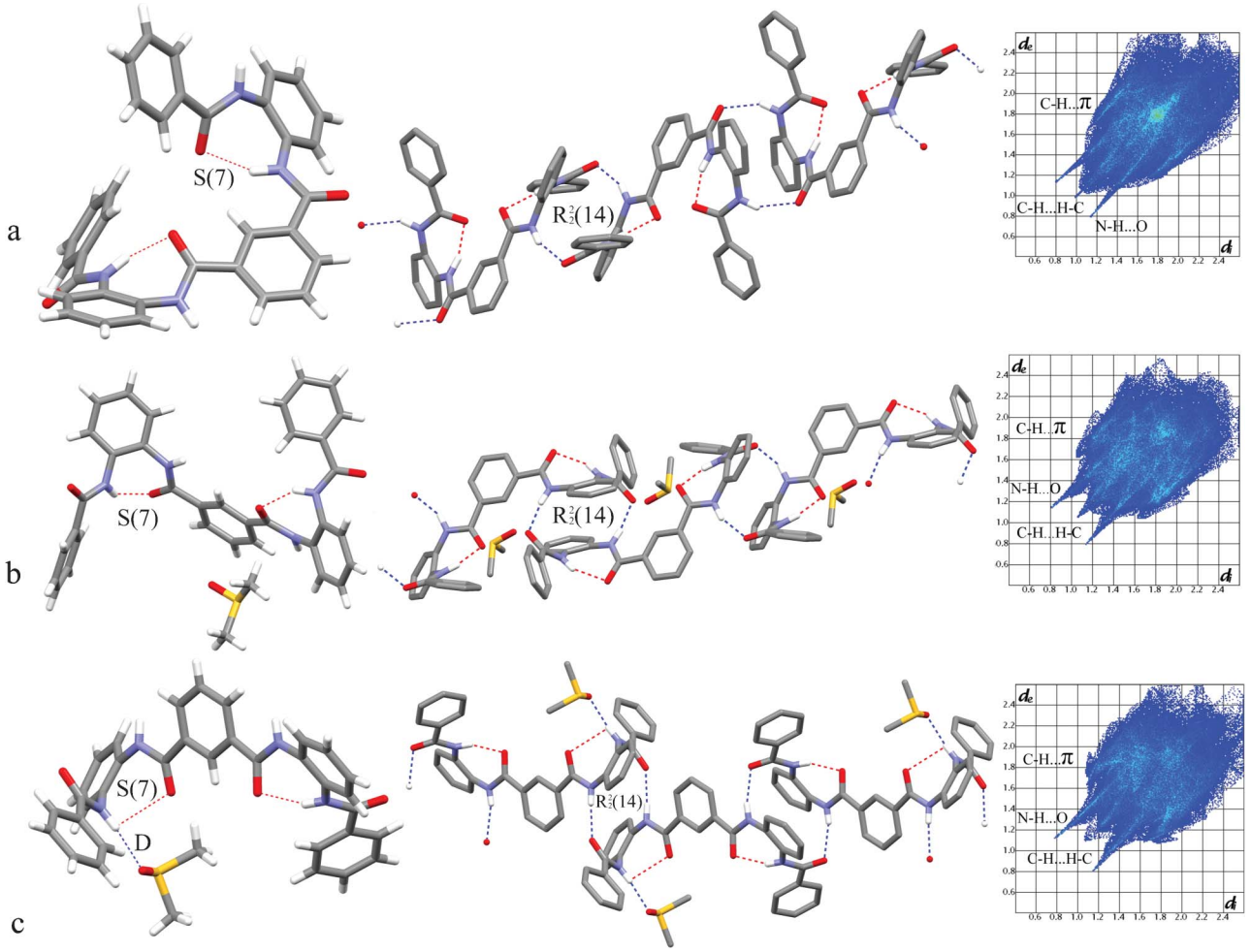

Fig. 1 The molecular conformation (left), the crystal packing (middle) and the fingerprint plot (right) of the benzene variant **2** showing (a) **2**-form I, (b) **2**-DMSO solvate I and (c) **2**-DMSO solvate II. Non-hydrogen bonding hydrogen atoms and solvent disorder (**2**-DMSO I) have been omitted for clarity.

are relatively similar because all forms have four hydrogen bonds with the neighbouring molecules of **2** and two intramolecular hydrogen bonds. The intermolecular hydrogen bonds are represented by the two long spikes in the fingerprint plot (marked by N–H···O in Fig. 1). The "wings" on the sides of the fingerprint plots represent the C–H···π interactions and the short spike represents the short H–H contacts.

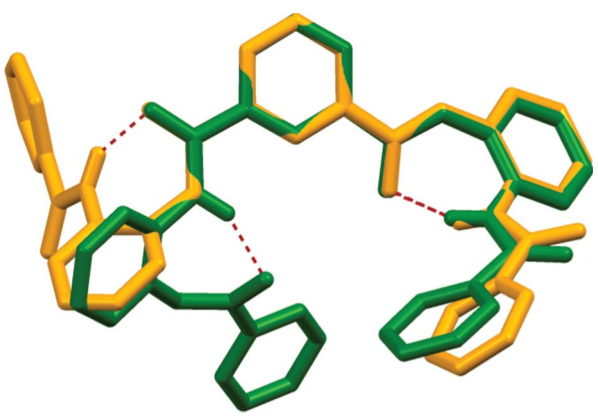

Fig. 2 The overlaid structures of **2**-form I (green) and **2**-DMSO I solvate (yellow) of the benzene variant **2**. Non-contact hydrogen atoms have been omitted for clarity.

The aromatic interactions play an important role in the crystal packing because the chains of the molecules in all three structures are connected by the interactions between the aromatic hydrogen atoms of a molecule in one chain and the aromatic carbons in the other chains, along with the weak hydrogen bonds between the carbonyl oxygens and the aromatic hydrogens. The packing coefficients suggest that the **2**-DMSO I solvate is the best packed of the three, but the differences are relatively small (**2**-form I: 0.722, **2**-DMSO I: 0.724 and **2**-DMSO II: 0.717). This suggests that the efficiency of the different packing patterns is almost equal.

In addition to the single crystal studies, powder X-ray diffraction revealed five crystal forms for the oligoamide **2**. Crystallization of **2** from DCE, EtOH, MeCN and MeOH and slurries from MeCN and EtOH were identified to produce **2**-form I by PXRD (Fig. 3). However, crystals suitable for single crystal X-ray diffraction were not obtained. Crystallizations from EtOAc–DMSO, DCM and THF, and slurries from DCM and THF produced solvates, which are isomorphous with the

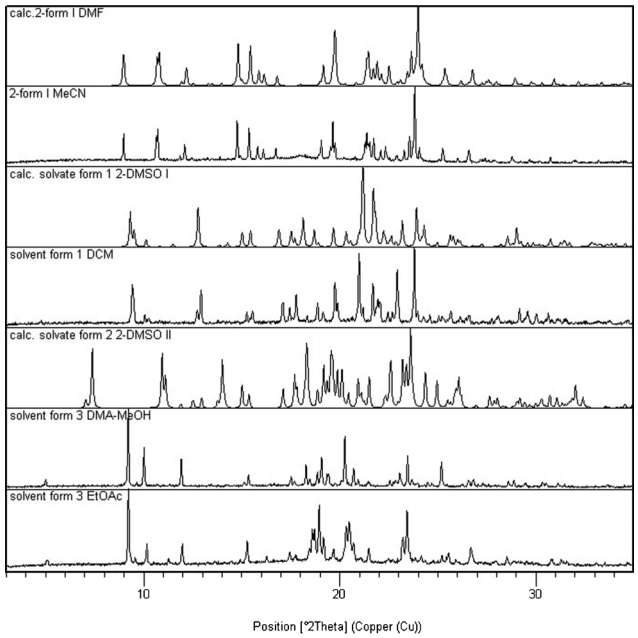

Fig. 3 The measured and the calculated PXRD patterns of the polymorphic and the solvate forms of the benzene variant **2**. Notes on the upper left corners of patterns indicate the solvent or solvents used in the experiment.

structure **2**-DMSO I based on their PXRD patterns (Fig. 3). In addition, crystals obtained from crystallization from EtOAc, and crystallizations from solvent mixtures of DMF with chloroform, EtOAc, THF and toluene; from solvent mixtures of DMA with EtOH, MeOH and MeCN; and a slurry from EtOAc were assigned into a third isomorphous group of oligoamide **2** solvates based on their PXRD patterns (ESI†). PXRD patterns of DMF and DMA with other solvents were so similar that most likely the crystals from these experiments are the same as the **2**-DMSO I solvate. Meaning that they are either DMF or DMA solvates, which have a different structure than if they would have been formed from crystallizations with just DMA or DMF. TG analysis performed on the MeCN, EtOAc and THF slurries support the results of the PXRD studies. Slurries other than MeCN are solvates. The samples were also analyzed using ATR-IR spectroscopy, but the different forms could not be unambiguously identified likely due to the simultaneous presence of the different crystalline forms and the solvents in the samples.

The recurring chain structure observed in the crystal structures of **2** may explain both the low solubility of the compound, as well as the strong tendency of **2** to form isomorphous solvates readily with many different solvents. Solvent layers form between and around the chains.

Crystal forms of the pyridine variant 3

Seven single crystal structures were obtained for the pyridine variant **3** (Table 2, Fig. 4, ESI†). One of the structures is a loosely packed unsolvated **3**-form I and the six others are solvates: isomorphous **3**-MeOH and **3**-EtOH solvates, isomorphous **3**-EtOAc and **3**-toluene solvates, **3**-DMF solvate and **3**-DMSO solvate. Hydrogen bonding parameters for the structures can be found in the ESI.†

The single crystal structure of **3**-form I was obtained from the slow evaporation crystallizations from EtOAc and MeCN solutions. The **3**-form I has three intramolecular hydrogen bonds that are all formed between the same outer C=O groups (1 or 4) and three of the N–H groups with S(7), S(13) and S(16) motifs (Fig. 4a). This causes the molecule to adopt a strongly folded structure. There are also two hydrogen bonds between the nitrogen of the pyridine ring and the inner N–H (2 and 3) hydrogen atoms with an S(5) motif that stabilize the folded conformation. The crystal packing of **3**-form I is composed of molecule pairs held together by two hydrogen bonds between the carbonyl and the amide groups with an $R_2^2(14)$ motif (Fig. 4a). There are also indigenous 33 $Å^3$ voids in the structure. The voids found in the structure are either evidence of inefficient packing, or an indication of a possible solvate formation before the formation of **3**-form I.

The **3**-DMF solvate structure has the same five intramolecular hydrogen bonds that cause a similar strongly folded structure as in **3**-form I (Fig. 4b). The molecules pack into chains connected *via* C=O···N–H hydrogen bonds with a C(7) motif. The DMF solvent does not form any medium or strong hydrogen bonds with the other molecules. PXRD studies also indicate that the DMF solvate of the pyridine variant **3** has five isomorphous solvates (acetone, 1,4-dioxane, DMA, pyridine and THF), but only DMF produced crystals suitable for single crystal XRD measurement.

The ethyl acetate solvate was at first discovered during the recrystallization phase of the synthesis when the crude product was dissolved in hot EtOAc and cooled in a refrigerator. The structure has one EtOAc molecule for every two molecules of the pyridine variant **3**. The molecular conformation is again similar to the **3**-form I and the DMF solvate, but the packing is slightly different. The molecules form a chain with a C(11) motif (Fig. 4c). The ethyl acetate solvate has an isomorphous toluene solvate formed from evaporation crystallization from toluene.

The isomorphous solvates **3**-MeOH and **3**-EtOH have a similar molecular conformation as the **3**-DMF, **3**-EtOAc and **3**-toluene solvates and **3**-form I. The molecules pack into chains of molecules with a C(16) motif (Fig. 4d). The solvent is hydrogen bonded to one of the inner C=O groups (2 or 3) with a D motif. The **3**-MeOH and **3**-EtOH solvates have identical structural features apart from solvent disorder, which is observed with the smaller MeOH, but not with EtOH.

The **3**-DMSO solvate crystallized overnight from a sample where the pyridine variant **3** was dissolved in DMSO by heating the sample. It has a slightly different molecular conformation than the other forms crystallized from the pyridine variant **3** (Fig. 4e). The solvate has two S(5) hydrogen bonds, one S(7) and one S(13) hydrogen bond, but the S(16) hydrogen bond is not formed. Instead a hydrogen bond is formed with the DMSO molecule with a D motif (Fig. 4e). The molecules of the pyridine variant **3** form chains with a C(11) motif, but the conformation of the molecules in the chain differs from the C(11) motif chain formed in the **3**-EtOAc and **3**-toluene solvates. The chain of molecules formed by the **3**-DMSO solvate is more consistent in shape than the other C(11) chain (Fig. 4c and 4e).

Nothing certain can be said about the possible hydrogen bonding between the pyridine variant **3** and EtOAc because the solvent molecule had to be removed from the final refinement of

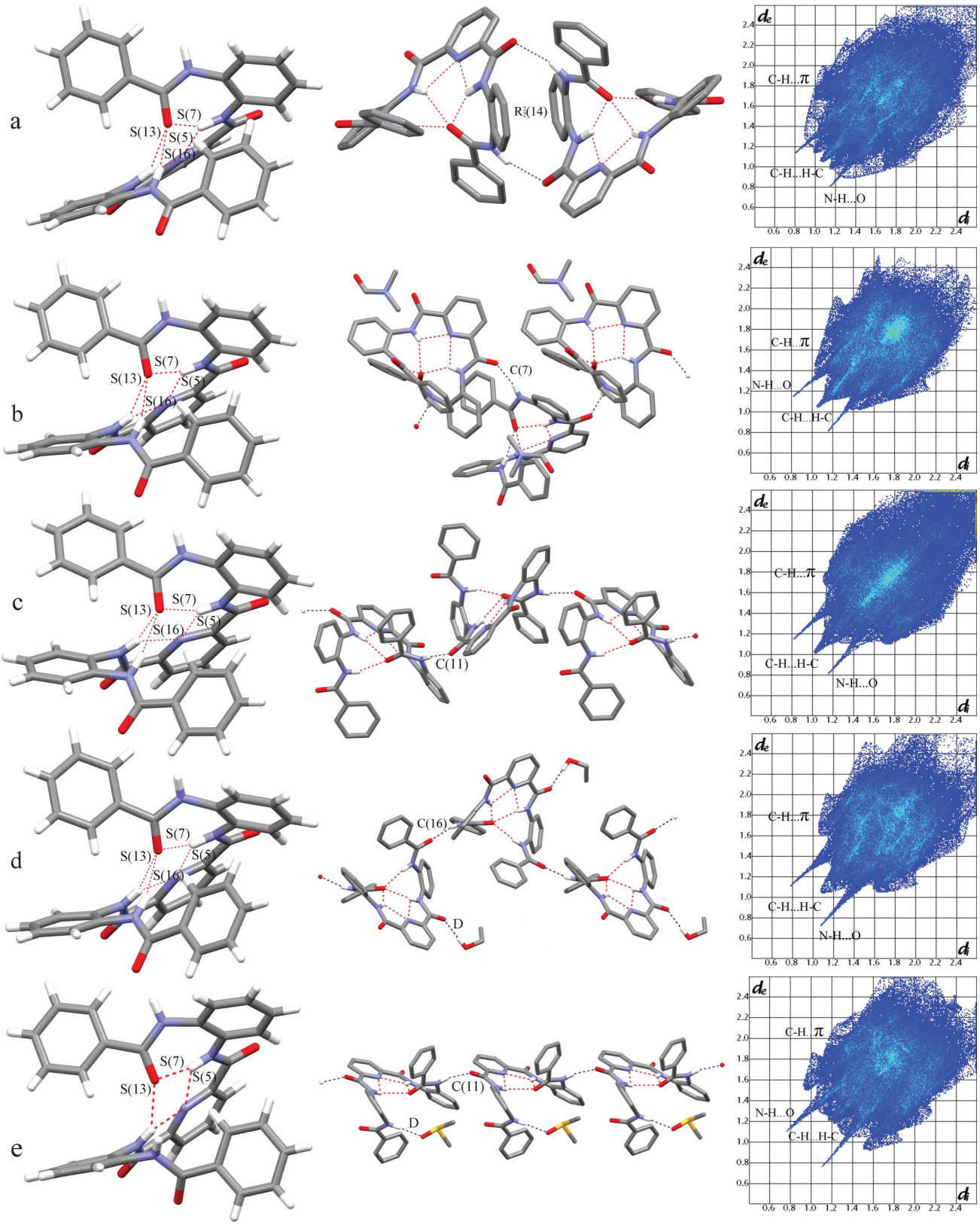

Fig. 4 The molecular conformation (left), packing (middle) and fingerprint plot (right) of the pyridine variant **3** showing (a) **3**-form I, (b) the **3**-DMF solvate, (c) the **3**-EtOAc solvate, (d) the **3**-EtOH solvate and (e) the **3**-DMSO solvate. Non-contact hydrogen atoms, form I benzene ring disorder and DMF solvate solvent disorder have been omitted for clarity.

the 3-EtOAc solvate structure by SQUEEZE due to severe disorder. Most likely the **3**-EtOAc solvate does not form any hydrogen bonds because it has no hydrogen bond donor groups and the molecules of the pyridine variant **3** are in a molecular conformation where only one hydrogen donor group is facing outside the molecule. In addition, this same donor group is already forming a hydrogen bond with the neighboring pyridine variant **3** molecule (Fig. 4c). Also, based on the isomorphous **3**-toluene solvate, which possesses the same molecular ratio, conformation and structure as the **3**-EtOAc solvate, it seems that the role of the solvent is again merely to fill the interstice between the chains. The same applies to the **3**-DMF solvate. In the **3**-DMSO solvate the molecular conformation is changed and a hydrogen bond is formed between the solvate and the pyridine variant **3** molecule (Fig. 4e). This is most likely due to the fast crystallization process and the powerful hydrogen bond forming tendencies of DMSO.

As the molecular conformations in all the crystal structures, aside from the DMSO solvate, are so similar, the differences between these structures clearly stem from the differences in the crystal packing and the hydrogen bonding. The packing coefficient of the **3**-DMF solvate is the highest ($C(k)$ = 0.735) followed by the **3**-MeOH and **3**-EtOH solvates (0.731 and 0.732, respectively), **3**-form I (0.712), DMSO solvate (0.709) and the **3**-toluene and **3**-EtOAc solvates (0.701 and 0.699). The differences in the stability and the packing efficiency between **3**-form I and the **3**-EtOAc solvate predicted by their packing coefficients are confirmed by the experimental observations. The **3**-EtOAc solvate only forms when a fast change in the temperature of the solvent causes a fast crystallization. When the temperature changes more slowly, the crystallization from EtOAc produces **3**-form I. The lower packing efficiency of the **3**-DMSO solvate indicated by its packing coefficient is also most likely the result of its fast crystallization. The difference between the packing efficiency of **3**-form I and the **3**-EtOH, **3**-MeOH and **3**-DMF solvates is also understandable because the crystal structures show that **3**-form I has voids in its structure that are not found in these solvate structures.

The fingerprint plots of the structures also demonstrate the differences (Fig. 4). Compared to **3**-form I, the **3**-DMSO, **3**-MeOH and **3**-EtOH solvates have an extra intermolecular hydrogen bond to the solvent molecule. The fingerprint plots of the solvates also have clearly defined ''wings'' caused by the C–H$\cdots\pi$ interactions that connect the different molecular chains. While these interactions are relatively weak alone, together they can have a significant effect on the stability of the crystal structure. The **3**-form I has a well defined center spike caused by the short C–H$\cdots$H–C distances between the molecular pairs. These short distances between the aromatic hydrogen atoms can make the structure more unstable, but at the same time are too weak to affect the overall molecular conformation caused by the intramolecular hydrogen bonds, or break the hydrogen bonds that form the molecular pairs. The molecular pairs and the chains of molecules formed in the structures are connected by weak hydrogen bonds, van der Waals interactions and parallel displaced and T-shaped π-stacking.

In addition to the single crystal structures, the pyridine variant **3** has also at least one other polymorphic form (**3**-form II) that was found using PXRD, TGA-DTA and ATR-IR measurements

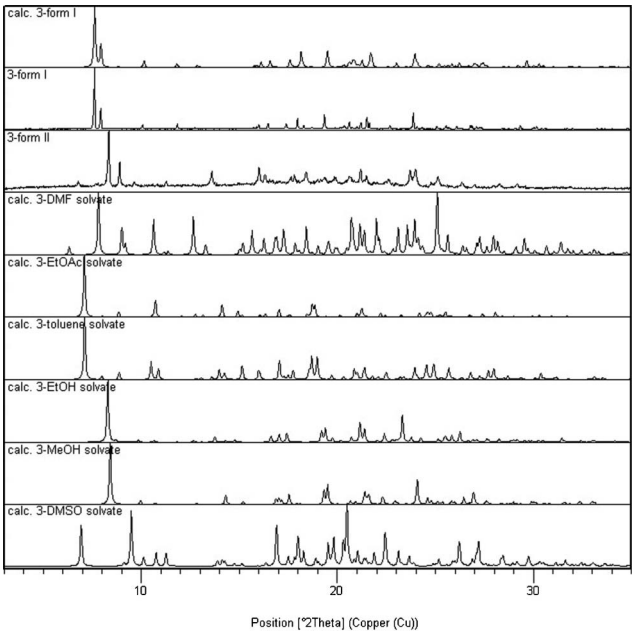

Fig. 5 The measured and the calculated PXRD patterns of the polymorphic and the solvate forms of the pyridine variant **3**.

(Fig. 5 and 6). The IR spectra of **3**-form II is easily distinguishable from the spectra of **3**-form I by its carbonyl peak at 1675 cm^{-1}. Unlike **3**-form II, the carbonyl peak of **3**-form I is split between a stronger and a weaker peak, at 1687 cm^{-1} and 1673 cm^{-1}. The splitting is caused by one carbonyl oxygen that is more strongly hydrogen bonded than the other three, whereas the single carbonyl peak of **3**-form II indicates

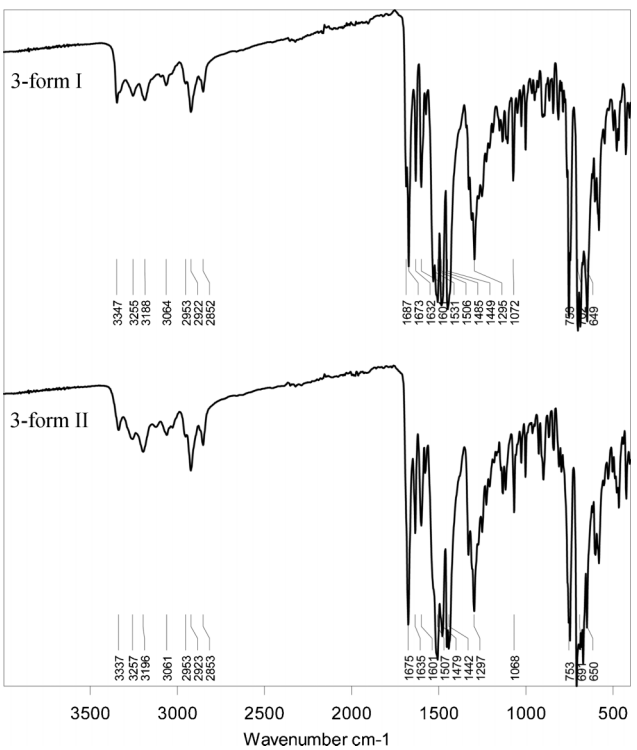

Fig. 6 IR spectra of the polymorphic forms of the pyridine variant **3**.

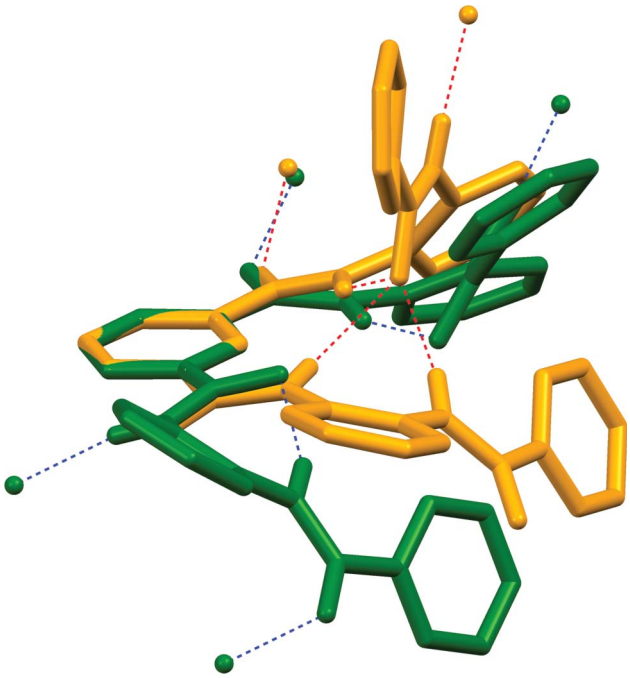

Fig. 7 Overlaid structures of the benzene variant **2**, **2**-form I (green), and the pyridine variant **3**, **3**-form I (yellow). The hydrogen bonds of the benzene variant are shown in blue and the bonds of the pyridine variant are shown in red. Non-contact hydrogen atoms have been omitted for clarity.

that all of its carbonyl groups are in a more similar environment. **3**-form II is formed from evaporation crystallizations from DCM and MeCN. TGA-DTA measurement confirmed that the **3**-form II is indeed a polymorph and not a solvate (ESI†).

Structural comparison of the compounds

The differences in the molecular conformations and the crystal structures of the benzene and pyridine variant are significant despite the very small difference in their molecular structure (Fig. 7). The exchange of the central phenyl ring to a pyridine ring causes a drastic change from a relatively loose molecular conformation to a more folded structure with a unique hydrogen bond pattern of five intramolecular hydrogen bonds, three of which are to the same carbonyl group. The benzene variant **2**, on the other hand, has only two intramolecular hydrogen bonds. The hydrogen bonds of the benzene variant **2** are more evenly distributed resulting in a structure that has no unused hydrogen bond donors or acceptors. Whereas the pyridine variant **3**, because of its many hydrogen bonds to single carbonyl oxygen, has two unused strong hydrogen bond acceptors (Fig. 7). Because of the different intramolecular hydrogen bond patterns the chains of molecules of the benzene variant **2** are held together by two intermolecular hydrogen bonds for each molecule and the chains of the pyridine variant **3** only by one.

Conclusions

Two new potential oligoamide foldamers, the benzene and the pyridine variants, were prepared and their solid-state structures were analyzed using various crystallographic and spectroscopic methods. For the benzene variant **2** four crystal forms, either polymorphs or solvates, were found and three structures were solved using single crystal X-ray diffraction. All the crystal structures of the benzene variant **2** consist of molecular chains formed by two intermolecular hydrogen bonds, where all the hydrogen bond acceptor and donor groups in the molecule are in efficient use.

For the pyridine variant **3** eight different polymorphs or solvates were found and the single crystal structures of seven of these were solved. Six of the forms are solvates: the **3**-DMSO solvate and the isomorphous **3**-MeOH and **3**-EtOH solvates, in which the solvent forms a hydrogen bond with the pyridine variant **3**; the isomorphous **3**-EtOAc and **3**-toluene solvates; and the **3**-DMF solvate, in which the solvent does not hydrogen bond with the pyridine variant, but interacts with compound **3** molecules by van der Waals interactions and possibly weak hydrogen bonds.

The molecular conformation of the pyridine variant **3** in all crystal structures (except in the **3**-DMSO solvate) consists of a unique hydrogen bonding pattern, where three of the N–H groups of each molecule form hydrogen bonds to the same carbonyl group. This leaves two unused hydrogen bond acceptors, which makes the pyridine variant **3** a good candidate for further co-crystallization experiments with compounds that have strong hydrogen bond donor groups. In addition, this type of multiple hydrogen bonding to a single carbonyl oxygen also indicates a possible catalytic effect on the carbonyl group of the compound.

Acknowledgements

M.Sc. Jussi Ollikka, B.Sc Hélène Campos Barbosa and B.Sc. Miia-Elina Puranen are thanked for the help with the synthesis and crystallization. We would also like to thank Spec. Lab. Technician Mirja Lahtiperä for measuring the ESI-TOF mass spectra, Spec. Lab. Technician Elina Hautakangas for the elemental analysis, Spec. Lab. Technician Reijo Kauppinen for measuring the ^{1}H, ^{13}C, COSY, HMBC and HMQC NMR spectra and Spec. Lab. Technician Esa Haapaniemi for measuring the NOESY NMR spectra.

References

1 E. Arunan, G. R. Desiraju, R. A. Klein, J. Sadlej, S. Scheiner, I. Alkorta, D. C. Clary, R. H. Crabtree, J. J. Dannenberg, P. Hobza, H. G. Kjaergaard, A. C. Legon, B. Mennucci and D. J. Nesbitt, *Pure Appl. Chem.*, 2011, **83**, 1637.
2 C. B. Aakeröy and N. Schultheiss, in *Making Crystals by Design*, ed. D. Braga and F. Grepioni, WILEY-VCH Verlag GmbH & Co. KGaA, Weinheim, Germany, 2007, pp. 209.
3 A. R. Fersht, J.-P. Shi, J. Knill-Jones, D. M. Lowe, A. J. Wilkinson, D. M. Blow, P. Brick, P. Carter, M. M. Y. Waye and G. Winter, *Nature*, 1985, **314**, 235.
4 P. M. Pihko, S. Rapakko and R. K. Wierengain *Hydrogen Bonding in Organic Synthesis*, ed. P.M. Pihko, WILEY-VCH Verlag GmbH & Co. KGaA, Weinheim, Germany, 2009, p. 43.
5 C. N. Fuhrmann, M. D. Daugherty and D. A. Agard, *J. Am. Chem. Soc.*, 2006, **128**, 9086.
6 C. Martinez, A. Nicolas, H. van Tilbeurgh, M.-P. Egloff, C. Cudrey, R. Verger and C. Cambillau, *Biochemistry*, 1994, **33**, 83.
7 J. Bernstein, *Polymorphism in Molecular Crystals*, Oxford University Press, United States, 2002.
8 U. J. Griesser in *Polymorphism in the Pharmaceutical Industry*, ed. R. Hilfiker, WILEY-VCH Verlag GmbH & Co. KGaA, Weinheim, Germany, 2006, p. 211.

9 S. H. Gellman, *Acc. Chem. Res.*, 1998, **31**, 173.
10 D. J. Hill, M. J. Mio, R. B. Prince, T. S. Hughes and J. S. Moore, *Chem. Rev.*, 2001, **101**, 3893.
11 J. Zhu, R. D. Barra, H. Zeng, E. Skrzypczak-Jankun, X. C. Zeng and B. Gong, *J. Am. Chem. Soc.*, 2000, **122**, 4219.
12 R. R. Araghi and B. Koksch, *Chem. Commun.*, 2011, **47**, 3544.
13 P. Claudon, A. Violette, K. Lamour, M. Decossas, S. Fournel, B. Heurtault, J. Godet, Y. Mély, B. Jamart-Grégoire, M.-C. Averlant-Petit, J.-P. Briand, G. Duportail, H. Monteil and G. Guichard, *Angew. Chem., Int. Ed.*, 2010, **49**, 333.
14 C. Baldauf, R. Günther and H.-J. Hofmann, *J. Org. Chem.*, 2006, **71**, 1200.
15 Y. Hamuro, S. J. Geib and A. D. Hamilton, *J. Am. Chem. Soc.*, 1996, **118**, 7529.
16 Y. Hamuro, S. J. Geib and A. D. Hamilton, *J. Am. Chem. Soc.*, 1997, **119**, 10587.
17 V. Berl, I. Huc, R. G. Khoury and J.-M. Lehn, *Chem.–Eur. J.*, 2001, **7**, 2798.
18 V. Berl, I. Huc, R. G. Khoury and J.-M. Lehn, *Chem.–Eur. J.*, 2001, **7**, 2810.
19 I. Huc, V. Maurizot, H. Gornitzka and J.-M. Léger, *Chem. Commun.*, 2002, 578.
20 B. Baptiste, J. Zhu, D. Haldar, B. Kauffmann, J.-M. Léger and I. Huc, *Chem.–Asian J.*, 2010, **5**, 1364.
21 H. Jiang, J.-M. Léger and I. Huc, *J. Am. Chem. Soc.*, 2003, **125**, 3448.
22 E. R. Gillies, C. Dolain, J.-M. Léger and I. Huc, *J. Org. Chem.*, 2006, **71**, 7931.
23 N. Delsuc, J.-M. Léger, S. Massip and I. Huc, *Angew. Chem., Int. Ed.*, 2007, **46**, 214.
24 D. Sánchez-Garcia, B. Kauffmann, T. Kawanami, H. Ihara, M. Takafuji, M.-H. Delville and I. Huc, *J. Am. Chem. Soc.*, 2009, **131**, 8642.
25 Y. Ferrand, A. M. Kendhale, J. Garric, B. Kauffman and I. Huc, *Angew. Chem., Int. Ed.*, 2010, **49**, 1778.
26 PANalytical B.V., 2006, 2.2b.
27 G. M. Sheldrick, *Acta Crystallogr., Sect. A*, 2008, **64**, 112.
28 Z. Otwinowski, D. Borek, W. Majewski and W. Minor, *Acta Crystallogr., Sect. A: Found. Crystallogr.*, 2003, **59**, 228.
29 A. I. Kitaigorodsky, *Organic Chemical Crystallography*, Consultants Bureau, New York, 1961.
30 M. A. Spackman and J. J. McKinnon, *CrystEngComm*, 2002, **4**, 378.
31 (*a*) M. C. Etter and J. C. MacDonald, *Acta Crystallogr., Sect. B: Struct. Sci.*, 1990, **46**, 256; (*b*) J. Bernstein, R. E. Davis, L. Shimoni and N.-L. Chung, *Angew. Chem., Int. Ed. Engl.*, 1995, **34**, 1555.
32 X. Bao and Y. Zhou, *Sens. Actuators, B*, 2010, **147**, 434.

II

FOLDING PATTERNS IN A FAMILY OF OLIGOAMIDE FOLDAMERS

by

Minna Kortelainen, Aku Suhonen, Andrea Hamza, Imre Pápai, Elisa Nauha, Sanna Yliniemelä-Sipari, Maija Nissinen & Petri M. Pihko, 2015

Chem. Eur. J., **2015**, *21*, 1096-1099

ChemPubSoc Europe

DOI: 10.1002/chem.201406521

CHEMISTRY
A European Journal
Full Paper

Conformation Analysis

Folding Patterns in a Family of Oligoamide Foldamers

Minna Kortelainen,[a] Aku Suhonen,[a] Andrea Hamza,[b] Imre Pápai,*[b] Elisa Nauha,[a] Sanna Yliniemelä-Sipari,[a] Maija Nissinen,*[a] and Petri M. Pihko*[a]

Abstract: A series of small, unsymmetrical pyridine-2,6-dicarboxylamide oligoamide foldamers with varying lengths and substituents at the end groups were synthetized to study their conformational properties and folding patterns. The @-type folding pattern resembled the oxyanion-hole motifs of enzymes, but several alternative folding patterns could also be characterized. Computational studies revealed several alternative conformers of nearly equal stability. These folding patterns differed from each other in their intramolecular hydrogen-bonding patterns and aryl–aryl interactions. In the solid state, the foldamers adopted either the globular @-type fold or the more extended S-type conformers, which were very similar to those foldamers obtained computationally. In some cases, the same foldamer molecule could even crystallize into two different folding patterns, thus confirming that the different folding patterns are very close in energy in spite of their completely different shapes. Finally, the best match for the observed NOE interactions in the liquid state was a conformation that matched the computationally characterized helix-type fold.

Introduction

The oxyanion hole is perhaps one of the most studied motifs in the active sites of enzymes.[1,2] Oxyanion holes stabilize high-energy intermediates and transition states that bear negatively charged oxygen atoms in enzymatic reactions that involve tetrahedral intermediates (e.g., hydrolytic cleavage reactions of (thio)esters and amides) and reactions that involve enolate intermediates.[2] In both cases, a charge builds up on the carbonyl oxygen atom on the way to a negatively charged intermediate, such as a tetrahedral intermediate or an enolate ion.[2]

In the realm of small-molecule catalysis, hydrogen-bond donors, such as (thio)urea and squaramide functionalities, could be viewed as analogues of the oxyanion holes.[3] These functionalities are relatively rigid and flat two-point hydrogen-bond donors. In contrast, the oxyanion holes in enzymes are three-dimensional, with two, or even three, hydrogen-bond donors that stabilize the charge at the oxyanion. The hydrogen-bond donors that comprise the oxyanion hole are separated by rotatable bonds of the amino acids. As such, mimicking the hydrogen-bond donor patterns of oxyanion holes with simple peptides might be extremely challenging due to the flexibility of the peptide backbone. However, peptide-type foldamers[4] that bear more rigid subunits[5] might offer better possibilities for folding into oxyanion-hole-type conformations. A variety of rigid aromatic oligomers composed of, for example, pyridine-2,6-carboxamide,[6] anthranilamide,[7] quinoline,[8] quinoxalene,[9] and other aryl–amide monomers,[10] have been studied since the 1990s. Still, only scattered examples of non-peptidic structures in which amide or ester carbonyl groups act as multiple hydrogen-bond acceptors have previously been described,[11] and foldamers that bear oxyanion-hole-type structures have not been systematically studied at all. In the previous examples of oligomers, the emphasis was placed on control of the folding properties, governed mainly by the repeating hydrogen-bond patterns[5–10] and aromatic interactions, which were adjusted by varying the functionalization of the aromatic rings.[10a] In many cases, the foldamers also contained an interior cavity of varying size at the center of the fold instead of a tight fold stabilized by multiple interactions.[5c–e]

Herein, we show that simple unsymmetrical pyridine-2,6-dicarboxylamide-derived oligoamides can adopt several alternative conformers (folding patterns, or in short folds) of nearly equal stability. Importantly, one of these conformers, observed in both the solid and liquid states, has two or even three NH groups hydrogen bonded to the terminal amide carbonyl group, thus closely resembling an oxyanion-hole motif. Although the amide carbonyl group is not an oxyanion in the classical Lewis sense, it is important to note that the oxygen

[a] M. Kortelainen,[+] A. Suhonen,[+] Dr. E. Nauha, Dr. S. Yliniemelä-Sipari, Prof. Dr. M. Nissinen, Prof. Dr. P. M. Pihko
Department of Chemistry, Nanoscience Center
University of Jyväskylä
P.O. Box 35, 40014 JYU (Finland)
Fax: (+358) 14-260-2501
E-mail: papai.imre@ttk.mta.hu
maija.nissinen@jyu.fi
petri.pihko@jyu.fi

[b] Dr. A. Hamza, Dr. I. Pápai
Institute of Organic Chemistry
Research Center for Natural Sciences
Hungarian Academy of Sciences
Magyar Tudósok Körútja 2, 1117, Budapest (Hungary)

[+] These authors contributed equally to this work.

Supporting information for this article is available on the WWW under http://dx.doi.org/10.1002/chem.201406521.

atom of the amide carbonyl unit already bears a substantial charge; that is, the net atomic charge (Q(O)) in *N*-methylacetamide is −0.65, whereas the corresponding value for *S*-methylthioacetate enolate is −0.77.[12] In other words, the amide group can be viewed at least as a crude mimic of the enolate anion.[12] As such, the search for foldamers that can stabilize oxyanions might well start with systems that bear an amide group that is intramolecularly hydrogen bonded through its carbonyl oxygen atom to multiple hydrogen-bond donors.

The point of departure of the present study was the single-crystal X-ray structure previously described by three of us,[13] in which one of the amide carbonyl groups is hydrogen bonded to three other amide NH groups (Figure 1). The structure of

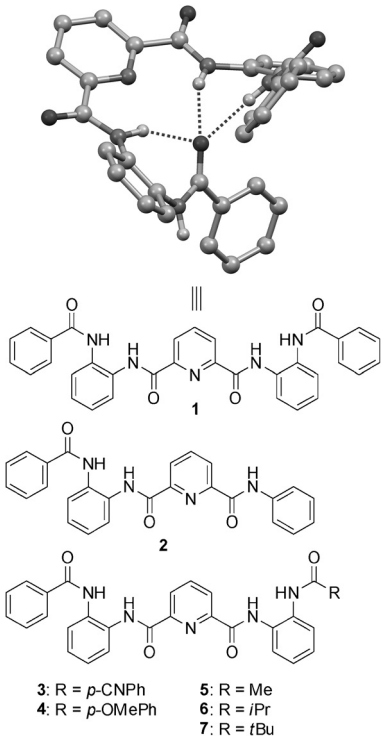

Figure 1. Structure of foldamer **1**[13] and schematic presentation of unsymmetrical derivatives **2**–**7**. The solvated EtOH molecule and non-hydrogen-bonding hydrogen atoms have been omitted for clarity from the X-ray structure (top).

1 raised hopes that similar motifs could be used as triple hydrogen-bonding oxyanion-hole motifs,[3b] but the stability and possibility of alternate conformers that were energetically as favorable have remained open questions. To address these questions, we embarked on a more comprehensive study of a family of foldamers, including the original foldamer **1**. By using a combination of computational and X-ray crystallographic studies, we show that **1** and related asymmetric foldamers **2**–**7** indeed adopt structures similar to the original structure of **1**, but alternate folds that are close in energy in the gas phase can also be experimentally characterized.

Results and Discussion

The present study involved the synthesis of unsymmetrical oligopeptide foldamers **2**–**7**, conformational analysis of the foldamers by means of computational studies, and structural characterization by X-ray crystallography and solution-phase NMR spectroscopic measurements.

Synthesis of unsymmetrical foldamers

For the synthesis of unsymmetrical foldamers **2**–**7**, monofunctionalized versions of the core building blocks pyridine-2,6-dicarboxylic acid and 1,2-diaminobenzene **8** were required (see Scheme 1). Monoprotected pyridine-2,6-dicarboxylic acid **14** was readily prepared by using the method developed by Schmuck and Machon.[14] Monoacylation of **8** could be achieved directly with HOBt/EDC coupling, but better results were obtained for aliphatic carboxylic acids when 2-nitroaniline **11** was used as a starting material (alternative 1, Scheme 1), followed by reduction of the resulting nitroanilide **12**. Standard HOBt/EDC coupling reactions could be used to assemble the oligoamide framework from **14** and **10** in two steps (Scheme 1).

Six different unsymmetrical foldamers were synthesized. The simplest foldamer **2** possessed only three amide linkages instead of four (Figure 1). Others were variants of **1** (R = Ph) with different side chains, namely, two different aryl rings (R = *p*-NC-Ph (**3**) and *p*-OMe-Ph (**4**)) and three different aliphatic side chains (R = Me (**5**), R = *i*Pr (**6**), or R = *t*Bu (**7**)) to probe the electronic and steric effects of the folding process.

Computational studies

A computational analysis for a set of foldamers was performed with the main aim of identifying the nature of the stabilizing interactions that govern the conformational distribution of these compounds. An extensive conformational search was carried out by using a combination of MM and DFT methods. Geometry optimizations, vibrational analysis, and an estimation of the solvent effects were carried out at the ωB97X-D/6-311G(d,p) level of theory; however, the electronic energies were further refined by additional single-point-energy calculations with the extended 6-311++G(3df,3pd) basis set. The relative stabilities were analyzed in terms of gas-phase Gibbs free energies. Further details of the applied methodology are provided in the Computational Approach section.

Three different conformers (folds) could be computationally identified for the simplest truncated foldamer **2**. The optimized structures and their relative stabilities are shown in Figure 2. For the clarity of further discussion, the identified folds were classified as follows:

1) The fold in which the outer carbonyl group serves as a hydrogen-bond acceptor, that is, a focal point around which the rest of the structure folds, is called the @-fold.
2) The fold in which the hydrogen-bond formed between an inner carbonyl group and the adjacent amide NH unit en-

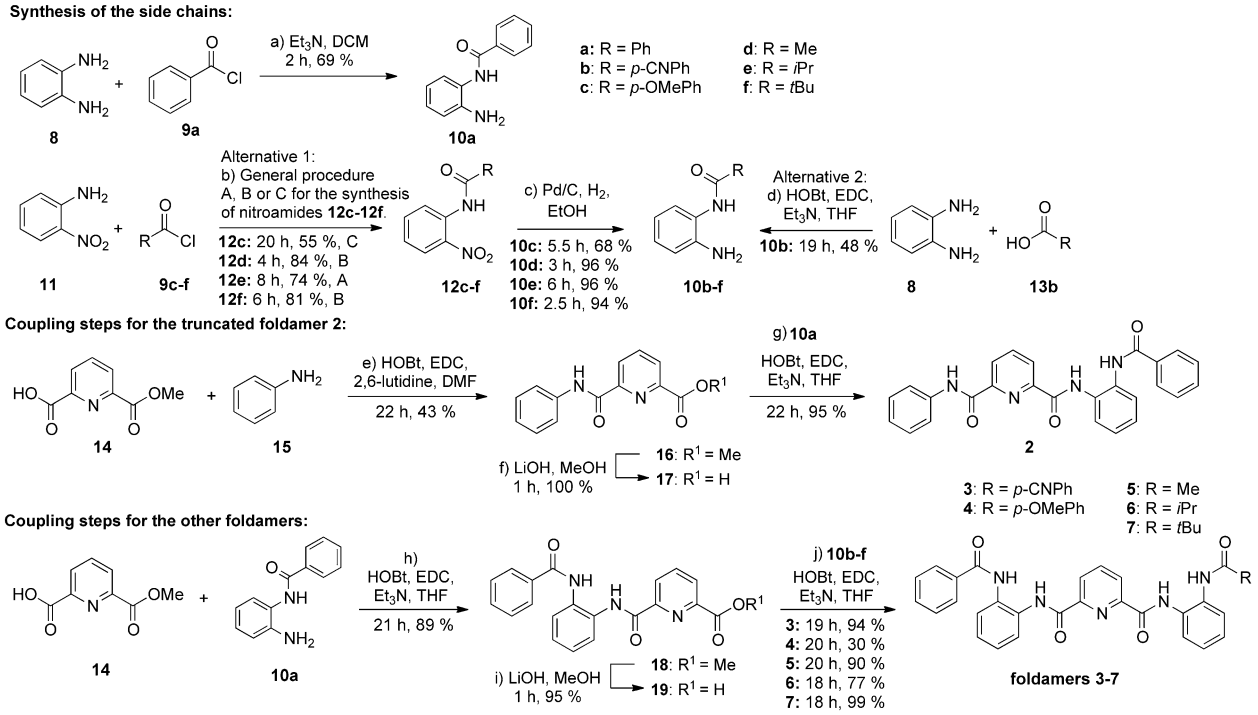

Scheme 1. Synthesis of unsymmetrical foldamers **2**–**7** (see the Experimental Section for details). EDC = *N*′-(3-dimethylaminopropyl)-*N*-ethylcarbodiimide, HOBt = 1-hydroxybenzotriazole.

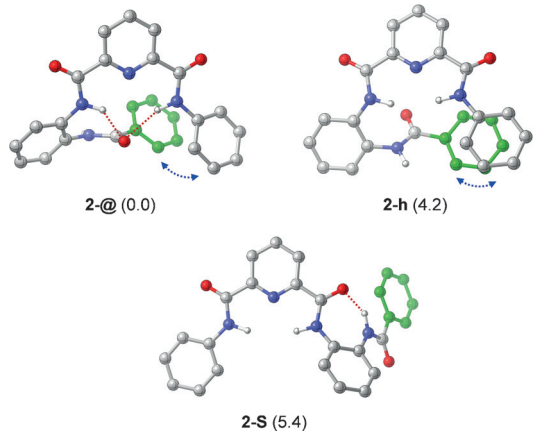

Figure 2. Optimized structures of the conformers identified computationally for foldamer **2**. The relative stabilities are shown in parenthesis (in kcal mol^{-1}). Intramolecular hydrogen bonds are indicated by dotted lines and aromatic interactions are highlighted by blue arrows. The CH hydrogen atoms have been omitted for clarity. Note: hydrogen bonds to the pyridine nitrogen atoms have been omitted for clarity in all the structures.

forces a turn that results in an S-shaped molecule is called the S-fold.

3) The remaining conformer is referred to as an h-fold based on its helical shape.

Conformer **2**-@ is predicted to be the most stable form, which is clearly separated from the other two forms in free energy. This structure is stabilized by a double hydrogen bond. The van der Waals contact between the terminal phenyl groups is also apparent, but the aromatic rings are somewhat displaced from the optimal parallel arrangement. No hydrogen bonds are present in structure **2-h**, which lies 4.2 kcal mol^{-1} above **2**-@ in free energy. This structure is stabilized by aromatic-stacking interactions. In the third structure (**2-S**), only a single hydrogen bond that involves one of the inner carbonyl groups provides intramolecular stabilization. Conformer **2-S** is computed to be at 5.4 kcal mol^{-1} in free energy.

For the symmetrical foldamer **1**, four different low-lying conformers that feature multiple hydrogen bonds and aromatic interactions could be identified (Figure 3). The structures of **1-S**, **1**-@, and **1**-@′ are analogous to **2**-@ in the central hydrogen-bonding pattern, but **1-S** has a turn as a result of a terminal hydrogen bond. The two @ conformers (**1**-@ and **1**-@′) have very similar folded shapes, but they differ in the number of hydrogen bonds (i.e., three and two, respectively) and also in the orientation of the terminal phenyl groups. Conformer **1-h** can be derived from **2-h**. Calculations predict **1-S** to be the most favored form; however, the other conformers are at the most 1.3 kcal mol^{-1} less stable. Aryl–aryl interactions seem to provide additional stabilization in all these structures (highlighted in Figure 3). In conformer **1-h**, both terminal phenyl groups are involved in an aromatic-stacking interaction that results in a compact helix structure that lies only 0.4 kcal mol^{-1} above **1-S**. Unlike in structure **2-h**, hydrogen-bonding interactions can also be identified in conformer **1-h**. An additional conformer with two turns that lead to a W-shape structure could also be located on the potential-energy surface (**1-W** in Figure 3). This conformer is far less stable than the other forms, which is relat-

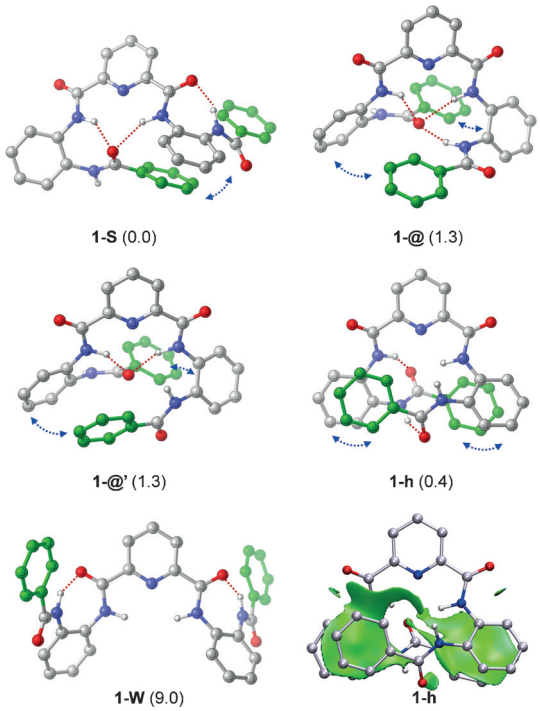

Figure 3. Optimized structures of the conformers identified computationally for foldamer **1** and an NCI plot generated for structure **1 h**. Characteristic van der Waals contacts are represented by the green regions. An applied cutoff for the gradient is 0.3 au.

ed to the absence of oxyanion-type hydrogen-bonding and aromatic-stacking interactions in **1-W**.

Thus, these computational results confirm that the conformational distribution of oligoamides **1** and **2** is primarily governed by N—H···O type hydrogen bonds, but these results also point to stabilizing effects due intramolecular van der Waals contacts between the aromatic rings. For an illustration of these latter noncovalent interactions (NCIs), we generated a reduced gradient (RDG) isosurface plot for structure **1-h** by using the method developed by Yang and co-workers.[15,16] The NCI plot depicted in Figure 3 indeed displays broad contact areas between the interacting aryl groups.

The strength and the balance of these noncovalent forces can be notably altered by introducing various substituents at the *para* position of the terminal phenyl group, as exemplified by foldamers **3** and **4**. The conformers of molecules **3** and **4** were derived from the conformers of the symmetrical foldamer **1**, and these conformers were all subjected to geometry optimization. Each conformer of **1** gives rise to a pair of folds that differ in the position of the substitution. Thus, additional labeling to distinguish the two types of unsymmetrical conformer is introduced: labels S_1, $@_1$, $@'_1$, and h_1 refer to conformers in which the carbonyl oxygen atom adjacent to the substituted phenyl end serves as the central hydrogen-bond acceptor, whereas S_2, $@_2$, $@'_2$, and h_2 correspond to conformers in which the hydrogen-bond acceptor is next to the unsubstituted phenyl group. The relative stabilities of these two conformers may vary appreciably, as shown by the relative Gibbs free energies of various conformers for foldamers **1**, **3**, and **4** in Table 1.

Table 1. Relative stabilities of various forms of foldamers **1**, **3**, and **4**.[a]

Conformers	Foldamer **1**	Foldamer **3**	Foldamer **4**
S	0.0	0.0 (S_2)	0.0 (S_1)
		2.5 (S_1)	1.6 (S_2)
@	1.3	3.4 ($@_2$)	2.5 ($@_1$)
		–[b]	3.4 ($@_2$)
@′	1.3	0.7 ($@'_2$)	2.4 ($@'_2$)
		3.3 ($@'_1$)	2.4 ($@'_1$)
h	0.4	0.2 (h_1)	0.9 (h_2)
		1.4 (h_2)	1.2 (h_1)

[a] Reported data are relative Gibbs free energies (in kcal mol^{-1}) with respect to the most stable conformer. [b] Only a single structure could be identified computationally in this particular case (optimization converged to conformer **3 h** for the other structural variant).

For instance, the preferred conformer for foldamer **3** is **3-S_2**, with a cyano group on the phenyl ring that does not take part in the aryl–aryl interaction (Figure 4). The alternative folding pattern (i.e., **3-S_1**) with a cyano group at the opposite terminus yields a less stable structure by 2.5 kcal mol^{-1}. On the other hand, the order of relative stabilities of these two conformers is reversed for foldamer **4**, and these stabilities differ by 1.6 kcal mol^{-1} (**4-S_1** is shown in Figure 4). The observed variations in the relative stabilities of these conformers can be associated with the electronic properties of the CN and OMe substituents, which strengthen or weaken the hydrogen-bonding interactions in the proximity of the substituents and likely affect the nature of the aromatic interactions as well. Similar effects are also expected for the other classes of fold. Interestingly, the $@_1$-type conformer of foldamer **3** is spontaneously transformed into conformer **3-h_1** upon geometry optimization, and its structural counterpart (i.e., **3-$@_2$**) is predicted to be relatively high in free energy (at 3.4 kcal mol^{-1}).

Computational studies were carried out for foldamers **5** and **7** with methyl and *tert*-butyl groups replacing one of the terminal phenyl groups in foldamer **1**, respectively. The geometry optimizations indeed yielded structures analogous to **1** (Figure 4). The conformers of unsymmetrical foldamers **5** and **7** can be classified into the same categories as introduced above. Thus, the fold labels S_1, $@_1$, $@'_1$, and h_1 refer to conformers in which the carbonyl group next to the Ph→R replacement is involved in the central hydrogen-bonding interaction, and S_2, $@_2$, $@'_2$, and h_2 refer to folds in which the hydrogen-bond acceptor is next to the unsubstituted phenyl group.

The computational data also reveal that the S_2 conformers are the most stable forms of these foldamers, but the other folds are typically higher in free energy by only 1–2 kcal mol^{-1} (Table 2). On the basis of the electron-donating nature of the Me and *t*Bu alkyl groups, particular stabilization for conformers with these groups next to the central hydrogen-bonding pattern is expected. This outcome is indeed the case for @-conformers (the $@_1$ forms are favored). However, the computational studies predict the S_2 and $@'_2$ variants to be more favorable for the S and @′ folds (Figure 4). These results suggest that the electronic-stabilization effects are counterbalanced by the loss of the aromatic interactions upon the Ph→R replacement. The

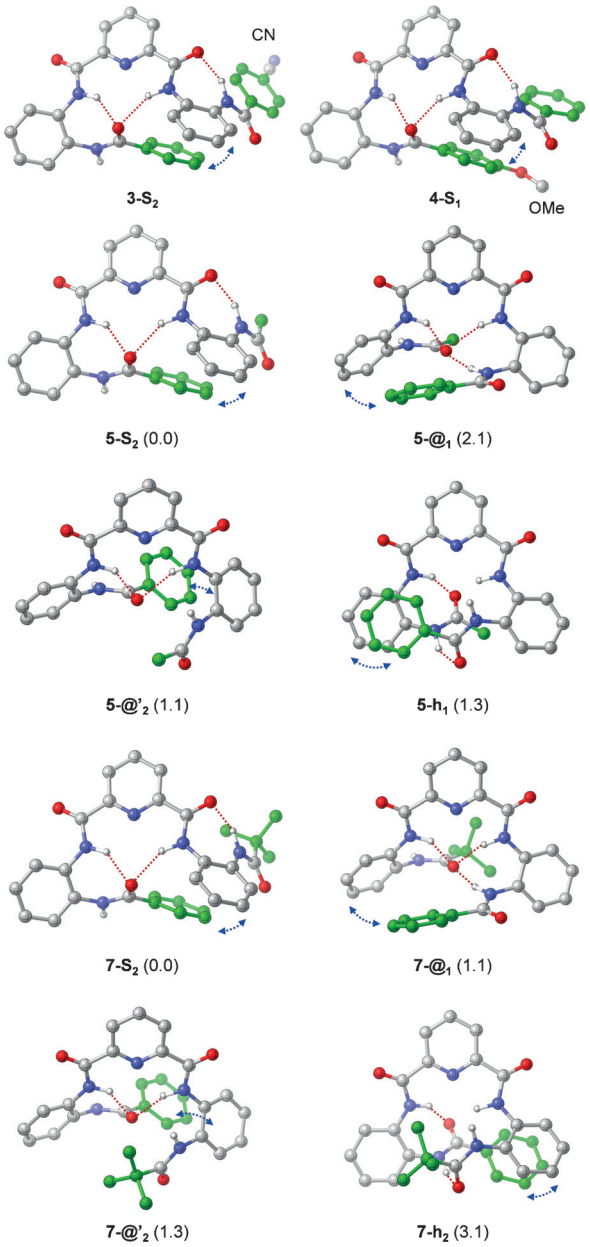

Figure 4. Most stable conformers of foldamers **3**–**5** and **7**.

Table 2. Relative stabilities of various forms of foldamers **1**, **5**, and **7**.[a]

Conformers	Foldamer **1**	Foldamer **5**	Foldamer **7**
S	0.0	0.0 (S_2)	0.0 (S_2)
		2.0 (S_1)	1.2 (S_1)
@	1.3	2.1 ($@_1$)	1.1 ($@_1$)
		2.7 ($@_2$)	1.8 ($@_2$)
@′	1.3	1.1 ($@'_2$)	1.3 ($@'_2$)
		2.2 ($@'_1$)	1.5 ($@'_1$)
h	0.4	1.3 (h_1)	2.3 (h_2)
		2.2 (h_2)	3.1 (h_1)

[a] Reported data are relative Gibbs free energies (in kcal mol^{-1}) with respect to the most stable conformer.

relative stabilities of the less favored conformers of **5** and **7** vary only slightly with respect to those of the original symmetrical molecule and stay within a narrow energy range relative to the most stable forms.

Solid-state conformations

Single-crystal structures were obtained for all the foldamers, except for the methoxyphenyl derivative **4**. For foldamers **2**, **3**, and **6**, both structures with the @ and S conformers were obtained equally by crystallization under various conditions (Table 3 and Figure 5). Although computational studies showed only a slight difference in stability toward the h conformation, the latter was not observed in the solid state. Typically, the @ conformer was obtained in unsolvated structures with no solvent included in the crystal lattice, whereas the S conformer was observed both in the solvates and unsolvated structures, with a preference for the solvates.

Table 3. Conformers of foldamers **1**–**7** in the XRD structures.[a]

Foldamer	@ Conformation	**S** Conformation
1[13]	**1**-$@_2$-EtOH	–
2	**2**-@-Form I	**2**-**S**-MeCN
	2-@-**S**-DMF	
3	**3**-$@_2$-Form I	**3**-S_1-EtOAc
4	–	–
5	–	**5**-S_1-Form I
6	**6**-$@_2$-Form I	**6**-S_1-Form II
7	–	**7**-S_2-Form I

[a] Forms I and II denote polymorphic crystal forms and a solvent molecule indicates a solvate structure.

The solid-state conformers are very similar to those conformers identified computationally. This finding can be visually assessed from the overlay structures (Figure 5 a, e, and j), in which the computationally derived and X-ray structures display closely related geometries and hydrogen-bonding patterns.[17] Similar to the computed structures, the @ conformers are each stabilized by two or three hydrogen bonds to the C=O group of the outer phenyl ring. The S conformers are always stabilized by an intramolecular hydrogen bond between an outer NH group and an inner C=O group. Additionally, two intramolecular hydrogen bonds to a C=O group of the outer phenyl ring contribute to the stability of the S fold, except for the truncated foldamer **2**, in which such hydrogen bonding is not possible. The biggest difference in the computational and crystal structures is seen in the aryl–aryl interactions of the @ conformers, which played a significant role in the computational structures. In the solid state, however, intramolecular aryl–aryl interactions, although present, are not as significant (see the overlay in Figure 5 a, j for examples).

In general, the folds observed in the solid state are slightly looser relative to those folds obtained computationally. This situation could either be related to crystal-packing forces or

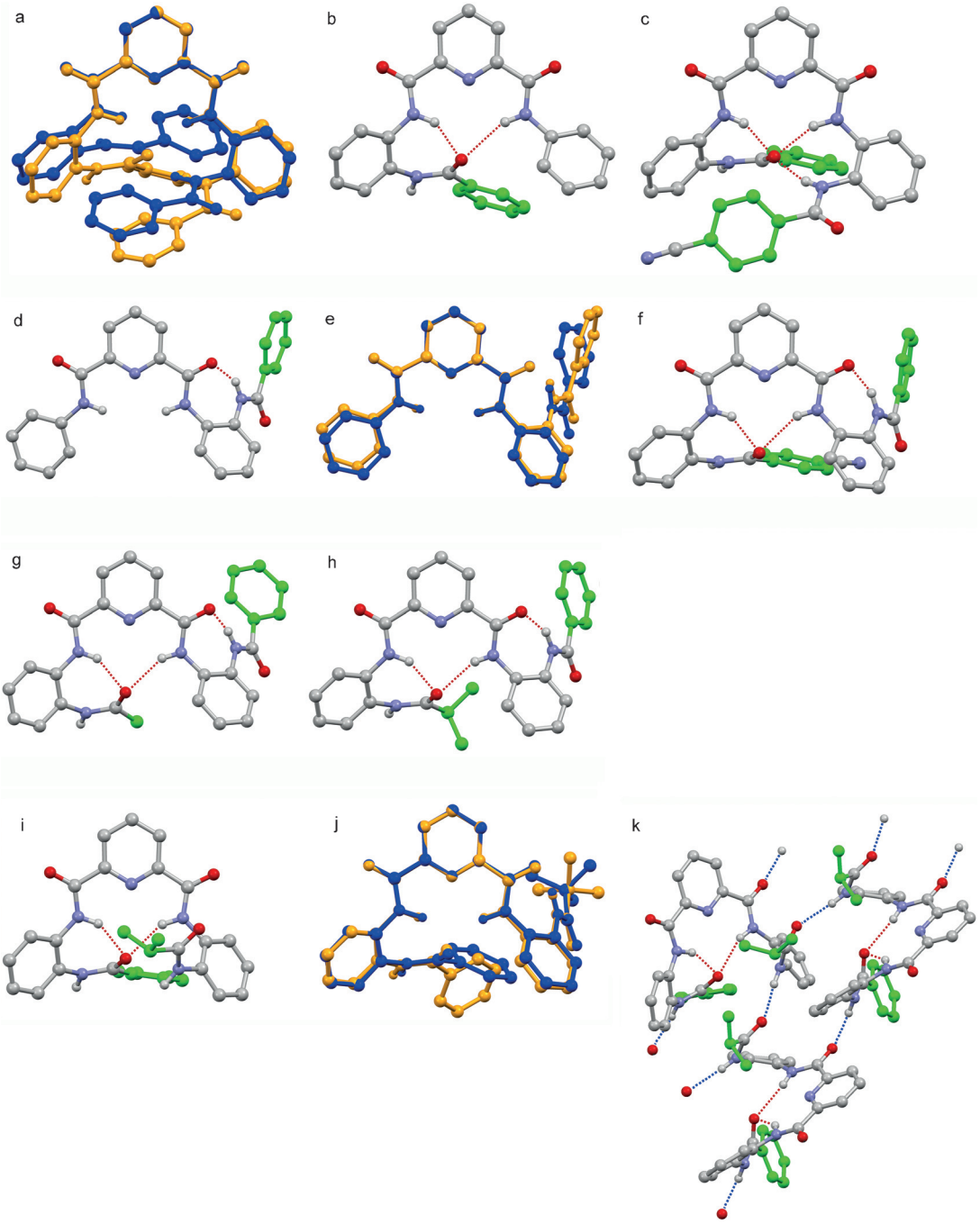

Figure 5. First row: a) An overlay structure of the calculated @ conformation (blue; see Figure 3) and the @ conformation in the XRD structure of an EtOH solvate of foldamer **1** (orange, from reference [6a]), b) XRD structure of foldamer **2** in the @ conformation (**2**-@-Form I), c) XRD structure of foldamer **3** in the $@_2$ conformation (**3**-$@_2$-Form I). Second row: d) XRD structure of foldamer **2** in the S conformation (**2**-**S**-MeCN), e) an overlay structure of the calculated **S**-conformation (**2**-**S**, blue; see Figure 2) and the XRD structure of foldamer **2** in the S conformation (**2**-**S**-MeCN, orange), and f) XRD structure of foldamer **3** in the S_1 conformation (**3**- $\mathbf{S_1}$-EtOAc).Third row: XRD structures of g) foldamer **5** in the S_1 conformation (**5**-$\mathbf{S_1}$-Form I), h) foldamer **6** in the S_1 conformation (**6**-$\mathbf{S_1}$-Form II). Fourth row: i) foldamer **6** in the @ conformation (**6**-$@'_2$-Form I), and j) an overlay structure of the calculated S_2 conformation (**7**-$\mathbf{S_2}$, blue; Figure 2) and XRD structure of foldamer **7** in the S_2 conformation (**7**-$\mathbf{S_2}$-Form I, orange), k) crystal-packing structure of foldamer **6** in the $@'_2$ conformation (**6**-$@'_2$-Form I). The intramolecular hydrogen bonds are presented in red and the intermolecular hydrogen bonds in blue. The non-amide hydrogen atoms and hydrogen bonds to the pyridine nitrogen atoms have been omitted for clarity.

the present computational method may slightly overestimate the strength of the aryl–aryl interactions. In analogy with the computationally identified structures, two different types of S conformer could also be characterized in the solid state, whereas the @ conformers were always of the $@_2$ type.

In the solid-state structures obtained so far, foldamer **1** always adopted the standard @ conformer (Figure 5).[13] The aromatic interactions described in the calculations are also seen in the solid-state structure of **1**, but the relative positions of the interacting aryl groups are different (i.e., the distances

of the centroids are fairly long; see Figure 5a and the Supporting Information).

The truncated foldamer **2**, a special case among the series due to its diminished hydrogen-bonding possibilities, can still adopt both @ and S conformations in the solid state (Figure 5), although calculations indicate a preference for the @ conformation. In the calculated structure, the orientation of the end aryl groups is slightly displaced parallel, whereas the orientation in the solid state is T-shaped.[11]

Interestingly, foldamer **2** was the only foldamer that crystallized with both the @ and S conformer appearing within the same crystal structure. This scenario suggests that foldamer **2** is likely to populate both conformations in a solution in significant proportions.

As expected, the $@_2$ conformer is observed in the unsolvated crystal structure of foldamer **3** due to the electron-withdrawing cyano substituent (Figure 5). The aryl–aryl interactions within the $@_2$ conformer of **3** are very weak (Figure 5c). Although the computations predict that the S_2 fold is more stable for **3** than S_1 (Table 1), the S_1 conformer appears to be more accessible in the solid state (Table 3, entry 3) possibly because of the effect of the solvent in the crystal lattice; that is, two molecules of foldamer **3** adopt the S_1 fold and form a pair with a void big enough for partial solvent inclusion. This particular crystal form seems to be very stable because altogether four isomorphous solvate structures (in EtOAc, THF, $CHCl_3$, and DMA) have been obtained so far.[18]

Acetyl foldamer **5** also seems to prefer the $\mathbf{S}_1$ fold in the solid state exclusively (Figure 5), even in the unsolvated form, although the computational studies again predicted that the S_2 conformer is slightly more stable (see Table 2 and Figure 4). However, the energy difference in the computational results was relatively small (2 kcal mol^{-1}), thus indicating that these conformations are almost equally stable and that environmental factors during the crystallization may drive the conformation to either fold.

Isopropyl foldamer **6** crystallized as two unsolvated polymorphs, one with a loose $@'_2$ conformer and one that adopted an S_1 conformer (Figure 5). In contrast to the other @ conformers, the $@'_2$ conformer of **6** has only two intramolecular hydrogen bonds to a central hydrogen-bond acceptor. The third hydrogen bond from the outer amide group makes an intermolecular hydrogen bond to the adjacent molecule of **6**. This interaction may be because of a more efficient crystal-packing mode or because of the relatively large size of the isopropyl group, which prohibits tighter folding due to steric hindrance with one of the inner benzene rings. Aromatic interactions are also observed, but the distances are also fairly long in this case (Figure 5i). In the polymorphic structure of foldamer **6** with an S_1 conformer, there is no significant steric hindrance and the electron-rich carbonyl oxygen atom near the isopropyl group can form the two intramolecular hydrogen bonds.

The *tert*-butyl foldamer **7** was the only foldamer that crystallized with an S_2 conformer (Figure 5), which is in agreement with the computational studies. The crystal packing of this structure consists of molecular chains, and the large *tert*-butyl group fits better at the outer edge of the molecule in the S_2 conformer in this packing structure, whereas the large *tert*-butyl group in the inner part of the molecule in the S_1 conformer would hinder the formation of the intramolecular hydrogen-bonding network that is important to the stability of the packing structure.

In conclusion, the foldamers generally adopt solid-state conformers that are remarkably similar to those obtained in the computational studies. Interestingly, many of the foldamers (i.e., **2**, **3**, and **6**) crystallized in both @- and S-folded conformers, thus indicating that it is likely that both of these conformers are also present in solution and that the environment during the crystallization affects which conformer is formed in the solid state.

Solution-state studies (NMR)

For the solution-state studies, foldamer **5** was selected as a probing compound due to its good solubility in $CDCl_3$ and clear ^{1}H NMR spectrum with a well-separated CH_3 singlet from the aromatic and the N–H signals. Foldamers **1**–**4** only have good solubility in solvents with good hydrogen-bond donation (such as DMF or DMSO), and these solvents might disrupt the intramolecular hydrogen bonds of some of the folds.

The 2D NOESY and 1D NOE experiments of **5** in $CDCl_3$ clearly showed that the methyl protons correlate to all four N–H signals, whereas no correlation between the N–H groups and the pyridine ring was observed (see the Supporting Information for details). This finding indicates that a conformer in which all the N–H groups face inside the folded molecule, most likely an @ or h conformer, is populated in solution. In the S conformer, one of the N–H groups is too far from the methyl group to display a correlation with the CH_3 group.

NOE interactions show the best match of the computationally derived h conformer with a nonplanar arrangement of the three central aryl groups (Figure 6) because most of the correlations match well, and even the distances for the N–H–methyl group are in the correct order based on the observed NOE interactions (Table 4). These results indicate that, at least in $CDCl_3$, the acetyl foldamer seems to favor the h-like conformer or there is constant conformational variation in solution between the @, S, and other conformers, and that the averaged structure, on the NMR timescale, matches best with the h-like conformer. Such a conformational variation would

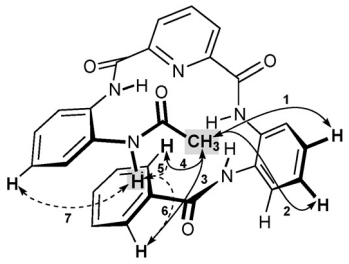

Figure 6. Schematic representation of the acetyl foldamer **5** in the h conformation. Key diagnostic NOE interactions from the acetyl CH_3 group (solid arrows) and from the acetamide N–H group (dashed arrows) are shown.

Table 4. Calculated key diagnostic NOE distances of **5**[a] and experimental NOE enhancement.

NOE interaction	C−H···H-N/H_3C [Å][b]	NOE enhancement [%][c]
1	4.628	0.08[d]
2	4.606	0.08[d]
3	4.758	0.05[e]
4	4.635	0.05[e]
5	3.208	0.95[f]
6	3.979	0.95[f]
7	4.610	0.52

[a] h conformer; see Figure 4. [b] The shortest distance to a Me hydrogen atom has been used when measuring the distances [c] See Figure 6 for labeling of the NOE interactions. [d]–[f] Same peaks.

enable the crystallization of the acetyl foldamer **5** in the S_1 conformation.

Conclusion

We have described herein the folding patterns of seven different oligoamide foldamers based on a 2,6-pyridinedicarboxamide core. In spite of seemingly minute variations in their structures, these foldamers have exhibited a remarkable variety in their folding patterns, as seen in the computationally derived gas-phase structures and in the solid-phase structures obtained by X-ray crystallography studies. Two major folds were identified in the gas and solid phases, the compact @ fold, which resembles an oxyanion-hole motif, and the more extended S fold. Both of these folds were characterized by three intramolecular hydrogen bonds. For some foldamers, both the @- and S-folded conformers could be characterized in the solid state, thus providing experimental confirmation that these conformers are close in energy. The computationally derived energies of these two folds were also within 1–2 kcal mol^{-1} for most of the foldamers. A third h fold, a helix, was characterized in the computational studies and was a likely alternative in solution for foldamer **5** with an *N*-acetyl terminus. Computational studies indicated that both hydrogen bonds and dispersion interactions (aryl–aryl or aryl–alkyl) are responsible for the stability of these folds. However, the aryl–aryl interactions in the crystal structures appear to be less significant, thus causing slightly looser conformers.

The fact that these conformationally very distinct folds are computationally so close in energy suggests that these foldamers could be used as conformational switches because they can readily attain at least two stable states. Studies toward understanding the dynamics of the folding and the effects of further substitution are in progress.

Experimental Section

All the reactions were carried out in an argon atmosphere in oven-dried glassware, except for the hydrolytic reactions. When needed, nonaqueous reagents were transferred under argon by syringe or cannula and dried prior to use. Dichloromethane, THF, and toluene were obtained by passing deoxygenated solvents through activated alumina columns (MBraun SPS-800 Series solvent purification system). MeOH, DMF, and pyridine were distilled and placed over molecular sieves (4 Å). The EtOH used in reduction reactions with Pd/C was placed over molecular sieves (4 Å). Other solvents and reagents were used as obtained from the supplier. Analytical TLC was performed on Merck silica gel 60 F_{254} (230–400 mesh) plates and analyzed with UV light and staining by heating with vanillin solution (vanillin (2.4 g), conc. H_2SO_4 (2 mL), conc. CH_3COOH (1.2 mL), absolute EtOH (100 mL)), anisaldehyde solution (anisaldehyde (2.8 mL), conc. H_2SO_4 (2 mL), conc. CH_3COOH (1.2 mL), absolute EtOH (100 mL)), or ninhydrin solution (ninhydrin (200 mg), absolute EtOH (95 mL), 10% CH_3COOH (5 mL)). For chromatography on silica gel, the flash chromatography technique was used with Merck silica gel 60 (230–400 mesh) and p.a. grade solvents.

The ^1H and ^{13}C NMR spectra were recorded in $CDCl_3$ or [D_6]DMSO on Bruker Avance 500 or 250 spectrometers. The chemical shifts are reported in ppm relative to $CHCl_3$ or [D_5]DMSO ($\delta = 7.26$ and 2.50 ppm, respectively) for the ^1H NMR spectra and to $CHCl_3$ or [D_5]DMSO ($\delta = 77.16$ and 39.52 ppm, respectively) for the ^{13}C NMR spectra. High-resolution mass-spectrometric data were measured on a MicroMass LCT spectrometer and the IR spectra were recorded on Bruker Tensor 27 FTIR spectrometer. Melting points (mp) were determined in open capillaries on a Stuart Scientific Melting Point Apparatus SMP3.

***N*-(2-Aminophenyl)benzamide (10a)**: Et_3N (2.6 mL, 18 mmol, 100 mol%) was added dropwise to a stirred solution of *ortho*-phenylenediamine (**8**; 4.00 g, 37 mmol, 200 mol%) in dichloromethane (100 mL) at room temperature. The solution was heated to reflux and benzoyl chloride (**9a**; 2.15 mL, 18 mmol, 100 mol%) in dichloromethane (80 mL) was added dropwise through a dropping funnel over 90 min. The solution was heated to reflux for 2 h and concentrated in vacuo. The residue was purified by flash chromatography (hexane/EtOAc 1:1) to afford amide **10a** (2.71 g, 69%) as a white solid.

R_f (hexane/EtOAc 55:45) = 0.37; mp 149–151 °C; IR (film): $\tilde{\nu} = 3401$, 3269, 3059, 1642, 1602, 1577, 1525, 1499, 1450, 1315, 1290, 748 cm^{-1}; ^1H NMR (500 MHz, [D_6]DMSO): $\delta = 9.64$ (s, 1H), 7.98 (d, 2H, $J = 7.3$ Hz), 7.59–7.56 (m, 1H), 7.53–7.50 (m, 2H), 7.18 (d, 1H, $J = 7.5$ Hz), 6.97 (td, 1H, $J_1 = 8.0$, $J_2 = 1.5$ Hz), 6.79 (dd, 1H, $J_1 = 8.0$, $J_2 = 1.5$ Hz), 6.60 (td, 1H, $J_1 = 7.$, $J_2 = 1.5$ Hz), 4.88 ppm (s, 2H); ^{13}C NMR (125 MHz, [D_6]DMSO): $\delta = 165.3$, 143.1, 134.6, 131.3, 128.2, 127.7, 126.6, 126.4, 123.3, 116.2, 116.1 ppm; HRMS (ESI+): *m/z* calcd for [$C_{13}H_{12}N_2ONa$]: 235.0847 $[M+Na]^+$; found: 235.0843; $\Delta = -1.8$ ppm (the NMR data is consistent with previous reports).[19]

General procedure for the nitro-amide preparation: Three different reported procedures were used.[20–22] Procedure A:[20] Et_3N (130 mol%) was added to a stirred solution of *ortho*-nitroaniline (**11**) in THF at room temperature. Acyl chloride **9** was added dropwise through a dropping funnel. The solution was stirred at room temperature for 8 h and concentrated in vacuo. The residue was purified by flash chromatography (hexane/EtOAc 8:2) to afford the nitro-amide **12e**.

Procedure B:[21] Similar to procedure A, but a mixture of dichloromethane and pyridine (1:1) was used as a solvent, 4-dimethylaminopyridine (DMAP) was used (5 mol%) instead of Et_3N, and the reaction was carried out at 0 °C for 2 h, allowed to warm to room temperature, and stirred for 4 h at room temperature. The solution was washed with 1 M HCl (4×50 mL), saturated $NaHCO_3$ (50 mL), and brine (50 mL) and dried over Na_2SO_4, filtered, and concentrated in vacuo. The residue was purified by flash chromatography to afford the nitro-amides **12d** and **12f**.

Procedure C:[22] Similar to procedure A, but neat pyridine was used as a solvent and Et_3N was not used. The reaction time was 20 h. The solution was concentrated in vacuo; dissolved in $CHCl_3$; washed with 1 M HCl (4×50 mL), water (2×50 mL), and brine (50 mL); dried over Na_2SO_4; filtered; and concentrated in vacuo. The residue was purified by flash chromatography (hexane/MtBE 1:1) to afford the nitro-amide **12c**.

***N*-(2-Nitrophenyl)pivalamide (12e)**: Procedure A: R_f (hexane/EtOAc 8:2) = 0.55; mp 42–44 °C; IR (film): $\tilde{\nu}$ = 3371, 2963, 1704, 1607, 1582, 1494, 1332, 1265, 1136, 744, 672 cm^{-1}; ^1H NMR (500 MHz, $CDCl_3$): δ = 10.72 (br s, 1H), 8.83 (dd, 1H, J_1 = 8.6, J_2 = 1.3 Hz), 8.22 (dd, 1H, J_1 = 8.5, J_2 = 1.6 Hz), 7.64 (dddd, 1H, J_1 = 8.6, J_2 = 7.2, J_3 = 1.6, J_4 = 0.4 Hz), 7.16 (ddd, 1H, J_1 = 8.5, J_2 = 7.2, J_3 = 1.3 Hz), 1.36 ppm (s, 9H); ^{13}C NMR (125 MHz, $CDCl_3$): δ = 178.0, 136.5, 136.1, 135.6, 125.9, 123.1, 122.3, 40.7, 27.6 ppm; HRMS (ESI$^-$): *m/z* calcd for $[C_{11}H_{13}N_2O_3]$: 221.0926 $[M-H]^-$; found: 221.0925; Δ = −0.5 ppm.

General procedure for the nitro-amide reduction: This procedure was adapted from a previous report.[22] Pd/C catalyst (5%) was added to a stirred solution of amide derivative **12** in absolute EtOH under argon at room temperature. The reaction mixture was placed under vacuum and the atmosphere was replaced with hydrogen. The reaction mixture was stirred for 3 h at room temperature, the solution was filtered through a pad of celite with EtOAc, and the filtrate was concentrated in vacuo to afford amide **10**.

***N*-(2-Aminophenyl)pivalamide (10e)**: R_f (hexane/EtOAc 8:2) = 0.08; mp 143–145 °C; IR (film): $\tilde{\nu}$ = 3373 3232, 2952, 1652, 1617, 1497, 1457, 1224, 744 cm^{-1}; ^1H NMR (500 MHz, [D$_6$]DMSO): δ = 8.73 (s, 1H), 7.01 (dd, 1H, J_1 = 7.8, J_2 = 1.2 Hz), 6.95–6.92 (m, 1H), 6.75 (dd, 1H, J_1 = 8.0, J_2 = 1.3 Hz), 6.57 (td, 1H, J_1 = 7.5, J_2 = 1.3 Hz), 4.63 (s, 2H), 1.24 ppm (s, 9H); ^{13}C NMR (125 MHz, [D$_6$]DMSO): δ = 176.6, 143.0, 126.7, 126.2, 123.8, 116.4, 116.1, 38.7, 27.5 ppm; HRMS (ESI+): *m/z* calcd for $[C_{11}H_{17}N_2O]$: 193.1335 $[M+H]^+$; found: 193.1332; Δ = −1.8 ppm.

Dimethylpyridine-2,6-dicarboxylate: The procedure was adapted from a previous report.[14] Conc. H_2SO_4 (0.93 mL, 18 mmol, 35 mol%) was added dropwise to a stirred solution of pyridine-2,6-dicarboxylic acid (8.36 g, 50 mmol, 100 mol%) in MeOH (50 mL) at room temperature. The solution was heated to reflux for 48 h and the reaction was quenched by the addition of sat. $NaHCO_3$ (40 mL). The mixture was concentrated in vacuo and the residue was re-dissolved in $CHCl_3$ (50 mL). The product was washed with water (3× 50 mL) and brine (50 mL), dried over Na_2SO_4, filtered, and concentrated in vacuo to afford the product (7.85 g, 80%) as a white solid.

R_f (hexane/EtOAc 8:2) = 0.67; mp 122–124 °C; IR (film): $\tilde{\nu}$ = 3063, 2969, 1739, 1571, 1449, 1434, 1288, 1241, 994, 951, 755, 694 cm^{-1}; ^1H NMR (500 MHz, $CDCl_3$): δ = 8.29 (d, 2H, J = 7.8 Hz), 8.00 (dd, 1H, $J_1 = J_2$ = 7.8 Hz), 4.01 ppm (s, 6H); ^{13}C NMR (125 MHz, $CDCl_3$): δ = 165.2, 148.4, 138.4, 128.1, 53.3 ppm; HRMS (ESI+): *m/z* calcd for $[C_9H_9NO_4Na]$: 218.0421 $[M+Na]^+$; found: 218.0429; Δ = −3.9 ppm (the NMR data is consistent with that reported previously).[23]

6-(Methoxycarbonyl)pyridine-2-carboxylic acid (14): The procedure was adapted from a previous report.[14] KOH (1.11 g, 20 mmol, 100 mol%) was dissolved in the minimal amount of water (0.5 mL) and was added to the cooled solution of dimethylpyridine-2,6-dicarboxylate (3.87 g, 20 mmol, 100 mol%) in MeOH (100 mL) at 0 °C. The solution was stirred at 0 °C for 2.5 h and warmed to room temperature. The mixture was concentrated in vacuo, and the residue was re-dissolved in water (80 mL) and washed with dichloromethane (2×50 mL). The aqueous layer was acidified with 1 M HCl (10 mL), and the product was extracted with EtOAc (4×50 mL). The combined organic layers were washed with brine (70 mL), dried over Na_2SO_4, filtered, and concentrated in vacuo to afford the product **14** (2.67 g, 74%) as a white solid.

The product could not be visualized by TLC analysis; mp 147–149 °C; IR (film): $\tilde{\nu}$ = 1724, 1698, 1325, 1306, 1264, 1154, 1141, 750, 648 cm^{-1}; ^1H NMR (500 MHz, [D$_6$]DMSO): δ = 8.25–8.22 (m, 2H), 8.17 (dd, 1H, J_1 = 7.9, J_2 = 7.5 Hz), 3.92 ppm (s, 3H); ^{13}C NMR (125 MHz, [D$_6$]DMSO): δ = 165.6, 164.7, 148.8, 147.6, 139.0, 127.8, 127.5, 52.6 ppm; HRMS (ESI$^-$): *m/z* calcd for $[C_8H_6NO_4]$: 180.0297 $[M-H]^-$; found: 180.0296; Δ = −0.2 ppm (the NMR data is consistent with that reported previously).[23]

Methyl-6-(phenylcarbamoyl) pyridine-2-carboxylate (16): R_f (hexane/EtOAc 1:1) = 0.46; mp 95–96 °C; IR (film): $\tilde{\nu}$ = 3487, 3447, 3253, 1721, 1678, 1598, 1532, 1495, 1433, 1327, 1300, 1238, 768, 735, 686 cm^{-1}; ^1H NMR (500 MHz, [D$_6$]DMSO): δ = 10.38 (s, 1H), 8.33–8.32 (m, 1H), 8.26–8.22 (m, 2H), 7.83 (d, 2H, J = 8.5 Hz), 7.40–7.37 (m, 2H), 7.17–7.13 (m, 1H), 3.96 ppm (s, 3H); ^{13}C NMR (125 MHz, [D$_6$]DMSO): δ = 164.6, 161.9, 150.4, 146.5, 139.6, 137.9, 128.8, 127.4, 125.6, 124.2, 120.2, 52.8 ppm; HRMS (ESI+): *m/z* calcd for $[C_{14}H_{12}N_2O_3Na]$: 279.0740 $[M+Na]^+$; found: 279.0747; Δ = 2.5 ppm.

6-(Phenylcarbamoyl)pyridine-2-carboxylic acid (17): The procedure was adapted from a previous report.[14] LiOH (0.41 g, 17.1 mmol, 200 mol%) was added to a stirred solution of carboxylate **16** (2.18 g, 8.5 mmol, 100 mol%) in MeOH (100 mL) at room temperature. The mixture was stirred at room temperature for 1 h and MeOH was removed in vacuo. The residue was dissolved in water (100 mL) and acidified with 1 M HCl (30 mL). The product was extracted with EtOAc (2×100 mL and 2×50 mL), and the combined organic layers were dried over Na_2SO_4, filtered, and concentrated in vacuo to afford the product **17** (2.06 g, 100%) as a white solid.

The product could not be visualized by TLC analysis; mp 169–172 °C; IR (film): $\tilde{\nu}$ = 3330, 1698, 1664, 1600, 1535, 1445, 1322, 1242, 756, 686, 666, 644 cm^{-1}; ^1H NMR (500 MHz, [D$_6$]DMSO): 10.83 (s, 1H), 8.39 (d, 1H, J = 7.5 Hz), 8.32–8.25 (m, 2H), 7.82 (d, 2H, J = 8.1 Hz), 7.42 (t, 2H, J = 7.8 Hz), 7.17 (t, 1H, J = 7.4 Hz), 3.38 ppm (br s, 1H); ^{13}C NMR (125 MHz, [D$_6$]DMSO): δ = 164.7, 161.4, 149.2, 146.1, 140.1, 137.9, 128.8, 127.0, 125.8, 124.4, 120.7 ppm; HRMS (ESI$^-$): *m/z* calcd for $[C_{13}H_9N_2O_3]$: 241.0613 $[M-H]^-$; found: 241.0611; Δ = −1.0 ppm.

6-((2-benzamidophenyl)carbamoyl)pyridine-2-carboxylic acid (19): *N*-(2-Aminophenyl)benzamide **10a** (2.02 g, 9.52 mmol, 100 mol%) and HOBt (1.29 g, 9.52 mmol, 100 mol%) were added to a stirred solution of 6-(methoxycarbonyl)pyridine-2-carboxylic acid (**14**; 1.72 g, 9.52 mmol, 100 mol%) in THF (100 mL) at room temperature. The solution was cooled to 0 °C and stirred for 40 min. EDC (1.85 mL, 10.47 mmol, 110 mol%) and Et_3N (1.46 mL, 10.47 mmol, 110 mol%) were added to the reaction mixture and the solution was stirred for further 45 min at 0 °C. The solution was warmed to room temperature, stirred for 20 h, and concentrated in vacuo. The residue was dissolved in dichloromethane (80 mL), washed with 1 M HCl (3×75 mL), sat. $NaHCO_3$ (100 mL), and water (80 mL) and dried over Na_2SO_4, filtered, and concentrated in vacuo to afford the product **18** (3.16 g, 89%) as a light-yellow solid. The product included small amounts of impurities, but it was used without further purification.

LiOH (0.11 g, 4.44 mmol, 200 mol%) was added to product **18** (0.83 g, 2.22 mmol, 100 mol%) in MeOH (40 mL) at room temperature. The formed suspension was stirred at room temperature for 1 h. The mixture was concentrated in vacuo and the residue was dissolved in water (50 mL). The solution was acidified with 1 M HCl

(10 mL) and the product was extracted with EtOAc (4×50 mL). The combined organic layers were dried over Na_2SO_4, filtered, and concentrated in vacuo to afford product **19** (0.76 g, 95%) as a white solid.

The product could not be visualized by TLC analysis; mp 208–210 °C; IR (film): $\tilde{\nu}$ = 3270, 1753, 1673, 1645, 1601, 1519, 1484, 1452, 1339, 1317, 757, 742, 697, 678 cm^{-1}; ^1H NMR (500 MHz, [D$_6$]DMSO): δ = 10.74 (s, 1H), 10.20 (s, 1H), 8.40 (dd, 1H, J_1 = 7.3 Hz, J_2 = 1.6 Hz), 8.30–8.24 (m, 2H), 8.04–8.02 (m, 2H), 7.98 (dd, 1H, J_1 = 8.0, J_2 = 1.5 Hz), 7.63 (dd, 1H, J_1 = 7.9, J_2 = 1.5 Hz), 7.60–7.57 (m, 1H), 7.52–7.49 (m, 1H), 7.36 (td, 1H, J_1 = 7.7, J_2 = 1.6 Hz), 7.31 ppm (td, 1H, J_1 = 7.7, J_2 = 1,6 Hz); ^{13}C NMR (125 MHz, [D$_6$]DMSO): δ = 166.2, 165.0, 161.6, 149.2, 146.8, 140.1, 134.2, 131.74, 131.70, 130.4, 128.4, 127.9, 127.3, 126.7, 126.1, 125.5, 125.4, 124.4 ppm; HRMS (ESI$^-$): *m/z* calcd for [$C_{20}H_{14}N_3O_4$]: 360.0984 [$M-H$]$^-$; found: 360.0978; Δ = −1.8 ppm.

General procedure for the coupling reactions:[24] HOBt and the amide derivative were added to a stirred solution of an asymmetric pyridine carboxylic acid in THF at room temperature. The mixture was cooled to 0 °C and stirred for 30 min. EDC and Et_3N were added to the reaction mixture and the solution was stirred for further 30 min at 0 °C. The solution was warmed to room temperature, stirred overnight, and concentrated in vacuo. The residue was dissolved in EtOAc, washed with several portions of 1 M HCl and finally with brine, dried over Na_2SO_4, filtered, and concentrated in vacuo to afford the product.

***N*^{2}-(2-Benzamidophenyl)-*N*^{6}-phenylpyridine-2,6-dicarboxamide (2)**: Prepared according to the general procedure for a coupling reaction with carboxylic acid **17** (1.080 g, 4.46 mmol, 100 mol%) in THF (20 mL), HOBt (0.603 g, 4.46 mmol, 100 mol%), amide **10a** (0.947 g, 4.46 mmol, 100 mol%), EDC (0.84 mL, 4.73 mmol, 106 mol%), Et_3N (0.66 mL, 4.73 mmol, 106 mol%), and THF (30 mL) to yield the product (1.843 g, 95%) as a white solid. R_f (hexane/EtOAc 1:1) = 0.41; mp 229–232 °C; IR (film): $\tilde{\nu}$ = 3316, 3232, 1677, 1660, 1645, 1597, 1528, 1445, 1312, 750, 706 cm^{-1}; ^1H NMR (500 MHz, [D$_6$]DMSO): δ = 11.14 (s, 1H), 10.76 (s, 1H), 10.34 (s, 1H), 8.40 (td, 2H, J_1 = 7.7, J_2 = 1.1 Hz), 8.31–8.28 (m, 1H), 7.89–7.86 (m, 3H), 7.77 (d, 2H, J = 8.1 Hz), 7.64 (dd, 1H, J_1 = 7.8, J_2 = 1.4 Hz), 7.45–7.33 (m, 5H), 7.27 (t, 2H, J = 7.8 Hz), 7.18–7.15 ppm (m, 1H); ^{13}C NMR (125 MHz, [D$_6$]DMSO): δ = 166.4, 161.3, 148.6, 148.5, 140.1, 137.7, 134.0, 131.7, 131.0, 128.6, 128.2, 127.6, 125.94, 125.88, 125.6, 125.2, 125.1, 124.4, 121.0 ppm; HRMS (ESI+): *m/z* calcd for [$C_{26}H_{20}N_4O_3Na$]: 459.1433 [M+Na]$^+$; found: 459.1426; Δ = −1.6 ppm.

***N*^{2}-(2-Benzamidophenyl)-*N*^{6}-(2-(4-cyanobenzamido)phenyl)pyridine-2,6-dicarboxamide (3)**: Prepared according to the general procedure for a coupling reaction with carboxylic acid **19** (359 mg, 1.00 mmol, 100 mol%), amide **10b** (237 mg, 1.00 mmol, 100 mol%), HOBt (135 mg, 1.00 mmol, 100 mol%), EDC (0.19 mL, 1.10 mmol, 110 mol%), Et_3N (0.15 mL, 1.10 mmol, 110 mol%), and THF (50 mL) to yield the product (544 mg, 94%) as a light-brown solid. R_f (hexane/EtOAc 3:7) = 0.56; mp 252–254 °C; IR (film): $\tilde{\nu}$ = 2230, 1667, 1599, 1515, 1480, 1441, 1306, 754 cm^{-1}; ^1H NMR (500 MHz, [D$_6$]DMSO): δ = 11.00 (s, 1H), 10.85 (s, 1H), 10.38 (s, 1H), 10.29 (s, 1H), 8.38–8.36 (m, 2H), 8.30–8.27 (m, 1H), 7.91 (d, 2H, J = 8.4 Hz), 7.77–7.75 (m, 1H), 7.72 (d, 2H, J = 7.2 Hz), 7.65–7.63 (m, 2H), 7.59 (d, 2H, J = 8.5 Hz), 7.56–7.54 (m, 1H), 7.45–7.42 (m, 1H), 7.39–7.31 (m, 4H), 7.22–7.19 ppm (m, 2H); ^{13}C NMR (125 MHz, [D$_6$]DMSO): δ = 166.1, 164.5, 161.3, 161.1, 148.33, 148.29, 140.3, 138.2, 133.7, 131.9, 131.7, 131.1, 130.8, 130.7, 130.5, 128.3, 128.1, 127.7, 126.2, 126.0, 125.7, 125.6, 125.5, 125.2, 125.09, 125.06, 125.0, 118.1, 113.7 ppm; HRMS (ESI+): *m/z* calcd for [$C_{34}H_{24}N_6O_4Na$]: 603.1751 [M+Na]$^+$; found: 603.1745; Δ = −1.0 ppm.

***N*^{2}-(2-Benzamidophenyl)-*N*^{6}-(2-(4-methoxybenzamido)phenyl)pyridine-2,6-dicarboxamide (4)**: Prepared according to the general procedure for a coupling reaction with carboxylic acid **19** (183 mg, 0.51 mmol, 100 mol%), amide **10c** (136 mg, 0.56 mmol, 110 mol%), HOBt (83 mg, 0.56 mmol, 110 mol%), EDC (0.11 mL, 0.61 mmol, 120 mol%), Et_3N (0.09 mL, 0.61 mmol, 120 mol%), and THF (50 mL) to yield the product (90 mg, 30%) as a white solid. R_f (hexane/EtOAc 3:7) = 0.51; mp 172–174 °C; IR (film): $\tilde{\nu}$ = 3345, 1698, 1682, 1648, 1633, 1605, 1509, 1439, 1307, 1258, 755 cm^{-1}; ^1H NMR (500 MHz, [D$_6$]DMSO): δ = 11.04 (s, 1H), 10.98 (s, 1H), 10.22 (s, 1H), 10.11 (s, 1H), 8.38–8.36 (m, 2H), 8.30–8.27 (m, 1H), 7.76 (dd, 2H, J_1 = 8.2, J_2 = 1.0 Hz), 7.73–7.71 (m, 4H), 7.68–7.67 (m, 1H), 7.62–7.61 (m, 1H), 7.44–7.41 (m, 1H), 7.37–7.32 (m, 4H), 7.20 (t, 2H, J = 7.8 Hz), 6.70 (d, 2H, J = 8.9 Hz), 3.74 ppm (s, 3H); ^{13}C NMR (125 MHz, [D$_6$]DMSO): δ = 166.0, 165.5, 161.9, 161.3, 161.2, 148.3, 148.2, 140.4, 134.0, 131.6, 131.10, 131.07, 130.8, 129.5, 128.1, 127.5, 125.9, 125.9, 125.8, 125.7, 125.6, 125.3, 125.11, 125.07, 113.3, 55.3 ppm; HRMS (ESI+): *m/z* calcd for [$C_{34}H_{27}N_5O_5Na$]: 608.1904 [M+Na]$^+$; found: 608.1903; Δ = −0.2 ppm.

***N*^{2}-(2-Acetamidophenyl)-*N*^{6}-(2-benzamidophenyl)pyridine-2,6-dicarboxamide (5)**: Prepared according to the general procedure for a coupling reaction with carboxylic acid **19** (479 mg, 1.33 mmol, 100 mol%), amide **10d** (230 mg, 1.53 mmol, 115 mol%), HOBt (207 mg, 1.53 mmol, 115 mol%), EDC (0.30 mL, 1.66 mmol, 125 mol%), Et_3N (0.23 mL, 1.66 mmol, 125 mol%), and THF (70 mL) to yield the product (588 mg, 90%) as a white solid. R_f (hexane/EtOAc 2:8) = 0.55; mp 227–229 °C; IR (film): $\tilde{\nu}$ = 3227, 3037, 1693, 1666, 1646, 1597, 1511, 1481, 1445, 1311, 754, 705 cm^{-1}; ^1H NMR (500 MHz, $CDCl_3$): δ = 11.25 (s, 1H), 11.12 (s, 1H), 9.65 (s, 1H), 9.07 (s, 1H), 8.47 (d, 1H, J = 7.6 Hz), 8.43 (d, 1H, J = 7.8 Hz), 8.11 (t, 1H, J = 7.8 Hz), 7.94 (d, 1H, J = 7.5 Hz), 7.80 (d, 2H, J = 7.5 Hz), 7.72–7.69 (m, 2H), 7.40 (t, 1H, J = 7.4 Hz), 7.28–7.24 (m, 3H), 7.22–7.16 (m, 3H), 7.08–7.05 (m, 1H), 1.71 ppm (s, 3H); ^{13}C NMR (125 MHz, $CDCl_3$): δ = 170.8, 166.4, 162.7, 161.7, 149.0, 148.4, 139.6, 133.8, 132.1, 131.1, 130.8, 130.2, 129.7, 128.7, 127.5, 126.66, 126.64, 126.33, 126.25, 125.9, 125.7, 125.53, 125.51, 125.1, 124.8, 23.4 ppm; HRMS (ESI+): *m/z* calcd for [$C_{28}H_{23}N_5O_4Na$]: 516.1627 [M+Na]$^+$; found: 516.1642; Δ = −3.0 ppm.

***N*^{2}-(2-Benzamidophenyl)-*N*^{6}-(2-isobutyramidophenyl)pyridine-2,6-dicarboxamide (6)**: Prepared according to the general procedure for a coupling reaction with carboxylic acid **19** (310 mg, 0.85 mmol, 100 mol%), amide **10e** (170 mg, 0.95 mmol, 110 mol%), HOBt (129 mg, 0.95 mmol, 110 mol%), EDC (0.19 mL, 1.05 mmol, 120 mol%), Et_3N (0.15 mL, 1.05 mmol, 120 mol%), and THF (50 mL) to yield the product (383 mg, 77%) as a white solid. R_f (hexane/EtOAc 3:7) = 0.50; mp 192–193 °C; IR (film): $\tilde{\nu}$ = 1650, 1599, 1513, 1480, 1450, 1302, 750 cm^{-1}; ^1H NMR (500 MHz, $CDCl_3$): δ = 11.06 (s, 1H), 10.97 (s, 1H), 9.54 (s, 1H), 8.72 (s, 1H), 8.46 (d, 1H, J = 7.7 Hz), 8.44 (d, 1H, J = 7.8 Hz), 8.12 (t, 1H, J = 7.8 Hz), 7.87 (dd, 1H, J_1 = 7.8, J_2 = 1.6 Hz), 7.80–7.77 (m, 3H), 7.59 (d, 1H, J = 7.7 Hz), 7.34 (t, 1H, J = 7.4 Hz), 7.20–7.10 (m, 5H), 7.05–7.02 (m, 1H), 2.40 (septet, 1H, J = 6.9 Hz), 0.89 ppm (d, 1H, J = 6.9 Hz); ^{13}C NMR (125 MHz, $CDCl_3$): δ = 177.6, 166.6, 162.1, 162.0, 148.7, 148.6, 139.7, 133.8, 132.0, 130.7, 130.4, 130.1, 128.7, 128.6, 127.6, 127.5, 126.6, 126.5, 126.1, 125.6, 125.53, 125.45, 125.2, 124.9, 36.1, 19.3 ppm; HRMS (ESI+): *m/z* calcd for [$C_{30}H_{28}N_5O_4$]: 522.2135 [M+H]$^+$; found: 544.1946; Δ = −0.9 ppm.

***N*^{2}-(2-Benzamidophenyl)-*N*^{6}-(2-pivalamidophenyl)pyridine-2,6-dicarboxamide (7)**: Prepared according to the general procedure for a coupling reactions with carboxylic acid **19** (340 mg, 0.95 mmol, 100 mol%), amide **10f** (200 mg, 1.04 mmol, 110 mol%), HOBt (141 mg, 1.04 mmol, 110 mol%), EDC (0.20 mL, 1.13 mmol, 120 mol%), Et_3N (0.16 mL, 1.13 mmol, 120 mol%), and THF (50 mL)

to yield the product (502 mg, 99%) as a white solid. R_f (hexane/EtOAc 1:1) = 0.37; mp 210–212 °C; IR (film): $\tilde{\nu}$ = 1691, 1676, 1638, 1601, 1524, 1481, 756, 707 cm^{-1}; ^1H NMR (500 MHz, [D_6]DMSO): δ = 11.04 (s, 1H), 10.88 (s, 1H), 10.20 (s, 1H), 9.05 (s, 1H), 8.41 (dd, 1H, J_1 = 7.7, J_2 = 1.2 Hz), 8.38 (dd, 1H, J_1 = 7.8, J_2 = 1.2 Hz), 8.31 (dd, 1H, J_1 = J_2 = 7.8 Hz), 7.87 (dd, 1H, J_1 = 7.9, J_2 = 1.5 Hz), 7.75 (dd, 2H, J_1 = 8.3, J_2 = 1.2 Hz), 7.62 (dd, 1H, J_1 = 7.9, J_2 = 1.3 Hz), 7.56 (dd, 1H, J_1 = 7.8, J_2 = 1.7 Hz), 7.52 (dd, 1H, J_1 = 7.7, J_2 = 1.7 Hz), 7.44–7.41 (m, 1H), 7.37 (td, 1H, J_1 = 7.7, J_2 = 1.6 Hz), 7.33–7.25 (m, 3H), 7.22–7.19 (m, 2H), 1.03 ppm (s, 9H); ^{13}C NMR (125 MHz, [D_6]DMSO): δ = 176.8, 166.1, 161.5, 161.3, 148.5, 148.1, 140.4, 133.8, 131.63, 131.62, 131.0, 130.9, 130.4, 128.1, 127.5, 126.00, 125.98, 125.9, 125.8, 125.6, 125.4, 125.3, 125.2, 125.1, 125.0, 38.8, 26.9 ppm; HRMS (ESI+): *m/z* calcd for [$C_{31}H_{29}N_5O_4Na$]: 588.2111 [M+Na]$^+$; found: 558.2117; Δ = 0.9 ppm.

Crystallographic analysis

The compounds were dissolved in solvents of analytical purity (foldamer **2**: acetone, MeCN/ dimethylacetamide (DMA), DMF; foldamer **3**: MeCN, EtOAc; foldamer **5**: acetone; foldamer **6**: EtOAc, toluene; foldamer **7**: acetone; see the Supporting Information for details) and allowed to evaporate at room temperature until crystals formed. Aliquots of 10–50 mg of the compounds and up to 6 mL of the solvents were used in the crystallization experiments. Heating and stirring were used to help the dissolving process.

Single-crystal X-ray diffraction data was collected on a Bruker Nonius KappaCCD diffractometer at 173 K with a Bruker AXS APEX II CCD detector and graphite-monochromated $Cu_{K\alpha}$ radiation (λ = 1.54178 Å). The structures were solved by using direct methods and refined by using Fourier techniques with the SHELX-97 software package.[25] Multiscan absorption correction was applied to all structures with Denzo-SMN 1997.[26] All the non-hydrogen atoms were refined anisotropically. The hydrogen atoms were placed in their idealized positions, except for the N−H hydrogen atoms that were found from the electron-density map and included in the structure-factor calculations. Isotropic temperature factor of 1.2 was used to refine the hydrogen atoms. Details of the crystal data and the refinement are presented in Tables 2 and 3 in the Supporting Information.

CCDC 1038215 (**2**-@-Form I), CCDC 1038216 (**2**-**S**-MeCN), CCDC 1038217 (**2**-@-**S**-DMF), CCDC 1038218 (**3**-@$_2$-Form I), CCDC 1038219 (**3**-**S**$_1$-EtOAc), CCDC 1038220 (**5**-**S**$_1$-Form I), CCDC 1038221 (**6**-@′$_2$-Form I), CCDC 1038222 (**6**-**S**$_1$-Form II), and CCDC 1038223 (**7**-**S**$_2$-Form I) contain the supplementary crystallographic data for this paper. These data can be obtained free of charge from The Cambridge Crystallographic Data Centre through www.ccdc.cam.ac.uk/data_request/cif.

Computational approach

The geometries of the stationary points were optimized by using the density-functional theory (DFT) at the ωB97X-D/6–311G(d,p) level. Herein, ωB97X-D denotes the long-range corrected hybrid density functional with damped atom–atom dispersion corrections developed by Chai and Head-Gordon.[27,28] This functional is a very promising DFT method[29] that yields reasonably accurate data for general main-group thermochemistry, kinetics, and noncovalent interactions (all of which are relevant to the present work). The initial structures for the geometry optimizations were obtained from a Monte Carlo conformational search by using the OPLS 2005 force fields as implemented in the MacroModel software.[30] The preliminary conformational analysis involved a systematic search and DFT potential-energy surface scans along specific dihedral angles.

Normal coordinate analysis was carried out at the ωB97X-D/6–311G(d,p) level of theory for all the optimized structures. The results were utilized to verify the nature of the stationary points (i.e. minima) and to estimate the zero-point energies and the thermal and entropic contributions to the Gibbs free energies. For each located structure, additional single-point energy calculations were performed at the ωB97X-D/6–311++G(3df,3pd) level to increase the accuracy of the electronic-structure predictions. In all the DFT calculations, the ultrafine integration grid was employed, as implemented in the Gaussian09 package.[31]

The thermochemical data were obtained within the ideal-gas (i.e., rigid rotor) harmonic-oscillator approximation for T = 298.15 K and P = 1 atm. The solvation free energies (solvent = $CHCl_3$) were estimated at the ωB97X-D/6–311G(d,p) level by using the integral-equation-formalism variant of the polarizable-continuum model (IEFPCM).[32] The atomic radii and nonelectrostatic terms in the IEFPCM calculations were those introduced recently by Truhlar and co-workers (SMD solvation model).[33]

Acknowledgements

We thank the Finnish Cultural Foundation, University of Jyväskylä, Academy of Finland (Grant no. 259532), and the Hungarian Scientific Research Fund (OTKA, grant NN-82955) for financial support.

Keywords: crystal growth · foldamers · protein folding · hydrogen bonds · oligomerization

[1] D. Blow, *Structure* **2000**, *8*, R77–R81.
[2] P. M. Pihko, S. Rapakko, R. K. Wierenga in *Hydrogen Bonding in Organic Synthesis* (Ed. P. M. Pihko), Wiley-VCH, Weinheim, **2009**, pp. 43–72.
[3] For a discussion, see: a) R. R. Knowles, E. N. Jacobsen, *Proc. Natl. Acad. Sci. USA* **2010**, *107*, 20678; for a recent example of a synthetic oxyanion mimic, see: b) E. V. Beletskiy, J. Schmidt, X.-B. Wang, S. R. Kass, *J. Am. Chem. Soc.* **2012**, *134*, 18534–18537; c) see also ref. [2]; d) B. Kótai, G. Kardos, A. Hamza, V. Farkas, I. Pápai, T. Soós, *Chem. Eur. J.* **2014**, *20*, 5631–5639.
[4] a) S. H. Gellman, *Acc. Chem. Res.* **1998**, *31*, 173–180; b) D. J. Hill, M. J. Mio, R. B. Prince, T. S. Hughes, J. S. Moore, *Chem. Rev.* **2001**, *101*, 3893–4011; c) S. Hecht, I. Huc, *Foldamers: Structure, Properties and Applications*, Wiley-VCH, Weinheim, **2007**; d) D.-W. Zhang, X. Zhao, Z.-T. Li, *Acc. Chem. Res.* **2014**, *47*, 1961–1970; e) G. Guichard, I. Huc, *Chem. Commun.* **2011**, *47*, 5933–5941.
[5] a) D.-W. Zhang, X. Zhao, J.-L. Hou, Z.-T. Li, *Chem. Rev.* **2012**, *112*, 5271–5316; b) I. Huc, *Eur. J. Org. Chem.* **2004**, 17–29; c) B. Gong, *Chem. Eur. J.* **2001**, *7*, 4336–4342; d) A. R. Sanford, K. Yamato, X. Yang, L. Yuan, Y. Han, B. Gong, *Eur. J. Biochem.* **2004**, *271*, 1416–1425; e) K. Yamato, M. Kline, B. Gong, *Chem. Commun.* **2012**, *48*, 12142–12158.
[6] a) V. Berl, I. Huc, R. G. Khoury, J.-M. Lehn, *Chem. Eur. J.* **2001**, *7*, 2798–2809; b) V. Berl, I. Huc, R. G. Khoury, J.-M. Lehn, *Chem. Eur. J.* **2001**, *7*, 2810–2820; c) I. Huc, V. Maurizot, H. Gornitzka, J.-M. Léger, *Chem. Commun.* **2002**, *6*, 578–579; d) B. Babtiste, J. Zhu, D. Haldar, B. Kauffmann, J.-M. Léger, I. Huc, *Chem. Asian J.* **2010**, *5*, 1364–1375.
[7] a) Y. Hamuro, S. J. Geib, A. D. Hamilton, *Angew. Chem. Int. Ed. Engl.* **1994**, *33*, 446–448; *Angew. Chem.* **1994**, *106*, 465–467; b) Y. Hamuro, S. J. Geib, A. D. Hamilton, *J. Am. Chem. Soc.* **1996**, *118*, 7529–7541; c) Y. Hamuro, S. J. Geib, A. D. Hamilton, *J. Am. Chem. Soc.* **1997**, *119*, 10587–10593.
[8] a) H. Jiang, J.-M. Léger, I. Huc, *J. Am. Chem. Soc.* **2003**, *125*, 3448–3449; b) E. R. Gillies, C. Dolain, J.-M. Léger, I. Huc, *J. Org. Chem.* **2006**, *71*, 7931–7931; c) N. Delsuc, J.-M. Léger, S. Massip, I. Huc, *Angew. Chem. Int.*

Ed. **2007**, *46*, 214 – 217; *Angew. Chem.* **2007**, *119*, 218 – 221; d) D. Sánchez-García, B. Kauffmann, T. Kawanami, H. Ihara, M. Takafuji, M.—H. Delville, I. Huc, *J. Am. Chem. Soc.* **2009**, *131*, 8642 – 8648.

[9] Y. Ferrand, A. M. Kendhale, J. Garric, B. Kauffman, I. Huc, *Angew. Chem. Int. Ed.* **2010**, *49*, 1778 – 1781; *Angew. Chem.* **2010**, *122*, 1822 – 1825.

[10] a) J. T. Ernst, J. Becerril, H. S. Park, H. Yin, A. D. Hamilton, *Angew. Chem. Int. Ed.* **2003**, *42*, 535 – 539; *Angew. Chem.* **2003**, *115*, 553 – 557; L. A. Estroff, C. D. Incarvato, A. D. Hamilton, *J. Am. Chem. Soc.* **2004**, *126*, 2 – 3; I. Saraogi, C. D. Incarvito, A. D. Hamilton, *Angew. Chem. Int. Ed.* **2008**, *47*, 9691 – 9694; *Angew. Chem.* **2008**, *120*, 9837 – 9840; b) C. Li, S.-F. Ren, J.-L. Hou, H.-P. Yi, S.-Z. Zhu, X.-K. Jiang, Z.-T. Li, *Angew. Chem. Int. Ed.* **2005**, *44*, 5725 – 5729; *Angew. Chem.* **2005**, *117*, 5871 – 5875; c) J.-L. Hou, X.-B. Shao, G.-J. Chen, Y.-X. Zhou, X.-K. Jiang, Z.-T. Li, *J. Am. Chem. Soc.* **2004**, *126*, 12386 – 12394; H.-P. Yi, X.-B. Shao, J.-L. Hou, C. Li, X.-K. Jiang, Z.-T. Li, *New J. Chem.* **2005**, *29*, 1213 – 1218; H.-P. Yi, C. Li, J.-L. Hou, X.-K. Jiang, Z.-T. Li, *Tetrahedron* **2005**, *61*, 7974 – 7980; d) J. Zhu, R. D. Parra, H. Zeng, E. Skrzypczak-Jankun, X. C. Zeng, B. Gong, *J. Am. Chem. Soc.* **2000**, *122*, 4219 – 4220.

[11] K. Mitsui, S. A. Hyatt, D. A. Turner, C. M. Hadad, J. R. Parquette, *Chem. Commun.* **2009**, 3261 – 3263; b) N. T. Salzameda, D. A. Lightner, *Monatsh. Chem.* **2007**, *138*, 237 – 244.

[12] a) I. Pápai, A. Hamza, P. M. Pihko, R. K. Wierenga, *Chem. Eur. J.* **2011**, *17*, 2859 – 2866; b) for a seminal study of the preferred hydrogen-bond orientation in oxyanion holes, see: L. Simón, J. M. Goodman, *J. Org. Chem.* **2010**, *75*, 1831.

[13] A. Suhonen, E. Nauha, K. Salorinne, K. Helttunen, M. Nissinen, *CrystEngComm* **2012**, *14*, 7398 – 7407.

[14] C. Schmuck, U. Machon, *Chem. Eur. J.* **2005**, *11*, 1109 – 1118.

[15] The RDG data were computed by using the NCIPLOT program; for a basic reference, see: a) E. R. Johnson, S. Keinan, P. Mori-Sánchez, J. Contreras-García, A. J. Cohen, W. Yang, *J. Am. Chem. Soc.* **2010**, *132*, 6498; b) J. Contreras-García, E. R. Johnson, S. Keinan, R. Chaudret, J. Piquemal, D. N. Beratan, W. Yang, *J. Chem. Theory Comput.* **2011**, *7*, 625.

[16] RDG isosurface plots were visualized by using the visual molecular dynamics (VMD) program: W. Humphrey, A. Dalke, K. Schulten, *J. Molec. Graphics* **1996**, *14*, 33.

[17] See the Supporting Information for additional overlay structures and the distances of the intramolecular aromatic interactions in the XRD structures.

[18] The details of the effects of solvation and crystal packing will be discussed elsewhere; A. Suhonen, M. Kortelainen, E. Nauha, S. Yliniemelä-Sipari, P. Pihko and M. Nissinen, *Manuscript in preparation*.

[19] H. Zhao, H. Fu, R. Qiao, *J. Org. Chem.* **2010**, *75*, 3311 – 3316.

[20] Y.-W. Legrand, M. Gray, G. Cooke, V. M. Rotello, *J. Am. Chem. Soc.* **2003**, *125*, 15789 – 15795.

[21] J. Duchek, A. Vasella, *Helv. Chim. Acta* **2011**, *94*, 977 – 986.

[22] H. Koshio, F. Hirayama, T. Ishihara, R. Shiraki, T. Shigenaga, Y. Taniuchi, K. Sato, Y. Moritani, Y. Iwatsuki, S. Kaku, N. Katayama, T. Kawasaki, Y. Matsumoto, S. Sakamoto, S. Tsukamoto, *Bioorg. Med. Chem.* **2005**, *13*, 1305 – 1323.

[23] W. Ong, H. Zhao, Z. Du, J. Z. Y. Yeh, C. Ren, L. Z. W. Tan, K. Zhang, H. Zeng, *Chem. Commun.* **2011**, *47*, 6416 – 6418.

[24] F. Stomeo, C. Lincheneau, J. P. Leonard, J. E. O'Brien, R. D. Peacock, C. P. McCoy, T. Gunnlaugsson, *J. Am. Chem. Soc.* **2009**, *131*, 9636 – 9637.

[25] G. M. Sheldrick, *Acta Crystallogr. Sect. A* **2008**, *64*, 112 – 122.

[26] Z. Otwinowski, D. Borek, W. Majewski, W. Minor, *Acta Crystallogr. Sect. A* **2003**, *59*, 228 – 234.

[27] a) J.-D. Chai, M. Head-Gordon, *Phys. Chem. Chem. Phys.* **2008**, *10*, 6615 – 6620; b) J.-D. Chai, M. Head-Gordon, *J. Chem. Phys.* **2008**, *128*, 084106/1 – 084106/15.

[28] a) R. Krishnan, J. S. Binkley, R. Seeger, J. A. Pople, *J. Chem. Phys.* **1980**, *72*, 650 – 654; b) A. D. McLean, G. S. Chandler, *J. Chem. Phys.* **1980**, *72*, 5639 – 5648; c) T. Clark, J. Chandrasekhar, G. W. Spitznagel, P. v. R. Schleyer, *J. Comput. Chem.* **1983**, *4*, 294 – 301; d) M. J. Frisch, J. A. Pople, J. S. Binkley, *J. Chem. Phys.* **1984**, *80*, 3265 – 3269.

[29] L. Goerigk, S. Grimme, *Phys. Chem. Chem. Phys.* **2011**, *13*, 6670 – 6688.

[30] Schrödinger Release 2013 – 3: MacroModel, version 10.2, Schrödinger, LLC, New York, NY, **2013**.

[31] Gaussian 09, Revision A.02, M. J. Frisch, G. W. Trucks, H. B. Schlegel, G. E. Scuseria, M. A. Robb, J. R. Cheeseman, G. Scalmani, V. Barone, B. Mennucci, G. A. Petersson, H. Nakatsuji, M. Caricato, X. Li, H. P. Hratchian, A. F. Izmaylov, J. Bloino, G. Zheng, J. L. Sonnenberg, M. Hada, M. Ehara, K. Toyota, R. Fukuda, J. Hasegawa, M. Ishida, T. Nakajima, Y. Honda, O. Kitao, H. Nakai, T. Vreven, J. A. Montgomery, Jr., J. E. Peralta, F. Ogliaro, M. Bearpark, J. J. Heyd, E. Brothers, K. N. Kudin, V. N. Staroverov, R. Kobayashi, J. Normand, K. Raghavachari, A. Rendell, J. C. Burant, S. S. Iyengar, J. Tomasi, M. Cossi, N. Rega, J. M. Millam, M. Klene, J. E. Knox, J. B. Cross, V. Bakken, C. Adamo, J. Jaramillo, R. Gomperts, R. E. Stratmann, O. Yazyev, A. J. Austin, R. Cammi, C. Pomelli, J. W. Ochterski, R. L. Martin, K. Morokuma, V. G. Zakrzewski, G. A. Voth, P. Salvador, J. J. Dannenberg, S. Dapprich, A. D. Daniels, Ö. Farkas, J. B. Foresman, J. V. Ortiz, J. Cioslowski, D. J. Fox, Gaussian, Inc., Wallingford CT, **2009**.

[32] J. Tomasi, B. Mennucci, E. Cancès, *J. Mol. Struct.* **1999**, *464*, 211 – 226.

[33] A. V. Marenich, C. J. Cramer, D. G. Truhlar, *J. Phys. Chem. B* **2009**, *113*, 6378 – 6396.

Received: December 17, 2014
Published online on May 12, 2015

III

EFFECT OF A RIGID SULFONAMIDE BOND ON MOLECULAR FOLDING: A CASE STUDY

by

Aku Suhonen, Ian S. Morgan, Elisa Nauha, Kaisa Helttunen, Heikki M. Tuononen & Maija Nissinen, 2015

Cryst. Growth Des., **2015**, *15*, 2602-2608

CRYSTAL GROWTH & DESIGN

Article

pubs.acs.org/crystal

Effect of a Rigid Sulfonamide Bond on Molecular Folding: A Case Study

Aku Suhonen, Ian S. Morgan, Elisa Nauha, Kaisa Helttunen, Heikki M. Tuononen, and Maija Nissinen*

Department of Chemistry, Nanoscience Center, University of Jyvaskyla, P.O. Box 35, FI-40014 University of Jyväskylä, Finland

Supporting Information

ABSTRACT: A disulfonamide compound with bulky aromatic side chains was prepared, and its properties as a potential building block for foldamers were evaluated. Two different solvate crystal forms of the compound were identified and compared to the structures of an analogous oligoamide and related disulfonamides. The disulfonamide is unfolded in one of the solvates, whereas in the other one, a loosely folded conformer stabilized by an intramolecular hydrogen bond is found. Density functional calculations indicated that the loosely folded conformer is slightly more stable than its unfolded isomer. The calculations also identified a third, more tightly folded and more extensively hydrogen bonded, conformer that is even lower in energy.

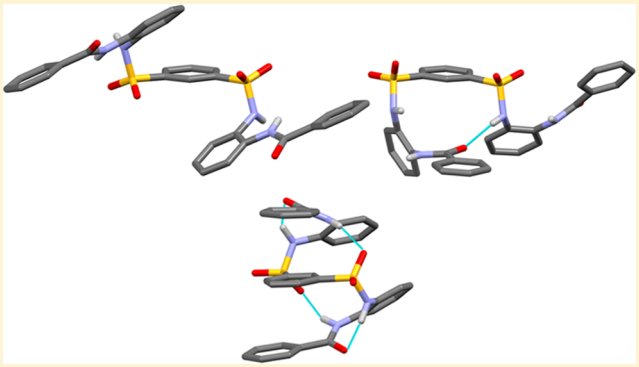

INTRODUCTION

The crystal form, the organization of molecules in a crystalline solid, depends on the conformational, functional, and interaction properties of the compound as well as on the crystallization environment, such as temperature and solvent. On the other hand, the crystal form affects the physical properties of crystalline materials and provides information on conformational preferences and the interplay of intra- and intermolecular interactions as well as their role in the formation of crystalline materials under varying conditions.[1] Molecular conformation is especially important in the case of synthetic compounds that adopt structures mimicking those of biological molecules, such as peptides and proteins. These biomimetic molecular scaffolds, called foldamers, are composed of relatively simple repeating structural units and have, to some extent, predictable secondary structures stabilized by weak interactions between nonadjacent units.[2,3] In addition to being artificial models for molecular folding,[4] foldamers may express enzyme-like functions such as receptor properties and catalysis.[5]

The most common bond type used in the construction of foldamers is the amide bond.[6,7] This is not only due to its analogy to peptide bonds but also because of its predictable hydrogen-bonding properties. Another interesting, yet rarely used, bond type is the sulfonamide bond in which the sp^2 carbon of an amide is replaced with an sp^3 sulfur.[8,9] This leads to differences in the preferred orientation of the C−N and S−N bonds and in the wideness of the OXN angles (120° and 106° for X = C and X = S, respectively). Compared to amides, sulfonamides have different possibilities for intra- and intermolecular hydrogen bonding,[10,11] which strongly affects their conformational properties and, hence, the propensity of sulfonamides to form polymorphs and co-crystals.[12,13] In small peptides, the amide-to-sulfonamide replacement has been reported to lead to both striking differences as well as surprising similarities in the folding patterns.[8,14]

Co-crystallization studies of sulfonamide compounds have been conducted to improve their properties, such as solubility, and to explore their potential as building blocks for new molecular assemblies with improved pharmaceutical properties.[15] Sulfonamides were the first clinically available antibacterial agents,[16] and they have been widely used in the design of drug candidates.[17,18] Another potential use for sulfonamide compounds is (stereoselective) organocatalysis because of their capacity to form fairly weak hydrogen bonds and their increased acidity compared to the amide group.[19,20]

In our previous study, we focused on aromatic oligoamides as potential foldamers and studied their conformational properties, polymorphism, and solvate formation.[21,22] In order to investigate the effect of amide-to-sulfonamide replacement on molecular conformation and folding, we have now prepared a sulfonamide analogue (**2**) of one of the previously synthesized oligoamides (**3**).[21] The structural properties of sulfonamide **2** were investigated in the solid state and in solution as well as by performing density functional theory (DFT) calculations. The results are compared and contrasted with the data of oligoamide **3** as well as with that for other related disulfonamides described in the literature.

Received: September 4, 2014
Revised: May 5, 2015
Published: May 11, 2015

DOI: 10.1021/acs.cgd.5b00424
Cryst. Growth Des. 2015, 15, 2602−2608

EXPERIMENTAL SECTION

Materials and Methods. All starting materials were commercially available and used as such unless otherwise noted. Analytical grade solvents and Millipore water were used for crystallizations. NMR spectra were measured with a Bruker Avance DRX 500 spectrometer, and chemical shifts were calibrated to the residual proton and carbon resonances of the deuterated solvent. Melting points were measured in open capillaries using a Stuart Scientific SMP3 melting point apparatus and are uncorrected. ESI-TOF mass spectra were measured with a LCT Micromass spectrometer. Elemental analyses were performed with a Vario EL III instrument.

Syntheses. All syntheses were carried out under a N_2 atmosphere. The glassware was dried at 120 °C prior to use. Dichloromethane was dried by distillation over $CaCl_2$ and stored over Linde type 3 Å molecular sieves under nitrogen gas. Compound **1** was prepared by a published method,[21] which is a slight modification of an earlier literature procedure.[23] Compound **2** was also prepared by a slightly modified literature procedure.[24]

***N*-Benzoyl-2-aminoaniline 1.** *O*-Phenylenediamine (8.97 g; 83.1 mmol) was dissolved in dry dichloromethane (350 mL). Triethylamine (3.0 mL; 21.6 mmol) was added, and the solution was heated to reflux with stirring. Benzoyl chloride (2.16 g; 20.7 mmol) dissolved in dry dichloromethane (200 mL) was added dropwise to the solution. The solution was allowed to reflux for 2 h. The product was separated by column chromatography using a silica column and an ethyl acetate–hexane (1:1) mixture as the eluent. Recrystallization from ethyl acetate–hexane afforded the product as a white solid (yield, 3.57 g, 81%). mp. 149–151 °C; ^{1}H NMR (500 MHz, DMSO-d_6, 30 °C): δ 4.87 (s, 2H; i), 6.60 (td, $^3J_{HH}$ = 1.2 Hz, $^3J_{HH}$ = 7.6 Hz, 1H; g), 6.79 (dd, $^3J_{HH}$ = 1.3 Hz, $^3J_{HH}$ = 8.1 Hz, 1H; e), 6.97 (td, $^3J_{HH}$ = 1.2 Hz, $^3J_{HH}$ = 7.6 Hz, 1H; f), 7.18 (d, $^3J_{HH}$ = 7.7 Hz, 1H; d), 7.51 (t, $^3J_{HH}$ = 7.4 Hz, 2H; b), 7.55–7.60 (m, 1H; a), 7.98 (d, $^3J_{HH}$ = 7.4 Hz, 2H; c), 9.63 (s, 1H; h) ppm; ^{13}C NMR (126 MHz, DMSO-d_6, 30 °C): δ 116.1, 116.2, 123.3, 126.4, 127.6, 128.2, 131.2, 134.6, 143.0, 165.2 ppm; MS (ESI-TOF) m/z $[M + Na]^+$ calcd for $C_{13}H_{12}N_2O$, 212.25; found, 235.08; Analysis calcd (%) for $C_{13}H_{12}N_2O$: C, 73.6; H, 5.7; N, 13.2. Found: C, 73.8; H, 5.6; N, 13.3.

***N*^{1},*N*^{3}-Bis(2-benzamidophenyl)benzene-1,3-disulfonamide 2.** *N*-Benzoyl-2-aminoaniline **1** (0.471 g; 2.22 mmol) was dissolved in pyridine (15 mL). The solution was stirred, and benzene-1,3-disulfonyl chloride (0.307 g; 1.11 mmol) dissolved in pyridine (15 mL) was added dropwise to the mixture. The solution was refluxed for 2 h, after which the stirring was continued for 24 h. Two molar HCl was added to the solution, and a precipitate formed; if the precipitate did not form, then 6 M HCl solution was added. The precipitate was filtered and washed with water. The precipitate was then dissolved in absolute ethanol and concentrated. The concentrated product was dissolved in ethanol, precipitated as a pink solid by adding water, and dried in vacuum (yield, 0.37 g, 63%). mp. 213-216 °C; ^{1}H NMR (500 MHz, DMSO-d_6, 30 °C): δ 6.90 (dd, 2H, $^3J_{HH}$ = 1.5 Hz, $^3J_{HH}$ = 8.1 Hz), 7.07 (td, 2H, $^3J_{HH}$ = 1.4 Hz, $^3J_{HH}$ = 7.8 Hz), 7.26 (td, 2H, $^3J_{HH}$ = 1.4 Hz, $^3J_{HH}$ = 7.8 Hz), 7.52–7.57 (m, 5H), 7.62 (tt, 2H, $^3J_{HH}$ = 1.5 Hz, $^3J_{HH}$ = 7.3 Hz), 7.76–7.80 (m, 4H), 7.81–7.84 (m, 4H), 8.00 (st, 1H, $^3J_{HH}$ = 1.8 Hz), 9.54 (s, 2H), 9.84 (s, 2H) ppm; ^{13}C NMR (126 MHz, DMSO-d_6, 30 °C): δ 124.7 (d), 125.3 (g), 126.2 (e), 127.0 (f), 127.3 (c), 127.8 (e′), 128.5 (b), 130.6 (j), 130.8 (h), 131.8 (a), 133.2 (d′), 134.0 (c′), 140.3 (j), 165.1 (k′); HRMS (ESI+) m/z $[M + Na]^+$ calcd for $[C_{32}H_{26}N_4O_6S_2Na]$, 649.1191; found, 649.1186, Δ = −0.8 ppm.

Crystallizations. X-ray quality crystals were obtained from ethyl acetate–hexane diffusion (EtOAc–Hex) and evaporation of acetonitrile (MeCN), 1,2-dichloroethane (DCE), or tetrahydrofuran (THF) solutions. However, only preliminary structures could be obtained for the MeCN and THF solvates (see Supporting Information for details). In all evaporation crystallizations, 20 mg of compound **2** was dissolved in 2–6 mL of the solvent. Heating and stirring were used to help the dissolving process. After the compound had fully dissolved, slow evaporation of the solvent was allowed at room temperature. In diffusion crystallization, 2 mg of compound **2** was dissolved in 0.5 mL of ethyl acetate and 2 mL of hexane was used as an antisolvent in a closed container. The sample was left to crystallize at room temperature.

X-ray Crystallography. Single crystal X-ray diffraction data was collected with a Bruker Nonius KappaCCD diffractometer at 173 K using a Bruker AXS APEX II CCD detector and graphite-monochromated Cu Kα radiation (λ = 1.54178 Å). The structures were solved with direct methods and refined using Fourier techniques with the SHELX-97 software package.[25] Absorption correction was performed with Denzo-SMN 1997.[26] All hydrogen atoms were placed to their idealized positions except for the N–H hydrogens, which were located from the electron density map and included in the structure factor calculations. Electron density of severely disordered solvent molecules in the EtOAc solvate structure was removed with the SQUEEZE[27] routine included in the PLATON[28] program in the WinGX package.[29] Full details of the crystallographic data and refinement are presented in Table 1 and in the Supporting Information. Graph set symbols for hydrogen bonding were assigned and used to compare the bonding between the different crystal structures.[30,31]

Table 1. Crystallographic Data for Solvate 2I (EtOAc) and Solvate 2II (DCE)

	solvate **2I** (EtOAc)	solvate **2II** (DCE)
formula	$C_{32}H_{26}N_4O_6S_2$	$C_{32}H_{26}N_4O_6S_2{\cdot}C_2H_4Cl_2$
MW/g mol^{-1}	626.69	725.64
crystal system	monoclinic	monoclinic
space group	$C2/c$	$P2_1/c$
a/Å	24.758(2)	13.1334(3)
b/Å	6.9874(5)	22.7870(6)
c/Å	21.0600(12)	11.6864(4)
β/deg	106.985(3)	104.874(10)
V/Å^3	3484.3(4)	3380.2(2)
Z	4	4
ρ_{calc}/g cm^{-3}	1.195	1.426
meas. reflns	4899	11 132
ind. reflns	2984	5889
R_{int}	0.0449	0.0427
R_1 $[I > 2\sigma(I)]$	0.0469	0.0449
wR_2 $[I > 2\sigma(I)]$	0.1216	0.1104
GoF	1.050	1.015

Computational Details. All calculations were performed with the Gaussian 09[32] program package using the ωB97XD density functional[33] and Ahlrichs' def2-TZVP basis sets.[34] The chosen density functional includes an empirical dispersion correction term which allows for better treat hydrogen bonding and van der Waals interactions than many conventional density functionals such as B3LYP. The initial geometries of conformers of **2** were taken directly from the single-crystal X-ray diffraction data. The global minimum conformation, **2III**, was obtained via potential energy surface scans in which the torsion angles of the sulfonamide substituents were systematically varied while keeping the other geometry parameters frozen. These scans were performed using a lower level basis set. The minima found were subjected to subsequent geometry optimizations using the same functional and basis set as those used for **2I** and **2II**. Gas-phase geometry optimizations were performed for all systems, and the nature of the located minima was confirmed by performing a full vibrational analysis. In addition to gas-phase calculations, a polarized continuum solvent model (IEFPCM)[35] was used to determine if the bulk properties of the solvents (EtOAc and DCE) had a significant influence on the energetic preference of different conformers of **2**. The energy values reported in the text are enthalpy differences obtained at 298 K and 1 atm.

DOI: 10.1021/acs.cgd.5b00424
Cryst. Growth Des. 2015, 15, 2602–2608

RESULTS AND DISCUSSION

The N^1,N^3-bis(2-benzamidophenyl)benzene-1,3-disulfonamide (**2**) was synthesized in good yield by a nucleophilic substitution reaction between *N*-benzoyl-2-aminoaniline (**1**) and benzene-1,3-disulfonyl chloride (Scheme 1). The product was characterized by ^{1}H and ^{13}C NMR spectroscopy including 2D techniques (COSY, HMQC, HMBC, and NOESY; see Supporting Information for details).

Scheme 1. Synthesis of Disulfonamide 2

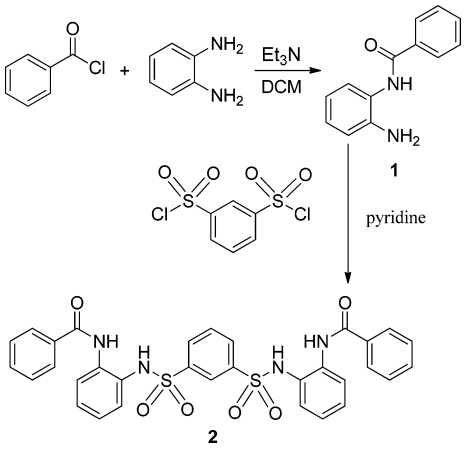

The ^{1}H NMR spectra of **2** in DMSO-d_6 and acetone-d_6 at room temperature are consistent with a symmetric structure for the molecular backbone, which indicates either the presence of a single preferred conformer with a C_2-symmetry axis or multiple conformers undergoing rapid exchange on the NMR time scale. Variable-temperature ^{1}H NMR measurements in acetone-d_6 showed no significant splitting of the proton signals when the temperature was gradually lowered to −80 °C, which confirmed that a rapid exchange process is unlikely. A NOESY NMR spectra of **2** in acetone-d_6 indicated NOEs between the protons of the terminal phenyl substituents and the hydrogen atoms of the sulfonamide groups, but this information was inconclusive for a detailed conformational determination.

Crystallographic Studies. Compound **2** was crystallized as two solvates, the ethyl acetate solvate (EtOAc, solvate **2I**) and the dichloroethane solvate (DCE, solvate **2II**), which differ by the conformation of **2** (Figure 1). Two lower-quality preliminary structures were also obtained: an acetonitrile (MeCN) solvate that is isomorphous with EtOAc solvate **2I** and a tetrahydrofuran (THF) solvate that is isomorphous with DCE solvate **2II** (see Supporting Information for details). In addition, powder diffraction data collected for the samples obtained from ethanol and methanol crystallizations of **2** suggest the existence of a third currently unknown crystal form, since the diffraction pattern bears very little resemblance to the patterns calculated from the single-crystal X-ray structures of solvates **2I** and **2II** (see Supporting Information for details).

In both conformers, the S−N bonds are roughly perpendicular to the plane of the central aromatic ring, which is typical to sulfonamides. In the structure of solvate **2I**, the conformation of **2** is unfolded and symmetrical, with the S−N bonds oriented on opposite sides of the central ring, whereas the conformation of **2** in solvate **2II** is loosely folded and asymmetric, with the S−N bonds on the same side of the central ring (Figure 1). In analogous oligoamide **3**, the C−N

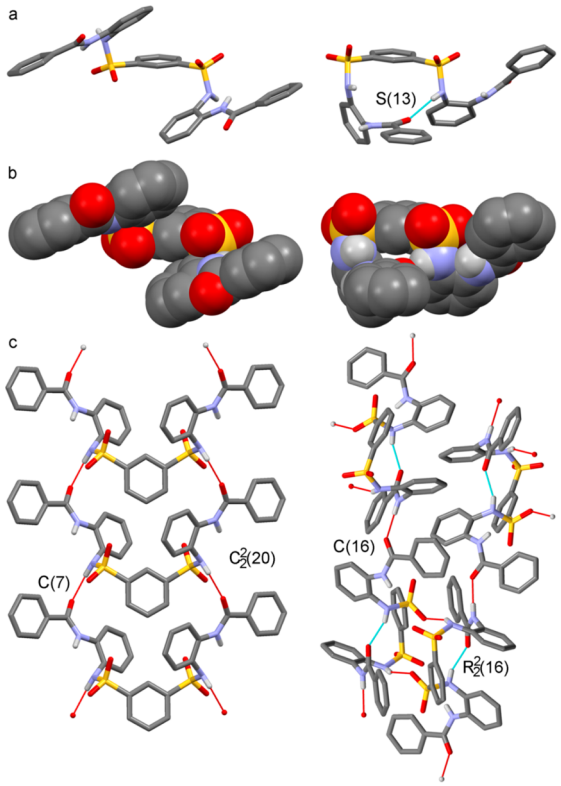

Figure 1. Two conformers of disulfonamide compound **2** crystallized from EtOAc (left, solvate **2I**) and DCE (right, solvate **2II**) shown as stick (a) and space filling (b) representations. Crystal packing highlighting intermolecular hydrogen bonding (c). Disordered solvent molecules and non-amide/sulfonamide hydrogen atoms have been removed for clarity.

bonds are on the same plane with the central aromatic ring, and a loosely folded conformer is stabilized by two intramolecular hydrogen bonds between neighboring amide groups (Figure 2).[21]

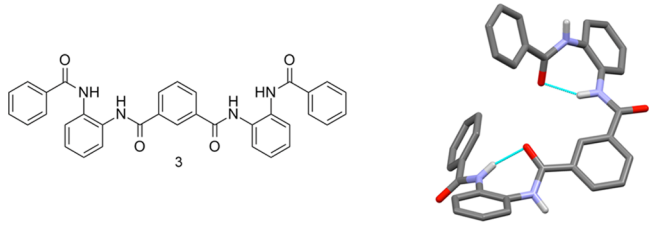

Figure 2. Loosely folded conformation of oligoamide **3**.[21] Non-amide hydrogen atoms have been removed for clarity.

The conformer of solvate **2I** is stabilized by two weak intramolecular amide-to-sulfonamide N−H···N hydrogen bonds (D···A 2.720(3) Å, ∠DHA 112(2)°) with no other significant intramolecular interactions present. Thus, the conformation in solvate **2I** appears to be mostly influenced by intermolecular interactions and packing effects instead of strong intramolecular interactions. Accordingly, disulfonamide **2** forms two intermolecular N−H···O=C hydrogen bonds (a *C*(7) motif) involving the sulfonamide (donor) and amide (acceptor) groups (D···A 2.793(3) Å, ∠DHA 171(3)°). The hydrogen bonding connects the molecules into chains along the crystallographic *b*-axis, giving rise to a double chain pattern ($C_2^2(20)$ motif) with head-to-tail arrangement of molecules in

DOI: 10.1021/acs.cgd.5b00424
Cryst. Growth Des. 2015, 15, 2602−2608

the chains (Figure 1). The individual chains exhibit offset $\pi-\pi$ stacking interactions between the outermost phenyl rings of neighboring molecules of **2** (see Supporting Information for details). The packing of **2** into parallel chains creates channels that contain severely disordered solvent molecules. This kind of disorder is expected, as there are no restricting interactions between the solvent and the channel walls.

The conformation of **2** in solvate **2II** reveals an intramolecular N−H···O═C hydrogen bond between the sulfonamide (donor) and amide (acceptor) groups (D···A 2.774(3) Å, ∠DHA 158(3)°) that gives **2** a folded conformation ($S(13)$ motif). The crystal packing is dominated by intermolecular N−H···O═C hydrogen bonding (D···A 2.834(3) Å, ∠DHA 161(3)°) that results in the formation of molecular chains along the crystallographic *b*-axis ($C(16)$ motif). The chains are further interconnected into sheet-like assemblies by two weak N−H···O═S hydrogen bonds ($R_2^2(16)$ motif) between the sulfonamide groups (D···A 3.079(3) Å, ∠DHA 157(3)°). The crystal packing of solvate **2II** also reveals $\pi-\pi$ stacking interactions between the $R_2^2(16)$ bonded molecular pairs (see Supporting Information for details). The disordered DCE molecules are located in the solvent-accessible voids between molecules of **2**.

The primary hydrogen-bonding networks in solvates **2I** and **2II** can be rationalized with the tendency of **2** to maximize interactions involving the amide carbonyls, since the amide carbonyl oxygen is known to be a better hydrogen-bond acceptor than the sulfonyl oxygen.[11] Consequently, the sulfonyl groups act as hydrogen-bond acceptors only between the molecular chains in the structure of solvate **2II**. This also means that there are amide and sulfonamide NH groups in both conformers of **2** that do not take part in the primary hydrogen-bonding network.

The reasons why different solvents and crystallization procedures lead to two different conformers of **2** are not obvious. The environmental conditions (temperature, moisture, and crystallization vessels) were kept as identical as possible for all experiments, and there are no clear trends in the results in relation to the physical and chemical properties of the solvents used. It can be argued that DCE is a poor hydrogen-bond acceptor compared to an amide carbonyl and therefore compound **2** should form intramolecular hydrogen bonds more willingly (solvate **2II**) than when better hydrogen-bond acceptors, such as EtOAc or MeCN, are used as solvent (solvate **2I**). However, the conformation of **2** in the THF solvate contradicts with this interpretation, as the hydrogen-bond acceptor properties of THF are more in line with those of EtOAc and MeCN than with DCE, but, still, a folded, isomorphous conformer to **2I** was nevertheless obtained.[36] Therefore, the likely explanation for two different conformers of **2** is that conformers are very close in energy and the interplay of inter- and intramolecular hydrogen bonding along with intramolecular steric hindrance caused by the bulky phenyl rings directs the organization of molecules to two different structures during crystal nucleation.

Computational Studies. In order to obtain more insight into the conformational features of **2**, its potential energy surface was analyzed with DFT by optimizing the structures of the two conformers observed in the solid state at the ωB97XD/def2-TZVPP level of theory.

The optimized structure of **2I** is similar to the conformer in solvate **2I** with major changes only in the hydrogen-bonding network. The weak N−H···N bonds observed in the crystal structure are replaced by two strong intramolecular N−H···O═S hydrogen bonds (D···A 2.869 Å, ∠DHA 154.1°) that result in a significantly more compact molecular geometry (Figures 3a and 4a). This is expected, as the orientation of the amide groups in the model system, a single molecule of **2**, is not fixed by intermolecular N−H···O═C hydrogen bonds whose formation is preferred in the solid state.

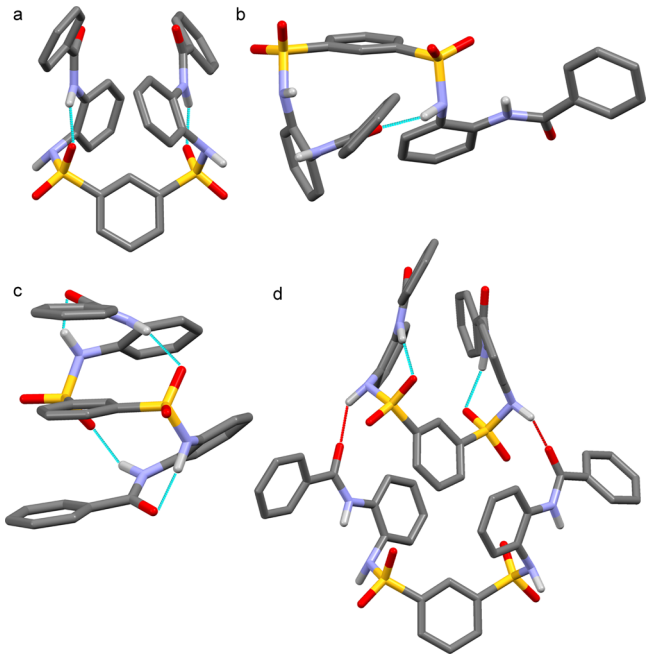

Figure 3. Optimized (ωB97XD/def2-TZVPP) structures of **2I** (a), **2II** (b), and **2III** (c) and a dimeric pair of **2I** (d). Non-amide/sulfonamide hydrogen atoms have been removed for clarity.

Unlike structure **2I**, the optimized geometry of **2II** is practically identical to the conformer in solvate **2II** (Figures 3b and 4b). The calculations reproduce well the intramolecular N−H···O═C hydrogen bond (D···A 2.842 Å, ∠DHA 155.4°) along with all other structural features of the molecular backbone. Only the torsional angles of the terminal phenyl groups are different, as the rotation of these groups is the most affected by crystal packing, which is not taken into account in calculations.

The computational results show that the conformer in solvate **2I** does not retain its crystal structure geometry without explicitly taking into account intermolecular interactions. Thus, the strong hydrogen bonding between neighboring molecules in the solid state plays a role in determining the conformation of the molecule. This was tested computationally by optimizing a dimeric pair of **2I** in the crystal structure geometry, in which case the intermolecular N−H···O═C hydrogen bonds kept the "tailing" molecule rather rigidly in place, whereas the geometry of the "heading" molecule changed from an open to a more compact form due to the formation of intramolecular N−H···O═S interactions (Figures 3d and 4c). Since the conformer of solvate **2II** was accurately reproduced even with the simplest possible model system, it seems that the folded conformer of **2**, once formed, can effectively guide the construction of a strong hydrogen-bonding network around it.

The energies of model systems **2I** and **2II** can also be compared for insight. If only intramolecular steric hindrance is considered, then the conformation of **2I** would be expected to

DOI: 10.1021/acs.cgd.5b00424
Cryst. Growth Des. 2015, 15, 2602−2608

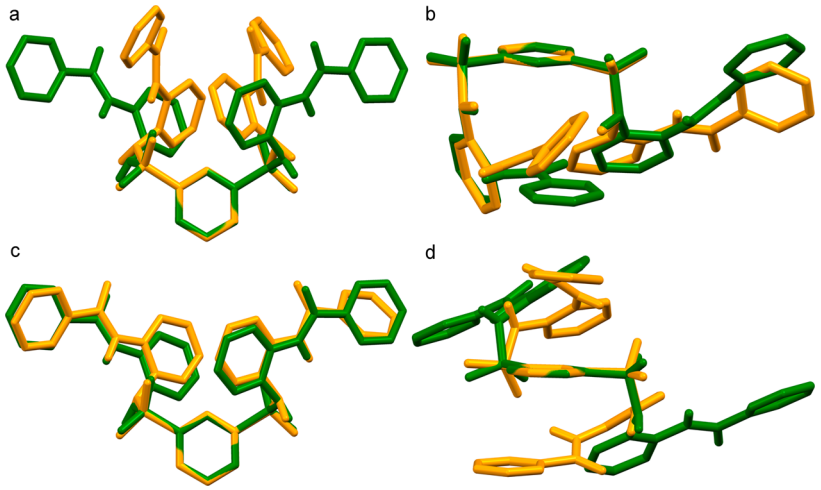

Figure 4. Overlay figures[37] of solvate conformer **2I** and calculated conformer **2I** (a), solvate conformer **2II** and calculated conformer **2II** (b), solvate conformer **2I** and an open conformer in the optimized dimeric pair of **2I** (c), and solvate conformer **2II** and calculated conformer **2III** (d). Crystal structure data and calculated structures are shown in green and yellow, respectively. Non-amide/sulfonamide hydrogen atoms have been removed for clarity.

be more favorable because of smaller repulsion between the bulky side chains. However, the calculations indicate that conformer **2II** is lower in energy, although only by approximately 7−11 kJ mol^{-1}, depending on whether the calculations were conducted in the gas phase or using a solvent model. The energy difference between the two conformers can be attributed to the strong intramolecular hydrogen bond in **2II**. It is also possible to compare the energy of the tailing monomer from the optimized dimeric pair of **2I**, denoted **2I***, with the optimized conformer **2II**, as both of these structures are very close to the geometries observed in the solid state (Figure 4). This comparison reveals that **2I*** is higher in energy than **2II** by 48 kJ mol^{-1} (approximately 35 kJ mol^{-1} for the solvated system), which further supports the notion that intermolecular interactions contribute much more to the stability of **2I** in the solid state than they do in the case of **2II**. Consequently, there seems to be an energetic preference toward structure **2II** in the gas phase and in solution which is then compensated by the external hydrogen-bonding network in the solid state, giving **2I** and **2II** nearly equal energies, as implied by the crystallization experiments. Unfortunately, the presence of severely disordered (and different) solvent molecules in the unit cells of solvates **2I** and **2II** prevents meaningful comparisons using computational energies based on unit cell data.

The potential energy surface of **2** is obviously complex with many different possibilities for the relative orientation of the side chains along with different secondary bonding interactions. An exhaustive search through all alternatives is beyond the scope of the present work. However, it was considered to be of interest to scan through some possible conformations that would maximize the intramolecular hydrogen bonding and therefore the folding of **2**. This led to the identification of conformer **2III** (Figures 3c and 4d) that has two N−H···O═C (D···A 2.714 Å, ∠DHA 141.4°) and two N−H···O═S (D···A 3.066 Å, ∠DHA 157.6°) hydrogen bonds that collectively give the molecule a symmetric S-shaped geometry. The terminal and central aromatic rings in **2III** adopt a mutually parallel orientation, but the distance between the rings does not indicate any significant $\pi-\pi$ interactions.

Due to extensive intramolecular hydrogen bonding, conformer **2III** is 39 kJ mol^{-1} more stable than **2II** (25 kJ mol^{-1} when using a solvent model). However, conformer **2III** was neither experimentally observed in the solid state nor could its presence in solution be identified. This could potentially be because of the presence of large energy barriers associated with the rotation of the bulky side chains, preventing such a folded structure from being adopted. Additionally, the hydrogen-bonding network in conformer **2III** is easily perturbed by appropriate solvent molecules, which could prevent its formation altogether.

Structural Comparisons. A search through the Cambridge Structural Database yielded only three sulfonamides related to **2** that contain a benzene-1,3-disulfonamide core with aromatic side chains (**4**−**6**; Figure 5).[24,38,39] In **4** and **5**, the S−N bonds are oriented on the opposite sides of the central ring in a manner similar to that in solvate **2I**. The rigidity of the

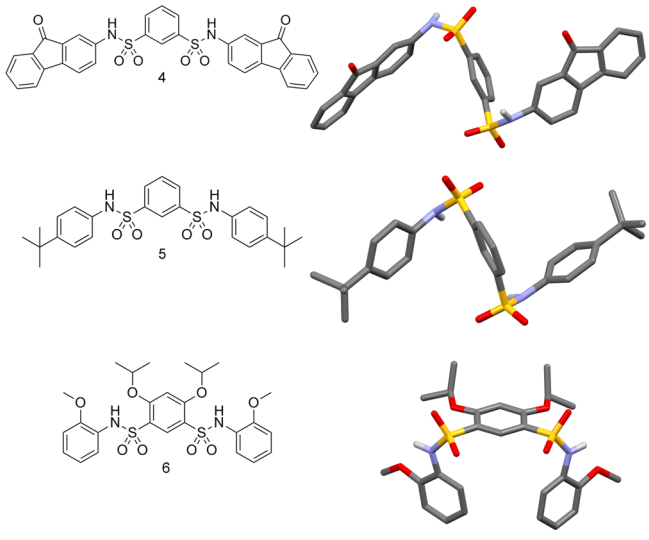

Figure 5. Molecular structures and conformations of disulfonamides **4**−**6**.[24,38,39] Non-amide/sulfonamide hydrogen atoms, solvent molecules, and the disorder of the *tert*-butyl substituents have been removed for clarity.

DOI: 10.1021/acs.cgd.5b00424
Cryst. Growth Des. 2015, 15, 2602−2608

molecules and the relative position of sulfonamide groups prohibit the formation of any intramolecular N−H···O═S hydrogen bonds. Instead, the solid-state structures of **4** and **5** exhibit intermolecular hydrogen bonds between the sulfonamide groups, which in the case of **5** results in the formation of molecular chains along the crystallographic *a*-axis.[38] In the case of **4**, the intermolecular hydrogen-bonding network involves one of the two carbonyl oxygen atoms on the aromatic side chains in addition to the sulfonamide groups.[24] Consequently, the conformation adopted by **4** and **5** is likely to be caused by favorable intermolecular hydrogen bonding and by steric hindrance associated with the bulky side chains. DFT calculations conducted for a single molecule of **5** predict a conformer with both aromatic side chains on the same side of the central ring to be lower in energy by 15 kJ mol^{-1} (see Supporting Information Figure S4). This supports the view that the conformation adopted by **5** in the solid state is strongly influenced by favorable intermolecular hydrogen-bonding interactions.

The conformation of compound **6** is similar to that of **2** in solvate **2II**. In this case, however, there is no intramolecular hydrogen bond to explain the orientation of the aromatic side chains on the same side of the central ring, but the conformation can be rationalized by the bulky isopropyl substituents, which direct the sulfonamide groups on the same side of the central ring. DFT calculations conducted for the two possible conformers of **6** indicate a small, 10 kJ mol^{-1}, energetic preference for the geometry observed in the solid state. In agreement with these structural features, it has been shown that the alkoxy-substituted diarylsulfonamide moiety in **6** is a convergent structural unit that can be used to build larger macrocyclic oligosulfonamides with predictable conformations.[38]

The Cambridge Structural Database was also searched for molecules similar to the folded conformer **2III** that was identified by calculations. A closely related conformer has been reported for compound **7** with a 4-methylphenol-2,5-disulfonamide core (Figure 6).[40] The conformational flexibility

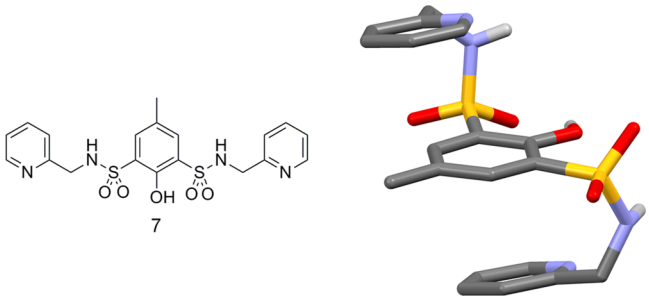

Figure 6. Molecular structure and conformation of disulfonamide **7** related to **2III**.[40] Non-amide and non-hydroxide hydrogen atoms have been removed for clarity.

of **7** can be ascribed to the methylene linkers between the sulfonamide groups and the terminal pyridyl rings, which, in the absence of significant steric strain, allow the molecule to adopt a folded S-shaped geometry in the solid state. Further stabilization for **7** is provided by intermolecular N−H···N and O−H···N hydrogen bonds and offset $\pi-\pi$ stacking interactions that organize the molecules into parallel columns along the crystallographic *a*-axis. DFT calculations for molecule **7** reproduce well the S-shaped geometry observed in the solid state (see Supporting Information for details). This strongly suggests that the folded conformation of the molecule is not just a result of packing effects and favorable intermolecular interactions in the solid state.

CONCLUSIONS

The folding of a disulfonamide compound **2** was studied both experimentally and computationally, and the results were compared to data reported for closely related oligoamide and disulfonamides **3**−**7**. Two significantly different conformers of **2** were observed in the solid state: one symmetrical and unfolded and the other unsymmetrical and loosely folded. Calculations at the density functional theory level showed that the observed conformers are relatively close in energy, which suggests that the adoption of a specific conformer during crystal nucleation involves a delicate interplay of intra- and/or intermolecular hydrogen bonding and steric hindrance caused by the bulky side chains. The calculations also indicated a third possible conformer of **2** with multiple intramolecular hydrogen bonds, giving the molecule both an S-shaped geometry and lower energy. The reason that this conformer was not observed experimentally was tentatively attributed to the energy barriers involved in the rotation of the side chains to adopt such a folded conformation.

The results indicate that oligomers with both amide and sulfonamide groups can easily assume at least two different stable conformers without apparent environmental factors. Thus, the controlled use of the sulfonamide bond as a component in foldamers is challenging and possibly requires synthetic modifications toward more flexible side chains or the use of a pyridine core. In analogous oligoamides, these changes have led to more folded structures and increased intramolecular hydrogen bonding. However, both the number of interaction sites in the sulfonamide derivative **2** and its ability to form channel structures suggest that it could potentially be used as a co-crystal host.

ASSOCIATED CONTENT

Supporting Information

Crystallographic data for two isomorphous preliminary structures of compound **2** (MeCN and THF solvates); notes on the crystallographic data; X-ray crystallographic information files (CIF) of solvates **2I**, **2IB**, **2II**, and **2IIB**; hydrogen-bonding parameters and relevant torsion angles (all structures); a figure of solvent channels in the structure of solvate **2I**; graphical representations of $\pi-\pi$ stacking interactions for solvates **2I** and **2II**; powder X-ray diffraction data of compound **2** (calculated and measured); ^{1}H, ^{13}C, COSY, HMBC, and HMQC NMR spectra of **2** in DMSO-d_6, a NOESY NMR spectra in acetone-d_6, and ^{1}H NMR spectra at 30 and −80 °C in acetone-d_6; optimized geometries (gas phase) of **2I**, **2I** dimeric pair, **2II**, and **2III** in *xyz* format; energies of structures **2I**, **2I***, **2II**, and **2III**; overlay figures of calculated and experimental structures of compounds **5**−**7**; and optimized structure of **5**. The Supporting Information is available free of charge on the ACS Publications website at DOI: 10.1021/acs.cgd.5b00424. Crystallographic information files are also available from the Cambridge Crystallographic Data Center (CCDC) upon request (http://www.ccdc.cam.ac.uk; CCDC deposition nos. 1022889−1022892).

DOI: 10.1021/acs.cgd.5b00424
Cryst. Growth Des. 2015, 15, 2602−2608

AUTHOR INFORMATION

Corresponding Author

*Tel: +358 50 428 0804. E-mail: maija.nissinen@jyu.fi.

Notes

The authors declare no competing financial interest.

ACKNOWLEDGMENTS

B.Sc. Hélène Campos Barbosa and B.Sc. Anniina Aho are acknowledged for their help with syntheses and crystallizations. We thank Dr. Elina Kalenius (ESI-TOF mass spectra), Laboratory Technician Elina Hautakangas (elemental analysis), and Chief Laboratory Technician Esa Haapaniemi (NMR spectroscopy). Financial support from the Academy of Finland (project no. 2100001911, K.H. and M.N.; project nos. 136929, 253907, and 272900, I.S.M. and H.M.T.) is gratefully acknowledged.

REFERENCES

(1) Grant, D. J. W. In *Polymorphism in Pharmaceutical Solids*; Brittain, H. G., Ed.; Marcel Dekker, Inc.: New York, 1999; pp 1−34.
(2) Gellman, S. H. *Acc. Chem. Res.* **1998**, *31*, 173−180.
(3) Hill, D. J.; Mio, M. J.; Prince, R. B.; Hughes, T. S.; Moore, J. S. *Chem. Rev.* **2001**, *101*, 3893−4011.
(4) Guichard, G.; Huc, I. *Chem. Commun.* **2011**, *47*, 5933−5941.
(5) Becerril, J.; Rodriguez, J. M.; Saraogi, I.; Hamilton, A. D. In *Foldamers: Structure, Properties, and Applications*; Hecht, S., Huc, I.; Eds.; Wiley-VCH Verlag GmbH & Co. KGaA: Weinheim, Germany, 2007.
(6) Zhang, D.-W.; Zhao, X.; Hou, J.-L.; Li, Z.-T. *Chem. Rev.* **2012**, *112*, 5271−5316.
(7) Huc, I. *Eur. J. Org. Chem.* **2004**, 17−29.
(8) Monnee, M. C. F.; Marjne, M. F.; Brouwer, A. W.; Liskamp, R. M. J. *Tetrahedron Lett.* **2000**, *41*, 7991−7995; Erratum. *Tetrahedron Lett.* **2001**, *42*, 965.
(9) Ramesh, V. V. E.; Kale, S. S.; Kotmale, A. S.; Gawade, R. L.; Puranik, V. G.; Rajamonahan, P. R.; Sanjayan, G. J. *Org. Lett.* **2013**, *15*, 1504−1507.
(10) Baldauf, C.; Günther, R.; Hofmann, H.-J. *J. Mol. Struct.: THEOCHEM* **2004**, *675*, 19−28.
(11) Adsmond, D. A.; Grant, D. J. W. *J. Pharm. Sci.* **2001**, *90*, 2058−2077.
(12) Sanphui, P.; Sarma, B.; Nangia, A. *Cryst. Growth Des.* **2010**, *10*, 4550−4564.
(13) Terada, S.; Katagiri, K.; Masu, H.; Danjo, H.; Sei, Y.; Kawahata, M.; Tominaga, M.; Yamaguchi, K.; Azumaya, I. *Cryst. Growth Des.* **2012**, *12*, 2908−2916.
(14) Vijayadas, K. N.; Davis, H. C.; Kotmale, A. S.; Gawade, R. L.; Puranik, V. G.; Rajamohanan, P. R.; Sanjayan, G. J. *Chem. Commun.* **2012**, *48*, 9747−9749.
(15) Caira, M. R. *Mol. Pharmaceutics* **2007**, *4*, 310−316.
(16) Wainwright, M.; Kristiansen, J. E. *Dyes Pigm.* **2011**, *88*, 231−234.
(17) Supuran, C. T.; Scozzafava, A. *Med. Res. Rev.* **2003**, *23*, 535−558.
(18) Maren, T. H. *Annu. Rev. Pharmacol. Toxicol.* **1976**, *16*, 309−327.
(19) Nakashima, K.; Murahashi, M.; Yuasa, H.; Ina, M.; Tada, N.; Itoh, A.; Hirashima, S.-I.; Koseki, Y.; Miura, T. *Molecules* **2013**, *18*, 14529−14542.
(20) Yang, H.; Carter, R. G. *Synlett* **2010**, 2827−2838.
(21) Suhonen, A.; Nauha, E.; Salorinne, K.; Helttunen, K.; Nissinen, M. *CrystEngComm* **2012**, *14*, 7398−7407.
(22) Kortelainen, M.; Suhonen, A.; Hamza, A.; Pápai, I.; Nauha, E.; Yliniemelä-Sipari, S.; Nissinen, M.; Pihko, P. M. *Chem.—Eur. J.* **2015**, DOI: 10.1002/chem.201406521.
(23) Bao, X.; Zhou, Y. *Sens. Actuators, B* **2010**, *147*, 434−441.
(24) Koivunen, J. T.; Nissinen, L.; Käpylä, J.; Jokinen, J.; Pihlavisto, M.; Marjamäki, A.; Heino, J.; Huuskonen, J.; Pentikäinen, O. T. *J. Am. Chem. Soc.* **2011**, *133*, 14558−14561.
(25) Sheldrick, G. M. *Acta Crystallogr., Sect. A: Found. Crystallogr.* **2008**, *64*, 112−122.
(26) Otwinowski, Z.; Borek, D.; Majewski, W.; Minor, W. *Acta Crystallogr., Sect. A: Found. Crystallogr.* **2003**, *59*, 228−234.
(27) van der Sluis, P.; Spek, A. L. *Acta Crystallogr., Sect. A: Found. Crystallogr.* **1990**, *46*, 194−201.
(28) Spek, A. L. *Acta Crystallogr., Sect. D: Biol. Crystallogr.* **2009**, *65*, 148−155.
(29) Farrugia, L. J. *J. Appl. Crystallogr.* **1999**, *32*, 837−838.
(30) Etter, M. C.; MacDonald, J. C.; Bernstein, J. *Acta Crystallogr., Sect B: Struct. Sci.* **1990**, *46*, 256−262.
(31) Bernstein, J.; Davis, R. E.; Shimoni, L.; Chung, N.-L. *Angew. Chem., Int. Ed. Engl.* **1995**, *34*, 1555−1573.
(32) Frisch, M. J.; Trucks, G. W.; Schlegel, H. B.; Scuseria, G. E.; Robb, M. A.; Cheeseman, J. R.; Scalmani, G.; Barone, V.; Mennucci, B.; Petersson, G. A.; Nakatsuji, H.; Caricato, M.; Li, X.; Hratchian, H. P.; Izmaylov, A. F.; Bloino, J.; Zheng, G.; Sonnenberg, J. L.; Hada, M.; Ehara, M.; Toyota, K.; Fukuda, R.; Hasegawa, J.; Ishida, M.; Nakajima, T.; Honda, Y.; Kitao, O.; Nakai, H.; Vreven, T.; Montgomery, J. A., Jr.; Peralta, J. E.; Ogliaro, F.; Bearpark, M.; Heyd, J. J.; Brothers, E.; Kudin, K. N.; Staroverov, V. N.; Kobayashi, R.; Normand, J.; Raghavachari, K.; Rendell, A.; Burant, J. C.; Iyengar, S. S.; Tomasi, J.; Cossi, M.; Rega, N.; Millam, J. M.; Klene, M.; Knox, J. E.; Cross, J. B.; Bakken, V.; Adamo, C.; Jaramillo, J.; Gomperts, R.; Stratmann, R. E.; Yazyev, O.; Austin, A. J.; Cammi, R.; Pomelli, C.; Ochterski, J. W.; Martin, R. L.; Morokuma, K.; Zakrzewski, V. G.; Voth, G. A.; Salvador, P.; Dannenberg, J. J.; Dapprich, S.; Daniels, A. D.; Farkas, O.; Foresman, J. B.; Ortiz, J. V.; Cioslowski, J.; Fox, D. J. *Gaussian 09*, revision D.01; Gaussian, Inc.: Wallingford, CT, 2009.
(33) Chai, J.-D.; Head-Gordon, H. *Phys. Chem. Chem. Phys.* **2008**, *10*, 6615−6620.
(34) Weigend, F.; Ahlrichs, R. *Phys. Chem. Chem. Phys.* **2005**, *7*, 3297−3305.
(35) Tomasi, J.; Mennucci, B.; Cammi, R. *Chem. Rev.* **2005**, *105*, 2999−3093.
(36) Marcus, Y. *Chem. Soc. Rev.* **1993**, *22*, 409−416.
(37) Overlay figures were drawn with Mercury CSD 3.5.1. Macrae, C. F.; Bruno, I. J.; Chisholm, J. A.; Edgington, P. R.; McCabe, P.; Pidcock, E.; Rodriguez-Monge, L.; Taylor, R.; van de Streek J.; Wood, P. A.; *J. Appl. Crystallogr.*, **2008**, *41*, 466−470.
(38) Eagle, C. T.; Kavallieratos, K.; Bryan, J. C. *J. Chem. Crystallogr.* **2002**, *32*, 165−170.
(39) He, L.; An, Y.; Yuan, L.; Feng, W.; Li, M.; Zhang, D.; Yamato, K.; Zheng, C.; Zeng, X. C.; Gong, B. *Proc. Natl. Acad. Sci. U.S.A.* **2006**, *103*, 10850−10855.
(40) Sundberg, J.; Witt, H.; Cameron, L.; Håkansson, M.; Bendix, J.; McKenzie, C. J. *Inorg. Chem.* **2014**, *53*, 2873−2882.

DOI: 10.1021/acs.cgd.5b00424
Cryst. Growth Des. 2015, 15, 2602−2608

IV

CONFORMATIONAL PROPERTIES AND FOLDING ANALYSIS OF A SERIES OF SEVEN OLIGOAMIDE FOLDAMERS

by

Aku Suhonen, Minna Kortelainen, Elisa Nauha, Sanna Yliniemelä-Sipari, Petri M. Pihko & Maija Nissinen, 2015

Manuscript, **2015**

Conformational Properties and Folding Analysis of a Series of Seven Oligoamide Foldamers

Aku Suhonen, Minna Kortelainen, Elisa Nauha, Sanna Yliniemelä-Sipari, Petri M. Pihko and Maija Nissinen*

33 crystal structures (11 unsolvated and 22 solvates) of a series of seven oligoamide foldamers were analysed. The crystal structures revealed that despite the structural and environmental differences the series of foldamers prefer only two general conformations, a protohelical @-conformation and a sigmoidal S-conformation. Both conformations have also preferred crystal packing motifs and solvate forming tendencies. Hydrogen bonding was found to be the most decisive factor in conformational preference, but steric properties, the type of the peripheral substituents, as well as solvent and aromatic interactions were also found to have an effect on the conformational details and crystal form.

Introduction

Foldamers are biomimetic molecular scaffolds composed of relatively simple repeating structural units, which makes their secondary structure somewhat predictable.[1,2] Foldamers are generally considered as artificial models for molecular folding,[3] but they may also find use in enzyme-like functions, for example as biomimetic receptors[4] and catalysts[5,6,7]. The most common bond type in foldamers is the amide bond with directional and relatively stable hydrogen bonding properties. Hydrogen bonding, and therefore also the molecular folding and crystal packing networks, are affected by the electronic environment created by the nearby functional groups with contribution from other possible weak interactions, hydrophobic forces and close packing effects.

Aromatic oligoamides present a promising class of foldamers because of their structural rigidity, functionalization potential of the aromatic rings, and the predictability of the hydrogen bonding properties of the amide bonds. Many studies have been conducted on the preparation, solution state folding and functionalization of a variety of aromatic amide foldamers; for example, helical and stranded pyridine-2,6-dicarboxamide and *N,N*-pyridine-2,6-formamide foldamers by Lehn *et al.*[8,9] and Huc *et al.*,[10,11] 1-3 stranded helices of quinoline and naphthyridine foldamers by Huc *et al.*,[12,13,14,15,16] and helical and linear aromatic oligoanthranilamides by Hamilton *et al.*[17,18] Solution state studies on the folding and aggregation behaviour of foldamers have mainly been done using NMR, and simulated with MD and DFT calculations. Single crystal X-ray diffraction studies have provided an important model and often a starting point when determining the solution state conformations of the foldamers. An in-depth understanding about the intermolecular solid state interactions and packing effects affecting the folding and conformational properties is therefore important to help to differentiate the conformational properties originating from the high density of the crystal structures from the universal conformational features and properties of the foldamer.

In our previous studies, we investigated the conformational variance of a series of oligoamide foldamers by computational, single crystal X-ray diffraction and NMR spectroscopic methods.[19,20] The oligoamide foldamers were able to adopt a conformation – among other almost equally stable conformers – where three intramolecular hydrogen bonds are formed to a single carbonyl oxygen, closely resembling an oxyanion hole motif found in the active sites of enzymes[21]. In enzymes, an oxyanion hole motif consists of two or more hydrogen bond donors, which can form hydrogen bonds to a negatively charged oxygen atom of a reaction intermediate. Multiple hydrogen bonds stabilize the intermediate and lower the energy cost of the reaction. Similar motifs can also arise when a single hydrogen bond acceptor, such as amide carbonyl, forms multiple hydrogen bonds to different hydrogen bond donors. The examples of non-peptidic systems mimicking this behaviour are still scarce, only a few examples of amide and ester carbonyls acting as an acceptor for multiple hydrogen bonds have been reported.[22,23]

Our previous studies showed that relatively small alterations in chemical structure and crystallization conditions have an effect on the preferred folding patterns of oligoamides and that the calculated energy difference between the observed folding

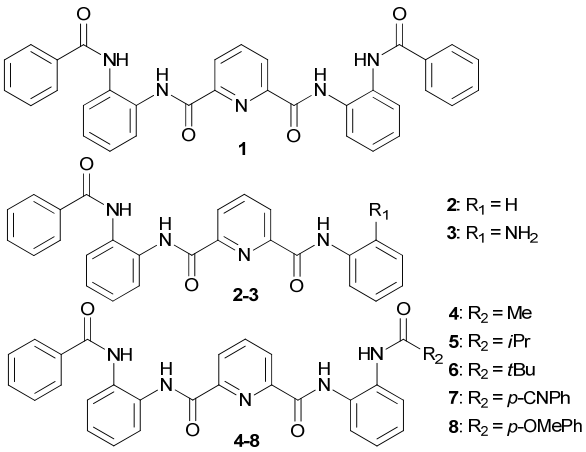

Scheme 1 Symmetrical oligoamide **1** and a series of asymmetric oligoamides **2**-**8**.

Nanoscience Center Department of Chemistry, University of Jyvaskyla, P.O. BOX 35 40014 JYU, Finland. E-mail: maija.nissinen@jyu.fi; Tel: +358 14 428 0804

Electronic Supplementary Information (ESI) available: Powder X-ray diffraction patterns, images of foldamer **2S**-DCM-2 solvate and foldamer **7** dioxane solvate, (**7S**$_2$-diox), notes on the crystallographic data including isomorphous crystal structures and hydrogen bonding parameters of the structures, lettering used in the NMR assignment of foldamer **3** and assigned ^{1}H and ^{13}C spectra and 2D COSY, HMBC and HMQC spectra of compound **3,** TGA-DTA graph of compound **2**-Form III. CIF files of the crystal structures. CCDC reference numbers 1436659-1436674 and 1438546.

patterns is very small (only 1-2 kcal/mol based on DFT calculations).[20] In this paper we present a more detailed solid state structural study of a series of seven oligoamide foldamers (Scheme 1) summarizing their conformational features, polymorphism and solvate formation, as well as the variance in crystal packing caused by the conformational preferences, small changes in their chemical structure and crystallization conditions.

Experimental

Materials and Methods

The oligoamide foldamers **1**,**2** and **4**-**8** (Scheme 1), as well as the intermediate products were prepared according to the literature procedures reported in our previous papers.[19,20] Compound **3** is previously unpublished and prepared according to the procedure outlined by Gunnlaugsson *et al.*[24] (Scheme 2). The starting materials were commercially available and used as such unless otherwise noted. The glassware was dried at 120°C prior to use. Dichloromethane was dried by distilling it over $CaCl_2$ and stored over Linde type 3 Å sieves under nitrogen atmosphere. Tetrahydrofurane (THF) was dried with MBraun solvent purification system. Triethylamine (Et_3N) was stored on molecular sieves (3 Å) and under nitrogen atmosphere. Analytical grade solvents and Millipore water were used for crystallizations.

NMR spectra were measured with Bruker Avance DRX 500 spectrometer and the chemical shifts were calibrated to the residual proton and carbon resonance of the deuterated solvent. The melting point was measured in an open capillary using a Stuart SMP30 melting point apparatus and is uncorrected. An ESI-TOF mass spectrum was measured with a LCT Micromass spectrometer. Elemental analysis was done with a Vario EL III instrument.

Synthesis of N2-(2-aminophenyl)-N6-(2-benzamidophenyl)-pyridine-2,6-dicarboxamide 3.[24] The synthesis was carried out under an argon atmosphere. *O*-phenylenediamine **9** (1.20 g; 11.13 mmol), 6-((2-benzamidophenyl)carbamoyl)picolinic acid **10** (1.00 g; 2.76 mmol) and hydroxybenzotriazole hydrate (HOBT) (0.43 g; 2.82 mmol) were dissolved in THF (120 ml). The solution was cooled to 0°C, and Et_3N (0.4 ml; 2.87 mmol) and 1-ethyl-3-(3-dimethylaminopropyl)carbodiimide (EDC) (0.5 ml; 2.82 mmol) were added to the solution. The cooled solution was stirred for an hour, allowed to warm to RT and stirred overnight. The solution was concentrated as oil and ethyl acetate (EtOAc) was added. This resulted in the product **3** precipitating as a white solid, yield 0.85 g (68%). mp. 243-245 °C; ^{1}H NMR (ESI†) (500 MHz, DMSO-d_6, 30 °C): δ = 4.92 (s, 2H; q), 6.61 (td, $^3J_{HH}$ = 1.4 Hz, $^3J_{HH}$ = 7.6 Hz 1H; k), 6.83 (dd, $^3J_{HH}$ = 1.4 Hz, $^3J_{HH}$ = 8.0 Hz, 1H; m), 7.00 (dd, $^3J_{HH}$ = 1.4 Hz, $^3J_{HH}$ = 7.9 Hz, 1H; j), 7.03-7.06 (m, 1H; l), 7.31-7.37 (m, 4H; b,e), 7.49-7.53 (m, 1H; a), 7.66-7.67 (m, 1H; d), 7.76-7.78 (m, 1H; f), 781-7.83 (m, 2H; c), 8.28 (t, $^3J_{HH}$ = 7.7 Hz, 1H; h), 8.33-8.35 (m, 1H; g/i), 8.38-8.40 (m, 1H; g/i), 10.20 (s, 1H; n), 10.44 (s, 1H; p), 11.14 (s, 1H; o), ^{13}C NMR (ESI†) (126 MHz, DMSO-d_6, 30 °C): δ = 116.05 (m/k), 116.19 (m/k), 122.15 (j'), 124.80 (g/i), 125.12 (g/i), 125.70 d/e/f), 125.81 (d/e/f), 125.94 (d/e/f), 127.17 (j,l), 127.59 (c), 128.34 (b), 130.63 (d'), 131.41 (f'), 131.74 (a), 133.85 (c'), 139.95 (h), 143.83 (m'), 148.36 (g'/i'), 148.79 (g'/i'), 161.66 (o',p'), 166.01 (n'); MS (ESI-TOF) *m/z*: 474.09 [M + Na^+]; Elemental analysis calcd (%) for $C_{26}H_{21}N_5O_3$: C 69.2, H 4.7, N 15.5; found C 68.8, H 4.7, N 15.3.

X-Ray crystallography

The crystal data and data collection parameters are presented in Table 1 and crystallization solvents in Table 2. The details of all crystallization experiments are reported in ESI.

Single crystal X-ray diffraction data of structures **2@**-Form II, **2@**-DMA, **2S**-DCM-1, **2S**-DCM-2, **4S**$_1$-Form II, **4S**$_1$-diox **7S**$_1$-THF and **7S**$_1$-DMA were collected with a Bruker Nonius KappaCCD diffractometer using a Bruker AXS APEX II CCD detector. The crystal structures of **1@**-MeCN, **1@**-Form II, **1@**-Ac and **1@**-DMSO-H_2O were measured with an Agilent Supernova Dualsource diffractometer using an Agilent Atlas CCD detector.

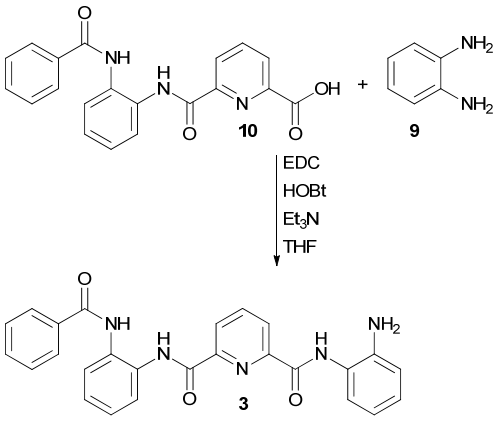

Scheme 2 The reaction scheme for the synthesis of compound **3**.

Table 1. Crystal data and collection parameters 1.

	1@-Form II	**1@**-DMA*	**1@**-DMSO-H_2O	**2@**-form II	**2@**-DMA	**2S**-DCM-1
Formula	$3C_{33}H_{25}N_5O_4$	$C_{33}H_{25}N_5O_4$• C_4H_9NO	$C_{33}H_{25}N_5O_4$• C_2D_6OS•H_2O	$C_{26}H_{20}N_4O_3$	$C_{26}H_{20}N_4O_3$• C_4H_9NO	$C_{26}H_{20}N_4O_3$• CH_2Cl_2
Crystallization solvent	DMSO-d_6	DMA	DMSO-d_6	DMA	DMA	DCM
M/gmol^{-1}	555.58	642.70	657.76	436.46	523.58	521.39
Crystal system	Triclinic	Monoclinic	Monoclinic	Orthorhombic	Triclinic	Triclinic
Space group	P-1	$P2_1/c$	$P2_1/c$	Pbca	P-1	P-1
a/Å	13.0733(2)	14.34241(19)	14.5114(7)	10.9333(6)	8.1890(2)	8.9343(1)
b/Å	16.7932(3)	19.5568(2)	19.1956(7)	18.0540(11)	12.1939(3)	12.0833(1)
c/Å	19.0162(2)	11.34410(16)	11.3102(4)	21.5317(14)	14.5599(3)	13.1298(1)
α/º	91.0697(11)	90	90	90	68.849(2)	112.097(1)
β/º	94.1916(12)	94.0477(12)	97.975(4)	90	80.180(3)	93.024(1)
γ/º	103.0744(14)	90	90	90	86.555(3)	101.520(1)
V/Å^3	4053.08	3173.98(7)	3120.0(2)	4250.1(4)	1336.1(1)	1263.1(3)
Z	6	4	4	8	2	2
ρ_{calc}/g cm^{-3}	1.366	1.345	1.400	1.364	1.301	1.359
Meas. reflns	84317	35938	10673	6664	6464	5929
Indep. reflns	17003	7844	6291	3634	4349	4297
T/K	123	173	123	173	173	173
Radiation	CuKα	MoKα	CuKα	CuKα	CuKα	CuKα
λ/Å	1.5418	0.7107	1.5418	1.54178	1.54178	1.54178
Monochromation	Mirror	Mirror	Mirror	Graphite	Graphite	Graphite
Absorption correction	analytical	analytical	analytical	multi-scan	multi-scan	multi-scan
Abs. Corr. program	CrysalisPro[25]	CrysalisPro	CrysalisPro	Denzo-SMN 1997[26]	Denzo-SMN 1997	Denzo-SMN 1997
Refinement programs	SHELX-2013,[27] ShelXle[28]	SHELX-2013, ShelXle	SHELX-2013, ShelXle	SHELX-97[27]	SHELX-97	SHELX-97
R_{int}	0.0345	0.0224	0.0655	0.0578	0.0588	0.0863
R_1 [I> 2σ(I)]	0.0425	0.0424	0.0610	0.0543	0.0512	0.0657
wR_2 [I> 2σ(I)]	0.1137	0.0981	0.1416	0.1132	0.1195	0.1671
GooF	1.087	1.024	1.093	1.039	1.027	1.052
	2S-DCM-2	**3@**-Form I	**4S$_1$**-Form II	**4S$_1$**-Diox	**4S$_1$**-DMSO	**6S$_2$**-Diox
Formula	$C_{26}H_{20}N_4O_3$• $0.5CH_2Cl_2$	$C_{26}H_{21}N_5O_3$	$C_{28}H_{23}N_5O_4$	$C_{28}H_{23}N_5O_4$• $0.5C_4H_8O_2$	$C_{28}H_{23}N_5O_4$• $2C_2H_6SO$	$C_{31}H_{29}N_5O_4$• $0.5C_4H_8O_2$
Crystallization solvent	DCM	MeCN	EtOAc	1,4-dioxane	DMSO	1,4-dioxane
M/gmol^{-1}	478.92	451.48	493.51	537.57	649.77	579.64
Crystal system	Triclinic	Triclinic	Monoclinic	Triclinic	Triclinic	Triclinic
Space group	P-1	P-1	C2/c	P-1	P-1	P-1
a/Å	9.0133(1)	8.5193(3)	28.6348(11)	8.7193(2)	8.7246(5)	9.6881(6)
b/Å	11.9653(1)	9.8054(4)	8.6348(3)	13.1332(3)	13.2012(5)	10.6294(7)
c/Å	12.0000(1)	14.3709(4)	21.4506(10)	13.2791(5)	15.2754(5)	15.8346(9)
α/º	83.142(1)	74.437(3)	90	114.688(1)	97.888(3)	105.487(5)
β/º	81.233(1)	75.224(3)	94.284(2)	97.288(1)	105.934(4)	103.244(5)
γ/º	69.213(1)	78.208(3)	90	103.683(1)	104.062(4)	102.241(5)
V/Å^3	1192.8(1)	1106.25(7)	4883.6(3)	1297.73(6)	1611.07(13)	1463.30(16)
Z	2	2	8	2	2	2
ρcalc/g cm^{-3}	1.333	1.355	1.342	1.376	1.339	1.316
Meas. reflns	5922	23956	6571	13017	11102	10347
Indep. reflns	4093	5460	4156	6647	7198	6610
T/K	173	173	173	173	173	173
Radiation	CuKα	MoKα	CuKα	MoKα	MoKα	MoKα
λ/Å	1.54178	0.7107	1.54178	0.71073	0.7107	0.7107
Monochromation	Graphite	Mirror	Graphite	Graphite	Mirror	Mirror
Absorption correction	multi-scan	multi-scan	multi-scan	multi-scan	multi-scan	multi-scan
Abs. Corr. program	Denzo-SMN 1997	CrysalisPro	Denzo-SMN 1997	Denzo-SMN 1997	CrysalisPro	CrysalisPro
Refinement programs	SHELX-97	SHELX-2013, ShelXle	SHELX-97	SHELX-97	SHELX-2013, ShelXle	SHELX-2013, ShelXle
Rint	0.0691	0.0265	0.0613	0.0700	0.0217	0.0222
R1 [I> 2σ(I)]	0.0582	0.0439	0.0518	0.0586	0.0516	0.0580
wR2 [I> 2σ(I)]	0.1498	0.1054	0.1129	0.1308	0.1138	0.0991
GooF	1.049	1.100	1.072	1.062	1.031	1.037

* Crystal data of the isomorphous solvate structures (acetone and acetonitrile solvates) are presented in the ESI.

	7S$_1$-$CHCl_3$	**7S**$_1$-DMA*
Formula	$C_{35}H_{25}N_6O_4$•$CHCl_3$	$C_{35}H_{25}N_6O_4$•C_4H_9ON
Crystallization solvent	$CHCl_3$	DMA
M/gmol^{-1}	699.96	667.71
Crystal system	Monoclinic	Monoclinic
Space group	$P2_1/n$	$P2_1/n$
a/Å	12.3983(2)	12.1856(5)
b/Å	19.7518(3)	20.3897(8)
c/Å	14.0691(2)	13.7195(5)
α/º	90	90
β/º	99.8562(16)	95.426(3)
γ/º	90	90
V/Å^3	3394.52(10)	3393.5(2)
Z	4	4
ρ_{calc}/g cm^{-3}	1.370	1.307
Meas. reflns	13725	9461
Indep. reflns	7694	5424
T/K	173	173
Radiation	MoKα	CuKα
λ/Å	0.7107	1.54178
Monochromation	Mirror	Graphite
Absorption correction	multi-scan	multi-scan
Abs. Corr. program	CrysalisPro	Denzo-SMN 1997
Refinement programs	SHELX-2013, ShelXle	SHELX-97
R_{int}	0.0161	0.0877
R_1 [I> 2σ(I)]	0.0501	0.0703
wR_2 [I> 2σ(I)]	0.1198	0.1653
GooF	1.024	1.021

* Crystal data of the isomorphous THF solvate is presented in the ESI.

The crystal structures of **1@**-DMA, **3@**-Form I, **4S**$_1$-DMSO, **6S**$_2$-Diox and **7S**$_1$-$CHCl_3$ were measured with an Agilent Supernova diffractometer using an Agilent Eos CCD detector. The structures were solved with direct methods and refined using Fourier techniques. All non-hydrogen atoms were refined anisotropically and the hydrogen atoms were placed in idealized positions except for N-H and H_2O hydrogen atoms which were found from the electron density map, and included in the structure factor calculations. Details of the crystal data and the refinement are presented in Table 1 and ESI.

The crystal structures were analysed by calculating the packing coefficients.[29] Graph set symbols[30,31] for hydrogen bonding were assigned and used to compare the hydrogen bonding between the different crystal structures.

Structures **2@**-Form I, **2S**-MeCN, **2@**-S-DMF, **4S**$_1$-Form I, **5@'**$_2$-Form I, **5S**$_1$-Form II, **6S**$_2$-Form I, **7@**$_2$-Form I and **7S**$_1$-EtOAc included in the discussion were published in our previous paper[20] and their details can be found there or free of charge from the Cambridge Crystallographic Data Centre via www.ccdc.cam.ac.uk/data request/cif, CCDC-1038215-1038223.

Results and Discussion

Folding patterns

The protohelical @-conformation originally found with compound **1**[19] provided an inspiration for the synthesis and folding studies of seven asymmetric analogues **2**-**8**[20] (Scheme 1) with different hydrogen properties and electron donating and withdrawing end groups. Foldamers **2** and **3** are shorter and lack one amide group at one end of the molecule. Foldamer **3**, however, has an amine group capable of hydrogen bonding at the ortho-position of the short end. The methyl (**4**), isopropyl (**5**) and *tert*-butyl (**6**) groups increase the electron density at the adjacent C=O group and show increasing steric hindrance, which affects their molecular conformation. Foldamers **7** and **8** have five aromatic rings connected by four amide bonds like foldamer **1** but also an electron density withdrawing cyano group (**7**) or, electron density donating

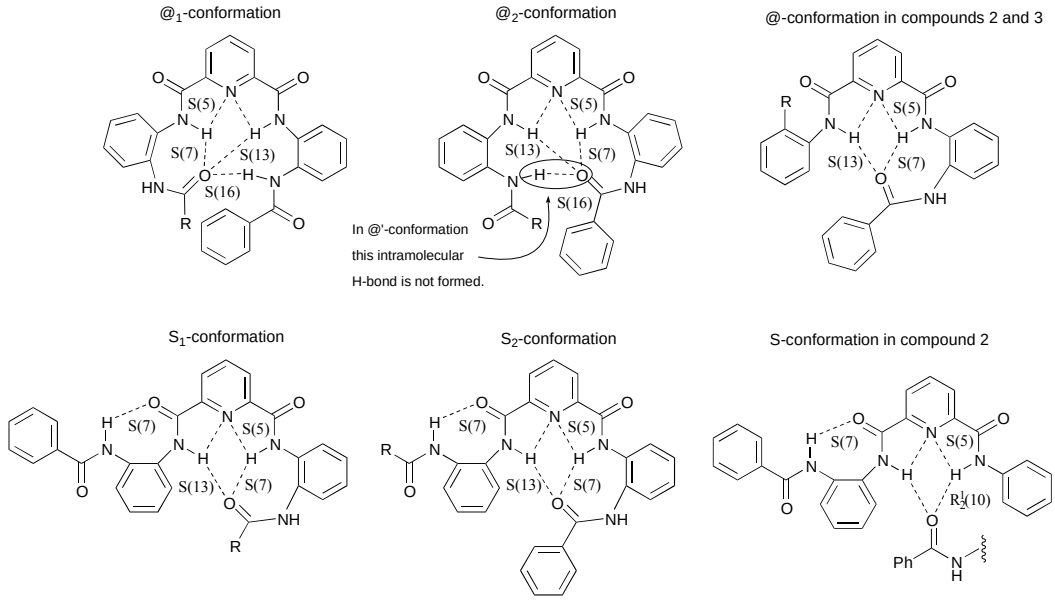

Scheme 3 Schematic representation of denotations of @ and S conformations. Subscripts describe which of the available carbonyls groups act as a hydrogen bond donor. With the smallest foldamers **2** and **3** only one type of @ conformation is possible and S conformer may also form via intermolecular hydrogen bonding.

Table 2. Crystal packing, packing coefficients and crystallizations solvents of the crystal structures of **1**-**7**.

Structure:	Packing motif:	Packing coefficient:	Coefficient Δ:	Crystallization solvent:
1@-Form I[19]	$R_2^2(14)$	0.7116	0.034330	EtOAc or MeCN
1@-Form II	$R_4^4(46), 2R_3^3(39)$	0.7270	0.018985	DMSO-d_6, 1:TBA-F $3H_2O$ (5:1)
1@-Ac	C(7)	0.7312	0.014780	Acetone-d_6, 1:TBA-Cl (3:1)
1@-DMA	C(7)	0.7374	0.008502	DMA
1@-DMF[19]	C(7)	0.7351	0.010803	DMF
1@-DMSO[19]	C(11)	0.7091	0.036808	DMSO
1@-DMSO-H_2O	C(7),$D_2^2(5)$	0.7459	0	DMSO-d_6, 1:TBA-F $3H_2O$ (1:4)
1@-EtOAc[19]	C(11)	0.6988	0.047159	EtOAc
1@-EtOH[19]	C(16)	0.7306	0.015293	EtOH
1@-MeCN	C(7)	0.7238	0.022152	MeCN
1@-MeOH[19]	C(16)	0.7317	0.014228	MeOH
1@-toluene[19]	C(11)	0.7011	0.044861	Toluene
2@-Form I[20]	C(11)	0.7121	0.018715	Acetone
2@-Form II	C(7)	0.7308	0	DMA
2S-DCM-1	$2R_2^1(10)$	0.6982	0.032628	DCM
2S-DCM-2	$2R_2^1(10)$	0.6984	0.032443	DCM
2@-DMA	D	0.7220	0.008799	DMA
2@-**S**-DMF[20]	$R_2^2(14), 2R_2^1(10)$	0.7200	0.010860	DMF
2S-MeCN[20]	$2R_2^1(10)$	0.7145	0.016341	MeCN
3@-Form I	$C_2^1(16)$	0.7224	0	MeCN, DMF, MeOH, EtOAc or Ac
4S$_1$-Form I[20]	$R_2^2(32)$	0.7106	0.028646	Acetone
4S$_1$-Form II	$R_2^2(32)$	0.7146	0.024712	EtOAc
4S$_1$-Diox	$R_2^2(32)$	0.7393	0	1,4-Dioxane
4S$_1$-DMSO	D	0.7189	0.020415	DMSO
5@'$_2$-Form I[20]	$C_2^2(23)$	0.7254	0	EtOAc
5S$_1$-Form II[20]	$R_2^2(14)$	0.699	0.025490	Toluene
6S$_2$-Form I[20]	C(11)	0.7151	0.008387	Acetone
6S$_2$-Diox	C(11))	0.7235	0	1,4-Dioxane
7@$_2$-Form I[20]	C(7)	0.7253	0	MeCN
7S$_1$-$CHCl_3$	$R_2^2(14)$	0.6811	0.044256	$CHCl_3$
7S$_1$-DMA	$R_2^2(14)$	0.7096	0.015744	DMA
7S$_1$-EtOAc[20]	$R_2^2(14)$	0.7135	0.011822	EtOAc
7S$_1$-THF	$R_2^2(14)$	0.6911	0.034294	THF

methoxy group (**8**) attached to the para position at one end of the molecule.

Foldamers **1-7** fold into two distinct conformations, denoted as the @- and S-conformation according to our previous article[20] (Scheme 3). Foldamers **2**, **5** and **7** were found to adopt both conformations, whereas foldamers **1** and **3** crystallized exclusively in the @-conformation and foldamers **4** and **6** only in the S-conformation. No crystal structures could be obtained for foldamer **8** despite several attempts in various solvents. In the @-conformation the oligoamide folds tightly around the pyridine core and forms two or three intramolecular hydrogen bonds to the same carboxyl oxygen (S(7), S(13) and S(16) motifs). In the conformational notation the number of hydrogen bonds is specified by an apostrophe, which designates that only two intramolecular hydrogen bonds are formed although three are possible.

In the S-conformation the molecule has a sigmoidal shape. One intramolecular hydrogen bond is formed from an outer amide N-H to an inner amide C=O group (S(7) motif) and two intramolecular hydrogen bonds are formed between the N-H groups next to pyridine, and the other outer amide bond C=O group (S(7) and S(13) motifs). Additionally, in all structures two weak intramolecular hydrogen bonds form from the central pyridine ring nitrogen to the inner amide bond N-H groups (S(5) motif). Both S- and @-conformers are further divided in categories 1 or 2 depending on which end of the molecule acts as a hydrogen bond acceptor to the pyridine core amide bonds (Scheme 3).

The main reason behind the popularity of the proto-helical @-conformation and the sigmoidal S-conformation is the potential to form several simultaneous intramolecular hydrogen bonds, which stabilize the conformers almost equally as evidenced by DFT calculations[20] and the prevalence of both conformers in crystal structures. The steric effects are likely to contribute to the conformation as well, especially in the case of foldamers **5** and **6** with bulkier aliphatic groups, which lead to a slight preference of more open and less compact S-conformer to minimize the steric strain.

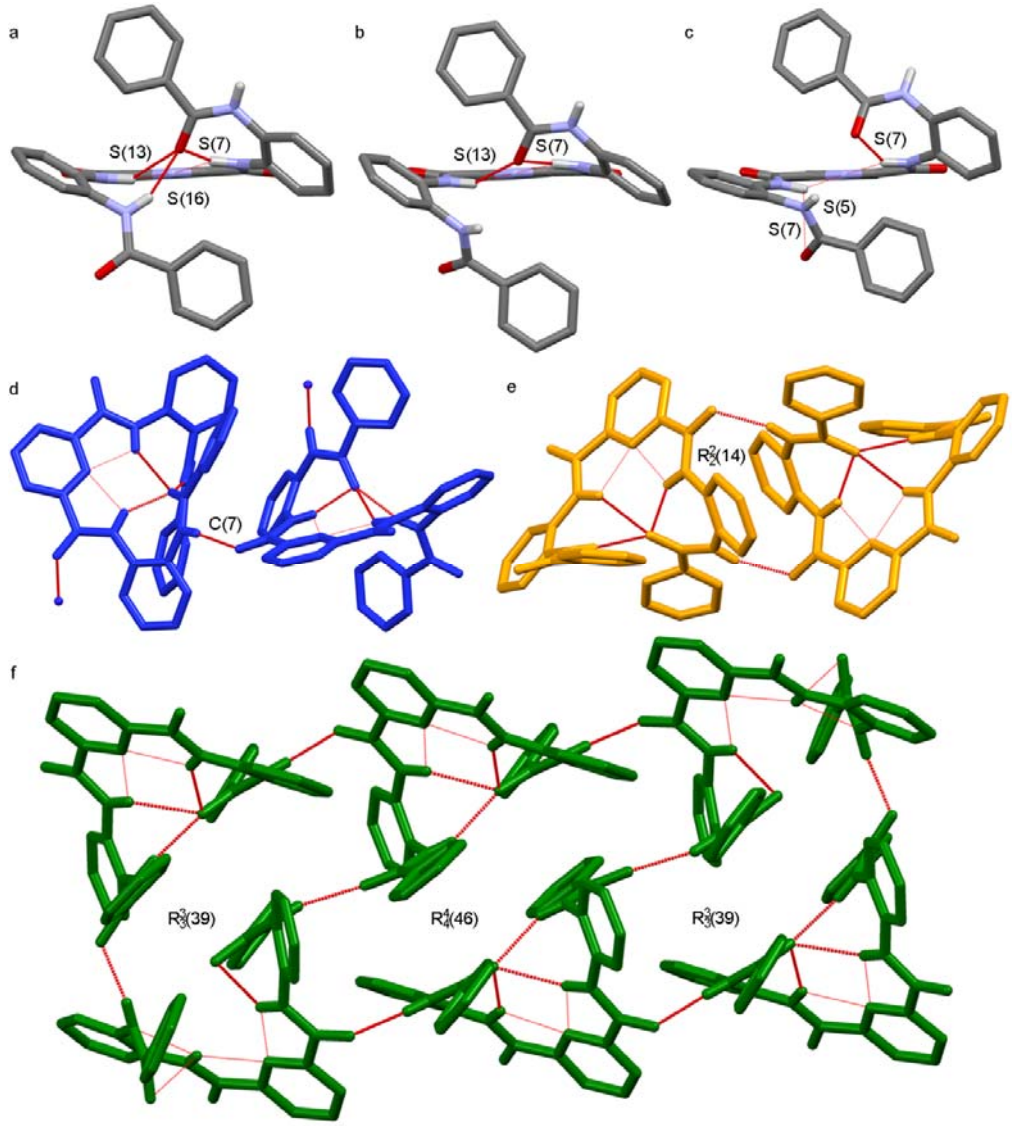

Figure 1. Variance in @-conformation of foldamer **1** a) @-conformation (**1@**-DMSO-H_2O), b) @'-conformation (**1@'**-DMSO)[20] and c) open @-like conformation (**1@**-Form II). Examples of foldamer **1** crystal packing d) a chain packing structure (C(7) motif, **1@**-DMA), e) a pair ring structure ($R_2^2(14)$motif **1@**-Form I) and f) six molecule double ring structure ($R_4^4(46)2R_3^3(39)$ motif, **1@**-Form II).

The effect of intramolecular aromatic interactions on the conformational properties is surprisingly small: although DFT calculations indicated stabilising aryl-aryl interactions, none are seen in the S-conformer structures, and only one or two weak T-stacking interactions are present and contribute to the stabilities of the @-conformers.

Structural analysis of individual compounds

Foldamer 1

Foldamer **1** proved to be a very versatile source of good quality crystals. Altogether 12 different crystal structures have been obtained for foldamer **1**: two polymorphs (previously published **1@**-Form I[19] and **1@**-Form II) and ten solvates with varying types of solvents, six of which are published previously[19]. The versatility of crystal formation was observed as nearly identical crystallization conditions produced several different crystal forms. For example, the crystallization experiments from DMSO solutions have produced three different crystal forms: unsolvated form II, DMSO/H_2O solvate and a DMSO solvate[19]. Ethyl acetate and acetonitrile crystallizations produced both **1@**-Form I, and respective solvates. However, some tendency to favour certain crystal forms according to solvent size and type was observed: DMF, DMA, acetonitrile and acetone solvates are isomorphous, as are also ethanol and methanol solvates and ethyl acetate and toluene solvates. The common theme in all crystal structures is still the tendency to strongly favour the @-conformation (Table 2, Figure 1a) with only a slight variation of conformational details: all other structures produce identical @-fold except for **1@**-Form II and **1@**-DMSO. In **1@**-Form II

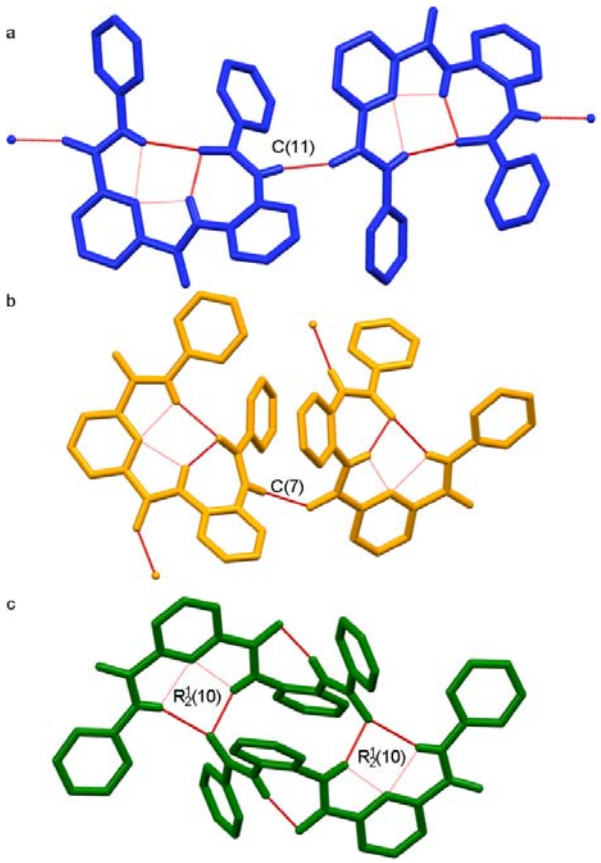

Figure 2. Crystal packing of foldamer **2**. a) Chain structure of **2@**-Form I (C(11) motif), b) Chain structure of **2@**-Form II (C(7) motif) and c) S-conformation pair structure ($2R_2^1(10)$ motif, **2@**-DCM-1).

the asymmetric unit contains three molecules, one of which is not in a perfect @-conformation, but instead found in a more open conformation, which nevertheless closely resembles the @-conformation (Figure 1c). This conformer has fewer and weaker hydrogen bonds and a different intramolecular hydrogen bond network (two S(7) motifs and S(5) motif). The @-conformer of foldamer **1** in the DMSO solvate[19] is classified as an @'-conformation (Figure 1b) as a slight twisting of the amide bond at the other end of the molecule prohibits the formation of a third hydrogen bond. Instead, the hydrogen bond is formed to a DMSO solvent molecule.

The crystal packing of the solvate structures of foldamer **1** favour chain-like motifs typical for most @-conformation structures, whereas two polymorphic forms, **1@**-Form I and **1@**-Form II, adopt a ring like packing motif. In **1@**-Form I the packing is based on pairs ($R_2^2(14)$ motif) and in **1@**-Form II as a triple ring formed by six molecules (see Table 2, Figure 1e and ESI, $2R_3^3(39), R_4^4(46)$ motif).

Foldamer 2

The lack of the fourth amide bond of foldamer **2** does not hinder the folding of the molecule and foldamer **2** crystallizes equally in @- and S-conformations. A fast overnight crystallization from DMF produced even a structure with both conformers present in the same crystal (Table 2). This indicates that, as suggested by DFT calculations,[20] the conformers are indeed close in energy and during the crystal nucleation the molecule is able to adopt both conformers depending on the conditions and the most favourable interactions.

Of seven obtained crystal structures five are solvates and two polymorphs, both of which are in the @-conformation (Figure 2a and 2b). In solvates both conformers are obtained and no clear solvent dependent pattern of which conformer crystallizes out is seen. As with foldamer **1** the same solvent may produce different crystal structures: form II and DMA solvate are both obtained from DMA solutions and two slightly different solvate types were obtained from DCM crystallizations (see ESI).

The crystal packing follows the general trends to each conformer, as @-conformers pack into chains (Figure 2a and 2b) and S-conformers as pairs. Notably, although the folding and adopted conformation is generally attributed to intramolecular hydrogen bonding, the shortest oligoamide foldamer **2** adopts the S-conformer because of intermolecular hydrogen bonding to an adjacent molecule, forming a pair (Scheme 3, Figure 2c).

Foldamer 3

Despite the close structural and chemical resemblance of foldamer **3** to foldamer **2** its crystallization modes were very different. Although many solvents were used and numerous crystallization attempts done, foldamer **3** always crystallized as the same unsolvated @-conformation structure (Table 1, Figure 3). The conformation closely resembles the @-conformation of foldamer **2** and the additional amine group does not participate in intramolecular bonding. Instead, the amine group is involved in forming a double chain crystal packing motif, which is likely very stable due to multiple hydrogen bonds and also the reason why only one crystal form is observed.

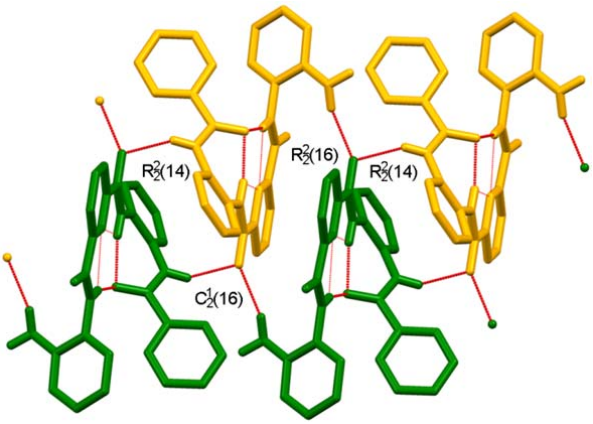

Figure 3. Crystal packing of foldamer **3**. Two ring motifs form a double chain.

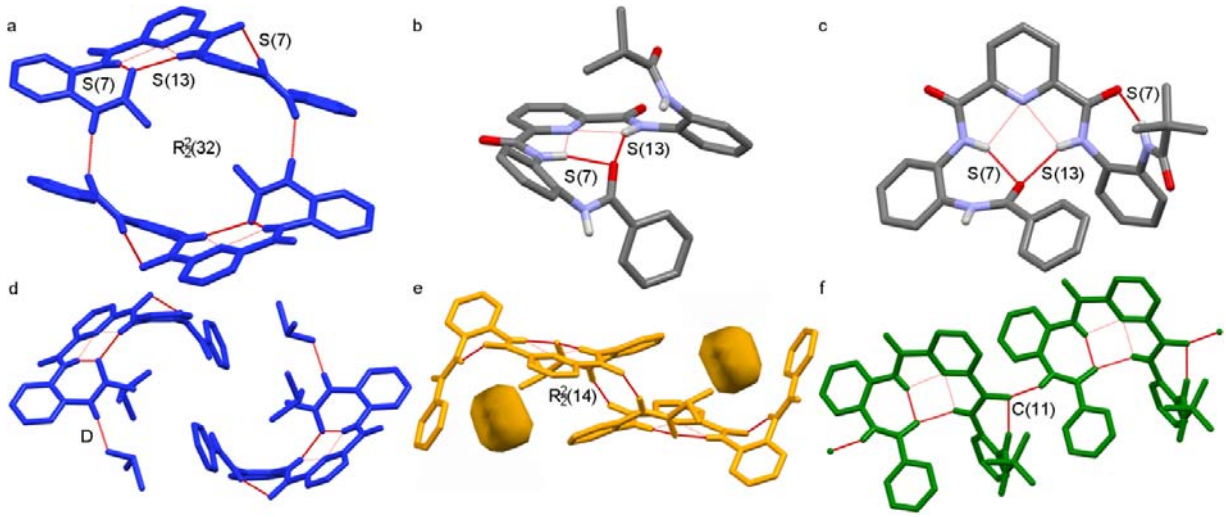

Figure 4. a) Stacked pair ($R_2^2(32)$ motif) in **4S**$_1$-Form I, b) foldamer **5** in @'$_2$ conformation (**5@**'$_2$-Form I), c) foldamer **6** in the S$_2$ conformation (**6S**$_2$-Form I), d) unpaired DMSO solvate **4S**$_1$-DMSO (D motif), e) crystal packing of foldamer **5**-Form II structure ($R_2^2(14)$ motif) showing non-solvent accessible voids, and f) chain-like crystal packing of foldamer **6** in **6S**$_2$-Form I (C(11) motif).

Foldamer 4

Foldamer **4** was exclusively found in the S$_1$-conformation both as polymorphs (**4S**$_1$-Form I and **4S**$_1$-Form II) and as two solvates (with DMSO and dioxane; Table 2). The result is surprising as the CH$_3$ group is small and provides only little steric hindrance for folding into an @-conformation. The prevalence of type 1 interactions (Scheme 3) can be rationalized by the fact that the methyl group at the acetyl moiety slightly increases the electron density of the closest C=O group thus making it more favourable as a hydrogen bond acceptor.

The crystal packing of foldamer **4** is defined by stacked pairs (Figure 4a), where the small CH$_3$-groups are efficiently nestled inside the dimer stabilized by two intermolecular hydrogen bonds ($R_2^2(32)$). The only example of an unpaired packing motif was seen with a DMSO solvate (**4S**$_1$-DMSO), where DMSO as a strong hydrogen bond acceptor forms a hydrogen bond to the foldamer (D motif) thus prohibiting the intermolecular hydrogen bonding network essential for the stacked pairs (Figure 4d).

Foldamer 5

Like foldamer **4**, foldamers **5** and **6** also have electron donating aliphatic groups with increasing size and bulkiness at one end of the molecule. Foldamer **5** was the other foldamer of the series, which did not crystallize as solvates, but only as two polymorphic forms, one in an @'$_2$-conformation and the other in an S$_1$-conformation (Figure 4b and 4e). The steric hindrance of the larger alkyl group affects the details of both structures. The @-conformer is stabilized by only two intramolecular hydrogen bonds and the alkyl end is slightly turned away from the fold interior. A double chain crystal packing motif ($C_2^2(23)$ motif, see ESI) contributes also to the stability of the @'$_2$-conformation. In the structure of **5S**$_1$-Form II stacked pairs are not possible because of the size of the isopropyl group. Instead, the foldamer molecules pack into parallel, displaced pairs ($R_2^2(14)$ motif). The structure contains small, non-solvent accessible voids (26 Å^3) and the packing coefficient is much smaller in comparison with the polymorphic forms of foldamer **4** and that of **5@**´$_2$-Form I (Table 2), which suggests a less efficient packing.

Foldamer 6

The crystallization experiments of foldamer **6** produced only one solvate and one unsolvated structure, both in the S$_2$-conformation, which is not observed with any other foldamer. The *tert*-butyl group causes considerable steric hindrance to the folding and is likely the main reason for the S$_2$-conformation (Table 2, Figure 4c and 4f). Exceptionally for the S-conformation, the foldamers pack into chains (C(11) motif). The reasons behind the unusual packing motif are not clear, but they could relate to the bulkiness of the *tert*-butyl group, as well as to the unique S$_2$-conformer.

Foldamer 7

Compared with the original foldamer **1**, foldamer **7** has a cyano substituent at the other end of the molecule, which withdraws the electron density from the phenyl ring and the closest carbonyl group. Therefore, one could assume that @$_2$- and S$_2$-conformations were favoured, but the crystallization studies yielded only one unsolvated structure in the @$_2$-conformation and four solvates in the S$_1$-conformation, two of which are isomorphous (THF and DMA). Although the *p*-cyanophenyl ring is large and bulky, the planar shape and possibility for aromatic interactions stabilise the @-conformation and alleviate the steric hindrance. As typical, the @-conformation packs into chains and the S$_1$-conformers as parallel, displaced pairs with solvent accessible voids, where the solvent molecules are located in all structures. The S$_1$-conformation and parallel stacked pair motif are probably due to steric reasons caused by the size of the *p*-cyanophenyl group: parallel displaced pairs

or stacked pairs could not form in S_1-conformation due to the size of the cyanophenyl groups.

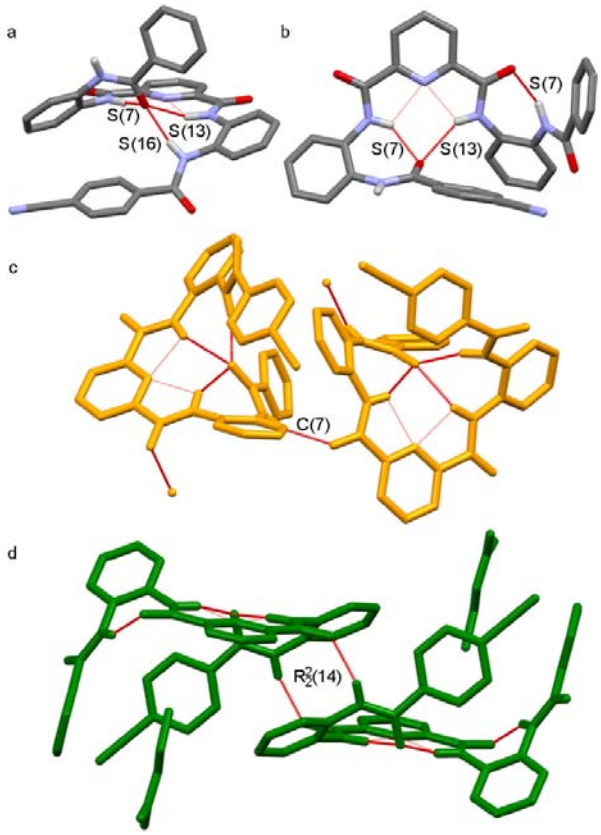

Figure 5. Conformations and crystal packing of foldamer **7** a) **7@**$_2$-Form I, b) **7S**$_1$-EtOAc, c) chain structure of **7@**$_2$-Form I (C(7) motif) and d) pair structure of **7S**$_1$-EtOAc ($R_2^2(14)$ motif).

Foldamer 8

Foldamer **8** is structurally very similar to foldamers **1** and **7**, but its solubility is much lower compared with the other foldamers. The methoxy group was designed to donate electron density to the carbonyl oxygen closest to it, but this small alteration in the structure caused such changes in the properties of the molecule that no crystal structures were obtained of foldamer **8**, which demonstrates how potent these small changes can be.

General trends in crystal packing and crystallization

General trends in the crystal packing show that the @-conformer enables more efficient crystal packing, as the packing coefficients of the @-conformers are generally higher than the packing coefficients of the S-conformers (Table 2). This could relate to a looser and more open form of the S-conformer, which together with the packing motif preferences may more easily lead to voids in the crystal structures.

The crystal packing of foldamers in the @-conformation favours the formation of continuous chains or discrete rings via hydrogen bonding (Figures 1-5, table 2). Hydrogen bonding to chains likely gives more stability to the protocrystal and allows an easy addition of foldamer molecules to the crystal phase during the crystal formation. There are also several intermolecular π-stacking interactions in an average structure that contribute to the stability of the packing.

S-conformers tend to favour a pairwise crystal packing (Figures 2 and 4-5, table 2). The S-conformation allows for efficient intermolecular pairing interactions thus creating a block-like unity that packs efficiently, but hinders the formation of hydrogen bonded chains like those in the @-conformation structures. Two types of paired structures were identified for the S-conformer structures; a stacked pair seen with the two smallest S-conformation foldamers **2** and **4** (Figure 2c and 4a) and a parallel displaced pair seen with foldamers **5** and **7** (Figure 4d and 5e). In the stacked pair the molecules are on top of each other whereas in the parallel displaced pair the molecules are only partially stacked. The parallel displaced pair allows enough space for the larger substituents, but also leads to a void near the pair (Figure 4d and ESI). The size of the void depends on the substituents: in the case foldamer **7** with a large aromatic ring the void is solvent accessible, but in the case of the foldamer **5** with a smaller substituent the void is non-solvent accessible (26 Å^3).[32]

The effect of the solvent and other crystallization conditions on the preferred conformations or crystal forms is fairly difficult to evaluate. Foldamers **1** and **2** showed remarkable crystallization tendencies in various solvents producing a variety of structures, both unsolvated polymorphs and solvates. This indicates great potential also as co-crystal formers and small molecule or ion hosts. Foldamer **3**, on the other hand, had a surprisingly uniform crystallization behavior as it repeatedly produced only one crystal form regardless of the solvent used. The other four foldamers have produced almost equally unsolvated and solvated forms, but the crystal formation is not as easy as with foldamers **1** and **2**.

Conclusions

Altogether 33 structures for a series of seven oligoamide foldamers were crystallized and analyzed. The compounds were found to fold in two distinct conformations with some variance in their intramolecular hydrogen bonding patterns. The nuances of the conformations were affected not only by hydrogen bonding but also by steric hindrance and variance in the electronic environment caused by the substituents. The effects of these substituents were the most visible for foldamer **8**, which did not crystallize at all. Nearly analogous foldamers **1** and **7**, both of which had much better solubility than foldamer **8**, produced readily good quality crystals from many different solvents. Although aromatic interactions were predicted to have effect on the conformation stability in previous DFT calculations, their effect in crystal structures was not as obvious.

Two of the foldamers (**1** and **3**) fold exclusively to a protohelical @-conformation, and two (**4** and **6**) exclusively to an S-conformation. For the other three (**2**, **5** and **7**) both conformers were observed with no clear pattern on the conformational preferences depending on crystallization conditions, such as solvent. This indicates that the

conformations are close in energy, as previous DFT calculations suggested, and that in solution both forms are likely present.

The crystal packing patterns vary depending on the conformation: the @-conformers favor chains while the S-conformers tend to form pairs. However, some exceptions to these patterns, caused by the interference of hydrogen bonding solvents, are seen. The crystal packing is mostly determined by intermolecular hydrogen bonding and the overall shape of the conformer.

The tendency to form solvates varied. Foldamer **2** forms several solvates, mostly in the S-conformation; while the nearly identical foldamer **3** did not form any solvates and repeatedly produced the same crystal form despite the solvent used. In general, the S-conformers are more likely to form solvates, whereas solvates and unsolvated structures are equally seen with @-conformation. This trend can be rationalized by inspecting the packing coefficients, which are larger with @-conformation structures indicating denser packing without voids.

Oligoamide foldamers have proven to be a very fruitful source of crystallographic information, as they, despite their size and flexibility, relatively easily produce good quality crystals in varying conditions and provide information on the subtle structural and environmental changes on the outcome of the solid state structures. Our future goal is to concentrate on the co-crystal and complex formation of the most versatile crystal formers, foldamers **1** and **2**, and, on the other hand, explore the uniform crystallization behavior of foldamer **3** and compare it with the conformational behavior in solution. This will clarify the reasons behind the crystal packing motifs and provide new insights for crystal engineering and crystal structure prediction.

Acknowledgements

We thank Spec. Lab. Technician Elina Hautakangas for the elemental analysis and Spec. Lab. Technician Esa Haapaniemi for measuring the ^{1}H, ^{13}C, COSY, HMBC and HMQC NMR spectra.

1 S. H. Gellman, *Acc. Chem. Res.*, 1998, **31**, 173.

2 D. J. Hill, M. J. Mio, R. B. Prince, T. S. Hughes and J. S. Moore, *Chem. Rev.*, 2001, **101**, 3893.

3 P. Claudon, A. Violette, K. Lamour, M. Decossas, S. Fournel, B. Heurtault, J. Godet, Y. Mély, B. Jamart-Grégoire, M.-C. Averlant-Petit, J.-P. Briand, G. Duportail, H. Monteil and G. Guichard, *Angew. Chem., Int. Ed.*, 2010, **49**, 333.

4 R. R. Araghi and B. Koksch, *Chem. Comm*, 2011, **47**, 3544.

5 J. Zhu, R. D. Barra, H. Zeng, E. Skrzypczak-Jankun, X. C. Zeng and B. Gong, *J. Am. Chem. Soc.*, 2000, **122**, 4219.

6 A. J. Neuvonen and P. M. Pihko, *Org. Lett.*, 2014, **16**, 5152.

7 N. Probst, Á. Madarász, A. Valkonen, I. Pápai, K. Rissanen, A. Neuvonen and P. M. Pihko, *Angew, Chem. Int. Ed.*, 2012, **51**, 8495.

8 V. Berl, I. Huc, R. G. Khoury and J.-M. Lehn, *Chem. Eur. J.*, 2001, **7**, 2798.

9 V. Berl, I. Huc, R. G. Khoury and J.-M. Lehn, *Chem. Eur. J.*, 2001, **7**, 2810.

10 I. Huc, V. Maurizot, H. Gornitzka and J.-M. Léger, *Chem. Commun.*, 2002, **6**, 578.

11 B. Baptiste, J. Zhu, D. Haldar, B. Kauffmann, J.-M. Léger and I. Huc, *Chem. Asian J.*, 2010, **5**, 1364.

12 H. Jiang, J.-M. Léger and I. Huc, *J. Am. Chem. Soc.*, 2003, **125**, 3448.

13 E.R. Gillies, C. Dolain, J.-M. Léger and I. Huc, *J. Org. Chem.*, 2006, **71**, 7931.

14 N. Delsuc, J.-M. Léger, S. Massip and I. Huc, *Angew. Chem. Int. Ed.*, 2007, **46**, 214.

15 D. Sánchez-Garcia, B. Kauffmann, T. Kawananni, H. Ihara, M. Takafuji, M.-H. Delville and I. Huc, *J. Am. Chem. Soc.*, 2009, **131**, 8642.

16 Y. Ferrand, A. M. Kendhale, J. Garric, B. Kauffman and I. Huc, *Angew. Chem. Int. Ed.*, 2010, **49**, 1778.

17 Y. Hamuro, S. J. Geib and A. D. Hamilton, *J. Am. Chem. Soc.*, 1996, **118**, 7529.

18 Y. Hamuro, S. J. Geib and A. D. Hamilton, *J. Am. Chem. Soc.*, 1997, **119**, 10587.

19 A. Suhonen, E. Nauha, K. Salorinne, K. Helttunen and M. Nissinen, *CrystEngComm*, 2012, **14**, 7398.

20 M. Kortelainen, A. Suhonen, A. Hamza, I. Pápai, E. Nauha, S. Yliniemelä-Sipari, M. Nissinen and P. Pihko, Chem. Eur. J., 2015, **21**, 9493.

21 P. M. Pihko, S. Rapakko and R. K. Wierenga, in *Hydrogen Bonding in Organic Synthesis*, ed. P.M. Pihko, WILEY-VCH Verlag GmbH & Co. KGaA, Weinheim, Germany, 2009, pp. 43.

22 K. Mitsui, S.A. Hyatt, D.A. Turner, C.M. Hadad, J.R. Parquette, *Chem. Commun.* **2009**, 3261.

23 N.T. Salzameda, D.A. Lightner, *Monatsh. Chem.* **2007**, *138*, 237

24 F. Stomeo, C. Lincheneau, J. P. Leonard, J. E. O'Brien, R. D. Peacock, C. P. McCoy and T. Gunnlaugsson, *J. Am. Chem. Soc.*, 2009, **131**, 9636.

25 Agilent (2011), CrysAlisPRO, Agilent Technologies UK Ltd, Yarnton, England.

26 Z. Otwinowski, D. Borek, W. Majewski and W. Minor, *Acta Crystallogr. A.*, 2003, **59**, 228.

27 G. M. Sheldrick, *Acta Crystallogr. A.*, 2008, **64**, 112.

28 C. B. Hübschle, G. M. Sheldrick and B. Dittrich, *J. Appl. Cryst.*, 2011, **44**, 1281.

29 A. I. Kitaĭgorodskiĭ, Organic Chemical Crystallography, Consultants Bureau, New York, 1961.

30 M. C. Etter and J. C. MacDonald, *Acta Crystallogr., Sect. B: Struct. Sci.*, 1990, **46**, 256.

31 J. Bernstein, R. E. Davis, L. Shimoni and N.-L. Chung, *Angew. Chem., Int. Ed.*, 1995, **34**, 1555.

32 A. L. Spek, *Acta Cryst. D*, 2009, **65**, 148.

DEPARTMENT OF CHEMISTRY, UNIVERSITY OF JYVÄSKYLÄ
RESEARCH REPORT SERIES

1. Vuolle, Mikko: Electron paramagnetic resonance and molecular orbital study of radical ions generated from (2.2)metacyclophane, pyrene and its hydrogenated compounds by alkali metal reduction and by thallium(III)trifluoroacetate oxidation. (99 pp.) 1976
2. Pasanen, Kaija: Electron paramagnetic resonance study of cation radical generated from various chlorinated biphenyls. (66 pp.) 1977
3. Carbon-13 Workshop, September 6-8, 1977. (91 pp.) 1977
4. Laihia, Katri: On the structure determination of norbornane polyols by NMR spectroscopy. (111 pp.) 1979
5. Nyrönen, Timo: On the EPR, ENDOR and visible absorption spectra of some nitrogen containing heterocyclic compounds in liquid ammonia. (76 pp.) 1978
6. Talvitie, Antti: Structure determination of some sesquiterpenoids by shift reagent NMR. (54 pp.) 1979
7. Häkli, Harri: Structure analysis and molecular dynamics of cyclic compounds by shift reagent NMR. (48 pp.) 1979
8. Pitkänen, Ilkka: Thermodynamics of complexation of 1,2,4-triazole with divalent manganese, cobalt, nickel, copper, zinc, cadmium and lead ions in aqueous sodium perchlorate solutions. (89 pp.) 1980
9. Asunta, Tuula: Preparation and characterization of new organometallic compounds synthesized by using metal vapours. (91 pp.) 1980
10. Sattar, Mohammad Abdus: Analyses of MCPA and its metabolites in soil. (57 pp.) 1980
11. Bibliography 1980. (31 pp.) 1981
12. Knuuttila, Pekka: X-Ray structural studies on some divalent 3d metal compounds of picolinic and isonicotinic acid N-oxides. (77 pp.) 1981
13. Bibliography 1981. (33 pp.) 1982
14. 6th National NMR Symposium, September 9-10, 1982, Abstracts. (49 pp.) 1982
15. Bibliography 1982. (38 pp.) 1983
16. Knuuttila, Hilkka: X-Ray structural studies on some Cu(II), Co(II) and Ni(II) complexes with nicotinic and isonicotinic acid N-oxides. (54 pp.) 1983
17. Symposium on inorganic and analytical chemistry May 18, 1984, Program and Abstracts. (100 pp.) 1984
18. Knuutinen, Juha: On the synthesis, structure verification and gas chromatographic determination of chlorinated catechols and guaiacols occuring in spent bleach liquors of kraft pulp mill. (30 pp.) 1984
19. Bibliography 1983. (47 pp.) 1984
20. Pitkänen, Maija: Addition of BrCl, B_2 and Cl_2 to methyl esters of propenoic and 2-butenoic acid derivatives and ^{13}C NMR studies on methyl esters of saturated aliphatic mono- and dichlorocarboxylic acids. (56 pp.) 1985
21. Bibliography 1984. (39 pp.) 1985
22. Salo, Esa: EPR, ENDOR and TRIPLE spectroscopy of some nitrogen heteroaromatics in liquid ammonia. (111 pp.) 1985

23. Humppi, Tarmo: Synthesis, identification and analysis of dimeric impurities of chlorophenols. (39 pp.) 1985
24. Aho, Martti: The ion exchange and adsorption properties of sphagnum peat under acid conditions. (90 pp.) 1985
25. Bibliography 1985 (61 pp.) 1986
26. Bibliography 1986. (23 pp.) 1987
27. Bibliography 1987. (26 pp.) 1988
28. Paasivirta, Jaakko (Ed.): Structures of organic environmental chemicals. (67 pp.) 1988
29. Paasivirta, Jaakko (Ed.): Chemistry and ecology of organo-element compounds. (93 pp.) 1989
30. Sinkkonen, Seija: Determination of crude oil alkylated dibenzothiophenes in environment. (35 pp.) 1989
31. Kolehmainen, Erkki (Ed.): XII National NMR Symposium Program and Abstracts. (75 pp.) 1989
32. Kuokkanen, Tauno: Chlorocymenes and Chlorocymenenes: Persistent chlorocompounds in spent bleach liquors of kraft pulp mills. (40 pp.) 1989
33. Mäkelä, Reijo: ESR, ENDOR and TRIPLE resonance study on substituted 9,10-anthraquinone radicals in solution. (35 pp.) 1990
34. Veijanen, Anja: An integrated sensory and analytical method for identification of off-flavour compounds. (70 pp.) 1990
35. Kasa, Seppo: EPR, ENDOR and TRIPLE resonance and molecular orbital studies on a substitution reaction of anthracene induced by thallium(III) in two fluorinated carboxylic acids. (114 pp.) 1990
36. Herve, Sirpa: Mussel incubation method for monitoring organochlorine compounds in freshwater recipients of pulp and paper industry. (145 pp.) 1991
37. Pohjola, Pekka: The electron paramagnetic resonance method for characterization of Finnish peat types and iron (III) complexes in the process of peat decomposition. (77 pp.) 1991
38. Paasivirta, Jaakko (Ed.): Organochlorines from pulp mills and other sources. Research methodology studies 1988-91. (120 pp.) 1992
39. Veijanen, Anja (Ed.): VI National Symposium on Mass Spectrometry, May 13-15, 1992, Abstracts. (55 pp.) 1992
40. Rissanen, Kari (Ed.): The 7. National Symposium on Inorganic and Analytical Chemistry, May 22, 1992, Abstracts and Program. (153 pp.) 1992
41. Paasivirta, Jaakko (Ed.): CEOEC'92, Second Finnish-Russian Seminar: Chemistry and Ecology of Organo-Element Compounds. (93 pp.) 1992
42. Koistinen, Jaana: Persistent polychloroaromatic compounds in the environment: structure-specific analyses. (50 pp.) 1993
43. Virkki, Liisa: Structural characterization of chlorolignins by spectroscopic and liquid chromatographic methods and a comparison with humic substances. (62 pp.) 1993
44. Helenius, Vesa: Electronic and vibrational excitations in some

biologically relevant molecules. (30 pp.) 1993

45. Leppä-aho, Jaakko: Thermal behaviour, infrared spectra and x-ray structures of some new rare earth chromates(VI). (64 pp.) 1994
46. Kotila, Sirpa: Synthesis, structure and thermal behavior of solid copper(II) complexes of 2-amino-2- hydroxymethyl-1,3-pr opanediol. (111 pp.) 1994
47. Mikkonen, Anneli: Retention of molybdenum(VI), vanadium(V) and tungsten(VI) by kaolin and three Finnish mineral soils. (90 pp.) 1995
48. Suontamo, Reijo: Molecular orbital studies of small molecules containing sulfur and selenium. (42 pp.) 1995
49. Hämäläinen, Jouni: Effect of fuel composition on the conversion of fuel-N to nitrogen oxides in the combustion of small single particles. (50 pp.) 1995
50. Nevalainen, Tapio: Polychlorinated diphenyl ethers: synthesis, NMR spectroscopy, structural properties, and estimated toxicity. (76 pp.) 1995
51. Aittola, Jussi-Pekka: Organochloro compounds in the stack emission. (35 pp.) 1995
52. Harju, Timo: Ultrafast polar molecular photophysics of (dibenzylmethine)borondifluoride and 4-aminophthalimide in solution. (61 pp.) 1995
53. Maatela, Paula: Determination of organically bound chlorine in industrial and environmental samples. (83 pp.) 1995
54. Paasivirta, Jaakko (Ed.): CEOEC'95, Third Finnish-Russian Seminar: Chemistry and Ecology of Organo-Element Compounds. (109 pp.) 1995
55. Huuskonen, Juhani: Synthesis and structural studies of some supramolecular compounds. (54 pp.) 1995
56. Palm, Helena: Fate of chlorophenols and their derivatives in sawmill soil and pulp mill recipient environments. (52 pp.) 1995
57. Rantio, Tiina: Chlorohydrocarbons in pulp mill effluents and their fate in the environment. (89 pp.) 1997
58. Ratilainen, Jari: Covalent and non-covalent interactions in molecular recognition. (37 pp.) 1997
59. Kolehmainen, Erkki (Ed.): XIX National NMR Symposium, June 4-6, 1997, Abstracts. (89 pp.) 1997
60. Matilainen, Rose: Development of methods for fertilizer analysis by inductively coupled plasma atomic emission spectrometry. (41 pp.) 1997
61. Koistinen, Jari (Ed.): Spring Meeting on the Division of Synthetic Chemistry, May 15-16, 1997, Program and Abstracts. (36 pp.) 1997
62. Lappalainen, Kari: Monomeric and cyclic bile acid derivatives: syntheses, NMR spectroscopy and molecular recognition properties. (50 pp.) 1997
63. Laitinen, Eira: Molecular dynamics of cyanine dyes and phthalimides in solution: picosecond laser studies. (62 pp.) 1997
64. Eloranta, Jussi: Experimental and theoretical studies on some

quinone and quinol radicals. (40 pp.) 1997

65. Oksanen, Jari: Spectroscopic characterization of some monomeric and aggregated chlorophylls. (43 pp.) 1998
66. Häkkänen, Heikki: Development of a method based on laser-induced plasma spectrometry for rapid spatial analysis of material distributions in paper coatings. (60 pp.) 1998
67. Virtapohja, Janne: Fate of chelating agents used in the pulp and paper industries. (58 pp.) 1998
68. Airola, Karri: X-ray structural studies of supramolecular and organic compounds. (39 pp.) 1998
69. Hyötyläinen, Juha: Transport of lignin–type compounds in the receiving waters of pulp mills. (40 pp.) 1999
70. Ristolainen, Matti: Analysis of the organic material dissolved during totally chlorine-free bleaching. (40 pp.) 1999
71. Eklin, Tero: Development of analytical procedures with industrial samples for atomic emission and atomic absorption spectrometry. (43 pp.) 1999
72. Välisaari, Jouni: Hygiene properties of resol-type phenolic resin laminates. (129 pp.) 1999
73. Hu, Jiwei: Persistent polyhalogenated diphenyl ethers: model compounds syntheses, characterization and molecular orbital studies. (59 pp.) 1999
74. Malkavaara, Petteri: Chemometric adaptations in wood processing chemistry. (56 pp.) 2000
75. Kujala Elena, Laihia Katri, Nieminen Kari (Eds.): NBC 2000, Symposium on Nuclear, Biological and Chemical Threats in the 21st Century. (299 pp.) 2000
76. Rantalainen, Anna-Lea: Semipermeable membrane devices in monitoring persistent organic pollutants in the environment. (58 pp.) 2000
77. Lahtinen, Manu: *In situ* X-ray powder diffraction studies of Pt/C, CuCl/C and Cu_2O/C catalysts at elevated temperatures in various reaction conditions. (92 pp.) 2000
78. Tamminen, Jari: Syntheses, empirical and theoretical characterization, and metal cation complexation of bile acid-based monomers and open/closed dimers. (54 pp.) 2000
79. Vatanen, Virpi: Experimental studies by EPR and theoretical studies by DFT calculations of α-amino-9,10-anthraquinone radical anions and cations in solution. (37 pp.) 2000
80. Kotilainen, Risto: Chemical changes in wood during heating at 150-260 °C. (57 pp.) 2000
81. Nissinen, Maija: X-ray structural studies on weak, non-covalent interactions in supramolecular compounds. (69 pp.) 2001
82. Wegelius, Elina: X-ray structural studies on self-assembled hydrogen-bonded networks and metallosupramolecular complexes. (84 pp.) 2001
83. Paasivirta, Jaakko (Ed.): CEOEC'2001, Fifth Finnish-Russian Seminar: Chemistry and Ecology of Organo-Element Compounds. (163 pp.) 2001
84. Kiljunen, Toni: Theoretical studies on spectroscopy and

atomic dynamics in rare gas solids. (56 pp.) 2001

85. Du, Jin: Derivatives of dextran: synthesis and applications in oncology. (48 pp.) 2001
86. Koivisto, Jari: Structural analysis of selected polychlorinated persistent organic pollutants (POPs) and related compounds. (88 pp.) 2001
87. Feng, Zhinan: Alkaline pulping of non-wood feedstocks and characterization of black liquors. (54 pp.) 2001
88. Halonen, Markku: Lahon havupuun käyttö sulfaattiprosessin raaka-aineena sekä havupuun lahontorjunta. (90 pp.) 2002
89. Falábu, Dezsö: Synthesis, conformational analysis and complexation studies of resorcarene derivatives. (212 pp.) 2001
90. Lehtovuori, Pekka: EMR spectroscopic studies on radicals of ubiquinones Q-*n*, vitamin K_3 and vitamine E in liquid solution. (40 pp.) 2002
91. Perkkalainen, Paula: Polymorphism of sugar alcohols and effect of grinding on thermal behavior on binary sugar alcohol mixtures. (53 pp.) 2002
92. Ihalainen, Janne: Spectroscopic studies on light-harvesting complexes of green plants and purple bacteria. (42 pp.) 2002
93. Kunttu, Henrik, Kiljunen, Toni (Eds.): 4th International Conference on Low Temperature Chemistry. (159 pp.) 2002
94. Väisänen, Ari: Development of methods for toxic element analysis in samples with environmental concern by ICP-AES and ETAAS. (54 pp.) 2002
95. Luostarinen, Minna: Synthesis and characterisation of novel resorcarene derivatives. (200 pp.) 2002
96. Louhelainen, Jarmo: Changes in the chemical composition and physical properties of wood and nonwood black liquors during heating. (68 pp.) 2003
97. Lahtinen, Tanja: Concave hydrocarbon cyclophane B-prismands. (65 pp.) 2003
98. Laihia, Katri (Ed.): NBC 2003, Symposium on Nuclear, Biological and Chemical Threats – A Crisis Management Challenge. (245 pp.) 2003
99. Oasmaa, Anja: Fuel oil quality properties of wood-based pyrolysis liquids. (32 pp.) 2003
100. Virtanen, Elina: Syntheses, structural characterisation, and cation/anion recognition properties of nano-sized bile acid-based host molecules and their precursors. (123 pp.) 2003
101. Nättinen, Kalle: Synthesis and X-ray structural studies of organic and metallo-organic supramolecular systems. (79 pp.) 2003
102. Lampiselkä, Jarkko: Demonstraatio lukion kemian opetuksessa. (285 pp.) 2003
103. Kallioinen, Jani: Photoinduced dynamics of $Ru(dcbpy)_2(NCS)_2$ – in solution and on nanocrystalline titanium dioxide thin films. (47 pp.) 2004
104. Valkonen, Arto (Ed.): VII Synthetic Chemistry Meeting and XXVI Finnish NMR Symposium. (103 pp.) 2004

105. Vaskonen, Kari: Spectroscopic studies on atoms and small molecules isolated in low temperature rare gas matrices. (65 pp.) 2004
106. Lehtovuori, Viivi: Ultrafast light induced dissociation of $Ru(dcbpy)(CO)_2I_2$ in solution. (49 pp.) 2004
107. Saarenketo, Pauli: Structural studies of metal complexing schiff bases , Schiff base derived *N*-glycosides and cyclophane π-prismands. (95 pp.) 2004
108. Paasivirta, Jaakko (Ed.): CEOEC'2004, Sixth Finnish-Russian Seminar: Chemistry and Ecology of Organo-Element Compounds. (147 pp.) 2004
109. Suontamo, Tuula: Development of a test method for evaluating the cleaning efficiency of hard-surface cleaning agents. (96 pp.) 2004
110. Güneş, Minna: Studies of thiocyanates of silver for nonlinear optics. (48 pp.) 2004
111. Ropponen, Jarmo: Aliphatic polyester dendrimers and dendrons. (81 pp.) 2004
112. Vu, Mân Thi Hong: Alkaline pulping and the subsequent elemental chlorine-free bleaching of bamboo (*Bambusa procera*). (69 pp.) 2004
113. Mansikkamäki, Heidi: Self-assembly of resorcinarenes. (77 pp.) 2006
114. Tuononen, Heikki M.: EPR spectroscopic and quantum chemical studies of some inorganic main group radicals. (79 pp.) 2005
115. Kaski, Saara: Development of methods and applications of laser-induced plasma spectroscopy in vacuum ultraviolet. (44 pp.) 2005
116. Mäkinen, Riika-Mari: Synthesis, crystal structure and thermal decomposition of certain metal thiocyanates and organic thiocyanates. (119 pp.) 2006
117. Ahokas, Jussi: Spectroscopic studies of atoms and small molecules isolated in rare gas solids: photodissociation and thermal reactions. (53 pp.) 2006
118. Busi, Sara: Synthesis, characterization and thermal properties of new quaternary ammonium compounds: new materials for electrolytes, ionic liquids and complexation studies. (102 pp.) 2006
119. Mäntykoski, Keijo: PCBs in processes, products and environment of paper mills using wastepaper as their raw material. (73 pp.) 2006
120. Laamanen, Pirkko-Leena: Simultaneous determination of industrially and environmentally relevant aminopolycarboxylic and hydroxycarboxylic acids by capillary zone electrophoresis. (54 pp.) 2007
121. Salmela, Maria: Description of oxygen-alkali delignification of kraft pulp using analysis of dissolved material. (71 pp.) 2007
122. Lehtovaara, Lauri: Theoretical studies of atomic scale impurities in superfluid ^{4}He. (87 pp.) 2007
123. Rautiainen, J. Mikko: Quantum chemical calculations of structures, bonding, and spectroscopic properties of some sulphur and selenium iodine cations. (71 pp.) 2007
124. Nummelin, Sami: Synthesis, characterization, structural and

retrostructural analysis of self-assembling pore forming dendrimers. (286 pp.) 2008

125. Sopo, Harri: Uranyl(VI) ion complexes of some organic aminobisphenolate ligands: syntheses, structures and extraction studies. (57 pp.) 2008
126. Valkonen, Arto: Structural characteristics and properties of substituted cholanoates and *N*-substituted cholanamides. (80 pp.) 2008
127. Lähde, Anna: Production and surface modification of pharmaceutical nano- and microparticles with the aerosol flow reactor. (43 pp.) 2008
128. Beyeh, Ngong Kodiah: Resorcinarenes and their derivatives: synthesis, characterization and complexation in gas phase and in solution. (75 pp.) 2008
129. Välisaari, Jouni, Lundell, Jan (Eds.): Kemian opetuksen päivät 2008: uusia oppimisympäristöjä ja ongelmalähtöistä opetusta. (118 pp.) 2008
130. Myllyperkiö, Pasi: Ultrafast electron transfer from potential organic and metal containing solar cell sensitizers. (69 pp.) 2009
131. Käkölä, Jaana: Fast chromatographic methods for determining aliphatic carboxylic acids in black liquors. (82 pp.) 2009
132. Koivukorpi, Juha: Bile acid-arene conjugates: from photoswitchability to cancer cell detection. (67 pp.) 2009
133. Tuuttila, Tero: Functional dendritic polyester compounds: synthesis and characterization of small bifunctional dendrimers and dyes. (74 pp.) 2009
134. Salorinne, Kirsi: Tetramethoxy resorcinarene based cation and anion receptors: synthesis, characterization and binding properties. (79 pp.) 2009
135. Rautiainen, Riikka: The use of first-thinning Scots pine (*Pinus sylvestris*) as fiber raw material for the kraft pulp and paper industry. (73 pp.) 2010
136. Ilander, Laura: Uranyl salophens: synthesis and use as ditopic receptors. (199 pp.) 2010
137. Kiviniemi, Tiina: Vibrational dynamics of iodine molecule and its complexes in solid krypton - Towards coherent control of bimolecular reactions? (73 pp.) 2010
138. Ikonen, Satu: Synthesis, characterization and structural properties of various covalent and non-covalent bile acid derivatives of N/O-heterocycles and their precursors. (105 pp.) 2010
139. Siitonen, Anni: Spectroscopic studies of semiconducting single-walled carbon nanotubes. (56 pp.) 2010
140. Raatikainen, Kari: Synthesis and structural studies of piperazine cyclophanes – Supramolecular systems through Halogen and Hydrogen bonding and metal ion coordination. (69 pp.) 2010
141. Leivo, Kimmo: Gelation and gel properties of two- and three-component Pyrene based low molecular weight organogelators. (116 pp.) 2011
142. Martiskainen, Jari: Electronic energy transfer in light-harvesting complexes isolated from *Spinacia oleracea* and from three

photosynthetic green bacteria *Chloroflexus aurantiacus*, *Chlorobium tepidum*, and *Prosthecochloris aestuarii*.(55 pp.) 2011

143. Wichmann, Oula: Syntheses, characterization and structural properties of [O,N,O,X´] aminobisphenolate metal complexes. (101 pp.) 2011
144. Ilander, Aki: Development of ultrasound-assisted digestion methods for the determination of toxic element concentrations in ash samples by ICP-OES. (58 pp.) 2011
145. The Combined XII Spring Meeting of the Division of Synthetic Chemistry and XXXIII Finnish NMR Symposium. Book of Abstracts. (90 pp.) 2011
146. Valto, Piia: Development of fast analysis methods for extractives in papermaking process waters. (73 pp.) 2011
147. Andersin, Jenni: Catalytic activity of palladium-based nanostructures in the conversion of simple olefinic hydro- and chlorohydrocarbons from first principles. (78 pp.) 2011
148. Aumanen, Jukka: Photophysical properties of dansylated poly(propylene amine) dendrimers. (55 pp.) 2011
149. Kärnä, Minna: Ether-functionalized quaternary ammonium ionic liquids – synthesis, characterization and physicochemical properties. (76 pp.) 2011
150. Jurček, Ondřej: Steroid conjugates for applications in pharmacology and biology. (57 pp.) 2011
151. Nauha, Elisa: Crystalline forms of selected Agrochemical actives: design and synthesis of cocrystals. (77 pp.) 2012
152. Ahkola, Heidi: Passive sampling in monitoring of nonylphenol ethoxylates and nonylphenol in aquatic environments. (92 pp.) 2012
153. Helttunen, Kaisa: Exploring the self-assembly of resorcinarenes: from molecular level interactions to mesoscopic structures. (78 pp.) 2012
154. Linnanto, Juha: Light excitation transfer in photosynthesis revealed by quantum chemical calculations and exiton theory. (179 pp.) 2012
155. Roiko-Jokela, Veikko: Digital imaging and infrared measurements of soil adhesion and cleanability of semihard and hard surfaces. (122 pp.) 2012
156. Noponen, Virpi: Amides of bile acids and biologically important small molecules: properties and applications. (85 pp.) 2012
157. Hulkko, Eero: Spectroscopic signatures as a probe of structure and dynamics in condensed-phase systems – studies of iodine and gold ranging from isolated molecules to nanoclusters. (69 pp.) 2012
158. Lappi, Hanna: Production of Hydrocarbon-rich biofuels from extractives-derived materials. (95 pp.) 2012
159. Nykänen, Lauri: Computational studies of Carbon chemistry on transition metal surfaces. (76 pp.) 2012
160. Ahonen, Kari: Solid state studies of pharmaceutically important molecules and their derivatives. (65 pp.) 2012

161. Pakkanen, Hannu: Characterization of organic material dissolved during alkaline pulping of wood and non-wood feedstocks (76 pp.) 2012
162. Moilanen, Jani: Theoretical and experimental studies of some main group compounds: from closed shell interactions to singlet diradicals and stable radicals. (80 pp.) 2012
163. Himanen, Jatta: Stereoselective synthesis of Oligosaccharides by *De Novo* Saccharide welding. (133 pp.) 2012
164. Bunzen, Hana: Steroidal derivatives of nitrogen containing compounds as potential gelators.(76 pp.) 2013
165. Seppälä, Petri: Structural diversity of copper(II) amino alcohol complexes. Syntheses, structural and magnetic properties of bidentate amino alcohol copper(II) complexes. (67 pp.) 2013
166. Lindgren, Johan: Computational investigations on rotational and vibrational spectroscopies of some diatomics in solid environment. (77 pp.) 2013
167. Giri, Chandan: Sub-component self-assembly of linear and non-linear diamines and diacylhydrazines, formulpyridine and transition metal cations. (145 pp.) 2013
168. Riisiö, Antti: Synthesis, Characterization and Properties of Cu(II)-, Mo(VI)- and U(VI) Complexes With Diaminotetraphenolate Ligands. (51 pp.) 2013
169. Kiljunen, Toni (Ed.): Chemistry and Physics at Low Temperatures. Book of Abstracts. (103 pp.) 2013
170. Hänninen, Mikko: Experimental and Computational Studies of Transition Metal Complexes with Polydentate Amino- and Aminophenolate Ligands: Synthesis, Structure, Reactivity and Magnetic Properties. (66 pp.) 2013
171. Antila, Liisa: Spectroscopic studies of electron transfer reactions at the photoactive electrode of dye-sensitized solar cells. (53 pp.) 2013
172. Kemppainen, Eeva: Mukaiyama-Michael reactions with α-substituted acroleins – a useful tool for the synthesis of the pectenotoxins and other natural product targets. (190 pp.) 2013
173. Virtanen, Suvi: Structural Studies Of Dielectric Polymer Nanocomposites. (49 pp.) 2013
174. Yliniemelä-Sipari, Sanna: Understanding The Structural Requirements for Optimal Hydrogen Bond Catalyzed Enolization – A Biomimetic Approach.(160 pp.) 2013
175. Leskinen, Mikko V: Remote β-functionalization of β'-keto esters (105 pp.) 2014
176. 12th European Conference on Research in Chemistry Education (ECRICE2014). Book of Abstracts. (166 pp.) 2014
177. Peuronen, Anssi: N-Monoalkylated DABCO-Based N-Donors as Versatile Building Blocks in Crystal Engineering and Supramolecular Chemistry. (54 pp.) 2014
178. Perämäki, Siiri: Method development for determination and recovery of rare earth elements from industrial fly ash. (88 pp.) 2014

179. Chernyshev, Alexander, N.: Nitrogen-containing ligands and their platinum(IV) and gold(III) complexes: investigation and basicity and nucleophilicity, luminescence, and aurophilic interactions. (64 pp.) 2014
180. Lehto, Joni: Advanced Biorefinery Concepts Integrated to Chemical Pulping. (142 pp.) 2015
181. Tero, Tiia-Riikka: Tetramethoxy resorcinarenes as platforms for fluorescent and halogen bonding systems. (61 pp.) 2015
182. Löfman, Miika: Bile acid amides as components of microcrystalline organogels. (62 pp.) 2015
183. Selin, Jukka: Adsorption of softwood-derived organic material onto various fillers during papermaking. (169 pp.) 2015
184. Piisola, Antti: Challenges in the stereoselective synthesis of allylic alcohols. (210 pp.) 2015
185. Bonakdarzadeh, Pia: Supramolecular coordination polyhedra based on achiral and chiral pyridyl ligands: design, preparation, and characterization. (65 pp.) 2015
186. Vasko, Petra: Synthesis, characterization, and reactivity of heavier group 13 and 14 metallylenes and metalloid clusters: small molecule activation and more. (66 pp.) 2015
187. Topić, Filip: Structural Studies of Nano-sized Supramolecular Assemblies. (79 pp.) 2015
188. Mustalahti, Satu: Photodynamics Studies of Ligand-Protected Gold Nanoclusters by using Ultrafast Transient Infrared Spectroscopy. (58 pp.) 2015
189. Koivisto, Jaakko: Electronic and vibrational spectroscopic studies of gold-nanoclusters. (63pp.) 2015